MODELLING OF GASIFICATION OF POULTRY LITTER

A thesis submitted to The University of Manchester for the degree of Doctor of Philosophy in the Faculty of Engineering and Physical Sciences

2011

CAROLINA FONT PALMA

SCHOOL OF CHEMICAL ENGINEERING AND ANALYTICAL SCIENCE

CONTENTS

Word count: 69106

LIST OF FIGURES

LIST OF TABLES

NOMENCLATURE

$\Delta H_{R,gg}$	heat of reaction of homogeneous reactions
$\Delta H_{R,gs}$	heat of reaction of heterogeneous reactions
ΔG^{o}_{f}	standard Gibbs free energy of formation
a	number of atoms
A	pre-exponential factor
A	total number of gram atoms
AFT	Ash fusion test
Ar	Archimedes number
ASPEN	advanced system for process engineering
ASTM	American Society for Testing and Materials
ASU	air separation unit
A_t	cross-surface area of reactor
BFBG	biomass bubbling fluidised bed gasifier
BIG/GT	biomass integrated gasification/gas turbine
C	concentration
CC	combined cycle
CET	compressor exhaust temperature
CFB	circulating fluidised bed
CFBG	circulating fluidised bed gasifier
CFD	Computational Fluid Dynamic
CGE	cold gasification efficiency
C_p	heat capacity
CSFB	comprehensive simulation program for fluidised bed equipment
CSTR	continuous stirred-tank reactor
D	diffusion coefficient
d_b	diameter of bubbles
DPM	Discrete Particle Method
DSC	differential scanning calorimetry
DTG	differential thermogravimetric analysis
DTP	dynamic two-phase structure model
E	apparent energy of activation
EET	expander exhaust temperature
EFGT	Externally fired gas turbines
EIS	energy integration system
EIT	expander inlet temperature
ER	equivalence ratio
F_∞	total elutriation rate of the particles
F_0	total entrainment rate at the bed surface
F_C	flow rate of carbonaceous material
FDA	Food and Drug Administration
FTIR	Fourier Transform Infrared spectrometry
G	Gibbs free energy
GC	gas chromatography
GC/FID	gas chromatography/flame ionization detector
GC-MS	gas chromatography – mass spectroscopy
GT	gas turbine
HACA	H_2-abstraction-C_2H_2-addition

H_{be}	heat transfer coefficient between emulsion and bubble phases
$H_{C,in}$	enthalpy of the carbonaceous material calculated from ultimate analysis
H_f	enthalpy of formation
HHV	higher heating value
h_p	heat transfer coefficient between solids and gas
HRSG	heat recovery steam generator
HTU	hydro thermal upgrading
IGCC	Integrated gasification combined cycle
k_g	thermal conductivity
K_{gt}	mass transfer coefficient
LCPD	Large Combustion Plants Directive
LHV	lower heating value
m	mass flow rate in kg/s
MC	moisture content
n	reaction order
n	number of moles
Nu	Nusselt number
OCC	oxidizable carbon content
ODE	ordinary differential equation
PAH	polycyclic aromatic hydrocarbon
PF	plug-flow model
PFBC	Pressurised fluidised-bed combustion
Pr	Prandtl number
PR-BM	Peng-Robinson equation of state with Boston-Mathias alpha function
Q	volumetric flow rate of produced gases
Re	Reynolds number
R_{gg}	rate of reaction of gas-gas reactions
R_{gs}	rate of reaction of gas-solid reactions
SFR	steam fuel ratio
SPA	solid phase absorption
SR	stoichiometric ratio
STP	simple two-phase model
T	temperature
TCC	total carbon content
TDH	transport disengaging height
TGA	thermogravimetric analysis
TMA	Thermo-mechanical analysis
TOMC	total organic matter content
u_b	bubble velocity
u_f	gas velocity in the freeboard
u_{mf}	minimum fluidisation velocity
W	net gas turbine power output in Watts
W_a	actual work
W_i	ideal work
WID	Waste Incineration Directive
X_C	carbon conversion
XRF	X-ray fluorescence
y	mole fraction

z_{bed}	total bed height

Greeks

$\hat{\phi}_i$	fugacity coefficient
λ	Lagrange multiplier
η	process efficiency
ϕ	distribution coefficient of combustion products CO/CO_2
ϕ_S	sphericity
η_C	isentropic efficiency of compression
η_{CG}	cold gasification efficiency
ε_{mf}	bed voidage at minimum fluidisation
η_T	isentropic efficiency of expansion
δ	bubble fraction
μ	viscosity

Subscripts

b	bubble phase
bio	biomass
e	emulsion phase
f	freeboard
gas	product gases
i	species
k	element
P	pressure
s	solid
T	temperature

ABSTRACT

The poultry industry in Europe is vast and proper waste management is required in order to comply with environmental regulations. As a result, poultry litter represents a potential fuel candidate for thermal conversion technologies since it is an available source. Therefore, a process for the gasification of poultry litter is examined in this study. This process integrates a fluidised bed gasifier with a gas turbine with the aim of generating combustibles gases for energy production. This resulted in a viable solution for a small scale system to be installed on-site the biomass source. The system allows the treatment of waste with the additional benefit of generation of energy, and is suitable for a poultry farm to avoid the transportation of litter to centralised plants. Among the by-products generated during gasification, such as NO_x, SO_2, and fly ash, tar is a major issue when implementing this technology because tar can cause operational problems as a result of the possible formation of aerosols and soot formation due to repolymerization.

A process simulation using Aspen Plus was used to evaluate four levels of integration. The equilibrium model was applied to evaluate integration schemes involving recuperation of energy from the gas turbine exhaust gases. The recuperation of residual heat to preheat air and product gases was performed with the aim of achieving the highest electrical efficiency. For the conventional "atmospheric layout", the fuel gases have to be cooled down before being compressed to the desire pressure, which causes to waste energy from the hot fuel gases. The benefit of the "pressurised layout" is that all process stages can be maintained hot. Process efficiency analyses showed that even when the "atmospheric layout" was set with energy recuperation, the "pressurised layout" delivered higher efficiencies with or without the energy recuperation into the gasifier.

After a bibliographic review, the lignin content of biomass was concluded responsible for tar formation because of its aromatic nature. As lignin components, guaiacol, vanillin and catechol were chosen as tar precursors due to its presence in lignin structure. A reaction mechanism and its corresponding kinetics were derived. This mechanism was based on the three-lignin unit decomposition into lighter molecules and greater aromatic rings. Some of the tar products were involved in combustion and/or steam gasification reactions. The tar reaction mechanism was introduced into the kinetic model for the gasification of poultry litter. The results showed agreement with experimental work from previous reports for the evolution of primary tars. However, the model overestimated the total tar concentration. When the model was compared with the equilibrium model, the trends of the main product gases agreed as the air:fuel ratio was varied.

LAY ABSTRACT

The massive production of poultry in Europe generates waste referred as poultry litter. Proper waste management is required in order to comply with environmental regulations. As a result, poultry litter is an attractive source for energy generation while avoiding the disposal of litter to land. The process selected to transform litter to energy was gasification. Gasification consists of converting litter, using a controlled amount of air, into a combustible gas mixture at high temperatures. A process that integrates a fluidised bed gasifier with a gas turbine with the aim of generating combustibles gases for energy production is examined in this study. This resulted in a viable solution for a small scale system to be installed on-site to avoid the transportation of litter to centralised plants. Among the by-products generated during gasification, such as NO_x, SO_2, and fly ash, tar is a complex mixture of heavy compounds that causes major issues when implementing this technology because of causing operational problems or damaging downstream systems.

A process simulation using the engineering software Aspen Plus was used to examine the process performance. The equilibrium model was applied to evaluate integration schemes involving recuperation of energy from the gas turbine exhaust gases. The recuperation of residual heat to preheat air and product gases was performed with the aim of achieving the highest electrical efficiency. Two configurations were examined. One was a conventional "atmospheric layout" where the fuel gases had to be cooled down before being compressed to the desire pressure. This caused to waste energy from the hot fuel gases. The other was a "pressurised layout" that allowed all process stages to be maintained hot without heat wastage. Process efficiency analyses showed that even when the "atmospheric layout" was set with energy recuperation, the "pressurised layout" delivered higher efficiencies with or without the energy recuperation into the gasifier.

The second part of this work consisted of modelling the formation and evolution of tar components. The main assumption was that tar is generated from the presence of lignin in poultry litter. The lignin structure is known to have an aromatic structure which is similar to the tar compounds formed during gasification. To simplify the reaction pathways, three compounds were chosen as representative of tar units and primary products. A reaction mechanism and its corresponding kinetics were derived. This mechanism was based on the three-lignin unit decomposition into lighter molecules and greater aromatic rings. Some of the tar products were involved in combustion and/or steam gasification reactions. The tar reaction mechanism was introduced into the model for the gasification of poultry litter. The results showed agreement with experimental work from previous reports for the evolution of primary tars. However, the model overestimated the total tar concentration. When the model was compared with the equilibrium model, the trends of the main product gases agreed as the air:fuel ratio was varied.

DECLARATION

I hereby declare that no portion of the work referred to in the thesis has been submitted in support of an application for another degree or qualification of this or any other university or other institute of learning.

COPYRIGHT STATEMENT

DEDICATION

I want to dedicate this thesis to my husband Marco, who has always believed that any goal I wish can be fulfilled.

To my parents Luis and Mary, who have always given me their unconditional support, comfort and love.

To my sister Lupita, who has always encouraged me to keep going.

To my grandma, cousins and uncles, who were always concerned with my well-being and progress.

ACKNOWLEDGEMENTS

I would like to thank my supervisor, Dr. Alastair D. Martin, for his continuous support and advice leading to the submission of the thesis.

I would also like to thank the National Council on Science and Technology (CONACYT) of Mexico for financial support for the completion of the PhD studies, and Keld Energy Ltd. for their financial support to attend the Energy from Biomass and Waste UK (EBW UK) Conference.

Chapter 1

Introduction

The use of renewable fuels in energy conversion processes represents a favourable option to reduce greenhouse gas emissions. Therefore, biomass and agricultural waste are increasingly gaining attention as a promising initiative to address Climate Change as substitute to fossil fuels. In this chapter, an overview of biomass uses, agricultural waste, waste management practises and the current challenges for waste-to-energy technologies is given. In addition, the objectives of this work are described.

1.1 Background

The production of bioethanol started from sugar cane in the late 70's in Brazil and it was followed some years later by the USA using maize and sorghum. The total grain consumption for bioethanol was 57 million tonnes in 2005. In contrast, EU countries have focused on producing biodiesel. It was forecasted that the demand of arable land for oilseed production would increase from 3.2 million ha in 2005 to 13.3 million ha in 2010 [1]. However, the growing production of crops for bio-energy production may also pose negative environmental impacts, e.g. the reduction of tropical rain forests in Brazil due to sugar cane and soybean plantations. In addition, it has a social impact since food costs can increase affecting consumers, especially in developing countries. Instead of just dedicating land to the growth of crops for energy generation, agricultural residuals and animal manure represent an alternative source for fuels. This is especially important nowadays when food demands augment.

Intensive farming practices are promoted by the food demand of the continuously increasing world population. A consequence of these practices is the generation of significant amount of organic waste. For instance, in Mexico 18.3 and 8.95 million tonnes of maize for grains and maize for forage, respectively, were produced in 2007. The maize for grain required a surface of 5.65 million ha, the yield was 3.24 ton/ha and represented 28.5% of the total production. The yield of maize for forage was 29.3 ton/ha [2]. The production of poultry was 293 million chicks for meat and 164 million chicks for eggs in 2005. The major producer owns 600 farms with an average production of 263,000 chicks per year. Of the 24.25 million hectares of land in United Kingdom, 18.5 millions are used for agriculture (statistics from 2005); as a result agriculture is a large source of waste. In addition, the enormous poultry industry in the UK is producing 850 million birds every year [3]. Thus, the selection of the type of biomass employed will depend on the availability of the waste. Therefore, each country requires an evaluation of their resources in order to avoid the overuse of land for energy generation. Nevertheless, it is evident that biomass is already available as potential fuel without the need of using more arable land.

The poultry industry also generates the so-called litter which is the waste that consists of a mixture of manure, waste bedding, waste food and feathers. The term poultry litter encompasses total manure and litter generated from chicken and turkey broilers, breeder chickens and layer chickens. Broilers are pullets and cockerels that have not yet reached sexual maturity.

1.1.1 Poultry litter management

Normally it takes nine to ten weeks for a crop to reach the market weight and five to six crops are grown per year in a farm. After that period, with every new crop litter is removed and substituted with fresh bedding material. An approximate generation of 4.4 million tonnes of litter results from poultry operations in the UK, from which 2.5 tonnes derived from broiler and turkey units [4]. Bedding material is spread over the floors within the poultry houses. The main purpose of the bedding material is to absorb moisture and promote drying by increasing the surface area of the house floor. Materials typically used as bedding include sawdust, straw, wood shavings, shredded paper and peanut or rice hulls [5]. As a result, the composition

and physical characteristics of poultry litter vary within production facilities and between farms and regions. This variability is caused by differences in the amount and type of bedding material, the number of flocks raised on the litter, the amount of dirt removed with the litter, water system employed, method of clean-out and storage time. Therefore, the resulting litter compared to woody biomass is more complex and challenging to employ because of its higher concentration of ash, nitrogen, sulphur, chlorine and alkali metals [6].

Inappropriate management of the bedding material can cause serious problems to the poultry health. Since birds are in continuous contact with litter, hock burns marks can be found on the upper joints of birds. These marks are caused by ammonia. In contact with the skin, ammonia burns the skin of the leg and leaves a mark. Blackened skin occurs leading to erosion and fibrosis on the lower surface of the foot pad, at the back of the hocks and sometimes, in the breast area. Wet litter can also cause problems, when moisture content exceeds 35%, health problems are encountered. Wet litter increases the incidence of foot pad dermatitis (pododermatitis) and folliculitis. Serious cases of folliculitis can turn into gangrenous dermatitis which causes downgrading of the end product. As a result, it is recommended that the litter moisture should be kept between 20–25% [7]. In addition, wet litter promotes the proliferation of pathogenic bacteria and moulds, and toxic fungi which can create a mycotoxin (toxic chemical products produced by fungi) threat. The growth of bacterial flora in wet litter contributes to a higher release of ammonia. Continuous exposure to ammonia can cause damage to the respiratory organs, inflammation of cornea and blindness. Consequently, the bedding material is removed with every new flock to maintain the quality of the bedding material that guarantees the welfare of the broilers.

1.1.2 Poultry litter disposal: Environmental impacts

Traditionally, disposal of poultry litter includes its utilisation as fertiliser, but its improper application and/or overuse represent potential environmental problems, such as spread of pathogens [8] and emission of greenhouse gases and odorous compounds. Nitrogen present in poultry litter can be converted to ammonia and nitrates. Infiltration of soluble nutrients can cause ground water pollution and favour high levels of nitrate in drinking water. These high levels of NO_3 can cause cancer,

respiratory disease in humans, foetal abortion in livestock and methaemoglobinaemia, a blood disorder in infants commonly known as 'blue baby disease' [9]. Heavy rainfall can sweep the poultry litter applied to land into nearby ditches, streams and lakes. Surface water pollution by nutrients can lead to eutrophication, which is the excessive growth of algae that consumes aquatic nutrients and oxygen, and block sunlight [10]. As a result, the dispersion of nitrates is monitored under the Nitrates Directive (91/676/EEC), which was created for the protection of water through better farmyard management by the control of the application and storage of inorganic fertiliser and manure on farmland [11]. With this growing concern and new regulatory constraints, manure disposal is a less acceptable option. Therefore, an environmentally friendly method of disposing animal waste is needed and some methods are analysed in the following section.

1.1.3 Waste management practises

Alternative options for the treatment of poultry litter include composting, anaerobic digestion, combustion, pyrolysis and gasification. Composting is the aerobic degradation of biodegradable organic waste. It typically takes 4–6 weeks to reach a stabilised material. The composted poultry litter is odourless and pathogen free with low moisture content, and can be used as organic fertiliser. Poultry litter contains high levels of organic nitrogen from the high content of protein and amino acids. A disadvantage of composting is that nitrogen and other nutrients are lost during the process. Ammonia emissions during composting are of significant environmental concern. Therefore, additives had been tested to reduce NH_3 volatilisation, such as zeolites, clay, coir (fibres found between the hard, internal shell and the outer coat of coconut fruit), $CaCl_2$, $CaSO_4$, $MgCl_2$, $MgSO_4$ and $Al_2(SO_4)_3$; where zeolite and coir proved to be more successful for the reduction of ammonia losses during the composting of poultry manure [5].

Anaerobic digestion involves the degradation and stabilisation of organic matter by microbial microorganisms under anaerobic conditions [12]. The main products are methane (around 60% content) and inorganic gases such as carbon dioxide. The anaerobic digestion of poultry litter involves two stages. The first stage includes the hydrolisation and brake down of complex components, such as fats, proteins and polysaccharides, to their component units. This breakage is performed

by anaerobic bacteria and called acid fermentation wherein organic material is converted to organic acids, alcohols and new bacterial cells. The second stage includes the conversion of the hydrolysis products into gases (mainly methane and carbon dioxide) and is called methane fermentation. The residual sludge is stable and can be used as fertiliser. Poultry litter contains around 50–70% of total solid content which makes difficult to mix and requires dilution [13]. The purpose of mixing in anaerobic digestion is the dispersion of the incoming waste to improve contact with the microorganisms and replace the previously degraded products with fresh nutrients from the waste, and reduce stratification; in this manner, maintain a high rate of anaerobic biodegradation and high production of gases. Another issue during the anaerobic digestion of poultry litter is the minimisation of the levels of ammonia; this could also require dilution. Dilution, however, increases the volume of the material to be handled, and thus increases process energy requirements. Even though some ammonium anions formed can be used by some anaerobic bacteria, excess ammonium can inhibit the destruction of organic compounds and produce volatile fatty acids. Composting and anaerobic digestion practices reduce pathogens and generate a more uniform fertiliser. However, they require large facilities, control ammonia emissions and long processing times, from days to months [5].

Biomass energy conversion through thermochemical processes, such as pyrolysis, combustion and gasification, are preferred because they offer the following advantages: the process can be designed to suit on-site application allowing a more compact system; the conversion process takes shorter times (a matter of minutes) compared to the long periods required in anaerobic digestion; destruction of pathogens and pharmaceutical compounds due to high process temperatures; the option of employing seasonal residues from farms; and more efficient recovery of nutrients [14]. Direct combustion of poultry litter has been proposed to provide heating to poultry houses or for power generation depending on the scale of the combustion process [5]. In contrast to combustion, where mainly heat is the end product, gasification involves the conversion of biomass into a combustible gas mixture by partial oxidation. Therefore, besides solving the problem of waste treatment, gasification of poultry litter on-site represents a viable solution for the disposal of litter and energy generation [15].

A by-product from thermochemical processes, such as combustion and gasification of biomass, is ash. The resulting ash contains high phosphorus and potassium concentration that makes it a feasible fertiliser for agricultural crops. Poultry litter ash was evaluated as a potential phosphorus source for wheat and other crops, and showed similar effectiveness as potassium phosphate when the soils were limed [16]. The ash generated could be marketed as fertiliser. Poultry litter ash could be potentially sold at a price comparable to fertilisers with phosphorus and potassium of different ratios such as 0:7:30 and 0:10:20, at €11.45 per 50 kg bag. However, the ash might require formulation and granulation which might incur in additional costs. But at least the ash could be used in its original state and save the farmer the expenditure on agricultural fertiliser [13].

1.1.4 Challenges for waste-to-energy technologies

The size of the facility for a waste-to-energy process –when located in rural areas or small towns– has proven to be of great relevance for the success of a project. For instance, the project of the installation of a 5-MWe wood gasification plant near the town of Cricklade failed to obtain planning permission due to public opposition in 2000 [17]. The proposed plant was designed as 126 m long and 46 m wide, requiring 36,000 tons of wood from surrounding farms in order to provide power to over 10,000 homes. Among the main negative perceptions from residents were: visual effects due to the height of chimneys and proximity to local residents, increases in traffic due to trucks, accidents and noise, and negative effect on property prices. Therefore, the design of a biomass electricity plant requires a sensible sizing of the plant and proper selection of the site.

Additionally, the success for the wider application of the biomass gasification technology greatly depends on the control of ash-related problems and product gases quality. Among the ash-related problems are sintering, agglomeration, deposition, erosion and corrosion. Since poultry litter contains relatively high ash content, alkali metals can react with silica to form silicates or with sulphur to produce alkali sulphates. These compounds have melting points lower than 700°C which cause deposition on the reactor wall or if carried with the gases can cause corrosion and erosion of further equipments. In addition to the conversion of biomass to gases during gasification, char and tar are produced reducing the syngas yield and overall

conversion efficiency [18]. The presence of tar is undesirable because of the problems caused by condensation or formation of more complex tar compounds. These compounds can block and foul process equipment, engines and turbines used for the application of the product gases [19].

The understanding of the gasification process allows the operation and optimisation of the system. A useful tool to explore its complexity is the mathematical simulation of the gasification process. As a result, there is a vast literature on the modelling of coal gasification. However, coal and biomass differ in composition, the latter contains larger amount of volatile matter which makes it more reactive. This difference creates the need to develop models for biomass gasification and the state-of-the-art will be discussed in the next chapter. In addition, models often consider tar as a single lump in order to avoid the complexity of tars, which shows a need to include more detail models including tar formation and evolution.

Since the main product of biomass gasification is a valuable mixture of combustible gases, gasification is frequently coupled to power generation systems. Integrated gasification combined cycle (IGCC) puts together a gasification unit and a combined cycle power system. The combined cycle system combines one or several gas turbines (GT) and/or one or several steam turbines which can include a heat recovery steam generator (HRSG). There are currently 18 installed coal-fired plants of large size (200–300 MW) worldwide, mainly located in Japan, the USA, Germany and Holland, which have reached the demonstration stage of commercial-scale IGCC plants [20]. Thus, the IGCC technology focuses on high efficiency and large capacity.

Conventional IGCC systems employ gasification at atmospheric pressure, where the product gases are cooled to facilitate the compression to the required pressure for the gas turbine engine [21-23]. Pressurised gasification is, therefore, more advantageous to avoid the cooling of gases when compression is required and maintain all process stages hot. However, systems employing a pressurised gasifier are usually of medium to large scale. This work considers a small scale on-site pressurised gasification unit to avoid the transportation of litter to centralised plants and maintain all process stages hot.

1.2 Objectives

The aim of this project is the evaluation of a gasification process with poultry litter as a potential source of renewable energy. The proposed process consists of a fluidised bed gasifier integrated with a gas turbine engine.

The objectives of this work are six folded. These consist of:

- The simulation of a process that integrates a fluidised bed gasifier with a gas turbine with the aim of generating combustibles gases for energy production. This process should be suitable for a poultry farm in order to avoid the transportation of litter to centralised disposal facilities and maintain all process stages hot.
- Comparison of different energy integration configurations and identification of the most optimal option in order to recuperate energy from the hot exhaust gases from the gas turbine.
- Identification of the leading operating parameters that affect the process efficiency.
- Evaluation of the emissions potentially released based on the operating parameters chosen.
- Identification of a mechanism for the tar formation and evolution during the fluidised bed gasification. This mechanism will be incorporated into a two-phase model.
- Identification of operating parameters and properties that require to be tested experimentally based on the modelling work.

1.3 Outline

The remainder of the study is organised into six more chapters, references and appendixes. Chapter 2 describes the advances in biomass conversion by thermochemical processes. The characteristics of poultry litter and its evaluation as fuel are examined. An analysis of experimental work on biomass gasification is shown which identified the main operating parameters that affect the system. Mathematical models that have been employed from coal to biomass are described. The last section explains the main challenges of the technology.

Chapter 3 starts describing the methodology employed for the modelling of the gasification of poultry litter. This section explains the assumptions made and how the process was split into sub-processes that allowed the representation of each unit modelled, such as the gasifier and gas turbine. This chapter provides the different heat exchanger configurations explored in order to maximise the recuperation of energy. The heat exchanger configurations were compared in order to identify the most suitable network.

Chapter 4 presents the results obtained through an equilibrium approach. Two cases are compared, the conventional case versus the pressurised system. Subsequently, the gasification process is examined by varying the amount of gasifying agent (air) and moisture content of poultry litter. The effect of the ash constituents is also revised. The temperature approach of the heat exchangers is varied to find by how much the efficiency can be improved. Finally, the gas turbine is evaluated by changing pressure ratio and turbine inlet temperature.

Chapter 5 provides the description of the kinetic model development. It explains the model assumptions and reactions involved in the proposed mechanism. This chapter explains the numerical method employed to solve the mass and energy balance equations and outlines the program used.

Chapter 6 shows the results generated from the kinetic model. These results are compared with experimental data for wood gasification in order to verify the accuracy of the model. Finally, the kinetic and equilibrium models for the gasification of poultry litter are compared.

Chapter 7 provides an overview of this work and the conclusions generated after the evaluation of the process configuration and results from the model. In addition, future work is proposed for the gasification of poultry litter.

Chapter 2

Literature review

Biomass gasification emerged in the early 1900s to produce fuels, chemicals and hydrogen, but the discovery of low-cost natural gas provoked the abandonment of manufacturing synthetic gas [24]. However, in recent decades concerns on power plant emissions, domestic and agricultural waste disposals, and the increased focus on greenhouse gases reduction have renewed interest and awareness on gasification technologies. In this chapter, thermochemical conversion processes are discussed in order to introduce the main topic of this work: biomass gasification. A review of experimental work on biomass gasification and biomass characteristics is examined. Subsequently, mathematical approaches for the simulation of the gasification process are presented and its integration with power generation systems. As a final point, software employed in the simulation of gasification is described.

2.1 Thermochemical conversion processes

The increasing demand for energy favours interest on the development of processes that generate electricity from sources different than coal, petroleum or natural gas. Biomass is preferred as a source for renewable energy due to its lower impact on the environment. Two main processes for the conversion of biomass to energy are used: thermochemical and bio-chemical/biological processes. Thermochemical processes transform biomass into energy rich products [25]. Bio-chemical conversion comprises: anaerobic digestion for production of mainly methane and CO_2, and fermentation for the production of ethanol [12]. Thermochemical conversion includes: combustion, pyrolysis, liquefaction,

hydrogenation and gasification. The main characteristics of these processes are giving below.

a) Combustion. In this process, biomass is directly burnt using air to produce heat, mechanical power or electricity in boilers, furnaces, steam turbines, etc. The oxygen added should be at least the amount necessary for stoichiometric oxidation of the feedstock. The product gases are at temperatures around 800–1000°C. Any type of biomass can be burnt, but in practice only biomass with <50% of moisture content is feasible for combustion [12].

b) Pyrolysis. The process of pyrolysis is the conversion of biomass using external heating in the absence of oxygen to generate liquid, solid and gaseous products; pyrolysis starts at temperatures of 350–550°C and up to 700°C. Depending on the heating rate employed, pyrolysis can be categorised in: i) slow pyrolysis, which uses slow heating rates in the order of 5–7 K/min and favours char production; ii) fast pyrolysis, employs heating rates around 300°C/min and produces higher yields of liquid products, such as high-grade bio-oil; and iii) flash pyrolysis, requires special reactors for residence times of few seconds which increases the liquid and gaseous products. An extensive review of types of pyrolysis processes can be found in [25].

c) Liquefaction. In this process, a liquid hydrocarbon is obtained using low temperatures and high pressures with a catalyst in the presence of hydrogen [26].

d) Hydrothermal upgrading (HTU). HTU is a process that transforms biomass into partly oxygenated hydrocarbons in a wet environment and at high pressure [12].

e) Gasification. In a gasification process, biomass is converted into a combustible gas mixture by partial oxidation. The amount of oxygen employed is lower than the stoichiometric amount required for complete combustion [27]. The product gases can be burnt to generate heat and steam or used in gas turbines to produce electricity. The gasification reactions include:

Reaction	ΔH_R	Reference	
Combustion reactions:			
$C + ½O_2 \rightarrow CO$	-111 kJ/mol	[27]	R.1
$C + O_2 \rightarrow CO_2$	-393 kJ/mol	[28]	R.2

$CO + ½O_2 \rightarrow CO_2$	-283 kJ/mol CO	[29]	R.3
$H_2 + ½O_2 \rightarrow H_2O$	-241.9 kJ/mol H_2	[29]	R.4
Water gas reaction:			
$C + H_2O \rightarrow CO + H_2$	+131.4 kJ/mol C	[29]	R.5
Boudouard reaction:			
$C + CO_2 \rightarrow 2CO$	+172.5 kJ/mol C	[29]	R.6
Steam methane reforming reaction:			
$CH_4 + H_2O \rightarrow CO + 3H_2$	+206 kJ/mol	[27]	R.7
$CH_4 + 2H_2O \rightarrow CO_2 + 4H_2$	+165 kJ/mol	[28]	R.8

HTU and liquefaction are the least employed technologies since they are less practical: HTU is at the pilot stage [30] and liquefaction is an expensive process that produces a tarry lump difficult to handle [25]. The purpose of combustion technologies is the generation of heat or destruction of waste, whilst gasification produces a valuable product that can be use as chemical or fuel for energy production [24]. Conversion efficiencies for biomass combustion power plants are in the range of 20–40%. However, higher efficiencies require systems with a capacity of over 100 MW_{el} or co-combustion with coal [12]. Therefore, gasification represents a viable solution for a small scale system installed on-site the biomass source, with twofold benefits: the treatment of waste and the generation of energy. As a result, the following sections will be dedicated to biomass gasification.

2.1.1 Types of gasifiers

Gasifiers can be classified according to the reactor design. This classification is based on how the fluids or solids are transported through the gasifier and they are: fixed bed and fluidised bed gasifiers. The parameter that dictates whether a bed is fluidised or fixed is the velocity at which the fluid passes upwards through the bed [31]. For fluidised beds, fluidisation begins when the drag force by upward moving gas equals the weight of particles; this is the so-called minimum fluidisation velocity, a very important parameter for the operation of fluidised beds [32].

In the case of fixed bed gasifiers, reaction zones are distributed based on the type of gasifier: downdraft or updraft gasifier. In downdraft gasifiers, air and

biomass are introduced from the top. Pyrolysis and combustion take place simultaneously and reduction reactions in a separate zone. In updraft gasifiers, biomass enters from the top and the gasifying agent from the bottom. Pyrolysis, oxidation and reduction reactions occur in distinct zones, as showed in Figure 2.1 [33]. In fluidised bed gasifiers, biomass is very rapidly mixed with the bed material, and almost immediately heated up to the bed temperature. As a result, the fuel is pyrolysed very fast.

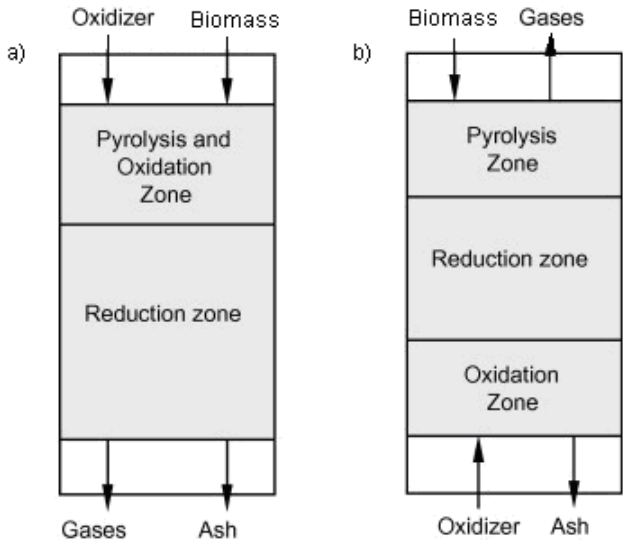

Figure 2.1 a) Downdraft and b) Updraft gasifiers [33]

The comparison between fixed bed and fluidised bed gasifiers had shown advantages and disadvantages of both technologies [34]. Fixed bed gasifiers provide high carbon conversion efficiency and stand high ash content in the feedstock. Moreover, updraft fixed bed gasifiers generate a product gas with low dust content. However, fixed bed gasifiers have some disadvantages, such as: non uniform temperature distribution allowing hot spots which might cause ash melting, the need for long periods for heat-up, and limited scale-up potential. In contrast, fluidised bed gasifiers produce a gas with higher dust content; furthermore, the use of high reaction temperatures to achieve good conversion efficiencies conflicts with the low melting points of ash components. On the other hand, fluidised beds have beneficial advantages as good heat and material transfer between gas and solids by providing good temperature distribution and fast heat-up, plus variation in fuel quality and broader particle size distribution in fuels are tolerable.

Fluidised beds are divided in bubbling and circulating fluidised beds. For bubbling fluidised beds, velocities are above the minimum fluidising velocity, but the bed expands no much further than its volume at minimum fluidisation; bubbles are formed providing more space. The bubbling action helps particles to mix and promotes uniformity in the bed temperature. Conversely, circulating fluidised beds have higher fluidising velocities that cause entrainment of particles. Most of the particles are blown out of the vessel which can be re-circulated to the reactor using cyclones. The circulation of particles promotes gas-to-particle contact and high carbon burnout efficiencies; however, this bed requires removal of heat to keep temperature lower than the ash melting temperature [31]. Therefore, the present work will focus on bubbling fluidised bed gasification.

2.1.2 Gasifying agents

In addition to the type of reactor, the gasification technology can be classified according to the gasifying agent employed. The type of gasifying agent affects the product gas composition, and in consequence its higher heating value (HHV). The selection of the gasifying agent can depend on the end use of the produced gas. They can be air, pure oxygen, steam, CO_2 or their mixtures. Main features of using different gasifying agents are:

a. Steam. The use of pure steam produces a gas with a high HHV and hydrogen content; however, the tar yield is higher [35]. Steam gasification requires indirect or external heat supply as well as catalytic tar reforming [18].

b. Steam-O_2. In order to supply heat for steam gasification, mixtures of steam and oxygen had been used [36]. The HHV of the product gases are slightly lower than when just gasifying with steam, and the tar yield is lower than when just using steam [35]. A H_2O/O_2 ratio of around 3 (mol/mol) and gasifier bed temperature between 800–860°C were recommended to generate a product gas with tar contents of around 5 g/Nm^3 [37].

c. Air. The HHV of the product gas is lower than when steam or steam mixtures are employed due to the diluting effect of nitrogen, but the tar content is significantly smaller than when pure steam is used [35].

d. CO_2. This gasifying agent produces a gas with high HHV, and H_2 and CO content, and low CO_2 content; however, it requires indirect or external heat supply and catalytic tar reforming [18].

Gasifying with air has been pointed out as suitable for electricity production, whilst with steam or steam-O_2 mixtures the produced H_2-rich gas can be best used in fuel cells. The lower heating value (LHV) of the product gas when gasified with pure steam was around 12.7–13.3 MJ/Nm^3; in contrast, with air gasification the LHV was 4.5–6.5 MJ/Nm^3 [35]. However, the use of steam or pure oxygen requires additional equipment for the generation of the gasifying agent which causes additional costs. This work, therefore, uses air-blown gasification because air is an available gasifying agent and produces a gas with lower tar content than steam gasification.

2.2 Biomass gasification

Even though coal gasification is a well established technology, its adaptation to biomass gasification poses challenges in the designing of the process. The main reason is the chemical and physical differences between biomass and coal. These differences are discussed in this section, as well as the most important physical and chemical characteristics of biomass.

2.2.1 Physical and chemical characteristics of biomass

Biomass is characterised by lower fixed carbon, and higher moisture and volatile matter contents than coal. Fuels are commonly characterised by proximate and ultimate analysis. Proximate analysis provides information on the content of volatiles, moisture, ash and fixed carbon. Fixed carbon is the mass that remains after the release of volatiles. Volatile matter, ash and moisture content are normally analysed by the standard test methods ASTM E (872), ASTM E (1755) and ASTM E (871), respectively, and the fixed carbon is determined by difference [38]. The ultimate analysis provides the elemental composition of biomass.

Biomass is also characterised by evaluating the energy content of the fuel, i.e. the heating value or calorific value. The energy released during complete combustion including the heat of vaporisation of water is known as the higher heating value (HHV) or gross calorific value. When the heat of vaporisation of water is subtracted

from the HHV, it is called net heating value or lower heating value (LHV) [27]. Over the years, numerous correlations to estimate the HHV from the elemental composition of fuels have been reported. Most of these correlations were developed from coal data such as the famous Dulong's formula. A correlation that unified the estimation of solid, liquid and gaseous fuels was derived from experimental data of HHV and elemental analysis from a number of fuels, including biomass, versus 18 HHV correlations; the resulting correlation for HHV (with an average absolute error of 1.45%) was:

$$HHV = 0.3491C + 1.1783H + 0.1005S - 0.1034O - 0.0151N - 0.0211A \quad (2.1)$$

where HHV is in MJ/kg, and C, H, O, N, S and A represent carbon, hydrogen, oxygen, nitrogen, sulphur, and ash contents of fuel, respectively, in mass percentages on a dry basis [39].

Among the identified biomass characteristics that affect the rate of gasification are size, shape, structure and ash content [40]. In the following section, the effects of the presence of ash will be discussed.

2.2.1.1 Ash content

Ash is the solid residue that remains after thermo-chemical or bio-chemical processes [27]. Ash consists of inorganic species such as alkali oxides and salts and its composition varies depending on the type of fuel. In general, potassium, sodium, and chlorine are the inorganics more problematic in fluidised bed gasification. The presence of ash in fluidised bed gasifiers represents a potential risk since bed agglomerates can lead to loss of fluidisation (defluidisation) and alkali vapours in the product gases can increase rates of hot corrosion on turbine surfaces in integrated systems [41]. For that reason, combustion turbine manufacturers recommend a total fuel-gas alkali content of less than 50 ppb which ensures the safe operation of the machines [42].

The analysis of ash constituents is normally reported in the form of oxides. However, ash is composed of different species and has been classified in three main groups that include [43]:

- salts ionically bound,
- inorganics bound organically to the carbonaceous material, and

- minerals present in the fuel structure and foreign material from biomass harvesting.

X-ray fluorescence (XRF, ASTM D4326) or Inductively Coupled Plasma spectrometry are normally used to determine the minor elemental composition of ash. For the speciation of the alkali salts and the organically bound inorganics present in biomass ash, the chemical fractionation method has been used, which uses strong leaching chemicals to extract ash constituents according to their solubility [43]. Table 2.1 shows a summary of species often found in biomass ash. Ash-forming matter in wood was grouped in three classes: water-soluble salts, minerals, and organically associated ash-forming elements, and shown in figure 2.2.

Table 2.1 Speciation of biomass ash [43]

Element	Ionic salts	Organically associated inorganics	Minerals
Na	Sodium nitrate		
	Sodium chloride		
K	Potassium nitrate		
	Potassium chloride		
Ca	Calcium nitrate	Calcium pectate	Calcium oxalate
	Calcium chloride		Calcite
	Calcium phosphate		
Mg	Magnesium nitrate	Chlorophyll	
	Magnesium chloride	Magnesium pectate	
	Magnesium phosphate		
Si	Amorphous silica		Phytolite
			Quartz
S	Sulphur tetraoxide-2ion	Sulfolipids	
N		Amino acids, protein	
		Sulfolipids	
P	Phosphate -3ion	Nucleic acids	Phytates
			Phytic acid
Cl	Chloride ion		
Al			Kaolinite
Mn		Organic structures of proteins and carbohydrates	
Fe		Chelates	Phytoferritin
		Organic sulphates	Iron oxide

Since ash agglomerates can create operating problems, agglomeration studies have identified two types of agglomerates. The first type is a melt-induced agglomeration in which bed materials are “glued” together by ash material in a melt phase; and the second type is a coating-induced agglomeration, where first the ash forms a uniform coating on the surface of bed grains and at certain coating thickness or temperature the coated bed grains start agglomerating. In order to study defluidisation as a function of temperature and fluidisation velocity, coated bed material was produced in a bubbling fluidised bed gasifier using willow, miscanthus and straw in a quartz tube reactor which allowed visual inspection. For straw, defluidisation was mainly caused by coating layer sintering and ash melting, whereas for willow and miscanthus, it was the sintering of coating layers at higher fluidisation velocities [44].

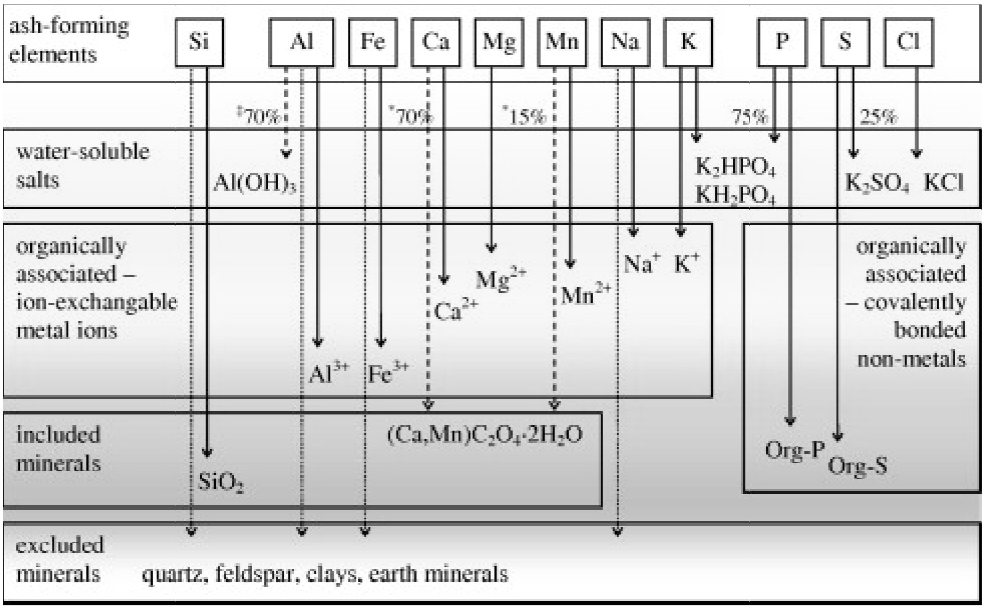

Figure 2.2 Ash-forming elements from wood [45]

Besides bed agglomeration, knowledge of the partition of inorganic elements between solid and gas streams is of interest. The partition was studied using banagrass (a tropical grass species) with different degrees of mechanical dewatering and leaching [41]. Tests were performed at 800°C in a bench fluidised bed gasifier and beads were used as bed material. The experiments showed that retention of alkali in the bed was: 80% of potassium, 20% of magnesium, and 30–60% of sodium. It was suggested that these values might affect the life of the bed material or lead to

bed agglomeration. In contrast, chlorine was predominantly found in the product gas stream.

Gas-phase concentration of alkali constitutes and low melting temperature of alkali ash components can cause ash deposit formation. As a result, work on the determination of melting and gas-phase release behaviour of biomass ashes have been conducted [46, 47]. Thermogravimetric analysis and differential scanning calorimetry (TGA/DSC) have been used simultaneously for the estimation of ash-melting characteristics. TGA/DSC analyses were performed on 12 biomasses and inorganic model compounds, such as SiO_2, KCl, K_2SO_4, K_2CO_3, $CaSO_4$, $CaCO_3$ and some mixtures, in order to elucidate the behaviour of biomass ashes. The initial melting temperatures were observed at 600-700°C for ash samples with high chlorine content (> 3 wt % in ash). The mechanisms identified as responsible for most of the weight lost consisted of: release of CO_2 from $CaCO_3$ at a temperature below 800°C; evaporation of potassium as KCl at temperatures of 850-1150°C; and the release of K_2O produced from the decomposition of K_2CO_3 at 1150–1450°C [46].

TGA/DSC tests combined with the Ash Fusion Test (AFT) and Thermo-mechanical analysis (TMA) were used to characterise the fusion behaviour of biomass ashes for a range of biomass, from woody and agricultural biomasses to poultry residues [47]. In the TMA, the change of height of a load of ash was measured to evaluate the sintering temperature while heating at a constant rate. The ashes were leached with water and ammonium acetate. For the chicken litter sample, a mass loss at 600-800°C was attributed to the decomposition of calcium carbonate and no clear melting point was observed. In contrast, for the leached chicken litter ashes, two endothermic peaks were noticed, one at 728°C (evaporation peak) with a mass loss of 30 % and the other at 958°C (melting point). The difference between the two samples was that the leached ashes were enriched with reactive inorganic and high melting point species. As a final point, the studies cited above, on ash agglomeration, inorganics partition, and ash melting, have shown that ash chemistry should be included in both experimental and modelling work.

2.2.2 Tars

Biomass gasification is one of the most promising technologies for renewable energy generation. During gasification many by-products are generated such as NOx,

SO_2, fly ash and tar. In particular, tar formation, as part of the product gases, is one of the major issues to resolve when implementing this technology. Tar is a complex mixture of condensable hydrocarbons comprising single-ring to 5-ring aromatic compounds plus other oxygen-containing hydrocarbons and complex PAH [48]. Tars are produced in series of reactions highly dependent on the operating conditions. A proposed scheme for the composition of biomass pyrolysis products and gasification tars as a function of process temperature showed the transition from primary products to aromatic hydrocarbons [49]:

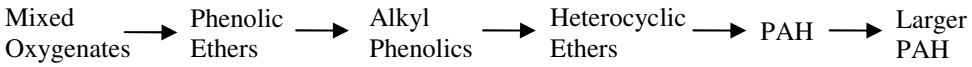

Table 2.2 shows that tars have been divided into five groups according to the molecular weight of individual tar compounds [19, 50].

Table 2.2 Classification of tar components based on molecular weight [19, 50].

Group	Class name	Representative compounds	Property
1	GC-undetectable	Determined by subtracting the GC-detectable tar faction from the total gravimetric tar	Very heavy tars, not detected by GC
2	Heterocyclic aromatics	Pyridine, phenol, cresols, quinoline	Highly water soluble compounds
3	Light aromatic (1 ring)	Toluene, xylene, styrene	Do not pose a problem regarding condensability and solubility
4	Light PAH compounds (2-3 rings)	Naphthalene, biphenyl, flourene, anthracene	Condense at low temperature even at very low concentration
5	Heavy PAH compounds (4-7 rings)	Flouranthene, pyrene, chrysene perylene, benzopyrene	Condense at high temperatures at low concentrations

The temperature at which the total partial pressure of tar equals the saturation pressure of tar that leads to condensation of the saturated gas is named the tar dew point. A calculation tool for predicting the tar dew point was developed based on the concentration of tar classes. From condensation curves, class 5 showed to dominate the tar dew point, e.g. even at a concentration of 0.1 mg/m^3 the dew point was 120°C

[51]. Tar is undesirable because of its propensity to condensate at temperatures lower than its dew point which causes blockage and fouling of lines, filters and gas turbines. Table 2.3 shows fuel requirements for gas turbines; these values had been proposed to avoid corrosion and deposition in the turbine expansion section [52].

Table 2.3 Fuel requirements for gas turbines [52]

Component	Allowable concentration
Particles	< 1 ppm
Tar	5 mg/m^3
HCl	< 0.5 ppm
S (SO_2 + H_2S + etc)	1 ppm
Na	< 1-2 ppm
K	< 1-2 ppm
Other metals	< 1-2 ppm

Methods to reduce and control tar formation during biomass gasification have been reported. These methods are classified in primary methods, when the tar is removed inside the gasifier; and secondary methods, when tar is removed in a separate step after gasification [48]. Primary methods include the appropriate selection of operating parameters, the proper design of the gasifier and the use of suitable bed additives or catalysts during gasification. In contrast, secondary methods comprise tar cracking either thermally or catalytically, or mechanical methods such as the use of cyclones and electrostatic filters.

Tar reduction methods are also categorised in five groups: mechanism methods, self-modification, thermal cracking, catalyst cracking and plasma methods [19]. Tars and particles have been simultaneously removed by plasma; 50% removal of naphthalene was achieved with a corona discharge using an energy density of 40J/L at 400°C in about 3 min [53]. A comprehensive review of tar reduction methods can be found in [19, 48].

Due to the importance of determining tar content in the product gas, sampling and analysis of tars is often performed during gasification experiments. Sampling tars has mostly included trapping tars by condensation on cold surfaces or filters,

through absorption in a cold organic solvent or adsorption on a sorbent. Subsequent to tar sampling, solvent and water are evaporated, followed by gas chromatographic or gravimetric analysis of tars. To unify methods for sampling and analysis, two sampling and analysis Tar Protocols were consented in 1998 [54, 55].

One protocol was developed for small scale, air blown fixed bed gasifiers at near atmospheric pressure with reciprocating engines. The agreed procedure includes the extraction of sample from the centre of the pipe, and then the gas passes through a stainless steel heated filter. To remove water vapour, the gas is passed into an ice bath, then through a series of three stainless steel or glass impinger bottles containing dichloromethane and placed in a cool box with an ice/acetone freezing mixture. To determine the dust content, filters are weight in an analytical balance. The amount of tar is estimated by solvent distillation and evaporation followed by weighing the tar sample. For the identification and quantification of tar components, gas chromatography (GC) was proposed either with a GC/MS or GC/FID technique [54].

The second protocol was developed to sample from large-scale atmospheric and pressurised gasifiers. The method includes the detection of tar components from benzene to pyrene. Moisture and tar are collected in a series of 6 impinger bottles. The first, the fifth and the sixth bottles are half-filled with glass beads. From the second to the fifth bottles contain dichloromethane. The first four bottles are placed in an ice bath, and the last two in an acetone/CO_2 ice bath. The organic compounds are also quantified gravimetrically and by gas chromatography [55]. These unified protocols can help the standardisation of reported tar concentrations which also benefit the development of more accurate models for tar formation.

2.2.3 Operating parameters for biomass gasification

Gasification produces a gaseous mixture mainly consisting of hydrogen (H_2), carbon monoxide (CO), methane (CH_4), carbon dioxide (CO_2) and water vapour (H_2O), and nitrogen (N_2) when air is employed as gasifying agent. In addition, a fraction of biomass converts to char and tar. For pine sawdust, a carbon conversion of 80% and char yield of around 10% were reported at a gasification temperature of 780°C in a steam/N_2 (90/10) fluidised bed gasifier [56]. The reduction and conversion of tar and char are of interest to increase the gas yield and conversion efficiency. Moreover, the removal of particulate dust and condensable tar from the

product gases is essential for the end use of the product gas, such as internal combustion engines, gas turbines or fuel cells for heat and power generation. Treatments inside the gasifier for char and tar reduction comprise: i) proper selection of operating parameters, ii) gasifier modifications (discussed in section 2.1.1), and iii) use of catalysts (section 2.2.4).

A variety of experimental studies have been performed to understand the leading operating parameters for biomass gasification. Among the parameters frequently analysed due to their influence on the gas product composition and tar content are: equivalence ratio, temperature of the gasifier bed, temperature of gasifier freeboard, secondary air injection in the freeboard, addition of catalysts [57], amount of fluidising agent, fuel composition [58] and fuel moisture content.

The equivalence ratio (ER) concept is widely used in energy conversion processes such as gasification. ER is the ratio of fed air to the stoichoimetric air for complete combustion. Its determination is straight forward for fuels of known chemical formula, e.g. ethanol; however, for biomass, the determination of the stoichiometric ratio (SR) of air to fuel for complete combustion is more complex. SR can be calculated from the elemental composition of the fuel:

$$SR = \left(\frac{C_C}{12} + \frac{C_H}{4} - \frac{C_O}{32}\right)\left(1 + \frac{79}{21}\right)\left(1 - \frac{C_A}{100}\right)\frac{28.84}{100} \qquad (2.2)$$

where C_C, C_H, and C_O represent the weight content of carbon, hydrogen and oxygen on an ash free basis, and C_A is the ash content; or by using a correlation between HHV and SR:

$$SR = 0.31HHV \qquad (2.3)$$

Then, the equivalence ratio (ER) is calculated using the actual air to fuel ratio divided by SR [59].

Increments of ER decreased CO and H_2 and increased CO_2 content; the inverse effect caused the increase of gasification temperature, CO and H_2 increased and CO_2 decreased [60]. The effect of temperature on the products distribution was studied in a downdraft fixed-bed gasifier using olive kernel and olive three cuttings [28]. The gasifier was operated at an ER of 0.42 varying the temperatures between 750–950°C. High temperatures favoured CO and slightly H_2 concentrations and decreased CO_2 concentration. Higher yields of H_2 and CO were obtained from olive

kernels and were attributed to the higher content of cellulose and hemicellulose compared to olive tree cuttings mainly composed of lignin. Then, at isothermal conditions (950°C), the ER was varied from 0.14 to 0.42, lower ER favoured CO and H_2 concentrations and higher ER increased CO_2 production. A maximum LHV of 11.33 MJ/Nm^3 using olive tree cuttings at an ER of 0.21 and 950°C was reported; however, the individual gas concentrations shown in graphs excluded the amount of N_2 in the gas composition.

Experiments in a small scale fluidised bed gasifier at atmospheric pressure using air and steam as fluidising agents showed that increases of temperature favoured H_2 concentration but not the CO production. An optimum ER of 0.23 was found which gave the maximum concentration of CO and H_2. The introduction of steam was favourable for improving gas quality; however, too much steam lowered the gasification temperature, and therefore reduced the product gas quality [61].

The effect of operating parameters on tar reduction has been reviewed in [48] and only major findings will be briefly summarised. Increases of operating temperature have shown to reduce the total number of detectable tars but favoured the formation of aromatics without substituent groups (such as benzene and naphthalene) on tests of indirectly heated fluidised bed gasification of sawdust [62]. Oxygen-containing compounds (phenol, cresol and benzofuran) were detected at temperatures below 800°C. Tests varying the equivalence ratio showed that the tar yield decreased with increases of ER. Tar oxygen-containing compounds decreased drastically with increases of ER. In contrast, two-ring, three-ring and four-ring tar compounds increased with higher ER values. Tar content decreases with increase of the gasification temperature and with a higher ER; however, increases of ER decreased the HHV and lowered hydrogen and carbon monoxide contents.

In addition, by increasing the temperature of the bed from 700 to 850°C during the bubbling fluidised air gasification of pine sawdust, it was observed an increase in the H_2 and CO contents, slight decrease in the CO_2 content and a drastic decrease in the tar content from 19 g/Nm^3 at 700°C to 5 g/Nm^3 at 800°C. Moreover, the increasing of temperature of the freeboard also contributed to reduce the tar content. This tar content reduction was caused by tar cracking and steam reforming reactions [57]. Experimental work in a fluidised bed gasifier with maple wood chips employed two process temperatures, 754 and 821°C [63]. The higher temperature

lowered the tar yield due to a decrease in water-soluble compounds, particularly phenol compounds. Likewise, operation at higher pressure from 8 to 21 bars using tree chips reduced oxygenated components and especially phenols were almost completely eliminated; conversely, the PAH fraction increased. However, high temperatures increase the risk of ash agglomeration and sintering as discussed in section 2.2.1.1.

Even though performing sensitivity analysis of operating variables has demonstrated usefulness, many hours of experimental work are required to vary all operating parameters and study their effects, as well as it involves operational costs. As a result, the use of mathematical models provides ease and reliable results, especially during the design of the gasifier.

2.2.4 Catalysts for tar elimination

Tar decomposition takes place as a result of a series of complex, multiple and simultaneous reactions. The main reactions occurring during catalytic treatment are:

Thermal cracking $$pC_nH_x \leftrightarrow qC_mH_y + rH_2$$ R.9

Steam reforming $$C_nH_x + mH_2O \leftrightarrow nCO + \left(m + \frac{x}{2}\right)H_2$$ R.10

Dry reforming $$C_nH_x + nCO_2 \leftrightarrow 2nCO + \left(\frac{x}{2}\right)H_2$$ R.11

Carbon formation $$C_nH_x \leftrightarrow nC + \left(\frac{x}{2}\right)H_2$$ R.12

where C_nH_x represents tar which can be a mixture of several individual tar compounds, and C_mH_y represents a hydrocarbon with a smaller carbon number than C_nH_x [64].

The selection of the optimal catalyst will require a catalyst that has a high level of activation, is not easily poisoned or deactivated over time plus is inexpensive. A variety of materials had been tested as additives for the reduction of tars inside the gasifier. These catalysts have been divided in groups as: dolomite catalysts, alkali metal and other metal catalysts, nickel catalysts, and novel metal catalysts [19].

Dolomite is a calcium magnesium ore [$CaMg(CO_3)_2$] widely employed since it is a cheap catalyst. The dolomite chemical composition varies depending on the source, and its composition and porosity affect its activity [65]. The use of 20–30 wt. % of dolomite and the rest silica sand in a gasifier was reported to reduce the tar content from 15 g/m^3 to around 1 g/m^3 with an ER of 0.3 [66]. In addition to the tar reduction, the use of dolomite increased the H_2, CO and CH_4 content as well as the LHV of the product gas. Olivine, a mineral containing magnesium, iron oxide and silica, was reported to convert 71% of the total heavy PAHs and 46% of the total tar in the hot gasification gases; calcined dolomite was also employed and showed 90% conversion of heavy PAHs and total tar conversions of 63%; these results were obtained using only 17% of catalyst and the rest silica sand [64]. Olivine showed to be active for tar decomposition at higher temperatures, but its activity was lower than for dolomite; this was attributed to the fact that olivine is not porous and with no available internal surface area. To improve olivine performance as tar removal additive, pre-treated olivine was utilised and achieved an 80% naphthalene conversion. In these experiments, naphthalene was used as a model tar compound and the pre-treatment consisted of heating the olivine at 900°C in the presence of air [64, 67]. Olivine [$(Mg,Fe)_2SiO_4$ with a ratio of 9/1 of Mg/Fe] and dolomite catalysts were compared in one bubbling fluidised bed and one circulating fluidised bed gasifiers using air as fluidising agent. Dolomite proved to be more active than olivine for tar elimination; however, dolomite produced more particulates in the product gas since dolomite is very soft and generates small particles [68].

Alkali catalysts have also been employed for tar reduction. Potassium carbonate was used impregnated on wood during steam gasification in a fluidised bed gasifier operated at 750°C. Phenolic tar compounds were reduced by a factor of five and PAH by a factor of ten; the concentrations of furans and ketones were also significantly reduced [69]. Since biomass has been pointed out as a source of inexpensive coal gasification catalyst, alkali metal salts contained in biomass ash, especially those containing potassium, have been found good promoters of gasification reactions. An almost eight-fold increase in co-gasification rate at 895°C was observed in a 10:90 mixture of coal char and switchgrass ash [70].

Significant work on hot gas cleaning for biomass gasification has used nickel catalysts. Nickel catalysts were employed as a secondary method for tar elimination,

where the raw gas was first cleaned with a dolomite or alkali catalyst for tar removal and then the gas composition was adjusted using a nickel steam reforming catalyst [36]. Nickel based catalysts were tested and three (ICI46-I, Z409 and RZ409) showed to be effective in eliminating heavy tars (> 99 % destruction efficiency) in a guard bed. In addition, the hydrogen yield was improved by 6–11 vol. % (dry basis). Space velocity showed little effect on gas composition whereas increases of temperature enhanced H_2 yield and reduced light hydrocarbons. Nickel supported on silica was described as active for tar catalyst cracking at relatively low temperature (823 K). But this catalyst was deactivated after a short time due to accumulation of large amounts of carbon on its surface [71].

Novel metals have been employed to overcome the limitations of more traditional catalysts while keeping high efficiency for tar conversion. $M/CeO_2/SiO_2$ (M = Rh, Pd, Pt, Ru, Ni) catalysts were tested during cedar wood gasification. The order of catalyst activity was Rh > Pd > Pt > Ni = Ru for gasification at 823 K. $Rh/CeO_2/SiO_2$ catalyst exhibited a carbon conversion rate of about 88% at 823 K and of 97% at 873 K. $Rh/CeO_2/SiO_2$ catalyst was used for cedar wood gasification, advantages were found when used at the low temperature and could produce high carbon conversion but the cost of the catalyst was relatively higher than conventional catalysts, since the work was done at laboratory level using high grade chemicals [72]. Instead, Ni/Dolomite catalyst used in biomass gasification was proposed as more appropriate catalyst due to its cost, preparation and life time [73].

In summary, olivine is a natural occurring mineral with high attrition resistance that allows its use directly in fluidised bed gasifiers but its activity for tar reduction is not enough for the end use of the product gases. Nickel catalysts present higher tar destruction activity in steam reforming but they are frequently used in a second fixed bed reactor due to its attrition phenomena [74] and rapid deactivation caused by carbon formation on the catalyst surface [65]. A combined catalyst, of olivine and nickel catalysts, was proposed that allowed tar destruction with high resistance for attrition and carbon formation [75]. Therefore, the selection of the optimal catalyst for tar reduction during gasification, as a primary method, is at present a compromise among effectiveness, stability, availability and cost.

2.2.5 Characteristics of poultry litter

Differences between coal and biomass are relevant to the adaptation of coal gasification to biomass applications. One difference between coal and biomass is the calorific value. For poultry litter, the calorific value has been reported as 14.4 MJ/kg (dry basis), this value is around 40% of that of coal [76]. However, the higher volatile matter content in biomass favours working at lower gasification temperatures. Poultry manure contains mainly organic matter as showed in table 2.4.

Table 2.4 Chemical and physicochemical characterisation of poultry manure

	Poultry manure
Organic matter [a]	85.38
pH	8.8
Moisture [b]	48.69
Total nitrogen [a]	3.56
Inorganic nitrogen [a]	1.74
Ammonia nitrogen [a]	1.76
OCC/nitrogen ratio	10.89
TCC/nitrogen ratio	12.24
P_2O_5 [a]	0.71
K_2O_5 [a]	3.79
Paraffinic C [c]	12.4
C in OCH_3, sterols and amino acids [c]	6.7
C in carbohydrates and aliphatics with OH groups [c]	68.1
Aromatic and N-heterocyclic C [c]	3.2
Phenolic C [c]	3.1
C in CO_2H [c]	6.5
Total aliphatic C [c]	87.2
Total aromatic C [c]	6.3
Aromaticity [c]	6.7

OCC: oxidizable carbon content, OCC = (TOMC – 15.356)/1.805

TCC : total carbon content, TCC = (TOMC – 9.33)/1.745

TOMC: total organic matter content

[a] in wt % dry basis from [5]

[b] in wt % wet basis from [5]

[c] distribution of C as % of total C from [77]

Nitrogen is present in several forms and is continuously converted by microbial activity and changes in temperature, pH, moisture, and oxygen concentration. 60–80% of the nitrogen in poultry litter is typically in organic form from urea, protein and amino acids. A large percentage of this organic nitrogen (40–90%) can be transformed to ammonia gas or ionised (NH_4^+) depending on environmental conditions. NH_4 can then be converted to nitrate by microorganism. During the poultry production cycle, accumulated manure is mixed with the bedding material which together form the so-called poultry litter [5].

Table 2.5 shows the composition of poultry litter, including proximate analysis, ultimate analyses, ash fusion and ash analysis, as earlier reported in some publications. The table illustrates that the composition can vary significantly depending on the origin of the litter and management practices of the farm. It shows that poultry litter ashes contain high concentrations of potassium (K), calcium (Ca) and phosphorous (P). The presence of K in ashes is known to be dependent on the type of bedding material used. For example, potassium content is very high, around 4–6%, when straw is employed; in contrast, wood shavings reduce the level of K to around 1.5% [78].

Poultry diet contains a range of trace elements, some of which are essential for healthy growth and development, such as zinc, copper, chromium, nickel and manganese, and others which have no known biological functions such as arsenic, cadmium and lead.

The addition of Cr, Ni, Cd, Pb and As to animal feedstuffs is not permitted under UK nor European Union regulations. The maximum permitted levels of heavy metals in poultry feeds are regulated according to the European Parliament and Council Directive 2002/32/EC and the amended 2003/100/EC, as indicated in table 2.6. These trace elements should not be added to compound feeds or blended with other feeding stuffs; therefore, levels in diets are those naturally present in the feeds. Arsenic, Cd and Pb are considered to be undesirable substances in livestock feeds.

The presence of arsenic in poultry litter is of great concern; however, arsenic is essential in the poultry diet which benefits arise from pharmacological effects on the gut microflora. The importance of the gut microflora relates to its effects on host nutrition, health and growth performance by interacting with nutrient utilisation [79].

Table 2.5 Composition of poultry litter

Components	Kirubakaran et al. 2007 [15]	Reardon et al. 2001 [80]	Antares Group Incorporated (1999) [81]	Whitely et al. 2006 [38]
HHV (MJ/kg)	9.56		10.73	12.0
		13.99 (dry)	14.79 (dry)	
		Proximate analysis (wt %)		
Fixed carbon	10.2	14.0	9.8	8.11
Volatile matter	50.3	62.2	47.3	54.72
Moisture	8.2	25.5	27.4	10.59
Ash	28.8	23.9	15.7	26.58
		Ultimate Analysis (wt %)		
C	24.84	35.6	27.22	29.09
H	1.9	4.6	3.72	5.11
O	33.76	29.8	23.10	
N	2.5	5.3	2.69	3.44
S	2.5	0.9	0.33	0.8
Cl	2.5	-	0.71	
Ash	28.8	23.9	15.7	26.58
Moisture	8.2	-	27.4	10.59
		Ash Composition (wt %)		
SiO_2	18.5	22.2	8.1	9.83
Al_2O_3	3.1	2.9	1.9	1.36
TiO_2	-	0.2	0.2	0.06
Fe_2O_3	2.1	1.7	1.16	0.58
CaO	18.5	21.3	17.3	3.72
MgO	4.2	5.0	5.0	1.26
Na_2O	3.6	3.9	9.2	1.61
K_2O	-	-	16.3	3.34
P_2O_5	25.7	20.2	24.4	4.23
SO_3	5.2	7.0	6.7	1.91
BaO	-	-	-	-
SrO	-	-	-	-
CO_2/other	-	0.3	9.4	-
		Ash fusion (°C)		
Initial deformation temperature	1139	-	-	-
Softening temperature	1149	-	-	-
Hemispherical temperature	1161	-	-	-
Fusion temperature	1163	-	-	-

Table 2.6 Maximum content of heavy metals in poultry feed and their presence in manure

Heavy metal	**Maximum content in poultry feed (mg/kg DM)** [3]	**Content in commercial poultry feed (mg/kg DM)** [82]	**Content in poultry manure (mg/kg DM)** [82]	**Estimated content in poultry litter (mg/m^3)** [82]
Zinc	284	106 –169	208 – 473	130
Copper	40	24.8 – 52.4	45.7 – 173	19
Nickel	Not stated. Poultry tolerance: 400 mg Ni/kg DM in sulphate or acetate form	1.1 – 3.9	2.2 – 12.3	2.4
Lead	5.6	<1 – 2.4	<1 – 9.28	2.0
Cadmium	0.56	<0.1 – 0.33	0.2 – 1.16	0.33
Arsenic	2.24	0.14 – 0.31	<0.1 – 41.1	0.3
Chromium	Not stated	<0.2 – 3.44	3.57 – 79.8	1.2
Manganese	284			
Fluorine	284			
Mercury	0.11			

Arsenic was added to poultry diets in the past as a growth stimulant at rates of around 90 mg As/kg DM [83]. Since the benefits were questionable, arsenic is no longer used as a growth promoter in the UK. However, the USA has continued the use of arsenic as Roxarsone (3-nitro-4-hydroxyphenylarsonic acid) because it has shown to increase growth and feed utilisation [84]. This addition causes the presence of 150 mg of As per 4.9 kg of poultry litter generated by a single broiler in a 48-day lifetime in the USA [85]. Recently, the US Food and Drug Administration (FDA) conducted studies of As levels in the liver of chickens; as a result, Alpharma, a subsidiary of Pfizer, Inc., is suspending the sales of Roxarsone by July 2011 [86]. A different situation is found in the UK, arsenic is not included in the poultry diet; therefore, As might be present in an insignificant amount in the poultry litter.

The data reported by Nicholson et al. [82] confirmed that none of the samples of compound or home-mix poultry feeds analysed exceeded the limit, as shown in table 2.6. This led to an arsenic content in manure of <0.1–41.1 mg/kg DM with a mean of 9.01 mg/kg DM, as shown in table 2.6. According to these low values of heavy metals found in poultry litter, the emission of heavy metals are expected to be below the limits established by the Waste Incineration Directive (WID), which should allow emissions of less than 0.5 mg/m^3. Table 2.7 shows WID average limits for heavy metal emissions including the vapour forms of the relevant heavy metal emissions and their compounds. The limits are established as average values over the sample period of a minimum of 30 min and a maximum of 8 h.

Table 2.7 Average limit values for heavy metal emissions according to the Waste Incineration Directive (273 K, 101.3 kPa, 11% O_2, dry)

Cadmium and its compounds, expressed as cadmium (Cd)	total 0.05 mg/m^3
Thallium and its compounds, expressed as thallium (Tl)	
Mercury and its compounds, expressed as mercury (Hg)	0.05 mg/m^3
Antimony and its compounds, expressed as antimony (Sb)	total 0.5 mg/m^3
Arsenic and its compounds, expressed as arsenic (As)	
Lead and its compounds, expressed as lead (Pb)	
Chromium and its compounds, expressed as chromium (Cr)	
Cobalt and its compounds, expressed as cobalt (Co)	
Copper and its compounds, expressed as copper (Cu)	
Manganese and its compounds, expressed as manganese (Mn)	
Nickel and its compounds, expressed as nickel (Ni)	
Vanadium and its compounds, expressed as vanadium (V)	

2.2.6 Gasification of poultry litter

Gasification comprises sequential steps: pre-heating and drying, pyrolysis, and char gasification and oxidation. The pyrolysis process normally takes place at 200–500°C, where the fuel decomposes into three often lumped products: char, volatiles (condensable hydrocarbon or tar) and gases (non-condensable) [87, 88]. Since pyrolysis is the first stage of thermal degradation during gasification, the

mechanisms of biomass pyrolysis have been studied to determine the pyrolysis rate and the amount, properties and composition of the resulting product [87, 89].

For wood pyrolysis, two types of models have been proposed for representing fast heating rates: the one-component mechanism and the multi-component reaction mechanism [87]. Figure 2.3a shows the reaction mechanism of the one-component model, wherein weight losses curves were combined with further measurements of the yields of the three considered products (char, tar and gases). There are fewer models for the multi-component mechanism of wood pyrolysis that include formation rates and yields of reaction products or solid phase and gas phase intermediates. An example of multi-component model is a three-step mechanism suggested for wood pyrolysis, which included secondary reactions for tar decomposition into gas and char; this mechanism is shown in figure 2.3b [90].

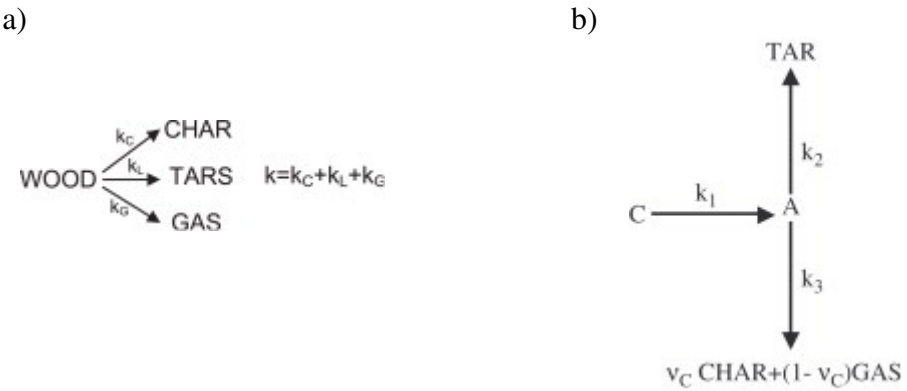

Figure 2.3 Examples of a) one-component mechanism [87], and b) multi-component mechanism [90]

There is a vast literature on wood pyrolysis, both experimental and modelling, for various types of wood, such as oak, hardwood, sweet gum, fir wood, pine and beech [87, 88]. However, work on the pyrolysis of poultry litter showed that the pyrolysis characteristics are very different from wood and other types of biomass [91]. As a result, experimental work on the pyrolysis of poultry litter has started. Fast devolatilisation experiments of poultry litter showed that weight is significantly lost to around 40% of weight loss at 500°C, and about 94% at 1300°C [92].

Table 2.8 shows product yields after the pyrolysis of poultry litter from the limited work found in the literature. The yields of products and pyrolysis rate are known to be affected by the heating rate, temperature and pressure, as well as by biomass characteristics, such as chemical composition, ash content, particle size and

shape, density, and moisture content [87]. Accordingly, the product yields reported vary greatly because of the quite different experimental conditions in each work, type of pyrolyser, and the differences in the poultry litter composition.

Table 2.8 Product yields from pyrolysis of poultry litter

Pyrolysis conditions	Reactor	Sample description	Yields (% wt)		
			Gas	Tar	Char
Fast pyrolysis at 550°C, sample feed rate 200 g/h (gas yield calculated by difference) [91]	Fluidised bed reactor of 5.08 cm pipe, 50.80 cm high and 13.97 cm preheater zone	Chicken litter with hardwood shavings	33.04	26.98	39.98
		Chicken litter with softwood shavings	42.28	20.66	37.14
		Wood chip	17.1	34.62	39.28
Heating rate: 100 K/min, sample of 21-37 mg, He flow rate of 400 ml/min	TGA coupled with FTIR (tar calculated by difference) [93]	Chicken litter with straw as bedding	49.75	23.37	26.88
Fast pyrolysis at 500°C, sample feed rate 200 g/h using N_2 flow rate of 18 L/min [94]	Bubbling fluidised bed reactor (50 mm pipe, 500 mm high and 140 mm preheater zone)	Chicken litter after one flock was raised, with hardwood shavings as bedding	13.6±5.7	45.7±2.9	40.6±6.2
		Chicken litter after two flocks were raised, hardwood shavings	22.3±2.5	36.8±1.2	40.8±1.9
		Turkey litter, pine wood	21.7±1.9	50.2±1.6	27.6±1.7
		Hardwood bedding	24	63.3±11.3	12.7±2
Fast pyrolysis 20°C/ms at 700°C, 1 mg sample [95]	CDS analytical pyroprobe, 1-cm quartz tube	Broiler litter, with softwood such as pine	9	66	25
Pyrolysis at 330°C [77]	Advanced prototype pyrolyzer	Chicken manure	23	50	27

The results from Lima et al. were the most different. In Lima's work [95], char and non-condensable gases were directly quantified; whereas the condensable gases (tar) might have been overestimated since they included non-condensable gases not calibrated, reaction water and pyrolytic oil vapours, that is, tar and hydrocarbon gases greater than C_4H_{10} which were not measured.

i) Char and ash production

Experimental work has shown that char yield is favoured at lower temperatures, and in order to maximise char yields low heating rate and long residence time are necessary, i.e. slow pyrolysis [95]. Table 2.9 shows the composition of poultry litter char. It is observed that carbon content is very high in the char. The ash content in char was between 21.55 and 66.26% for poultry litter [91], that is, higher than in the initial poultry litter. This higher ash content is because almost all the ash that was in the initial poultry litter remains in the char. In contrast, the ash content in char for bedding material was much lower between 1.4 and 27.28% [91, 94].

Table 2.9 Composition of poultry litter char from fast pyrolysis and ash content (% wt, on moisture- and ash-free basis)

Component	Schnitzer et al, 2007 [a]	575°C Agblevor et al, 2010 [b]	575°C Agblevor et al, 2010 [c]	Hardwood bedding, 575°C Agblevor et al, 2010 [94]
Carbon	82.7	41.63	74.20	61.33
Nitrogen	7.0	3.08	5.23	1.62
Oxygen	6.4	48.67	5.89	32.33
Hydrogen	3.3	2.42	3.74	2.70
Sulphur	0.6	1.48	3.56	0.39
Chlorine	-	2.72	7.37	1.22
Ash	48.6	43.79	54.53	27.28

[a] Chicken manure [77]

[b] Poultry litter after one flock was raised, hardwood shavings used as bedding material [94]

[c] Poultry litter after two flocks were raised, hardwood shavings used as bedding material [94]

Char contains several inorganics such as, potassium, phosphorous, silicon, calcium and trace elements, for instance cadmium, copper and zinc. Table 2.10 shows the inorganic speciation of char from two sources. The concentration of inorganics such as calcium, potassium and phosphorous were increased 2.8–7 times compared to the original samples. Inorganic species, such as potassium, are known to catalyse char formation [91]. The presence of these inorganic elements is what makes poultry litter char a potential soil conditioner or fertiliser. Chars from poultry litter contain between 1.68 wt % [94] and 3.7 wt % of phosphorus; in contrast, chars from coal, coconut shell and wood have less than 0.2 wt % [95].

Table 2.10 Inorganic components of char from poultry litter pyrolysis

	Chicken litter		Hardwood bedding
Element	wt % [94] [2]	mg/g char [95]	wt % [94]
P	1.68	36.8 ± 2.7	0.09
K	5.65	42.0 ± 5.3	1.06
Ca	6.55	53.0 ± 4.0	1.56
Mg	1.16	14.2 ± 1.2	0.17
Na	1.48	NA	0.17
Al	0.54	NA	0.03
Fe	0.62	NA	0.12
Mn	0.08	NA	0.02
Cu[1]	0.08	NA	0.01
Zn[1]	0.08	NA	0.01
Cd[1]	4.0	NA	1.0
Ni[1]	45	NA	26
Se[1]	1.2	NA	0.2
Mo[1]	11	NA	NA
S	NA	17.3 ± 2.3	NA

[1] ppm

[2] Poultry litter after one flock was raised, hardwood shavings used as bedding material

NA – not available

ii) Tar production

Table 2.11 shows the elemental analysis of condensable gases after pyrolysis. The carbon and nitrogen content were higher for poultry litter than for bedding material. The higher nitrogen content is attributed to the presence of manure in the litter, which contains mainly protein. Due to the higher content of carbon, the HHV of condensable gases from poultry litter was higher than for the bedding material. The higher HHV for poultry litter was caused by the higher protein content or lipids content. Decarboxylation and nitrogen lost of proteins cause higher hydrocarbon content and for this reason a higher HHV [94].

Table 2.11 Composition of condensable gases from fast pyrolysis of poultry litter at 500°C

Component	Content in % wt				
	Kim et al, 2009 [91]			Agblevor et al, 2010 [94]	
	Chicken litter	Turkey litter	Wood chip	Chicken litter	Hardwood bedding
Carbon	58.07	60.62	45.22	63.24	55.25
Nitrogen	8.30	4.21	<0.5	5.05	<0.5
Oxygen	22.77	28.68	48.73	23.89	37.58
Hydrogen	7.22	7.16	7.7	7.22	6.54
Sulphur	-	-	-	0.46	<0.05
Ash	1.37	0.71	0.1	<0.09	<0.08
Moisture	-	-	-	4.6	5.3
HHV (MJ/kg)	27.49	26.24	18.11	28.25	22.64

iii) Gases production

Attempts to understand the fast devolatilisation of poultry litter have also included the characterisation of volatiles. The main released non-condensable gases are carbon dioxide, carbon monoxide and hydrogen and small amount of low molecular weight hydrocarbons such as CH_4, C_2H_6, and C_3H_8 [95]. The yield of gases increased with increasing pyrolysis temperature. Methane yields were 3–8 times lower than CO and CO_2 yields [92]. CO_2 yields were the highest over the temperature range (400–1300°C) measured and reached an asymptotic value at

around 1000°C [92]. At temperatures higher than 700°C, CO_2 increase is suggested to be caused by decarboxylation of mineral-matter (such as $CaCO_3$); this mineral-matter in poultry litter might be the reason for lower tar yields than from other fuels and be the cause of tar destruction at an early stage [93].

The thermal conversion behaviour of poultry litter has also been analysed using thermogravimetric analysis (TGA). The release of nitrogen species was studied in detail in order to identify NO_x precursors [92, 93]. Experiments on the pyrolysis of poultry litter used TGA and Fourier Transform Infrared (FTIR) spectrometry to quantify evolved gases, mainly N-gases. A high percentage of chicken litter bound nitrogen was converted to NH_3, HCN and HNCO (isocyanic acid), and NH_3 was the main gas released of the three. These nitrogen species are of interest because they are considered NO_x precursors. However, no correlation was found between the amount of nitrogen species released and the nitrogen content in the litter. The gaseous nitrogen species yields were found to decrease with increasing heating rates. In addition, acetic acid (1.3–3.1% wt daf) and methane (1.2–3.4% wt daf) were released from poultry litter pyrolysis [93].

Other work employed a heated wire mesh to study fast pyrolysis and it was coupled with a FTIR spectrophotometer for the simultaneous analysis of gas species. It was found that CO_2 was predominant at low temperatures (< 800°C) and at high temperatures CO increased, which was attributed to tar decomposition. At low temperature (< 600°C), nitrogen was mainly retained in the char, and ammonia was the main N-gas product. At high temperature, more nitrogen was released, high yields of N-tar were produced and HCN was the main N-gas formed [92].

The combination of FTIR spectrometry with the TGA kinetic data generated was recommended for slow pyrolysis applications, like carbonization and biochar production, but also for modelling purposes using appropriate tools [96]. Figure 2.4 shows the DTG (differential thermogravimetric analysis) curve with the compounds analysed by FTIR from chicken manure using a heating rate of 10 °C/min. It was observed the drying step at 105 °C, and the water released subsequently was pyrolytic water. Some ammonia was released already during the drying step and it was assumed as physically absorbed NH_3 contained in the manure. CH_4 was released at around 530°C, probably due to the release of methoxyl groups mainly from lignin decomposition. In chicken manure protein-nitrogen is present mainly due to

undigested food, and it was considered responsible for the continuous release of NH_3 at lower temperatures. Since manure has also a high concentration of nitrogen in the form of urea, this component was assumed responsible for the high amount of HNCO released at around 430 °C, in connection with the release of NH_3 and HCN. The appearance of the second CO_2 peak, as can be observed in figure 2.4, was proposed as originated from the decomposition of HNCO into NH_3 and CO_2. A limitation of these works is that FTIR cannot detect H_2, since FTIR cannot measure diatomic molecules of the same element.

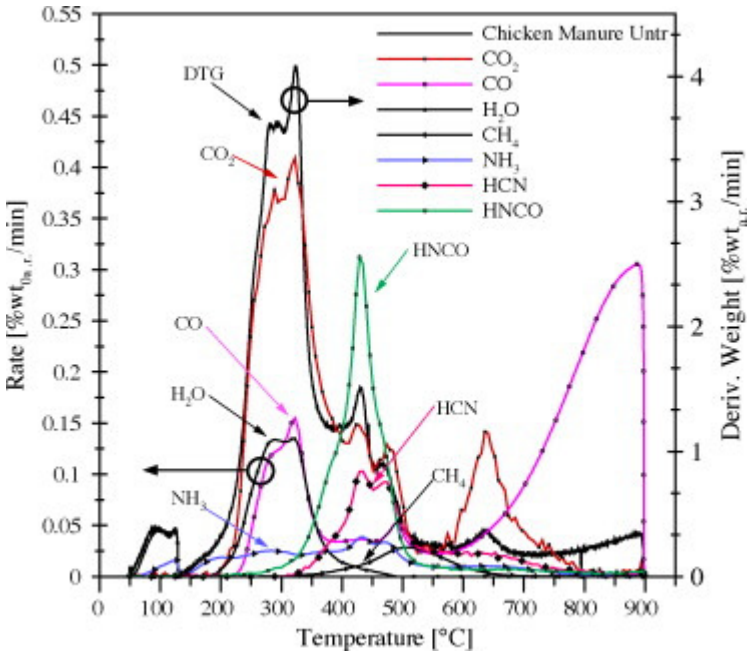

Figure 2.4 DTG curve with the compounds analysed by FTIR from chicken manure; heating rate 10 °C/min and He flow of 100 mL/min. Data are on an "as received" basis [96]

The understanding of the initial devolatilisation is necessary for the modelling of biomass thermal conversion processes. However, the limited data and the variation of feedstock properties make the simulation a challenge.

Since the application of poultry litter into land is restricted by the European Union, treatment of this waste has gained attention. One example is the work carried out at the Department of INETI in Portugal contracted by the University of Limerick from Ireland using a small-scale fluidised bed combustor [78]. The combustor is square (30 cm x 30 cm) with a height of 500 cm. Due to the fluidising velocity employed (0.4–0.5 m/s), a large amount of ashes was elutriated out of the combustor

and then collected in two cyclones. The measurement of the ashes showed that most remained in the bed (only 10–12%) and the ashes collected in the cyclones allowed to trace the partition of potassium, chlorine and heavy metals. Major problems arose from the feeding of poultry litter into the combustor since its moisture as received was 43% which led to unstable combustion. This high moisture content also affected the ignition temperature, which was found to be over 620°C at a moisture content of 20%. To help the combustion of chicken litter, a mixture with peat was also studied. The combustion efficiency was improved by introducing part of the air as secondary to the freeboard with some turbulence. This reduced the CO formed, as well as NO_x and N_2O levels were lower than the permitted emission values. It was reported that the ash fusion was determined as 931.9 K; however, it was mentioned a tendency for ash agglomeration above 1073 K, but in general no agglomeration tendency was observed because the bed was reported as shallow and well fluidised. In September 2010, it was announced the approval of Rose Energy Limited, a consortium of three agri-food companies in Glenavy, Ireland, for converting poultry litter into electricity using a fluidised bed combustion and steam turbine. The combustor will be fed with poultry litter and meat and bone meal (approximately 250,000 tonnes per annum), and power about 25,000 homes [97].

Another example of a small size waste disposal system for the farm industry, is the co-combustion of poultry litter with natural gas in a swirling fluidised bed combustor, where secondary air was injected in a tangential direction [98]. The resulting hot gas was passed through heat exchangers, one after the combustor and the second after the cyclone; the heat recovery efficiencies were 50 and 20%, respectively, which gave a total heat recovery efficiency of around 75%.

Examples of commercial facilities for the conversion of poultry litter to energy were reviewed in [5]. Fibropower opened as a poultry-litter-fired power plant at Eye in Suffolk, UK in November 1993. The plant generates a net output of 12.7 MW to supply a 33 kV power line for distribution of local electricity networks. Fibrowatt constructed two plants; one is a 38.5 MW plant in Thetford, England. The plant consists of a conventional moving grate boiler and steam cycle that employs 420,000 tonnes/yr of poultry litter [99]. The litter is combusted at more than 850°C with a residence time of 2 s. Based on the experience of the management team that built the world's first three poultry litter-fuelled power plants in the United Kingdom

in the 1990s, Fibrowatt LLC was founded in 2000 [100]. In mid 2007, the first poultry litter-fuelled power plant (Fibrominn) in the USA began operation in Benson, Minnesota. The 55-MW power plant uses more than 500,000 tonnes of poultry litter annually mainly supplied by Minnesota turkey growers and produces enough electricity for approximately 40,000 homes. This solution uses the heat from a furnace to produce high pressure and temperature steam in a boiler which is then used in steam turbines to generate electricity. However, this project requires that poultry litter be transported in trucks to the plant storage facility plus truck routing to minimise traffic impact on local communities.

In contrast to combustion applications of small and medium scale, little open literature exits for the gasification of poultry litter. A small scale study was performed at Texas A&M University in a updraft fixed-bed gasifier with a 10 kW capacity [101]. The gasifier worked at atmospheric pressure using air as gasifying agent. The apparatus had an internal diameter of 0.15 m and total height of 0.75 m, with a thick two-stage insulation of castable alumina refractory and insulating blankets. The product gas composition mainly consisted of CO (28%), CO_2 (3.7–11%), H_2 (6.1–7.3%) and CH_4 (0.9–1.4%) with a HHV of 4.28–4.64 MJ/m^3 (dry basis). However, the experiments were performed under a batch-mode operation (approximately for 1 hr) since steady-state was not achieved due to ash accumulation in the bed; tar measurements were not presented. This limited literature supports the need for studies on poultry litter gasification as part of the aims of this work.

2.3 Modelling of fluidised bed gasification

The understanding of the gasification process allows the operation and optimisation of the system. A useful tool to explore its complexity is the mathematical simulation of the gasification process. There is a vast literature on the modelling of coal gasification. However, coal and biomass differ in composition as mentioned in section 2.2.5; the latter contains a larger amount of volatile matter which makes it more reactive. This difference creates the need to develop models for biomass gasification.

There are fewer articles where the modelling of biomass bubbling fluidised bed gasifiers (BFBGs) is presented, as revealed in [102]. The work on the modelling

of biomass gasification has been classified in two approaches: modelling of a single fuel particle through a discrete particle model (DPM) and models for simulating the reactor [103]. The modelling of the fluidised reactor is divided in two types: a) a kinetic-free equilibrium approach and, b) an approach where kinetics and fluidised bed hydrodynamics are included [104].

2.3.1 Equilibrium modelling of biomass gasification

Most kinetic data are obtained under experimental conditions which are usually different from the actual fluidised bed gasifier operation. As a result, equilibrium models have been widely utilised to avoid problems due to the use of kinetic data [105, 106]. When chemical equilibrium is reached, the system is at its most stable composition. This condition is achieved when the system entropy is maximised while the system Gibbs free energy is minimised. The equilibrium approach has been reported when the operating temperatures are above 600°C, where the gases leaving the gasifier were found to approach equilibrium [105]. The equilibrium calculation provides the final composition and temperature of the product gases considered, CO, CO_2, H_2O, H_2 and CH_4. Since only CH_4 is thermodynamically stable under gasification, other hydrocarbons, such as C_2H_2 and C_2H_4, are normally not included despite being produced. Also, tar is not added in equilibrium models even though is normally present in the product gas [105].

A number of theoretical works on biomass gasification have used chemical equilibrium models [33, 105, 107-109]. There are two approaches to model chemical equilibrium: stoichiometric and non-stoichiometric [110]. In the stoichiometric approach, knowledge of the reaction mechanism is required as well as all chemical reactions and species involved. In contrast, the non-stoichiometric approach only requires the elemental composition of the feed.

A stoichiometric equilibrium approach was employed for the modelling of the reduction zone of a downdraft gasification of Douglas fir bark [33]. The set of chemical reactions that participated in the reduction reactions were presented for the mass balance. The model predicted equilibrium composition and equilibrium constants as well as unconverted char, calorific value of gas, gasification efficiency, and outlet gas temperature. A non-stoichiometric equilibrium model was used for the simulation of downdraft gasification of pine bark; the model predicted with accuracy

the influence of air/fuel ratio and moisture content on the composition of main product gases, adiabatic temperature and process efficiency [108].

Equilibrium models include assumptions that are not always valid in practice: a) the gasifier is assumed to operate under perfect mixing conditions and uniform temperature. In practice, different hydrodynamics are present which depend on the gasifier design; b) fast reaction rates and sufficiently long residence time are assumed to reach equilibrium; and c) heat losses are often ignored since the gasifier is considered entirely insulated [111]. Nonetheless, equilibrium models are helpful because they allow the prediction of the thermodynamic limits of the gasification reaction. In particular, non-stoichiometric models are more suitable for biomass where precise chemical compositions are normally unknown and the elemental composition of the feed can be taken from the ultimate analysis. As a result, a non-stoichiometric model was chosen for this work and employed in chapters 3 and 4.

2.3.2 Discrete particle model (DPM)

Fluidised bed behaviour has been studied with the aid of video techniques or probe measurements; however, these techniques can disturb the fluidisation behaviour and consequently the outcome [112]. To overcome these limitations computer models are widely used. Discrete particle model (DPM) comprises the gas-particle and particle-particle interactions, and enables the simultaneous evaluation of the gas and particle velocities and the porosity. During burning processes, solid fuel particles undergo: heating-up, drying, devolatilisation, primary fragmentation and char burn-out. Heating-up is normally neglected since the heating rates are very high in fluidised beds. Drying is assumed to start at the time the fuel particle enters the reactor. Primary fragmentation occurs during the devolatilisation of mainly big particles as a result of thermal shock and pressure increase of released volatile gases inside the particle. After devolatilisation, the remaining char particles start burning and gas-solid reactions occur [103]. The heterogeneous reactions can be described by the unreacted-core or shrinking-core model. The shrinking rate, the reduction of the particle radius with time, of a single particle was determined on the basis of the particle radius [113]:

$$\frac{dr_p}{dt} = -\frac{M_C \Theta}{\varphi \rho_c} K C_{O_2}^{*} \qquad (2.4)$$

where, r_p is the particle radius, M_C is the molar mass of carbon, φ is the carbon weight fraction of char, Θ is the mechanism factor char combustion, ρ_c is the density of char, K is the char combustion rate constant and $C^*_{O_2}$ is the O_2 concentration in the bulk phase. The factor Θ depends on the particle temperature at combustion conditions as expressed in equations 2.5 and 2.6:

$$p = \frac{n_{CO}}{n_{CO_2}} = \frac{2(\Theta - 1)}{2 - \Theta} \tag{2.5}$$

$$p = 2500 \exp\left(-\frac{6240K}{T_p}\right) \tag{2.6}$$

In addition to the burn-out of char particles, the released volatiles (CO, CH_4 and H_2) are oxidised. Even though the DPM offers the flow phenomena governing in fluidised beds, it does not provide an estimation of the performance and size of the gasifier. Therefore, other models were explored during this work, and will be described in the following section.

2.3.3 Models with kinetics and hydrodynamics

An alternative model for the gasification process incorporates kinetics and hydrodynamics. The types of models for fluidised bed reactors are divided by the number of phases assumed inside the reactor: one-, two-, and three-phase models. A one-phase model results in a very simplistic approach, and three-phase models are too complex and without providing any significant improvement over the two-phase model because the model predictions are more sensitive to the reaction kinetics than to hydrodynamics [114]. Therefore, fluidised bed gasifiers have been widely described by the two-phase model [29, 104, 114-118] where the gasifier is split in two regions: the fluidised bed and the freeboard. The fluidised bed is composed of the bubble and emulsion phases. The emulsion phase consists of solid particles and gas, whilst the bubble phase is free of solid particles. Mass and heat transfer occur between bubble and emulsion phases [32].

A model for beech wood gasification including the two-phase model to describe the fluidised bed was developed [104]. The assumptions considered were: pyrolysis as instantaneous in the feeding point since solid mixing proceeded more slowly than pyrolysis; kinetic models to determine yield of products, char and tar; carbon as only constituent of char; isothermal conditions on the bed; counter-current

back-mixing model used to describe char particles mixing in the fluidised bed; and in the freeboard, homogeneous reactions occurred such as tar cracking and water-gas shift reactions as a plug-flow model. It was found that a kinetic model at higher heating rates described better the product gas distribution and its heating value. The model predicted the gas product composition, HHV of the product gas and tar yield at different heights of the reactor, ER and bed temperatures. The predicted parameters were in good agreement with experimental data; however, tar measurements were not performed due to the low flow rate and tar deposition over cold surfaces.

A mathematical model that incorporated bed and freeboard hydrodynamics, and kinetics for drying, devolatilisation and gasification reactions was developed for the simulation of bubbling fluidised bed gasifiers. Experimental data from four fluidised bed gasifiers of different scales, from atmospheric laboratory scale to pressurised commercial scale, were used to test the model for brown coal, peat and sawdust feedstocks. The comparison between experimental and simulation data for freeboard temperature, carbon conversion and concentration of product gases agreed with a deviation of ± 10% [29].

A two-phase model, with a dense phase and a bubble phase, was developed by dividing a downdraft gasifier into several elemental reactors of dz thickness. Along the bed height, the resulting differential equations were solved versus the temperature and the product gas composition, for both dense and bubble phases. However, the freeboard zone was assumed chemically inert [117].

In order to predict the performance of an industrial-scale fluidised bed reactor, three hydrodynamic models were compared: simple two-phase (STP) model, dynamic two-phase structure (DTP) model, and plug-flow (PF) model. In contrast to the STP model, the DTP model allowed that the concentration of particles in the emulsion phase to be less than that at minimum fluidisation and bubbles could contain particles, that is, heterogeneous reactions could take place in both bubbles and emulsion phases. In the PF model, a uniform distribution of solids in the bed was assumed and the flow of gas passing through the bed was assumed as plug flow at high superficial gas velocities and high catalyst recirculation rates. The findings of the comparison were that: the STP model underpredicted the performance of the fluidised bed, the PF model predicted lower conversions at lower gas velocities and

higher conversions at higher gas velocities compared to the two-phase model, whilst the DTP model was able of predicting the performance of fluidised bed reactors over a broad range of superficial velocities [116].

For coal gasification, a model where the bed hydrodynamics followed the two-phase model was proposed. Devolatilisation and drying were considered instantaneous in the feed area. The solid was assumed as isothermal and its consumption uniform through the bed height. Chemical reactions, convection and diffusion were included in the differential equations for both phases. The fluid dynamics were represented by semi-empirical correlations for the estimation of velocities and diameters of the phases. Six experimental results were compared with the model and most of the calculations were between 20% error [119].

In the two-phase theory, the excess gas flow is the one in excess of that required to maintain fluidisation of the bed; in contrast, the assumption of net flow was included in the model to deal with the net gas generated in the emulsion phase through devolatilisation, homogeneous and heterogeneous reactions [114, 120, 121]. The net flow concept is especially relevant when a large amount of volatiles is released as in the case of biomass. In addition, the model also considered the non-isothermal behaviour of the bed resulting from gas-phase reactions in the bubble phase in the energy balance, and the heat transfer mechanisms in the fluidised bed [114]. The non-isothermal assumption showed better agreement in the prediction of the overall carbon conversion than the isothermal model. However, the non-isothermal assumption requires knowledge of the distribution coefficient (ϕ) of combustion products CO/CO_2 from the oxidation of carbon according to the following reaction,

$$C + \phi O_2 \rightarrow 2(1-\phi)CO + (2\phi - 1)CO_2 \qquad \text{R.13}$$

The value of ϕ changes the final gas product composition, as a result, it affects the overall energy balance and the char gasification reaction rates. The ϕ value depends on many factors such as particle temperature, particle size, reactivity, and O_2 concentration. It was suggested that due to the lack of experimental data, ϕ should be given a value between 0.75 and 0.85 [122].

A model that is regarded as complete comprises the simulation of fluidised bed equipment such as boilers, gasifiers, shale retorting reactors, dryers and

pyrolysers using various coal ranks and biomasses [115]. The model assumptions were: steady-state regime; two-phase model for bed; three possible solid phases: fuel, inert (ash) and catalysts; well-mixed model for the composition of solid particulate phases in the bed, however, the temperatures were calculated for each phase along the reactor; particles size distribution modifies due to chemical reactions, attrition between particles and with internal equipment walls; entrainment of fines to the freeboard; freeboard is composed of particles and gases where homogeneous and heterogeneous reactions occur; heat and mass transfers in the axial or vertical direction within each phase are considered as negligible compared to transfers in the horizontal direction between phases. Even though the model is commonly referenced as complete, ash was assumed as an inert solid where gas-solid reactions only involved fuel and bed additives or catalysts. The model involves 54 reactions including fuel and tar reactions with oxygen, hydrogen, steam, and NO; however, it is not shown how species such as C_2H_2, C_2H_6, C_3H_6, C_3H_8 and C_6H_6 appeared in the set of reactions since pyrolysis/devolatilisation reactions did not produce them. On the other hand, ash was assumed as inert because the model was mainly employed for coal gasification. Since poultry litter typically has higher ash content than coal, the ash chemistry needs to be incorporated in the model to account for its effects. Therefore, inclusion of the reactions involving ash constituents is of importance to guarantee the proper performance of the gasifier.

2.3.3.1 Bed hydrodynamics for biomass fluidisation

A substantial review of hydrodynamics and mixing of biomass particles in fluidised beds can be found in [123], only main findings will be discussed in this section. Extensive work on fluidisation of dry spherical particles of narrow size distributions is documented; however, biomass particles consist of non-standard shapes, such as broad size distribution and variety of shapes. As a result, studies of biomass fluidisation have been performed. Experimental work to study the fluidisation behaviour of fluidised beds normally consists of measuring pressure drop across the bed over a range of fluidising agent flows [124].

Since biomass particles are more difficult to fluidise owing to their shapes, sizes and densities, conventional correlations for minimum fluidisation velocity (u_{mf}) have been proven as unable to give reliable predictions. From experimental work, the

dependence of the fluidised bed performance on the hydrodynamics and preservation of bed fluidisation state were highlighted. However, the bed studied consisted of silica sand without biomass; accordingly, the predicted pressure drops and u_{mf} values agreed with experiments. Three sand particle diameter ranges were employed as well as various sand quantities, for the size range 425–500 μm, u_{mf} increased over sand quantity; however, it was highlighted that u_{mf} existing correlations do not include sand quantity [124]. Other study using mixtures of biomass (rice husks) and sand showed that the minimum fluidisation velocities increased with increasing biomass weight fraction and also with increasing sand density and particle size. Therefore, a modified correlation was introduced which included an average effective mixture density and an effective particle diameter [125]:

$$u_{mf,m} = \frac{d_{peff}^2 (\rho_{eff} - \rho_g) g}{1650 \mu_g} \tag{2.7}$$

$$\rho_{eff} = k \frac{w_1 \rho_1 + w_2 \rho_2}{w_1 + w_2} \tag{2.8}$$

$$d_{peff}^2 = k \left\{ d_{p1} \left[\left(\frac{\rho_1}{\rho_2} \right) \left(\frac{d_{p2}}{d_{p1}} \right) \right]^{w_2 / w_1} \right\}^2 \tag{2.9}$$

$$k = 20 d_{p1} + 0.36 \tag{2.10}$$

Another parameter that requires quantification is the so-called terminal velocity. The terminal velocity is reached when the drag force of the fluid is higher than the weight of particles, that is, the gas velocity that pushes the particles out of the reactor [119]. Therefore, knowledge of this velocity is important to avoid the entrainment of particles of determined diameter. From coffee husks with three mean diameters (1.6, 2.6 and 4.0 mm) employed in a small cold-model column, physical properties were investigated.

A correlation for minimum fluidisation velocity and terminal velocity u_t were presented [126]:

$$u_{mf} = 0.19 e^{0.305 d_p} \tag{2.11}$$

$$u_t = 1.55 e^{0.081 d_p} \tag{2.12}$$

Once fluidisation starts, bed expansion occurs; then, the fraction of the total volume which is occupied by gas is named the bed voidage, ε [103]. The bed voidage at minimum fluidisation, ε_{mf}, is known to increase with temperature (up to 8% at up to 500°C) for fine particles, though unaltered for coarse particles, and slightly increase (1–4%) with an augment in pressure [32]. An empirical correlation for ε_{mf} was proposed that neglects wall effects and particle diameter:

$$\varepsilon_{mf} = \left(\frac{1}{14\phi_S} \right)^{1/3} \tag{2.13}$$

where ϕ_S is the sphericity term which is defined as the surface area of a sphere having the same volume as the particle divided by the surface area of the particle [103].

On top of the fluidised bed there is a zone called freeboard. The freeboard functions as a space for disengaging of particles carried by the gas flow and for further homogeneous reactions. Hence, the cross-sectional area of the freeboard is normally larger than the one in the bed area. The height of the freeboard helps to decrease the ascendant flow of particles or entrainment; however, there is a certain height where the entrainment remains practically constant no matter how much the height is increased; this is called the transport disengaging height (TDH). This designing parameter for fluidised beds can be calculated as followed:

$$TDH = \frac{1}{a} \ln \left(\frac{F_0 - F_\infty}{0.01 F_\infty} \right) \tag{2.14}$$

where F_0 is the total entrainment rate at the bed surface, F_∞ is the total elutriation rate of the particles, and a is the constant in the entrainment equation that varies between 3.5 to 6.4 m^{-1} [103].

2.3.3.2 Kinetics of thermal conversion of poultry litter

The investigation of the thermal conversion behaviour of biomass includes the study of the mechanism and kinetics by which biomass decomposes. The kinetics parameters are normally determined by the curves obtained from experimental work from thermogravimetric analysis (TGA). With the TGA, the weight loss at different

temperatures is used to study the characteristics of devolatilisation and further conversion of biomass, and afterwards to elucidate the kinetics of reaction.

TGA results of wood chips and chicken litter (broiler and flock) were compared since chicken litter contains wood chips as bedding material. Wood chips showed two weight loss regimes, the first one attributed to the decomposition of cellulose, hemicellulose and lignin and the last one to further devolatilisation of residual charcoal. Whereas chicken litter presented three different weight loss regimes, the second loss regime was attributed to manure and lignin and the third one to further charcoal devolatilisation [127].

The kinetics parameters of pyrolysis of chicken litter were determined using the differential method from data obtained using DTG. The rate of reaction (-*r*) was expressed as:

$$-r = \frac{dX}{dt} = k \cdot f(X) \tag{2.15}$$

The reaction rate constant, *k*, follows the Arrhenius equation:

$$k = A\exp\left(-\frac{E}{RT}\right) \tag{2.16}$$

The combination of equations 2.15 and 2.16, and taking the natural logarithm yields the following equation:

$$\ln\left(\frac{dX}{dt}\right) = \ln A + n\ln(1-X) - \frac{E}{RT} \tag{2.17}$$

where *E* is the apparent energy of activation, *A* is the pre-exponential factor, *T* is the pyrolysis temperature, X is the conversion of sample, *t* is the pyrolysis time, *R* is the gas constant and *n* is the reaction order [127]. *E* and *A* were determined by linear regression from the lineal relationship between ln(d*X*/d*t*) and 1/*T* with slope −*E*/*R*, since TGA was run at different heating rates [103, 127, 128].

Another approach to elucidate the gasification kinetics of poultry litter employed static air and static nitrogen separately at a heating rate of 5°C/min [15]. From the TGA data, the rate of reaction was determined as the average of weight loss (d*X*/d*t*) between (*t* –1) and (*t*), and (*t*) and (*t* + 1). Assuming a first order reaction, *f*(*X*) was defined as the weight of biomass yet to be degraded (w) and calculated for each temperature. Using equation (2.15), *k* was calculated for each temperature. With

the natural logarithm of equation (2.16), a plot for ln*k* versus 1/*T* showed different zones of conversion; *E* and *A* were determined for each zone.

Table 2.12 summarises the results of kinetics parameters for poultry litter when a first order reaction was assumed.

Table 2.12 Kinetic parameters for chicken litter considering a first order reaction

TGA	Stages of conversion	E (kJ/mol)	A (s^{-1})	Reference
Pyrolysis carrier gas: N_2 at 20 ml/min Heating rates: 5, 10 and 20°C/min	60% conversion 80% conversion	99 464	$7.66x10^3$ $1.01x10^5$	[127]
Static N_2 Heating rate: 5°C/min	moisture removal: 30-120°C zone I: 200-310°C zone II: 310-440°C zone III: 440-600°C	36.54 87.19 52.46 58.76	1740 $9.82x10^5$ 20.22 29.35	[15]
Static air Heating rate: 5°C/min	moisture removal: 30-120°C zone I: 200-310°C zone II: 310-440°C zone III: 440-600°C	32 88.62 63.8 62.12	245.32 $1.34x10^6$ 193.67 55.09	[15]
Pyrolysis N_2 at 50 ml/min Heating rate: 20°C/min	20-160°C II (160-290°C) III. 290-390°C IV 390-500°C	100.6 52.11 193.9 242.3	$2.77x10^{13}$ 808.81 $4.18x10^{15}$ $4.81x10^{17}$	[128]
Combustion Air at 50 ml/min Heating rate: 20°C/min	I. moisture removal: 20-150°C II. Devolatilisation (150-350°C) III. Char precombustion (350-500°C) IV. Char combustion (500-650°C)	61.72 71.43 148.5 157.6	$4.41x10^6$ $2.64x10^4$ $4.49x10^8$ $1.69x10^9$	[38]

The activation energies shown in table 2.12 vary significantly as a result of different heating conditions, experimental devices such as classical thermogravimetry, sample characteristics, and mathematical treatment of the data [129]. These variations make difficult to identify proper kinetics of primary poultry litter degradation through fast pyrolysis for this work.

A kinetic model based on parallel first-order reactions with a Gaussian distribution of activation energies was proposed for devolatilisation of poultry litter [93]. In order to fit the experimental data, the pre-exponential factor was fixed to $2.2x10^{13}s^{-1}$. Since each volatile species evolved as one or more peaks, single or multiple precursors were assumed, respectively. Kinetic parameters were given for CO, CO_2, H_2O, CH_4, C_2H_4, CH_3COCH_3, CH_3OH, HCN, NH_3, CH_2O, HCOOH, CH_3COOH, C_2H_4O, HNCO and tar, with activation energies ranging from 124.7 to 323.3 kJ/mol.

2.3.3.3 Tar reaction kinetics and models

Due to the complexity of tar, the decomposition reactions have been studied using tar model compounds including phenol, toluene, naphthalene, etc. The catalytic activity of olivine via steam reforming was investigated using naphthalene as tar model. Naphthalene conversion was higher than 80 % when it was employed olivine pre-treated (10 h of pre-treatment with air at 900°C). The Arrhenius' law was employed to estimate the apparent activation energy over pre-treated olivine as 187 kJ/mol and frequency factor of $2.06x10^{9}$ m^3/kg h [67]. Toluene was also used as model component of tar in a laboratory scale fixed bed reactor for toluene steam-reforming. The highest conversion of toluene was achieved at temperatures above 650°C. The toluene conversion using Ni/olivine catalyst at 560°C was the same as with olivine at 850°C. The first order kinetic parameters for steam reforming of toluene on Ni/olivine were activation energy (*E*) of 196 kJ/mol and frequency factor (*A*) of $3.14x10^{13}m^3/(kg_{cat}h)$ [75]. Benzene was used as model component for kinetic studies at 750-925°C and ambient pressure in a fixed bed reactor with a mixture of simulated gasification gases using calcined dolomite as catalyst. The main assumed reactions were benzene reacting with water to produce CO, H_2 and CO_2 and benzene reacting with H_2 to form light hydrocarbons [130].

Experimental studies of fluidised bed gasification of pine sawdust using calcined dolomite as catalyst, and air and steam as gasifying agents were presented. After the gasifier, a fixed bed reactor with nickel based catalyst (Z409R) was incorporated for catalytic tar reduction. The temperature of the fixed bed reactor was varied by external heating and an optimal temperature of 750°C was found to deliver the maximum H_2/CO ratio. Tar was reduced in the presence of the nickel based

catalyst and also by increasing the temperature. All tar species were treated as one lump in order to avoid the complexity of the tar composition. Assuming a first order kinetic model, *E* and *A* were determined as 51 kJ/mol and 14476 $m^3(T_{b,wet})$/kg h, respectively [131].

Since most works have grouped all tar compounds as a single unit, an improved kinetic model was developed to treat tar as composed of six lumps. Each lump consisted of tar species with similar chemical structure. The six lumps considered were: i) benzene, ii) one-ring compounds (except benzene), iii) naphthalene, iv) two-ring compounds (except naphthalene), v) three- and four-ring compounds, and vi) phenolic compounds [132]. Based on the experimental work on the evolution of tar composition, a set of six kinetic equations with 11 different kinetic constants were presented. Reactivity rates were evaluated and it was found that phenolic compounds (296 mg destroyed/kg of catalyst/h) were the most reactive, and naphthalene (33.1 mg destroyed/kg of catalyst/h) was the hardest compound to destroy. The kinetic equations fitted well with the experimental results. On the other hand, the experimental data were obtained using the solid-phase adsorption method for tar sampling. However, heavy tars (compounds with high molecular weight) are not trapped by this sampling method; therefore, the developed kinetic model has the same limitations. This shows that care should be taken when using tar models which employed experimental data with selected tar compounds. Especially when heavy tar compounds are neglected since these compounds might condense even at high temperatures and low concentrations, as indicated in table 2.2.

2.4 Integrated gasification for energy production

Since the main product of biomass gasification is a valuable mixture of combustible gases, gasification is frequently integrated to gas turbines, steam turbines or fuel cells. To improve the performance of gas turbine (GT) cycles, the GT exhaust heat is recovered and reused for preheating air and/or process streams. The technologies for energy recuperation are categorised as: heat recuperation, steam recuperation and thermochemical recuperation [133]. The emerging combination of technologies for the generation of electricity has resulted in the development of

different configurations for gasification, power systems and energy recuperation technologies. Among the existing options for producing power using solid fuels are:

- Direct solid-fuel fired gas turbine
- Pressurised fluidised-bed combustion (PFBC)
- Integrated gasification combined cycle (IGCC)
- Externally fired gas turbines (EFGT)

Direct solid-fuel fired gas turbine consists of directly firing a gas turbine with biomass as a more cost effective option by avoiding the use of a heat exchanger or biomass gasification before combustion. Nonetheless, issues from biomass-fired gas turbine combustors are the formation of deposits on the turbine nozzles and rotors, erosion by solid particles and corrosion by molten ash. An attempt to reduce the formation of deposits consisted of a small four-stage gas turbine directly fired with woodchips using a downdraft gravel-bed combustor to promote intense combustion in a thin zone and control particulate growth by using high excess air. The average turbine blockage was 0.19 % per hour after 150 h of testing [134].

PFBC operates at elevated pressures and produces hot high-pressure gases used in a gas turbine. The heat in the fluidised bed is used to generate steam to drive a steam turbine which creates a highly efficient combined cycle system. The combination of fluidised bed advantages with advanced combined cycles shows potential for burning a wide range of fuels (even with high ash and sulphur contents). This produces electricity at higher thermal efficiencies and lower emission rates than when using conventional systems. Co-firing of coal with biomass has shown that the overall power plant efficiency declines as biomass fraction increases, and power plant equipment modifications may be not necessary if biomass percentage is kept below 10% [135].

The IGCC technology comprises four operating components: an air separation unit (ASU), a gasification unit, a gas clean-up system and a gas turbine combined cycle. The ASU is used to generate pressurised high purity oxygen which is sent to the gasifier. The gasification product gases are employed to produce electricity in a combined cycle (CC). The combined cycle consists of a gas turbine, a heat recovery steam generator (HRSG) and a steam turbine [136].

In contrast, an EFGT differs from a conventional IGCC by having a heat exchanger instead of a combustion unit. Thus, an EFGT employs an external combustion unit where biomass is burnt. The hot product gases are used to preheat the exhaust compressor air to rise the turbine inlet temperature, and then the turbine exhaust air is sent to the combustor. The advantages of the EFGT include that different solid fuels can be employed with little pretreatment and a gasifier is not required since the solid is directly burnt [137]. Nevertheless, in EFGT systems the critical element is the heat exchanger which has to stand high temperatures and the aggressive nature of the combustion gases, such as oxidation, corrosion and erosion on the surfaces.

Due to the advantages of IGCC systems and the focus on gasification, more emphasis will be given to IGCC applications. An IGCC plant in Värnamo, Sweden was built to demonstrate this technology using wood chips as fuel and a pressurised circulating fluidised bed gasifier (CFBG). Air was employed as gasifying agent and extracted from the gas turbine compressor by around 10%, but before entering the gasifier, the air was further compressed. The plant operated continuously at 20 bar and 950−1000°C for almost 1000 h. The hot product gas was cooled to a temperature of 350–400°C before entering a ceramic filter for particle removal. GT exhaust gases were used in a HRSG to generate steam and then injected into a steam turbine. The product gases were of a low calorific value of 5 MJ/Nm^3 and the plant generated 4 MW of electricity and 9 MW of heat for district heating [138].

In order to increase the IGCC efficiency, the injection of nitrogen produced from an ASU into the gas turbine combustor and the extraction of air from the gas turbine compressor to feed the ASU was proposed [139]. The purpose of extracting air from the compressor was to reduce the power consumption of the ASU. Then, nitrogen injection alone with an elevated pressure-ASU design showed to reduce NO_x emissions, produce higher efficiency and improve the system performance as the nitrogen injection was increased.

The use of biomass as fuel has originated the concept of biomass integrated gasification/gas turbine (BIG/GT). The GT exhaust gas is used as a heat source for steam generation for the biomass gasification process. A proposed energy recuperation integrated with a BIG/GT system, called energy-recuperative BIG/GT, was compared with a conventional BIG/GT [133]. Since the GT exhaust temperature

was higher than the gasification temperature, the GT exhaust gas was employed to heat the gasifier with internal indirect heating coils. The compressed air was preheated before entering the GT combustor in the HSRG. In addition, steam was generated in the HSRG to achieve a final GT exhaust temperature of 423 K. The energy recuperative BIG/GT system showed better thermal efficiency than the conventional system.

One of the main problems with the implementation of BIGGT/CC relates to the use of gas turbines with low LHV fuels. Since gas turbines are originally designed for natural gas, a larger biomass flow is necessary to achieve an equivalent heat input. To overcome the problems associated to using low calorific value fuels in gas turbine systems, some strategies have been proposed such as de-rating by lowering the temperature, bleeding air from the compressor, and redesigning the GT. De-rating includes lowering the burning temperature to keep the pressure ratio to acceptable levels; however, the overall cycle efficiency will decrease. Bleeding air from the compressor reduces the mass flow input to the expander; on the other hand, the continuous extraction of air might require some retrofit. As mentioned before, nitrogen from an ASU can be used to compensate the mass flow. Bleeding air is more advantageous when the BIGCC system uses a pressurised gasifier and the pressurised bled air is sent to the gasifier. Redesign of the GT includes modifying the geometry of the expander either by increasing the blade height or the nozzle discharge angle. Even though the latter strategy guarantees the operation of the GT under design conditions, it is the most expensive approach. It was shown that redesign of GT expander gave the best overall efficiency and power output followed by the bleeding air strategy [22].

Medium to large scale BIGCC systems as well as more complex systems that use a HRSG for generating high and low pressure steam and an air separation unit (ASU) for oxygen-blown gasification have been suggested as capable of achieving up to 40 % of net efficiency [52]. However, these systems require a large amount of biomass which involves the transportation of fuel to centralised plants. In contrast, the installation of compact on-site systems with the potential of achieving competitive efficiencies through the use of an energy integration system may be a more attractive option, as proposed in this work.

2.5 Software for biomass gasification

Process simulators have been used for the evaluation of biomass gasification and one widely employed is ASPEN Plus, which contains extensive thermal and property databases. Equilibrium calculations based on minimisation of free energy have been developed in ASPEN Plus. A proposed equilibrium model consisted of uncoupling the pyrolysis, combustion, Boudouard reaction and gasification processes to evaluate the effect of operating parameters in the gasification of wood. From a sensitivity analysis, it was found a maximum air temperature above which preheating is no longer beneficial, an optimum oxygen factor and a slight positive effect on gasification efficiency from varying operating pressure [140].

ASPEN Plus was also employed for the simulation of a fluidised bed gasifier and validated with experimental data of pine sawdust steam gasification. ASPEN plus units were used for the simulation of devolatilisation and volatile reactions; char gasification was modelled in a CSTR unit including reaction kinetics with the use of FORTRAN codes. For the hydrodynamic parameters, two reactors were used to simulate the two regions, bed and freeboard, and each region was simulated by one CSTR [141]. However, the model overestimated the H_2 production and underestimated the CO_2 generation due to the selection of ϕ and β (coefficient of the steam-gasification reaction) as 0.9 and 1.4, respectively.

The simulation of a circulating fluidised bed (CFB) combustor was performed using ASPEN Plus; the reaction steps included: decomposition (with a yield reactor) and volatile combustion (using a stoichiometric reactor), char combustion (use of kinetic model), NO_x formation (using an equilibrium reactor) and SO_2 absorption by limestone [142].

A CFB gasifier was simulated using also Aspen Plus. The gasifier was divided in eight separate steps: decomposition, carbon conversion by removing a specified fraction of carbon, gasification reactions using a Gibbs reactor, ash separation, gasification with temperature approach to restrict equilibrium, mixing of un-reacted carbon with product gases, solid separation in a cyclone, and recycle of solids to gasifier. The effect of varying the equivalence ratio, temperature, level of air preheating, biomass moisture and steam injection on the product gas composition, the gas heating value and the cold gas efficiency were studied [143]. The results

showed that methane was overpredicted when compared to experimental data, and heavier hydrocarbons were not included.

To improve the prediction capability, a semi-empirical model was proposed using Aspen Plus. The amount of carbon extracted to simulate incomplete carbon conversion was calculated from empirical correlations. According to proximate analysis, the volatiles were separated and introduced to a Rstoic block (Stoichiometric reactor) to calculate the formation of CH_4, C_2H_2, C_2H_4, C_2H_6 and NH_3 based on experimental data from fluidised-bed air gasification of pine sawdust. The remaining carbon, air, steam and unreacted volatiles were introduced to a gasification unit to generate gasification products according to thermodynamic equilibrium using an RGibbs block [144]. The model was tested with experimental data from six feedstocks and showed good agreement with pine, eucalyptus wood chips and forest residues, but was not suitable for pine bark and wheat straw due to the difference in reactivity with pine sawdust. Nonetheless, the model assumed ash as inert and ignored the behaviour of ash-forming species during gasification.

There are others commercial software found in the literature. One example is the comprehensive simulation program for fluidised bed equipment (CSFB), which is a commercial simulator software for pilot and industrial-size unit operations. The program can simulate boilers, gasifiers, dryers and pyrolysers with various coal ranks and biomasses [115]. The CSFB software has been used to evaluate the design of a bubbling bed gasifier to give an optimal performance by analysing the main operational parameters such as freeboard diameter and insulation, air factor, bed dynamic height and biomass feeding point [145]. An equilibrium model was developed in a commercial, equation-oriented simulation tool IPSEpro^{TM} for the simulation of steam gasification of beech chips with a combined heat and power station [58]. The commercial Computational Fluid Dynamic (CFD) software Fluent was employed for modelling coal gasification in a two stage entrained flow gasifier, and the particle flow was modelled by a DPM model [146]. In conclusion, the use of commercial software has shown to be a practical and useful tool that allows a comprehensive evaluation of gasification systems.

2.6 Summary of survey

The transformation of biomass waste by thermal conversion processes represents a potential solution for waste disposal. In particular, gasification offers a viable option for small scale plants. Among the types of gasifiers, fluidised bed reactors provide good temperature distribution and allow a wider range of fuels to be used.

The operating parameters, such as temperature, pressure, nature of the gasifying agent and its flow rate, and use of catalysts, have great influence on the gas yield, composition and calorific value of gases. The selection of the optimal operating parameters require careful analysis, e.g. high temperatures favour higher HHV and tar reduction but also increase the risk of bed agglomeration. Among the greatest challenges of the gasification technology is the reduction of tars. Tar has a complex composition; furthermore, sampling and measuring tars are difficult tasks that affect the accurate modelling of tars. For simplification, tar model compounds have been studied to understand tar cracking mechanisms. Another approach is the consideration of all tar compounds as a single lump to obtain apparent kinetic parameters. Whilst for ash, its constituents often are considered as inert in gasification models.

Large-scale systems are found on the literature, such as IGCC systems, for the generation of energy from biomass. However, these systems require an ASU, gas turbines, HRSG and steam turbines to deliver high overall plant efficiencies. In addition, poultry litter has been employed for energy production; however, the installed plants require transportation of the fuel to centralised facilities. Therefore, the present work proposes the use of a small-scale gasification process installed near a farm.

The modelling of biomass has included equilibrium approaches, and kinetics and hydrodynamic models. The two-phase model has been widely employed to simulate fluidised beds. Studies on biomass hydrodynamics have showed that conventional correlations for the minimum fluidisation velocity do not predict well biomass fluidisation since biomass is not uniform in particle shape and size. As a result, the need for biomass hydrodynamics becomes more evident. In the following sections, this work deals with an equilibrium model to reveal the thermodynamic limits of the gasification reactions of poultry litter.

Chapter 3

Model for gasification of poultry litter

The understanding of gasification allows for the optimisation of the process and its optimal operation. This chapter, therefore, describes the development of a model for the simulation of the gasification process integrated with a gas turbine. "Conventional" gasification systems are normally large scale centralised facilities; these systems use an atmospheric gasifier that requires cooling of the product gases before compression which results in significant wastage of energy. This work, however, considers a small scale on-site pressurised gasification unit to avoid transportation of litter to centralised plants and to maintain all process stages hot. This chapter evaluates system configurations after adding an energy integration system. The comparison of the different configurations provides an insight into the effects of the energy integration and the selection of the most beneficial configuration. Finally, a description of six case studies is given in order to evaluate the performance of the proposed system.

3.1 Equilibrium approach: model description

Gasification is a process wherein biomass is converted into a combustible gas mixture by partial oxidation. Thus, the amount of oxygen employed is lower than the stoichiometric amount required for complete combustion. The gasification process was modelled based on the chemical equilibrium between the reactants (poultry litter and air) and the specified product gas constituents generated after gasification. The composition of the product gases was estimated through the minimisation of the

Gibbs free energy (G). At constant temperature and pressure, the system was considered at equilibrium when [110],

$$dG_{T,P} = 0 \qquad (3.1)$$

The equilibrium composition can be determined using numerical methods. This computation requires to find the set of number of moles of species *i*, n_i, which minimise the value of G. There are two approaches which can be employed: a) stoichiometric and b) non-stoichiometric. The stoichiometric approach uses a set of stoichiometrically independent reactions which includes a clearly defined reaction mechanism that incorporates all chemical reactions and species involved. These reactions are generally selected arbitrarily from a set of possible reactions, which can lead to erroneous findings. In contrast, the non-stoichiometric approach uses direct minimisation of the Gibbs free energy for a given set of species [147, 148]. Only the elemental composition of the feed is specified, which can be readily obtained from ultimate analysis data. In this work, the non-stoichiometric approach was chosen because: there is no need for selecting a possible set of reactions and it is not necessary an estimation of the initial equilibrium composition.

The material balance is given by

$$\sum_i \left(n_i a_{ik}\right) - A_k = 0 \qquad k = 1, 2, \ldots, \mathrm{w} \qquad (3.2)$$

where A_k is the total number of gram atoms of the *k*th element present in the system, as determined by its initial constitution; a_{ik} is the number of atoms of the *k*th element present in each molecule of chemical species [149].

The equilibrium equation is

$$\Delta G^o_{fi} + RT \ln \frac{y_i \hat{\phi}_i P}{P^o} + \sum_k \lambda_k a_{ik} = 0 \qquad i = 1, 2, \ldots, \mathrm{N} \qquad (3.3)$$

where ΔG^o_{fi} is the standard Gibbs free energy of formation of species *i*, y_i is the mole fraction of species *i*, and $\hat{\phi}_i$ is the fugacity coefficient of species *i* in the gas mixture.

The unknowns in equations 3.2 and 3.3 are the n_i ($y_i = n_i/\sum_i n_i$) and the λ_k (Lagrange multiplier), respectively. The set of N equilibrium equations, one for each chemical species, and w material-balance equations, one for each element, are solved for all unknowns.

3.1.1 Methods and assumptions

A model that involves the evaluation of the gasification of poultry litter and the integration with a power generation engine was developed. The simultaneous solution of mass and energy balances was performed by modelling in the advanced system for process engineering (ASPEN Plus®) software. ASPEN Plus allows the use of processes involving solids and is equipped with physical, chemical and thermodynamic databases. The calculations provided the final composition and temperature of the considered product gases.

The following assumptions were considered for the modelling of the gasification process integrated with a gas turbine:

- The process is at steady state
- The fluidised bed reactor is treated as well-mixed
- Isothermal gasifier with no distinction between the dense and dilute phases present in the reactor
- The gasifier is well insulated with no heat losses
- The gasification reaction rates are fast enough to reach the equilibrium state
- Residence time is long enough to reach the equilibrium state
- Perfect mixing and uniform temperature are assumed for the gasifier
- The compressor and expander in the gas turbine are assumed as isentropic
- Combustion in the combustor gas turbine chamber is complete and adiabatic
- Tars are not modelled
- The gasification of poultry litter was performed with the aim of achieving 200 kW of net gas turbine power output

The 200 kW of net power output was targeted based on a farm that produces an average of 1,029,187 birds/year, and generates 1839 ton/year of litter. For poultry litter with a LHV of 11.4 MJ/kg and assuming a process efficiency of 30%, 5.04 ton/day will be required to be fed into the system.

3.1.2 Process flowsheet and units description

With the model assumptions defined, the process units were selected which represent each stage within the gasifier and gas turbine.

The process diagram of the gasification of poultry litter for energy generation is illustrated in figure 3.1. This figure shows that air (stream AIR1) is drawn into the compressor to reach the desired operating pressure. A fraction of the compressed air enters the gasifier (stream AIR4) and the rest is taken into the combustor unit (stream AIR3). The air stream for combustion (stream AIR3) is preheated with the exhaust gases (stream GT-EX1) from the gas turbine. Whereas poultry litter (stream POULTRY) is introduced into the gasifier and its contact with air results in gasification and combustion reactions. The resultant fuel gas leaves the gasifier as stream GAS1 and bottom ash as stream ASH1. The fuel gas (stream GAS2) is sent to the hot gas filter where carried dust is removed (stream ASH2). The clean fuel gas (stream GAS3) is divided, a small fraction is passed to the DE-NOX reactor (stream GAS5) and the rest (stream GAS4) passes to the combustor unit where the fuel gas is burned in the presence of excess hot air (AIR5). The resultant hot gases (stream COM-EX) enter the expander of the gas turbine where their sensible heat is converted into rotational energy. The exhaust gases (stream GT-EX2) are passed to a DE-NOX reactor to destroy NOx compounds. The process is composed of the following units:

Gasifier

To model the gasification process, it was split into three component sub-processes analogous to the flash pyrolysis, gasification and ash separation phases. This is achieved in ASPEN Plus using three units: DECOMP, GASIFIER, and S-1 respectively, as shown in figure 3.1.

The DECOMP unit is a reactor that simulates the flash pyrolysis of poultry litter by breaking it into its constituent elements (carbon, oxygen, nitrogen, hydrogen, sulphur, chlorine), ash and energy according to its ultimate analysis. This type of yield reactor is modelled using a RYIELD block, which only requires the yield distribution of elemental constituents.

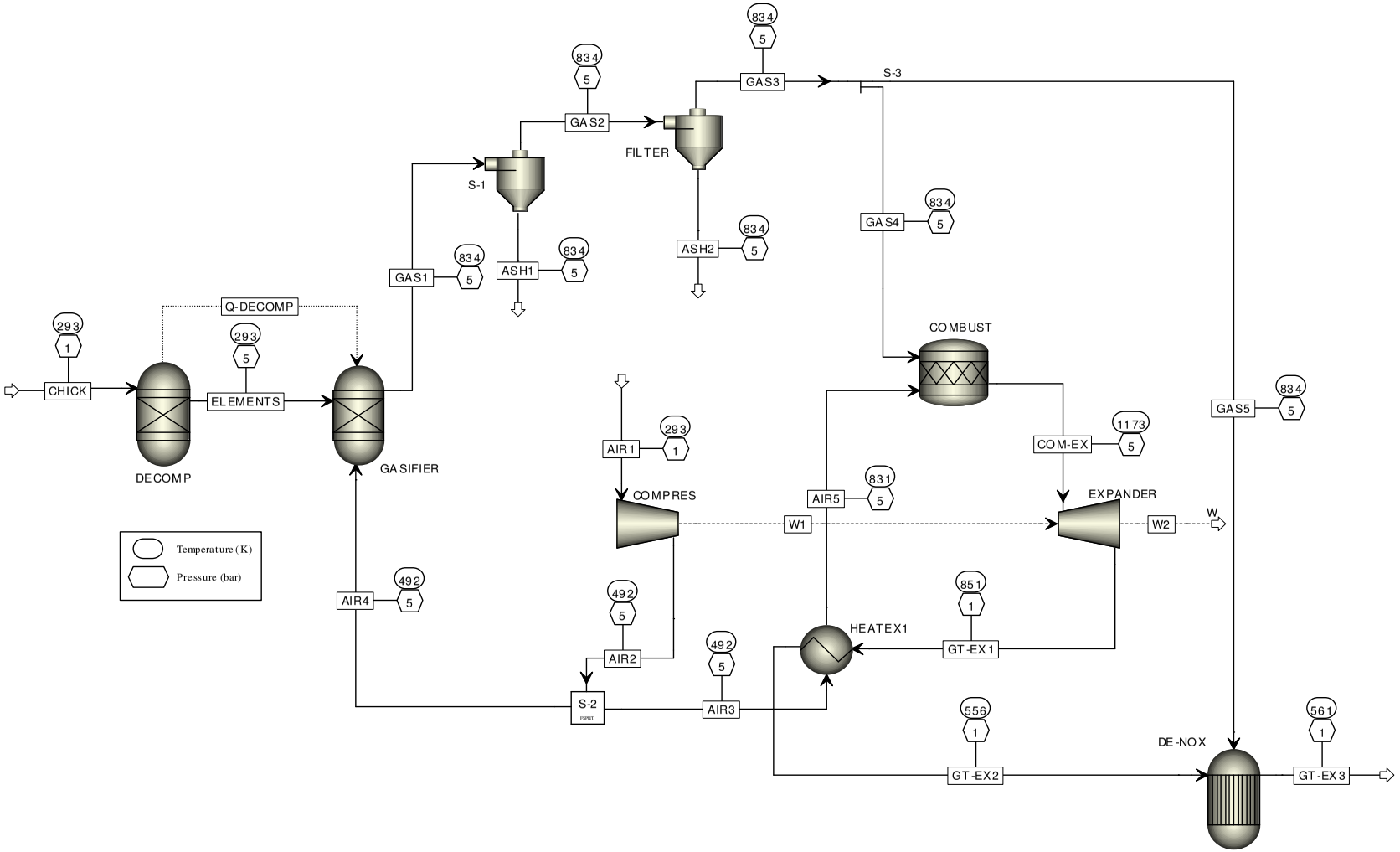

Figure 3.1 Diagram of the gasification integrated gas turbine system

The GASIFIER unit is a reactor that simulates the gasification phase based on the chemical equilibrium between the reactants and the specified product gas constituents. The composition of the product gases is estimated through the minimisation of the Gibbs free energy using a RGIBBS block. The specified product gases from the gasification reactions are CO, CO_2, H_2O, H_2, O_2, N_2, C, CH_4, H_2S, COS, SO_2, HCl, NH_3, NO, NO_2, and HCN. Longer chain hydrocarbons are not included as they are thermodynamically unstable under the gasification conditions [105]. The fluidised bed is treated as a simple well-mixed reactor with no distinction between the dense and dilute phases that might be present.

The S-1 unit simulates the disengagement of gas from the fluidised bed that allows the separation of ash and unconverted carbon from the fuel gas. This step is modelled simply by a SSPLIT block using a fractional carryover of the solid components (ash and carbon).

Hot filter

The FILTER unit simulates the hot gas dust filter which removes the remaining particles that are carried out of the gasifier together with the product gases. The filtration process is modelled simply by a SSPLIT block using a fractional carryover of the particles.

Gas turbine

In order to model the gas turbine (GT) unit, the GT was split into three component sub-processes that simulate compression, combustion and expansion, as shown in figure 3.1:

i) The COMPRES unit simulates the compression of air. The isentropic efficiency (η_C) and the desired pressure ratio are specified for the simulation. The compressor is modelled using a COMPR block. The isentropic efficiency is defined by

$$\eta_C = \frac{W_i}{W_a} \tag{3.4}$$

where W_i is the ideal work and W_a is the actual work of compression at the same final pressure.

ii) The COMBUST unit simulates the burner as an adiabatic stoichiometric reactor. This required knowledge of the stoichiometry of reactions and the extent of conversion of the species involved. The combustion reactions were specified and established as progressing to completion. This type of process is modelled in ASPEN Plus with an RSTOIC block.

iii) The EXPANDER unit simulates the expansion of hot gases to convert their sensible heat into rotational energy. The power generated was used for driving the compressor and the excess work for energy production. The isentropic efficiency was assumed as 85% and the desired pressure ratio specified for the simulation. The expander was modelled using a COMPR block. The isentropic efficiency is defined by,

$$\eta_T = \frac{W_a}{W_i} \tag{3.5}$$

where W_a is the actual work and W_i is the ideal work of expansion from the same initial state to the same final pressure.

De-NOx

The DE-NOX unit simulates the catalytic reduction of nitrogen oxides (NO_x) to nitrogen by a small flow of fuel gas. It is assumed that the effect of the unit is to bring the exhaust gases to chemical equilibrium at the reactor temperature. This process is modelled by a RGIBBS reactor block.

Heat recovery

The S-2 unit simulates the division of compressed air into two parts. The first part is directed to the gasifier whilst the second part is passed to the burner of the GT as combustion air. This second part of air is preheated by recovering heat from the GT exhaust gases. The HEATEX1 simulates heat exchange in counter flow between the hot GT exhaust gases and the air that is passed to the burner of the GT as combustion air.

3.1.3 Model and input parameters

The ultimate (elemental) analysis, moisture content, mass flow rate and higher heating value (HHV) of the fuel were used as input data to run the simulations. The ultimate analysis of poultry litter is shown in Table 3.1. The HHV for poultry litter was calculated by ASPEN PLUS using the IGT correlation [150], the value estimated was 13.23 MJ/kg (dry basis).

The stoichiometric ratio (SR) of air to fuel for complete combustion was estimated as equal to 4.73 according to equation (2.2) using the ultimate analysis of poultry litter from table 3.1. The equivalence ratio (ER) was calculated using the ratio of the actual flow of air fed to the gasifier and the fuel flow rate, divided by the SR value.

Table 3.1 Ultimate and proximate analysis of poultry litter

Ultimate analysis	Weight (%) (dry basis)	Proximate analysis	Weight (%) (dry basis)
Carbon	37.50	Fixed carbon	24.00
Oxygen	30.62	Volatile matter	54.37
Nitrogen	3.71	Ash	21.63
Hydrogen	5.12		
Sulphur	0.45		
Chlorine	0.97		
Ash	21.6		

In order to have accurate physical property data and models, the following ASPEN Plus properties were used:

- For nonconventional components, POULTRY and ASH streams, HCOALGEN is the model chosen for the estimation of enthalpy as recommended in the ASPEN Plus guidelines. The HCOALGEN model includes a number of empirical correlations. For the estimation of the heat of combustion, the IGT (Institute of Gas Technology) correlation was chosen. This correlation was obtained from 578 samples of coals. The heat-of-combustion-based correlation on ultimate and sulphur analyses was

selected for the estimation of the heat of formation. The Kirov correlation was preferred for the estimation of the heat capacity. The heat capacity is calculated as the sum of the heat capacity of the coal constituents;

- For nonconventional components, POULTRY and ASH components, DCOALIGT is the model chosen for the estimation of density as recommended in the ASPEN Plus guidelines. The standard deviation of this correlation for 190 points collected by IGT was $12x10^{-6}$ m^3/kg. The DCOALIGT model uses ultimate and sulphur analyses; however, this model was developed to calculate the density of coal on a dry basis;
- Solids method was chosen to compute thermodynamic and transport properties for the gasification section. This method uses ideal gas law, Henri's law, Raoult's law and solid activity coefficients;
- Peng-Robinson equation of state with Boston-Mathias alpha function (PR-BM) method was selected for the calculations of thermodynamic and transport properties for the gas turbine section, which it is appropriate for power generation processes [133].

Table 3.2 shows a summary of the main input variables specified for the ASPEN Plus simulations. A typical value for isentropic efficiencies was selected as recommended for modest values of pressure ratio and turbine inlet temperature [151].

Table 3.2 Model input data

Unit	Description	Assumption
Gasifier	Pressure	5 bar
Turbine	Compressor isentropic efficiency	0.85
	Expander isentropic efficiency	0.85
	Inlet temperature	1173 K
	Pressure ratio	5
Solid fuel	Moisture content of poultry litter	25 %

In order to set tasks during the simulation, calculator blocks and design specifications are employed. A calculator block allows inserting FORTRAN statements into flowsheet computations to perform user-defined tasks. A design specification allows setting the value of a variable that Aspen Plus would otherwise calculate. The design specification requires specifying a desired value for a flowsheet variable or some function of flowsheet variables. For each design specification, a block input variable or process feed stream variable must be also selected and adjusted to satisfy the design specification. This variable is the manipulated variable. Thus, the simulation in this work is controlled using two calculator blocks based on FORTRAN routines and two design specifications.

Calculator blocks

The first calculator block is used to determine the mass flow of each elemental component in the ELEMENTS stream. This calculation is done according to the ultimate and proximate analyses. This calculator block allows the easy modification of the value of moisture content since the ultimate analysis is specified on a dry basis. Ash constituents are calculated based on the specification of inorganic species found in ash.

The second calculator block determines the air flow rate required for gasification at a desired equivalence ratio and poultry litter flow rate. This block also calculates the fraction of air that leaves the S-2 unit to enter to the gasifier (stream AIR4), and the remaining air going into the gas turbine combustor (stream AIR3).

Design specifications

The first design specification calculates the required flow rate of poultry litter as a function of the gas turbine net power which was specified as 200 kW. A tolerance of 0.01 kW and a range of values for the flow rate of poultry litter were established. The iteration process consists of varying the flow rate of litter until achieving the specified GT net power output.

The second design specification calculates the air flow rate entering the gas turbine compressor as a function of the expander inlet temperature which was specified as 1173 K. A tolerance of 0.2 K and a range of values for the air flow rate were established. The iteration process consists of varying the inlet air flow rate until achieving the specified expander inlet temperature.

Ash constituents

Poultry litter contains a significant amount of ash, which consists of inorganic species such as alkali oxides and salts. The presence of ash may represent a problem due to the potential generation of bed agglomerates that can lead to loss of fluidisation or alkali vapours in product gas that can increase rates of hot corrosion on turbine surfaces. Inorganics species, such as potassium, calcium, sodium, and silicon were included as part of the ash fraction. Table 3.3 shows the ash components (K_2O, $CaCO_3$, Na_2CO_3, SiO_2) used as input data for the simulations.

Table 3.3 Ash components

Species	Concentration (wt %)
$CaCO_3$	41.75
K_2O	21.45
Na_2CO_3	4.6
SiO_2	2.7
Inert	29.50

The inorganics not identified were assumed as inert solids. In addition, other inorganic species were incorporated into the equilibrium calculations in order to identify how the inorganics partition into the solid and gas phases. The inorganics included during the simulations were: K_2O, KCl, K_2CO_3, K_2SO_4, CaO, $CaCO_3$, $CaSO_3$, $CaSO_4$, CaS, $CaCl_2$, $Ca(OH)_2$, NaCl, Na_2CO_3, Na_2O, Na_2SO_3, SiO_2, Na_2SiO_3, $Na_2Si_2O_5$, K_2SiO_3, $K_2Si_2O_5$, Ca_3SiO_5.

3.1.4 Parameters tested in the model

The model is capable of predicting the final composition and temperature of the product gases under different operating conditions, including varying the air flow rate, air preheating temperature and operating pressure. The influences of equivalence ratio, air temperature, pressure and turbine inlet temperature, as well as changes in the calorific value and moisture content of poultry litter were investigated. Their effects were evaluated on the product gas composition, product gas

temperature, carbon conversion, LHV of gases, cold gasification efficiency, process efficiency and emissions.

The carbon conversion (X_C) was calculated with the following equation:

$$X_C = \frac{[CO]+[CO_2]+[CH_4]}{[C_{PL}]} \times 100 \quad (3.6)$$

where $[C_{PL}]$ is the amount of carbon content in poultry litter in moles, and [CO], $[CO_2]$ and $[CH_4]$ are the produced amounts of CO, CO_2 and CH_4, respectively, in moles.

The HHV of the product gases at standard conditions was determined by:

$$HHV = \frac{12.75[H_2]+12.63[CO]+39.82[CH_4]}{100} \quad (3.7)$$

where the heats of combustion are in MJ/Nm^3 and $[H_2]$, [CO] and $[CH_4]$ are concentrations in %mol [152].

The LHV was determined by

$$LHV = \frac{(25.7[H_2]+30[CO]+85.4[CH_4]+151.3[C_nH_m]) \times 4.2}{1000} \quad (3.8)$$

where the LHV is in MJ/Nm^3 [61].

Cold gasification efficiency is commonly used as a parameter for evaluating the gasification process. The cold gasification efficiency (CGE) is calculated at standard conditions based on the LHV and using the following equation:

$$\eta_{CG} = \frac{Q_{gas} LHV_{gas}}{m_{bio} LHV_{bio}} \quad (3.9)$$

where Q_{gas} refers to the volumetric flow rate of produced gases in m^3/s, LHV_{gas} is the lower heating value of the produced gases in MJ/Nm^3, m_{bio} is the mass flow rate of biomass in kg/s, and LHV_{bio} is the lower heating value of biomass in MJ/kg, at standard conditions.

The process efficiency (η) is calculated by:

$$\eta = \frac{W}{m_{bio} LHV_{bio}} \quad (3.10)$$

where W refers to the net gas turbine power output in Watts.

3.2 Energy integration system

In order to obtain the best achievable efficiency, the hotter GT exhaust gases can be employed to preheat the air for gasification and the air for combustion in the GT section. In addition, when the outlet product gas temperature is lower than the GT exhaust temperature, product gases can be preheated before entering the GT combustion chamber. Four case studies with various levels of energy integration are, therefore, analysed and illustrated in figure 3.2. The objective of these heat exchangers networks is to explore the benefits of different stages of energy recuperation. This is done in order to maximise the transfer of energy from the GT exhaust gases into the air and fuel gas streams, whilst at the same time cooling down the GT exhaust gases stream before sending them to the stack.

The four stages of heat exchangers were added to the "pressurised layout" from figure 3.1. These four heat exchanger networks are described in detail below:

Stage 1

This stage corresponds to the heat exchanger shown in figure 3.1. This stage follows the Brayton (or Joule) cycle with heat-exchange. However, not all the compressed air is heated and continues its path in the cycle. A small portion of air is extracted at S-2 and used as gasifying air without any preheating. The rest of the air leaving the GT compressor is passed through a single heat exchanger in counter flow with the hot GT exhaust gases, as shown in figure 3.2a. Following pre-heating, the air stream is passed to the burner of the GT as combustion air.

Stage 2

In addition to preheating the air for combustion, fuel gas (syngas) is heated further in parallel using also the hot GT exhaust gases, as shown in figure 3.2b.

Stage 3

The GT exhaust gas is directed to the heat exchanger HEATEX1 to preheat one part of air before entering the gasifier. Then the GT exhaust gas is passed through the heat exchanger HEAXT2 to preheat compressed air. The hot air is divided in two parts. The first part is sent to HEATEX1 whilst the second part of the compressed air is sent to the GT burner. This is shown in figure 3.2c.

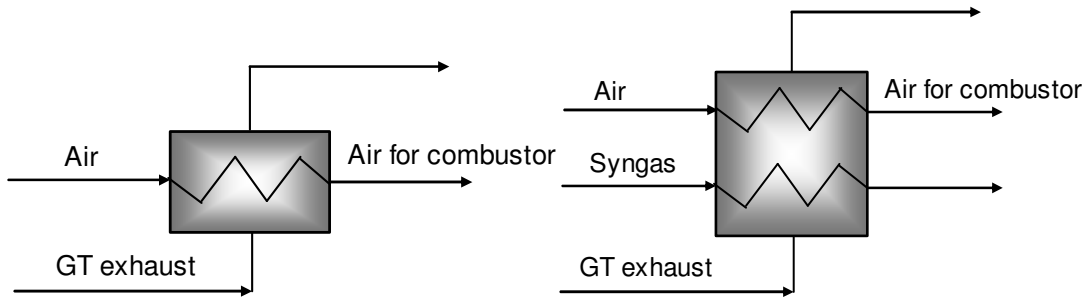

a) Stage 1 b) Stage 2

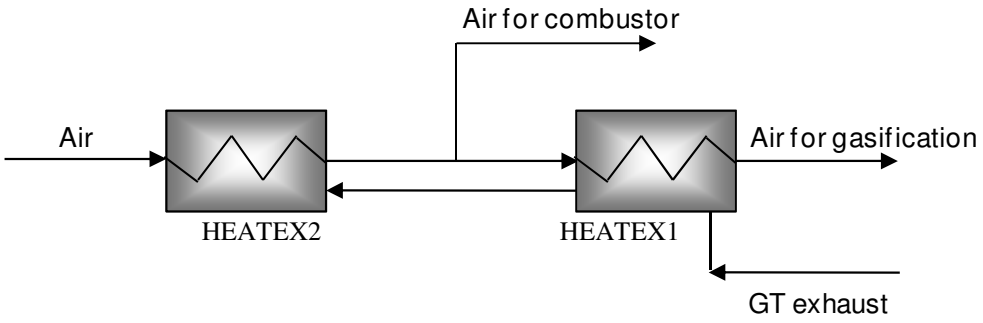

c) Stage 3

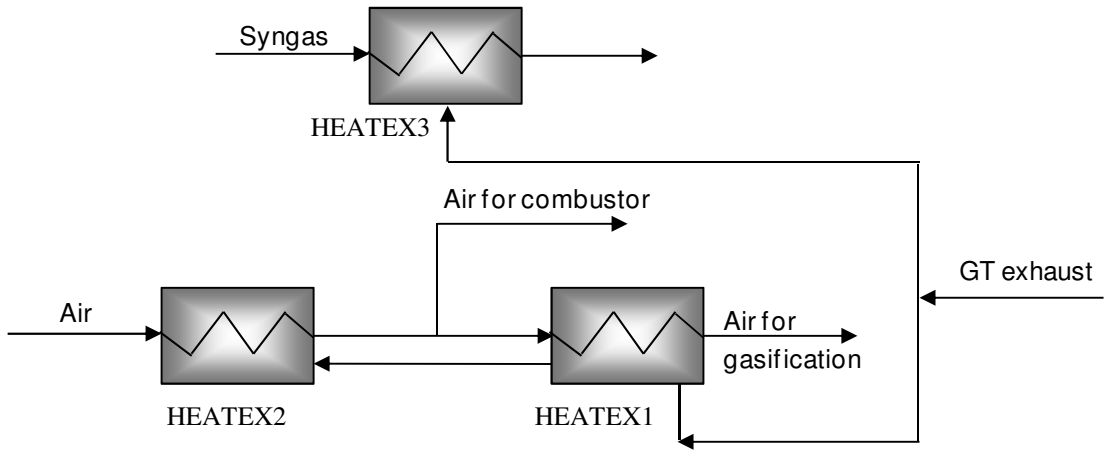

d) Stage 4

Figure 3.2 Heat exchanger networks for energy integration: a) stage 1, b) stage 2, c) stage 3 and d) stage 4.

Stage 4

GT exhaust gas is divided into two parts. The first part is directed to the heat exchanger HEATEX1 to preheat the air before entering the gasifier and followed the path described in stage 3, whilst the second part is passed through the heat exchanger

HEAXTE3 to heat the clean fuel gas between the gasifier and the GT burner. Compressed air leaving the GT compressor is passed through the heat exchanger HEAXT2 in counter flow to the total GT exhaust gas stream. The hot air is divided into two parts. The first part is directed to the burner of the GT as combustion air whilst the second part is passed to the HEATEX1 before entering the gasifier as shown in figure 3.2d.

3.3 Results and discussion

3.3.1 System configuration

Before starting the design of the heat exchanger network, energy targets should be established. When only one point is identified between the hot and cold streams with a minimum temperature difference, it is called the heat recovery pinch. Therefore, individual heat exchangers should not have a temperature approach smaller than the pinch temperature [153]. Pinch analysis, followed by an analysis of the four cases, is evaluated in this section.

Pinch analysis

To start the analysis of the heat exchanger network, the sources of heat (GT exhaust gas stream) and cold streams (air and product gases) were identified. Firstly, the simplest problem (stage 1) was analysed. Stage 1 involves the GT exhaust gases stream with a supply temperature of 850 K and the air for combustion stream with a supply temperature of 492 K.

Figure 3.3 shows a composite plot of enthalpy and temperature between the GT exhaust gases (stream GT-EX1) and compressed air for combustion (stream AIR3) with a minimum temperature difference of 20 K. The overlap of the two streams shows a possible heat recovery of 375 kW, value known as energy target. When the line of air for combustion is moved to achieve a minimum temperature difference of 10 K, the heat recovery increased to 389 kW. This shows the potential recovery of heat from the GT exhaust gases to preheat the cooler air. The pinch temperature is at 850 K in the hot curve and 830 K in the cold stream. Though, the problem becomes more complex when product gases can be preheated, e.g. when the product gas temperature is lower than the GT exhaust temperature when the fuel

moisture content is high or using low ERs, or when the pressure ratio in the GT is lower and the GT exhaust temperature increases as analysed in section 4.3.

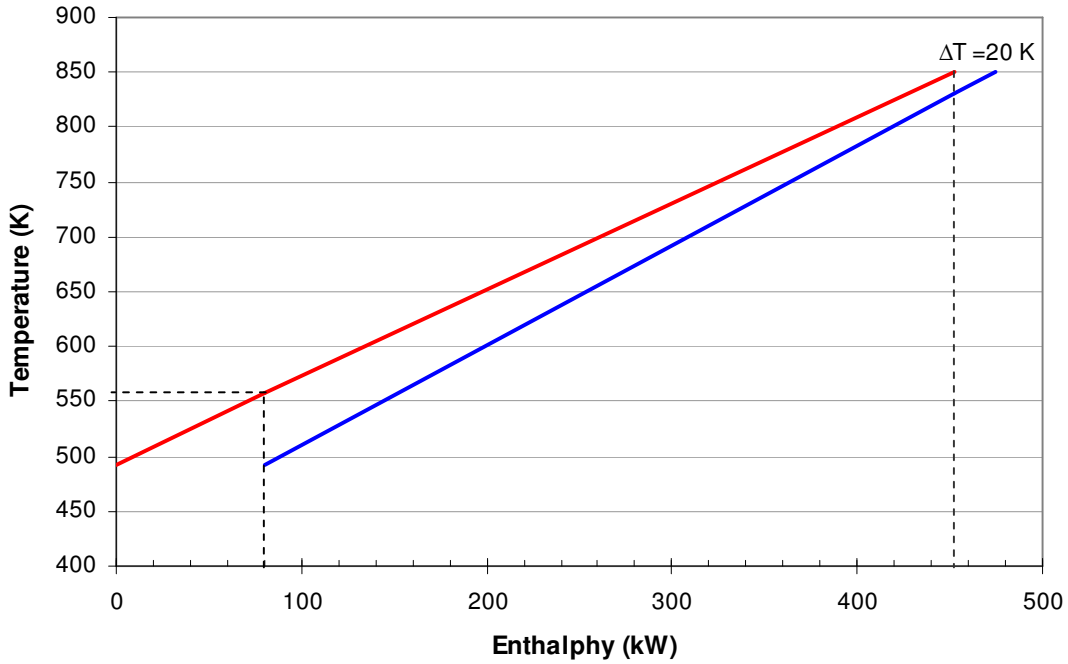

Figure 3.3 Composite curve for GT exhaust gases stream (red line) and compressed air for combustion (blue line) for stage 1

For stage 2, the cold streams are the air for combustion and the fuel gases. Figure 3.4 shows a grid diagram for the heat transfer between the hot stream (GT exhaust gases) and cold streams when it was assumed the moisture content of poultry litter as 30% and an ER of 0.20, which resulted in a gasification temperature of 793 K. In order to heat both streams up to pinch temperature respecting the minimum temperature constraint, stream splitting of the hot stream was necessary. With a minimum temperature difference of 20 K, a heat recovery of 376 kW is possible by heating the air for combustion (stream AIR3) and 6.6 kW by heating the fuel gas (stream GAS3).

Stream No.	Type	Supply temperature (K)	Target temperature (K)	Enthalphy (kW)	Heat capacity (kW/K)
1. GT-EX1	Hot	850	552	-414.6	1.33
2. AIR3	Cold	492	830	203.8	1.07
3. GAS3	Cold	793	830	-566.1	0.17

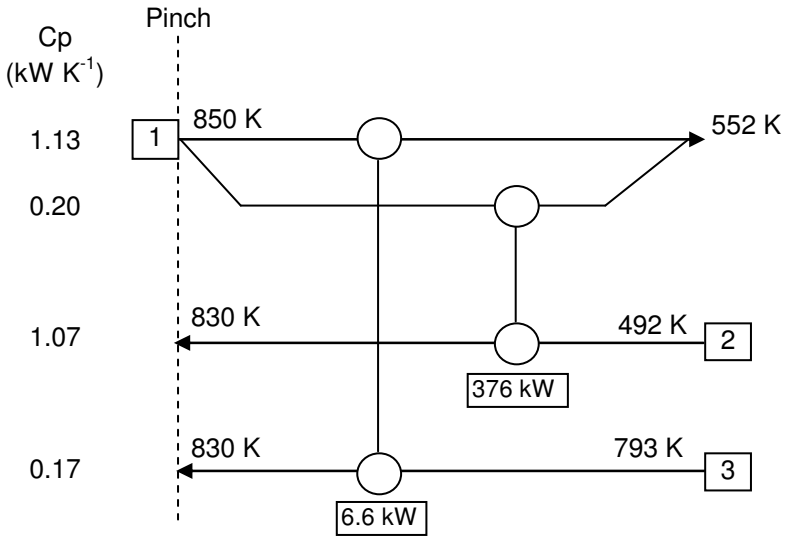

Figure 3.4 A grid diagram for stage 2

The third cold stream is the air for gasification as proposed in stages 3 and 4. However, when the gasifying air is preheated, the gasification temperature increases as well and can augment to values higher than the GT exhaust temperature, especially at high ERs and low moisture content of poultry litter.

The four stages were compared using a fuel moisture content of 30% and an ER of 0.20. The comparison included finding changes in carbon conversion, gasification temperature, electrical efficiency, and heat duties of heat exchangers. Stages 3 and 4 delivered the highest electrical efficiencies of 25.5%, followed by stage 2 of 24.2% and stage 1 of 23.9%, as shown in figure 3.5. For stages 1 and 2, a carbon conversion and gasification temperature of 82% and 792 K, respectively, were delivered because the same air temperature of 492 K was used. In contrast, for stages 3 and 4, the air temperature was 830 K giving as a result a gasification temperature of 825 K, and carbon conversion of 84%.

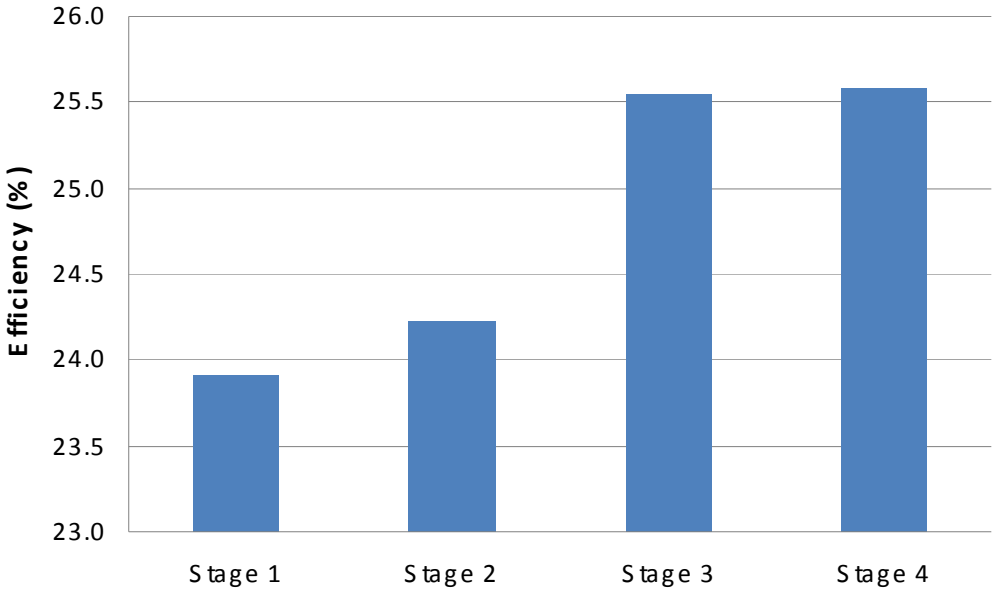

Figure 3.5 Comparison of electrical efficiency for each Stage (ER of 0.2 and moisture content of 30%)

The efficiency for stages 3 and 4 were of the same value for two reasons. The most evident was that gasification temperature was of 825 K for both stages, as shown in figure 3.6. Accordingly, the same carbon conversion of 84% was achieved for both stages (shown in figure 3.7). The second reason was that the fuel gases were not significantly preheated on the third heat exchanger in stage 4 due to the higher gasification temperature, and the GT exhaust temperature was of 850 K for a turbine inlet temperature of 1173 K and pressure ratio of 5. Benefits seem to be more evident for higher turbine inlet temperatures or lower pressure ratios, which is discussed in section 4.3.

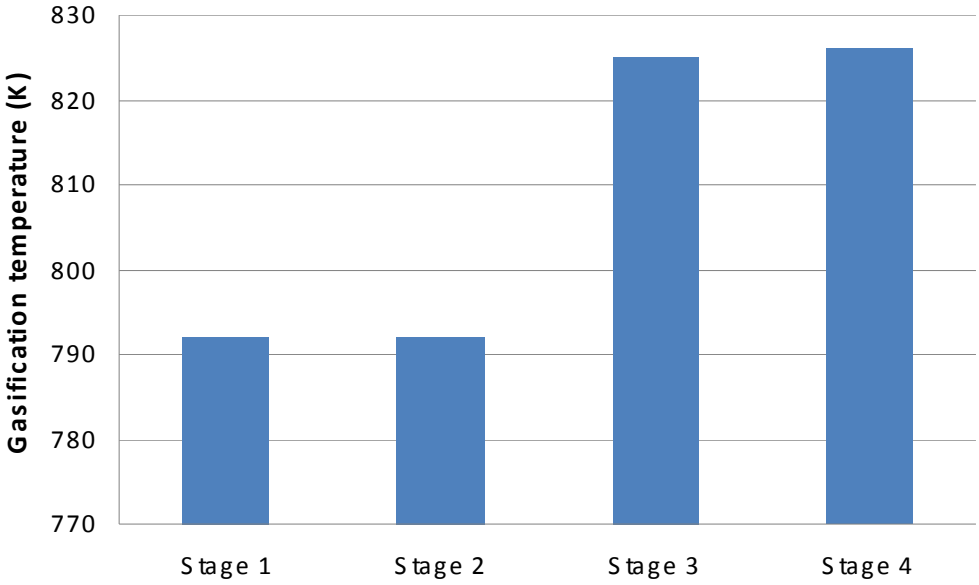

Figure 3.6 Comparison of gasification temperature for each Stage (ER of 0.2 and moisture content of 30%)

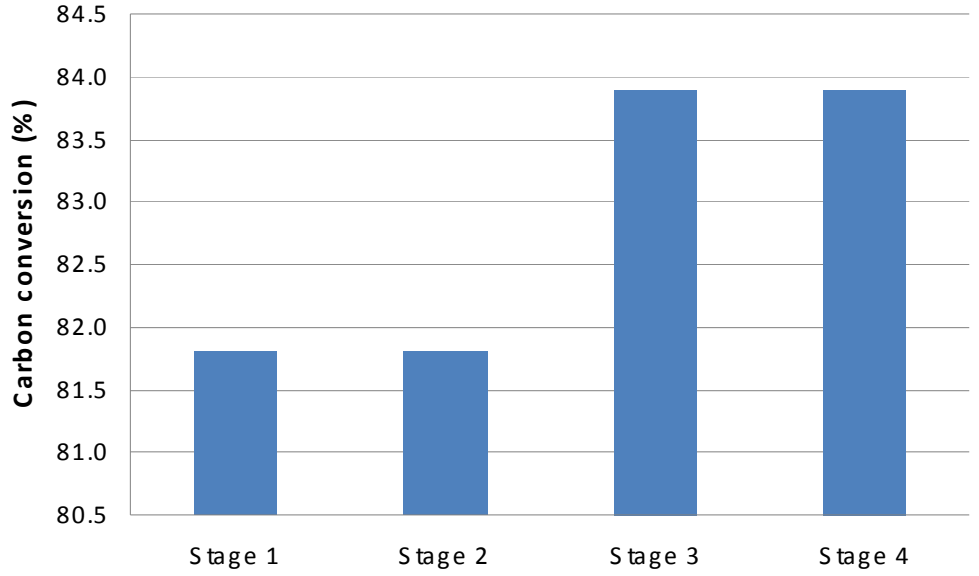

Figure 3.7 Comparison of carbon conversion achieved for each Stage (ER of 0.2 and moisture content of 30%)

Figure 3.8 shows the heat duties of the heat exchangers for each stage. The heat duties for HEx 2 and HEx 3 were significantly smaller than for HEx 1; this huge difference is due to the bigger flow of air for combustion compared to the small fraction of air extracted for gasification (between 4.2-4.5% of main air stream) and the fuel gases.

Preheating fuel gases improved the efficiency; however, a bigger benefit showed the preheating of air for gasification, because it improved the calorific value of the fuel gases and increased the fuel gas temperature. For stage 3, it is found that two heat exchangers were not necessary, and the whole air stream can be preheated with one heat exchanger.

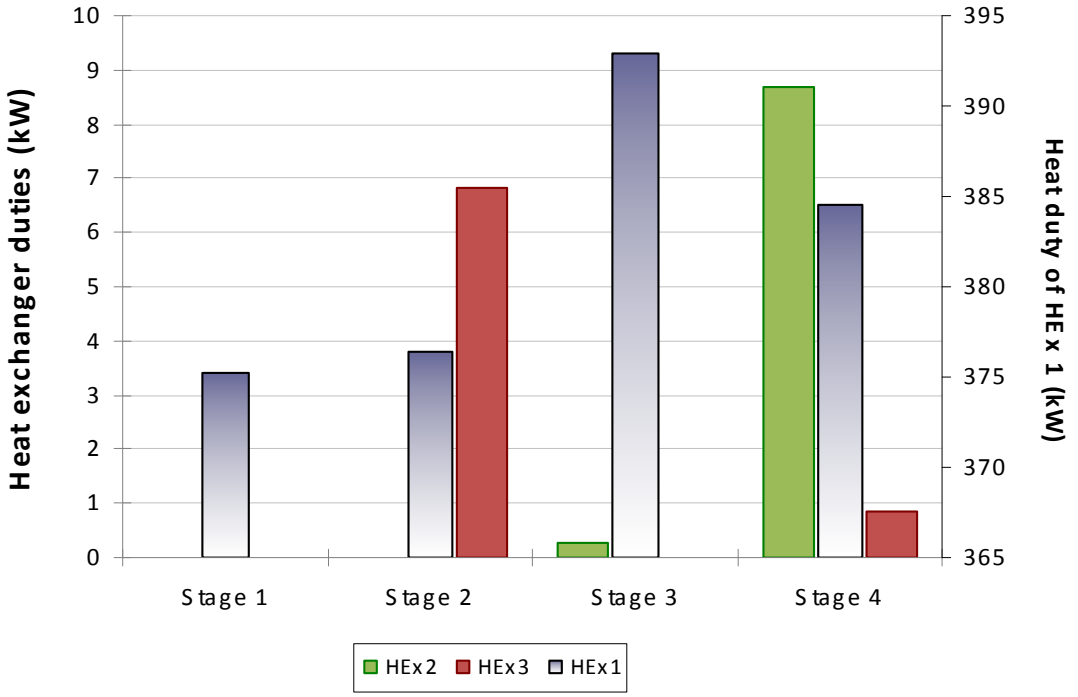

Figure 3.8 Comparison of heat duties of heat exchangers for each Stage (ER of 0.2 and moisture content of 30%)

Because gasification temperatures might exceed the GT exhaust temperature, it was evaluated if the heat exchanger to preheat gas products is redundant in this configuration.

Figure 3.9 shows the efficiency when only the two heat exchangers (Stage 3) to preheat air for combustion and gasification are included, varying the ER and the moisture content of the feedstock.

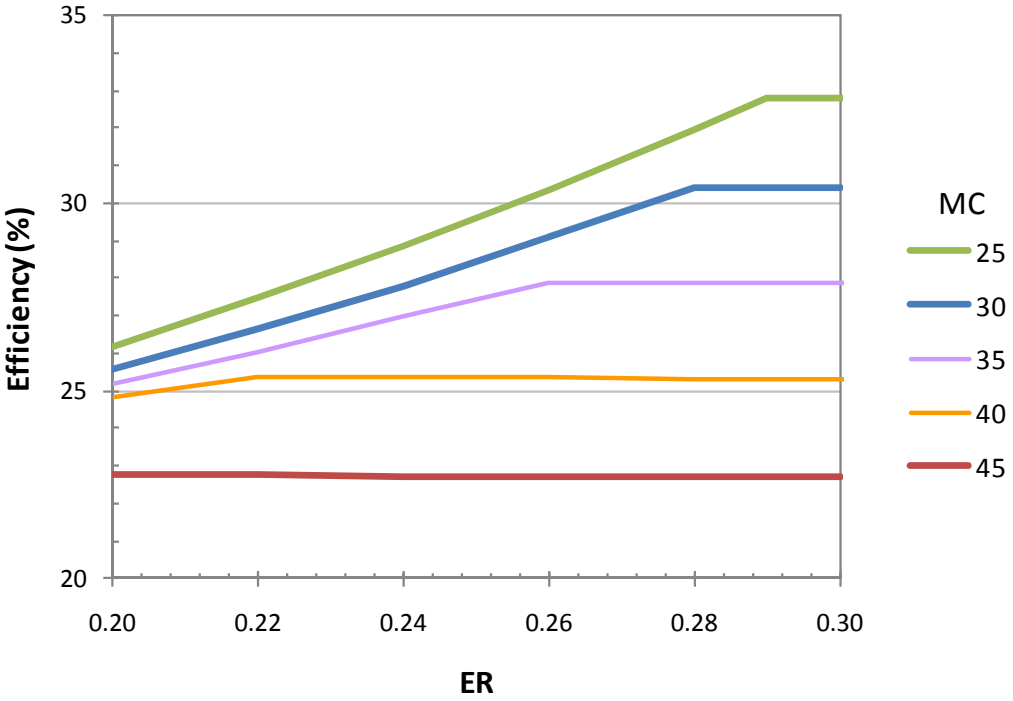

Figure 3.9 Process efficiency for stage 3 for various ERs and moisture content of poultry litter

Figure 3.10 shows the efficiency increment when the third heat exchanger (Stage 4) is added. This figure shows that high moisture contents (higher than 30%) and low ERs are required to make use of the third heat exchanger.

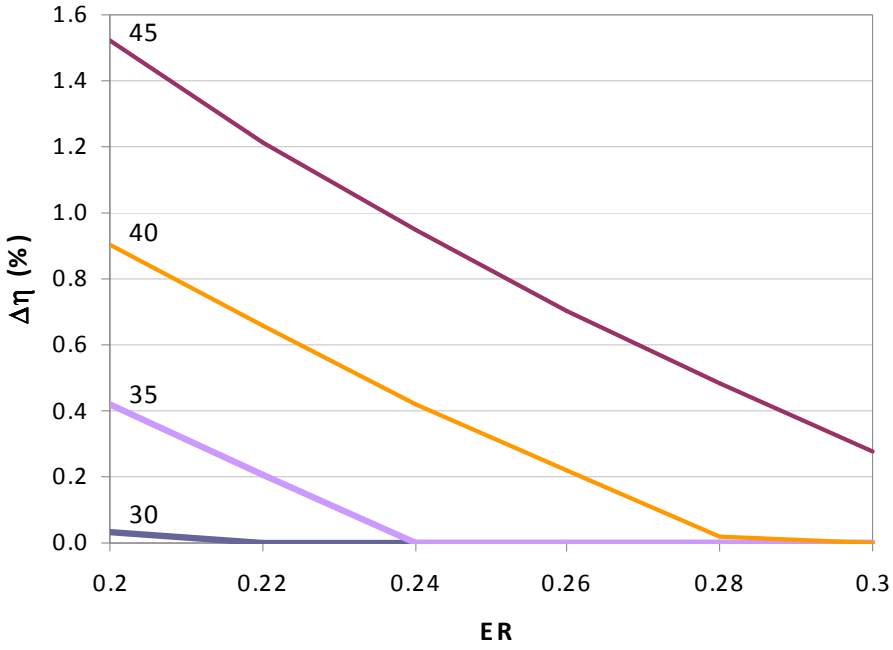

Figure 3.10 Efficiency increment when third heat exchanger is added (Stage 4) for various ERs and moisture content of poultry litter

Stage 4 was the process layout of choice since it delivers the best efficiencies, in particular with low ERs or high moisture content of biomass. Stage 4 was selected as the energy recuperation system to be added to a conventional system and to the proposed pressurised system, and their comparison is shown in the next chapter. Figure 3.11 shows the arrangement of heat exchangers to be added to both systems which deliver the maximum heat exchange and achieve pinch temperatures in all cold streams.

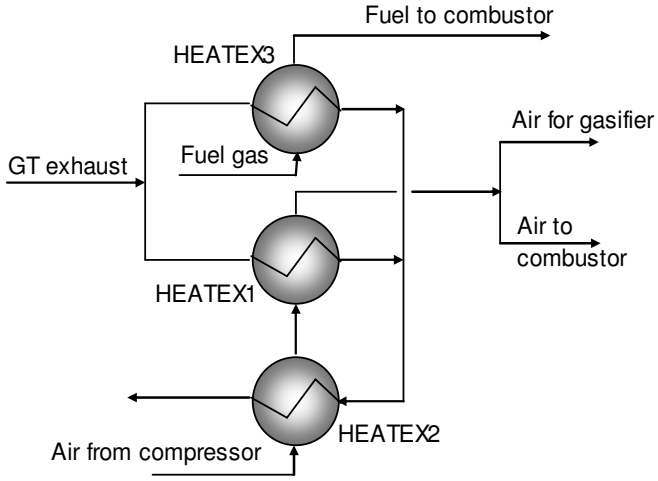

Figure 3.11 Arrangement of heat exchangers of Stage 4 for Aspen Plus flowsheet

3.4 Case studies description

Six case studies were identified in order to evaluate the proposed system, which include the comparison of the "conventional layout" versus "pressurised layout", by changing the calorific value and moisture content of poultry litter, pressure ratio of GT, variation of turbine inlet temperature, temperature approach of heat exchangers and pressure losses. The six cases are described below.

3.4.1 Conventional versus pressurised gasification

In order to evaluate the performance of the proposed "pressurised layout", it was compared to a "conventional layout" using an atmospheric gasifier, which is considered as the base case. Two more arrangements that include heat recovery using "stage 4" were analysed; where the exhaust gases from the GT were used to preheat the air for gasification and air for combustion used in the GT combustor chamber.

When the outlet product gas temperature was lower than the GT exhaust temperature, product gases were preheated before entering the combustor. Therefore, four case studies were evaluated as explained below.

Case A. The base case consists of a gasifier operating at atmospheric pressure where air was used as gasifying agent as illustrated in figure 3.12. Since the product gases carried particles, a filter was used to remove dust from the gas stream. The clean gases were cooled down to 40°C to condense water vapour and lower the work of the syngas compression to reach the required operating pressure. Then the fuel gases were injected into the combustion chamber of the GT and burnt with the previously compressed air. Following combustion, the gases entered the expander and then the De-NO_x unit for NO_x elimination. Figure 3.13 shows the Aspen Plus flowsheet employed; the additional units are HEATEX, COOLER and COMPR2.

The cooling of product gases was modelled using the COOLER unit. The COOLER unit was modelled using a FLASH2 block. The COMPR2 unit is a compressor to raise the pressure of product gases to the required pressure for the gas turbine. It was modelled by a COMPR block and assuming an isentropic efficiency of 85%.

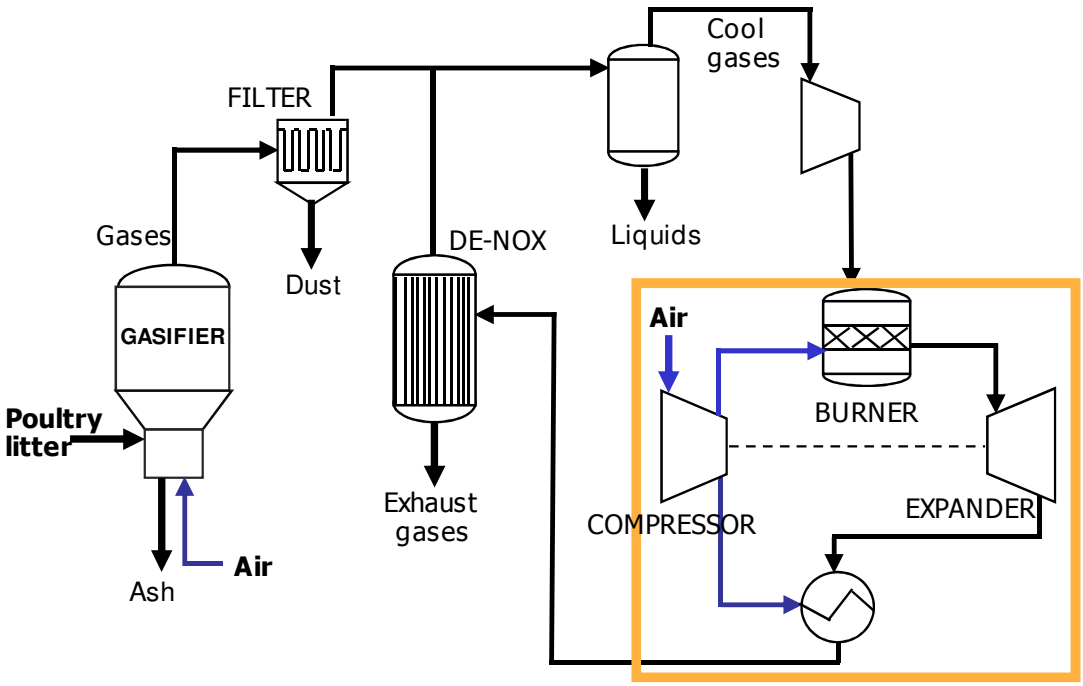

Figure 3.12 Schematic diagram of the base case

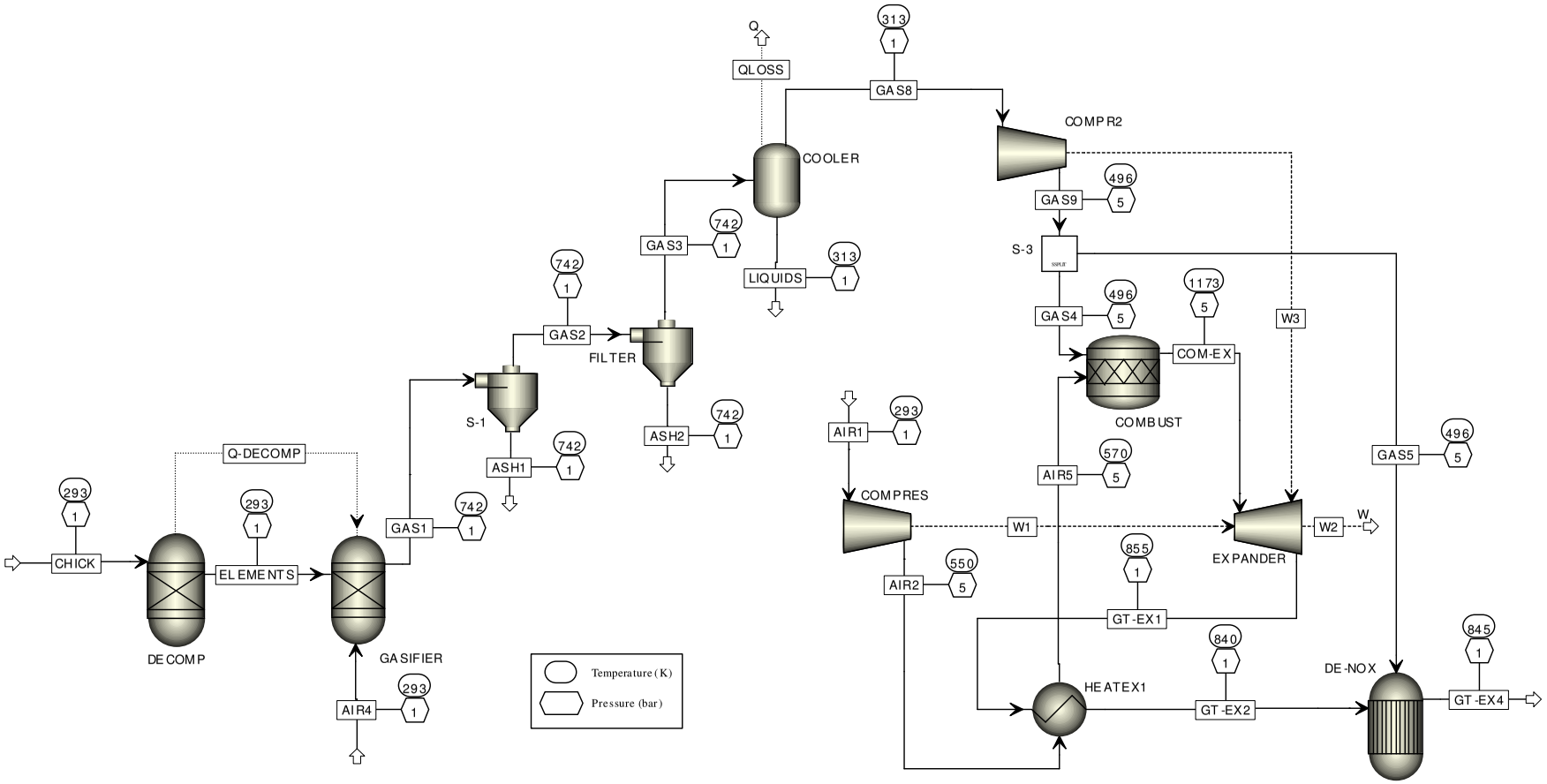

Figure 3.13 ASPEN Plus model of the base case

Case B. This process corresponds to the system described in section 3.1.2 and the diagram was illustrated in figure 3.1.

Case C. This arrangement contains the same process units as the base case (case A), but in this configuration an energy integration system (EIS) was added as shown in figure 3.14. In the EIS, the hot GT exhaust gases were used to preheat further the product gases after compression, air for gasification and air after compression. The clean gases before entering the compressor were cooled down to 400°C, and then further to 40°C to condense water vapour and lower the work of the syngas compression to reach the required operating pressure. After compression, the cool gases were used to lower the temperature of exhaust gases from the gasifier to 400°C. Then the preheated gases were injected into the combustion chamber of the GT and burnt with the previously compressed air.

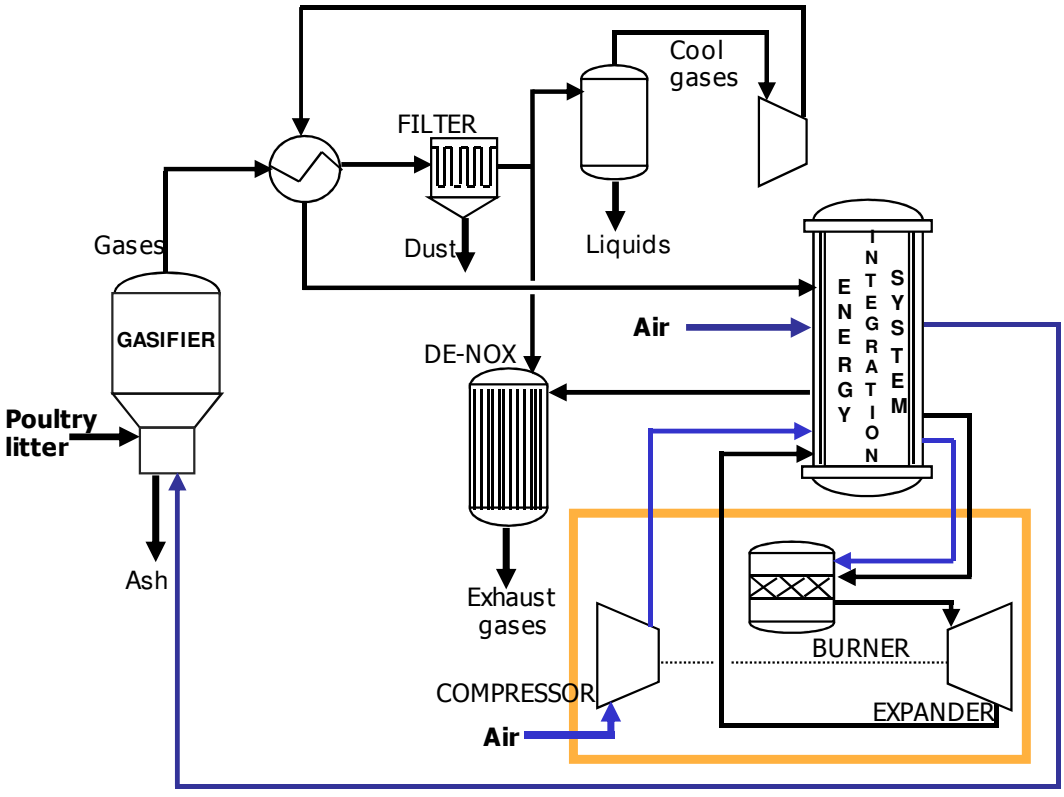

Figure 3.14 Process configurations: Case C

The cooling of product gases was modelled in two stages using the HEATEX and COOLER units. The HEATEX unit is a heat exchanger for cooling down the product gases firstly to 400°C. It is modelled as counter current using a HEATX

block and fixing the outlet temperature. The COOLER unit was used to cool further the product gases to 40°C and modelled using a FLASH2 block.

Case D. This arrangement contains the same process units as case B, but in this case an EIS using the Stage 4 was included as shown in figure 3.15. In the EIS, the hot GT exhaust gases were used to preheat air and the gases produced after gasification. Only one compressor was used for air compression, after which the air was preheated in the EIS.

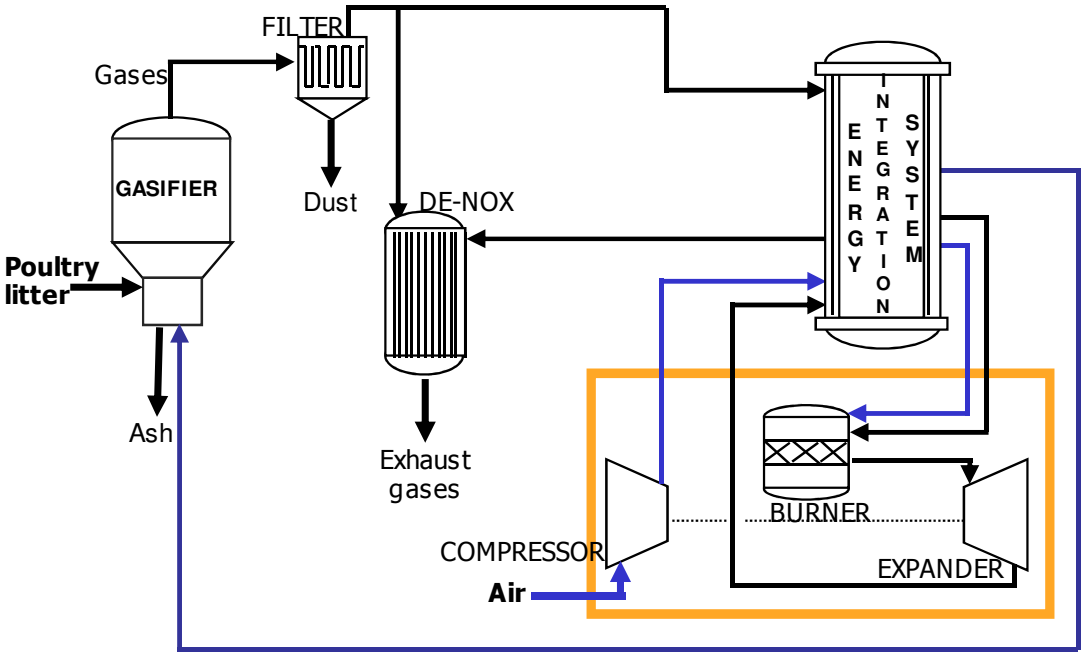

Figure 3.15 Process configuration: Case D

Following pre-heating the air was divided into two parts. The first part was directed to the gasifier whilst the second part was passed to the burner of the GT as combustion air.

In order to model the process configurations described above, the methods and assumptions explained in section 3.1.1, the units described in section 3.1.2, and the model input parameters indicated in section 3.1.3 were employed for the simulations. In addition, the heat exchangers were modelled assuming a temperature approach of 20 K.

3.4.2 Calorific value and moisture content of poultry litter

Biomass properties are of interest for gasification and the end gas product quality. Two properties selected are the calorific value and moisture content of poultry litter. The calorific value of a material is a property that shows the energy content released after being burnt in air, whilst the moisture content reduces the available energy from the biomass [154]. Therefore, the calorific value and moisture content of poultry litter were varied and their effects analysed.

3.4.3 Pressure ratio of gas turbine

An assessment of the effects of pressure on the gasifier and gas turbine performance, as well as on the overall process efficiency, was performed in order to identify an optimum pressure ratio.

3.4.4 Turbine inlet temperature

The effects of increasing the maximum expander inlet temperature (EIT) were evaluated with the objective of improving the process efficiency. This EIT is constrained by gas turbine materials.

3.4.5 Temperature approach of heat exchangers

The temperature approach for the heat exchangers will be varied to evaluate possible improvements in process efficiency. The setting of the temperature approach is normally a tradeoff between energy and capital costs.

3.4.6 Pressure losses

Frictional pressure losses can potentially occur in the passages on the air-side and gas-side. Pressure losses can decrease the turbine pressure ratio relative to the compressor pressure ratio and consequently reduce the net work output [151]. Pressure losses in the gasifier will be evaluated in order to identify their effects in the process efficiency.

3.5 Summary

Since the temperature of the GT exhaust gases is around 850 K, energy is available in the system which can be integrated to raise the temperature of cooler streams such as air. As a result, this option for energy integration was discussed.

Stage 4 was chosen as the configuration of heat exchangers for the energy integration system. This selection was based on the arrangement that allows the best energy recuperation into the gasifier and gas turbine.

The case studies were defined in order to evaluate: the conventional case versus the pressurised layout. The conventional case employs a gasifier that operates at atmospheric pressure and requires the cooling of the product gases before compression to minimise the work required for the compression of product gases. The cases are modelled based on the assumption of chemical equilibrium. The gasification process is modelled in three stages as flash pyrolysis, gasification and ash separation. For the pressurised layout, parameters such as calorific value of poultry litter, temperature approach of heat exchangers and turbine inlet temperature will be evaluated in the following chapter.

Chapter 4

Case studies: Process performance

Medium BIGCC systems that integrate gasification with combustion/heat recovery can deliver net efficiencies of 40–50% (based on LHV) for a plant with capacity of 30–60 MWe [12]. In order to achieve comparable efficiencies, in this work, the GT exhaust heat is recuperated into the system. This chapter presents the findings of the six case studies described in section 3.4. Case study one compares the "conventional layout" (Brayton cycle with heat exchange), which comprises an atmospheric gasifier coupled to a gas turbine with a "stage 1" (Case A) energy integration system (EIS), to a "pressurised layout" comprising a pressurised gasifier, gas turbine and "stage 1" EIS (Case B). It also compares the performance of the two layouts when coupled with "stage 4" EIS (Cases C and D respectively). The comparison of the different configurations provides an insight into the effects of the energy integration and the selection of the most convenient configuration. The partition of inorganic species is included in the analysis, in order to identify the optimum parameters to minimise the vaporisation of inorganics. To evaluate environmental impacts, emissions were assessed. For the following case studies, parameters such as calorific value and moisture content of poultry litter, pressure ratio, turbine inlet temperature, temperature approach and pressure losses, were varied and their effects evaluated.

4.1 Conventional versus pressurised gasification

The four cases previously described in 3.4.1 are compared in this section. This comparison includes the analysis of the effects of changes of ER on carbon conversion, lower heating value of product gases, cold gasification efficiency and process efficiency. For the four cases analysed, a moisture content of 25% was assumed.

4.1.1 Carbon conversion

Figure 4.1 shows that carbon conversion was improved with increasing ER for the four cases, since more oxygen was provided to react with the remaining carbon. This figure gives the optimum operating ER to achieve complete carbon conversion for the four cases. Complete carbon conversions were achieved for case A and case B at ER values equal or greater than 0.34 and 0.32, respectively, as shown in figure 4.1. At ERs lower than 0.32, carbon conversion for case A was improved by 4% points when the pressurised system was included (case B).

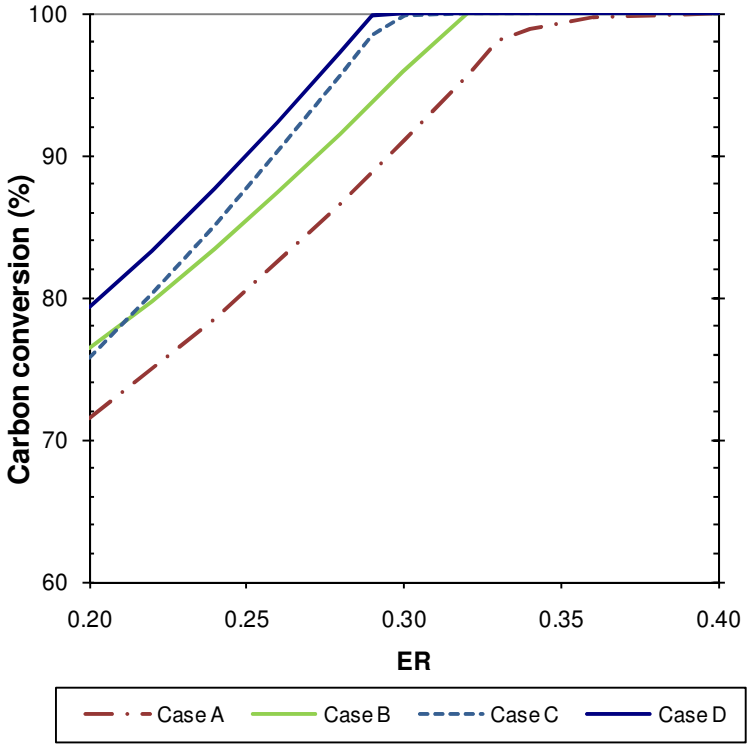

Figure 4.1 Comparison of carbon conversion for case studies

In the present work, carbon conversions for case A and case B were 75% and 80%, respectively, at an ER of 0.22. A similar carbon conversion of 78.17% was reported from experimental studies on the gasification of pine sawdust with moisture content of 8%, air temperature of 338 K, ER of 0.22 and gasifier temperature of 973 K [61]. However in Lv et al's work the steam biomass ratio of 2.7 was very much higher than in this work where it was effectively 0.33.

Cases C and D reach complete carbon conversion at a lower ER value of 0.29 than for case A and case B. This can be explained by the energy provided by the hotter gasifying air which can promote carbon conversion by endothermic reactions, such as the water-gas reaction ($C + H_2O \rightarrow CO + H_2$) and Boudouard reaction ($C + CO_2 \rightarrow 2CO$). At low ER values, carbon conversion is lower for case C than for case D, because for case C gasification temperatures inside the atmospheric gasifier are lower.

4.1.2 Lower heating value

Figure 4.2 shows the LHV of product gases versus ER for the four cases. It can be seen that the LHV decreases as expected with increasing ER. This occurs due to the changes in gas composition, since changes in the proportion of methane, hydrogen and carbon monoxide impact on the LHV. However, the LHV at low ER slightly decreased up to an ER of 0.32 and 0.34 for cases A and B, respectively; at higher ERs, the LHV decreases steadily because of the continuous depletion of methane progressing to elimination. Furthermore, a critical ER is predicted where the sudden change in LHV gradient occurs which corresponds to the ER of complete carbon conversion (shown in figure 4.1) and at which H_2O content of the gas starts increasing by the reaction $CH_4 + 2O_2 \rightarrow CO_2 + 2H_2O$.

For case C, the LHV at low ERs slightly decreased or remained almost constant up to the ER where complete carbon conversion (figure 4.1) was achieved. Higher LHVs were observed for case D at low ERs, because the CH_4 composition increased, whilst H_2 and CO formation decreased at the higher pressure of 5 bar, and CH_4 has greater influence on the LHV.

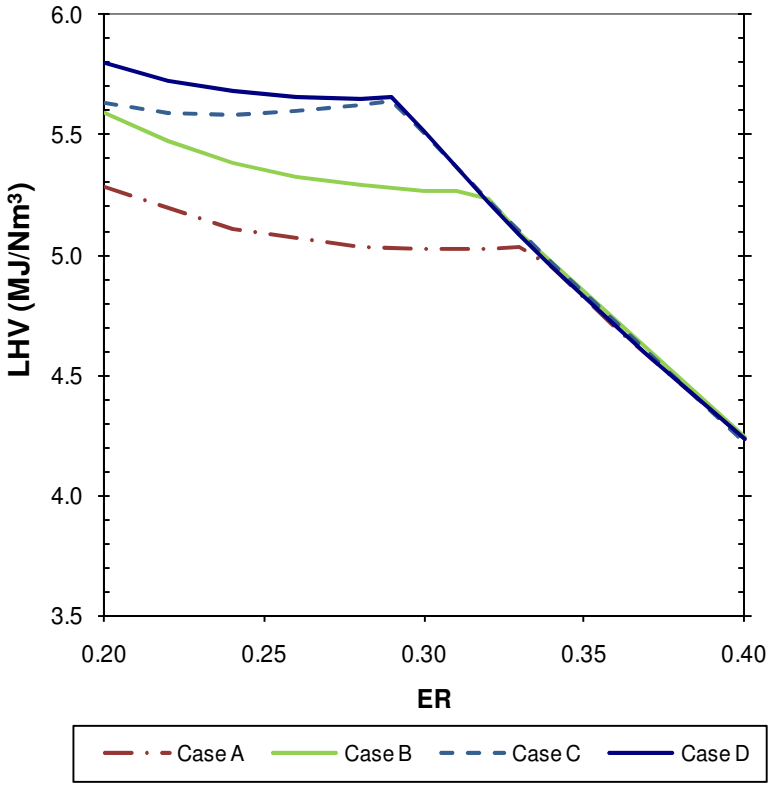

Figure 4.2 Comparison of LHV for case studies

These results are in agreement with a previous work on the gasification of olive kernel where fairly constant LHV values were obtained up to an ER of 0.21 which were followed by steadily decreasing values with further increases to the ER [28]. However, they did not associate the critical value of ER with complete conversion of the carbon. Above the respective critical ER values, the LHV of the gas decreases along a common trend for all four cases. This trend represents the progressive oxidation of the fuel components of the gases, such as CH_4 and H_2.

4.1.3 Cold gasification efficiency

Figure 4.3 shows the cold gasification efficiency (CGE) for the four process layouts, based on the LHV versus ER. For the four cases, maximum CGEs were obtained. For the cases C and D, the maximum CGEs were achieved at a lower ER value of 0.29 compared to the case A and case B where maximum CGEs were achieved at ERs of 0.34 and 0.32, respectively. Figure 4.3 also illustrates that the ER identified with the maximum CGE coincided with complete carbon conversion.

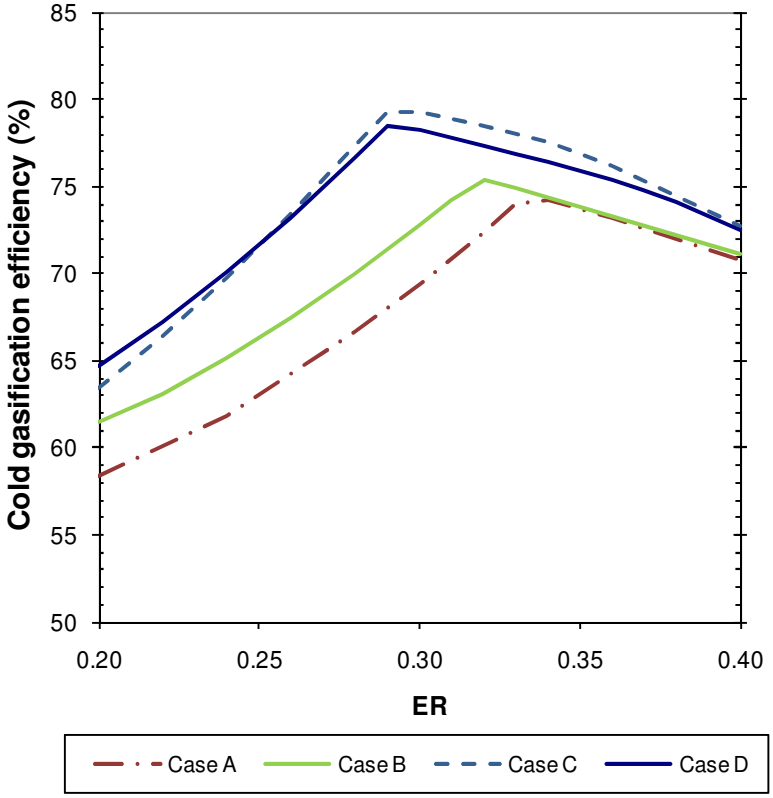

Figure 4.3 Comparison of cold gasification efficiency for case studies (based on LHV)

The maximum cold gasification efficiency of case A (74%) was increased by 8% points when the energy recuperative system (case C) was included. These results agree with the trends previously found for wood gasification with both 20% and 40% wood moisture content [155]. When the air inlet temperature was increased from 298 K to 873 K, the maximum cold gas efficiency showed an increase by nearly 6% points. In the present work, the air inlet temperature was raised from 293 K in case A, to 830 K in case C, and from 492 K in case B to 830 K in case D resulting in 8% and 6% points, respectively, increase in CGE.

Cases C and D show a similar trend for the cold gasification efficiency with values very close, with only up to 1% point difference, especially at ERs lower than 0.29. Figure 4.3 confirms that air preheating improves cold gasification efficiency and reduces the ER value necessary for maximum CGE. Even more advantageous is the fact that air was preheated by recovering heat from the gas turbine exhaust gases.

Sugiyama et al. [156] used a pebble bed slagging-gasifier with a high temperature air generator in order to obtain a syngas with higher calorific value.

They analysed the effect of increasing the ER when air was preheated to 1000°C. They found that by increasing the ER the carbon conversion efficiency and the cold gasification efficiency were improved whilst the HHV of the product gases decreased which is in agreement with these results.

4.1.4 Process efficiency

Figure 4.4 shows the process efficiency for the four cases versus ER. It is seen that the efficiency increased with increasing ER up to a maximum which coincides with the ER for complete carbon conversion, maximum cold gasification efficiency and where the sudden increase in the LHV gradient occurs.

The process efficiency of case A was improved by 5% points when the pressurised gasifier (case B) was included at the same ER. However, the maximum process efficiency was increased by 7% points but appeared at a lower ER, as shown in figure 4.4.

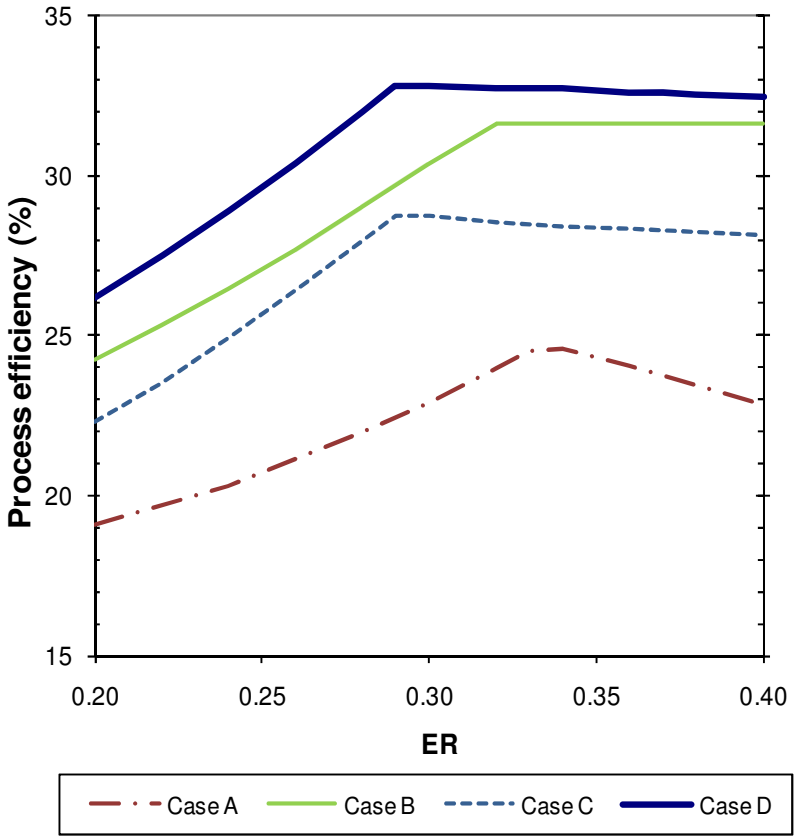

Figure 4.4 Comparison of process efficiency for case studies

An ER of 0.32 is enough to achieve the maximum efficiency (32%) for case B. For cases C and D, the maximum efficiencies were achieved at an ER of 0.29, which is also lower than for the case A at an ER of 0.34.

The difference seen between the efficiencies obtained for cases B and D shows the benefit of further heating the gasifying air from 492K to 830K, which raised the process efficiency by 3% points at the same ER and lowered the required ER value for complete conversion from 0.32 to 0.29.

The ERs for the maximum efficiency values for the four cases correspond to the points for maximum cold gasification efficiencies, complete carbon conversions and the starting of LHVs decrease. After the maximum process efficiencies were reached, the efficiencies remain fairly constant when ER was increased for cases B, C and D. In contrast, for case A after reaching the ER for maximum efficiency, the efficiency started decreasing with increasing ER. This decrease in ER is attributed to the cooling of the product gases in case A and the energy wasted during the cooling prior to compression.

Process efficiency analyses resulted in an alternative approach to evaluate the process configurations that complement cold gasification efficiency, carbon conversion and LHV analyses. Important variations in efficiency were observed as shown in figure 4.4. The figure illustrates that the process efficiencies between cases C and D differ by 4% points which show an unambiguous difference not observed when only cold gasification efficiency was analysed. Another benefit of these results is the identification of an optimal ER value, which can then be chosen as an operating parameter for future experimental work.

The process efficiencies obtained for case D in the range of ER evaluated were between 26% and 33%. These results are surprisingly within the efficiencies reported for larger and more complex systems [52, 133, 139]. A conventional IGCC system, with a gasification temperature of 873 K, expander inlet temperature of 1547 K, turbine pressure ratio of 15 and GT power output of 15.25 MW, gave a net efficiency of 32.6%, and with modification of 33.9%, on a coconut husk fuel with moisture content of 50% [133]. Higher net efficiencies have also been previously reported. One system included an ASU, gas turbine, HRSG, and steam turbine [139]. The efficiencies reported when nitrogen was injected to the combustor of the GT were from 38.2 to 40.8% with a net power output of 275–291 MW. The gasification

temperature was 1,589 K and the GT used a pressure ratio of 15.5 and an expander inlet temperature of 1,561 K. A second system showed an efficiency of 37.9% with a total power output of 17.9 MW [52]. The simulation parameters used were a pressure ratio of 15.5 and an air-blown gasifier operated at around 850°C. In this work, a small scale system was chosen (200 kW of net power output) with a pressure ratio of 5. These process parameters allow the installation of a compact system with the potential of achieving an efficiency of 33% according to the results from case D.

4.1.5 Air bleeding from compressor

Integration of the gasifier with a gas turbine was achieved by recuperating energy from the GT exhaust gases to preheat air for gasification and combustion. In addition, air was extracted from the compressor discharge to avoid the use of a separate air compressor for the gasifying air for cases B and D. According to GE Energy, up to 5% of airflow can be extracted from the compressor discharge without the need of modifications, and an air extraction between 6% and 20% may be possible but requires some modifications to the casings, piping and controls [157]. Figure 4.5 shows the required amount of extracted air from the GT compressor for the two pressurised cases in solid lines. It can be seen that case B demands an air extraction between 4.8–7.3%. This case will require modifications in the compressor at ER values greater than 0.22, as suggested by manufacturer.

In contrast for case D, figure 4.5 shows that less than 5% of air extraction is necessary when using low ER values of up to 0.3; at ERs higher than 0.3, up to 6.8% of air extraction is required. Since the preferred ER for maximum efficiency was of 0.29 for case D, the extracted air mass flow was of 4.9% from the compressor airflow, which value is just below the constraints of gas turbines as recommended by a manufacturer (GE Energy).

Figure 4.5 also shows the gasification temperatures for cases B and D in dashed lines. It can be seen that the change of air extraction gradient corresponds to a change in the gradient of the temperature of the gasifier product gases due to the increase of gasification temperature with increasing ER.

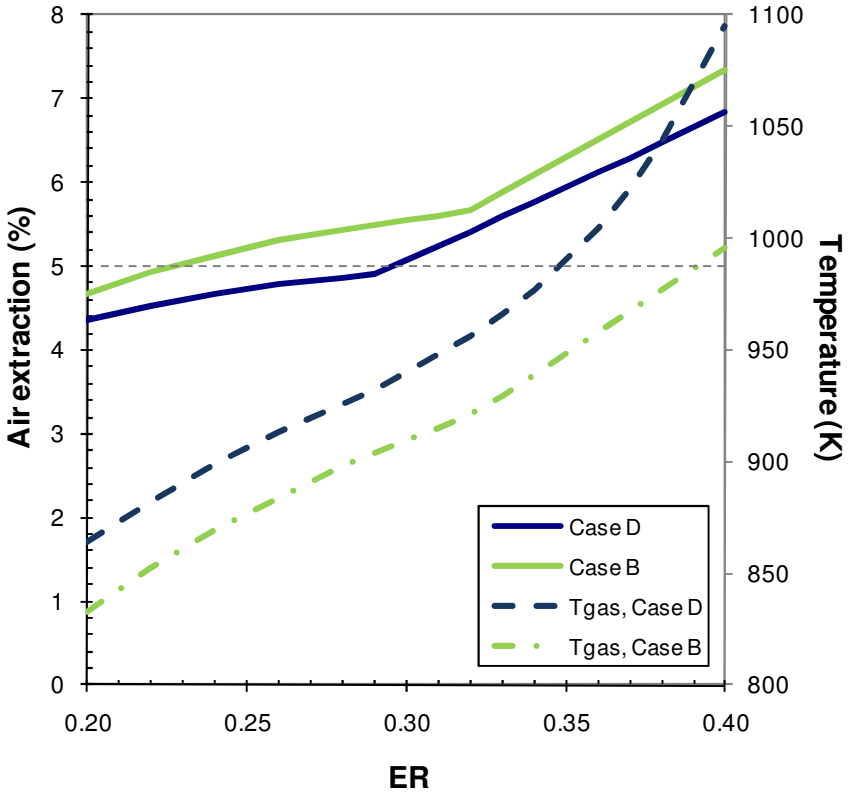

Figure 4.5 Air extraction from the compressor discharge and exit temperature of gasifier product gases for cases B and D

4.1.6 Air emissions

Any industrial and agricultural activity with the potential of polluting requires proper prevention and control of its emissions. As a result, the European Union has set out regulations in order to control industrial installations. The Council Directive 96/61/EC of 24 September 1996, which is concerned with integrated pollution prevention and control, specifies the main rules to allow and control new or existing installations after complying with certain obligations and requirements. Sectoral directives establish specific emission limit values and are intended to certain industrial activities, e.g. large combustion plants and waste incineration. The Large Combustion Plants Directive (LCPD, 2001/80/EC) applies to large combustion plants with a thermal output greater than 50 MW and regulates the emission of major pollutants, such as sulphur dioxide (SO_2), nitrogen oxides (NO_x), and particulates or dust. The Waste Incineration Directive (WID, 2000/76/EC) establishes limit emission values for incineration and co-incineration of both hazardous and non-hazardous wastes [11].

In this work, the WID applies to the gasification process being studied. In order to meet the emission limit values set out by the WID, installations should be designed, built and operated accordingly. Table 4.1 shows air emission limit values established by the WID for dust, organic carbon, HCl, HF, SO_2 and NOx as daily averages.

Table 4.1 Air emission limit values according to the Waste Incineration Directive (273 K, 101.3 kPa, 11% O_2, dry)

	Daily average
Total dust	10 mg/m^3
Total organic carbon	10 mg/m^3
Hydrogen chloride (HCl)	10 mg/m^3
Hydrogen fluoride (HF)	1 mg/m^3
Sulphur dioxide (SO_2)	50 mg/m^3
Nitrogen oxides (NOx)	400 mg/m^3

Figure 4.6 illustrates pollutant emissions from case D after being released from the De-NOx unit, which are regulated by the WID in table 4.1. HF is not included in the graph since fluorine is normally only present in poultry litter in an insignificant amount, and in this work the ultimate analysis does not include fluorine content.

NO_x emissions originate from the nitrogen contained in poultry litter. Nitrogen is firstly released as NH_3 from poultry litter during gasification. Later, in the GT combustion chamber, NH_3 is oxidised. However, NO_x formation is predicted to be insignificant due to the low combined nitrogen content in the fuel gas and the use of the De-NOx unit which reduces the amount of NO_x formed. Other reason for the low NO_x emissions is the diluting effect of the air used for the complete oxidation of gases inside the GT combustion chamber. Excess air was also added in order to constraint the temperature of combustion to 1173 K, this in accordance with the temperature limitations in the expander inlet. Due to this excess air, the oxygen content in the exhaust gases is around 16%, which value is higher than the WID specifications of 11% of oxygen content in table 4.1. As a result, NO_x emissions are

lower than 0.5 mg/m^3 which are under the emission limit value of table 4.1; therefore, its corresponding curve is unnoticeable in figure 4.6.

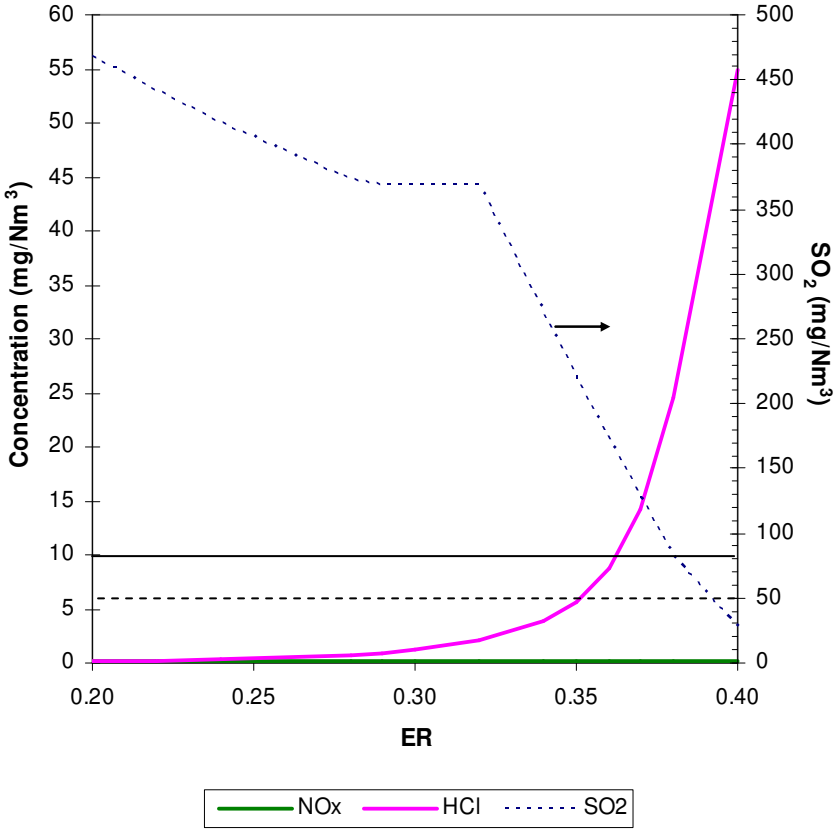

Figure 4.6 Effect of ER on pollutant emissions for Case D

Figure 4.6 shows a substantial decrease in SO_2 emissions at high ER values. At ER values greater than 0.33, gasification temperatures are greater than 970 K and calcium present in ash begins the retention of sulphur in the form of CaS, leading to the elimination of sulphur-containing gases, as seen in figure 4.7. This result agrees with a previous work from experiments of co-combustion of coal and poultry litter at a temperature of 1073 K that reported that poultry litter with high calcium and magnesium contents is capable of retaining sulphur in the ashes [158]. Therefore, the reduction of sulphur-containing gases during gasification decreases the formation of SO_2 inside the GT combustion chamber.

Figure 4.7 shows that at the ER value of 0.40 the calcination reaction occurs ($CaCO_3 \rightarrow CaO + CO_2$), wherein the gasification temperature is 1105 K. The calcination reaction is endothermic and favoured by higher gasification temperatures. It is known that above 800°C, the calcination reaction is kinetically favoured but at

temperatures above 900°C sintering may deteriorate the reactivity, porosity and surface area of the particles [159]. The reverse of the calcination reaction is carbonation, and is therefore exothermic.

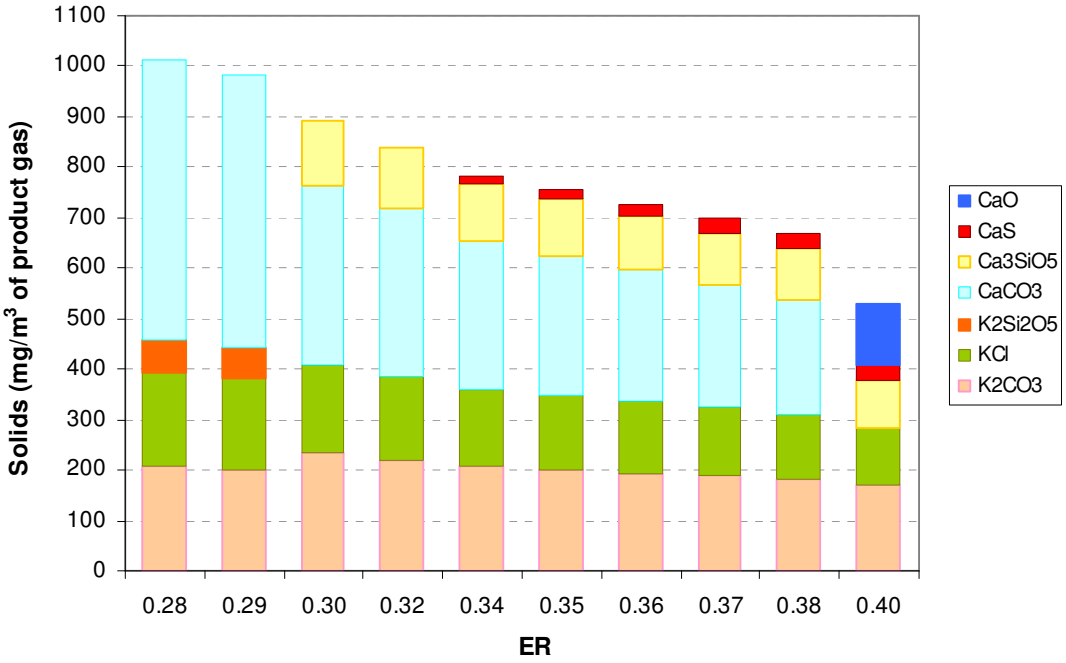

Figure 4.7 Potassium and calcium content in ashes in gasifier versus ER

Figure 4.8a shows that sulphur is initially released as H_2S and COS during gasification. These two sulphur-gases are converted to SO_2 during combustion inside the GT, as illustrated in figure 4.8b. At an ER value of 0.34, 73% of the sulphur present in poultry litter is converted to SO_2 inside the GT combustion chamber, whilst at an ER of 0.40 only 7% of fuel-sulphur in the form of SO_2 exits the De-NOx unit. The rest of the sulphur remains in the ashes as CaS. Thus, only at ER values greater than 0.39, SO_2 emissions are lower than 50 mg/m^3, as expected by the WID limits of table 4.1.

This work also showed that a molar ratio of calcium to sulphur of 3.3 in poultry litter retained up to 51.5% of the sulphur with a gasification temperature of 1027 K and an ER value of 0.40. The equilibrium calculations showed that when increasing the Ca/S molar ratio to 6.4, poultry litter ashes retain up to 79% at 1105 K and an ER of 0.40. Previous experiments on the combustion of coals of different sulphur contents showed that a much lower Ca/S mole ratio of 2.0 retained around 70% of sulphur in the ash using a combustion temperature of 1123 K [160].

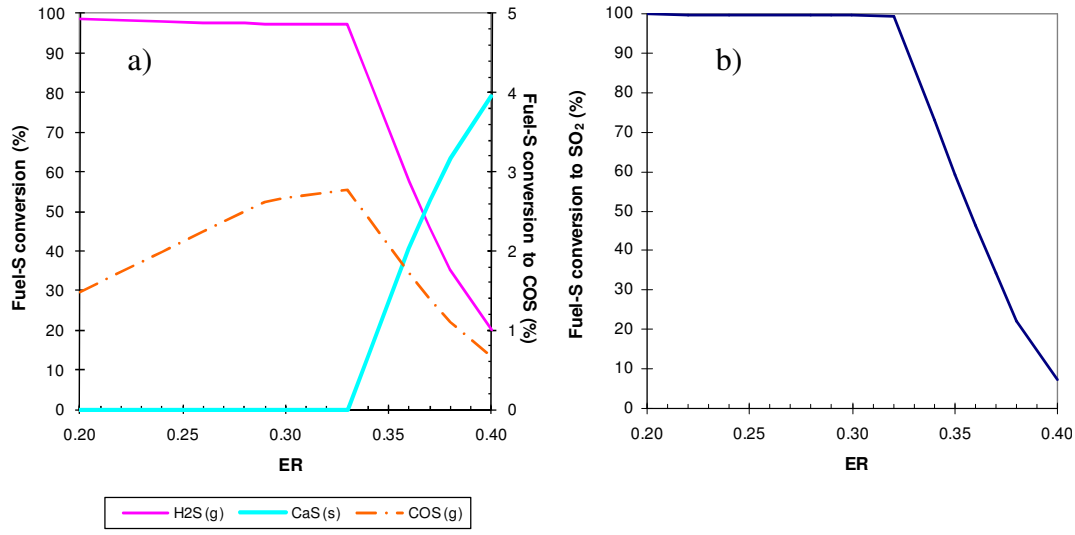

Figure 4.8 Fuel-sulphur conversion versus ER inside: a) gasifier and b) GT combustion chamber

Figures 4.7 and 4.9 show the fate of potassium during gasification. At ER values lower than 0.29, potassium remains in the solids as carbonate, chloride and disilicate ($K_2Si_2O_5$) fairly constantly. Figure 4.9 shows that at ER values greater than 0.29 the partition of potassium starts changing. The disilicate starts disappearing and KCl begins to evaporate at temperatures higher than 947 K. This agrees with a previous work on the simulation of KCl emissions from switchgrass combustion [162]. The Discrete Particle Method (DPM) was used to model the packed bed of solid fuel as composed of discrete particles with individual shapes and sizes. The fuel particles underwent various processes such as heating-up, drying, devolatilization, pyrolysis, gasification and combustion. They reported that the initial emission of potassium was caused by evaporation of KCl at 973–1103 K, and that the potassium that remained in the solids consisted of KCl, K_2CO_3, potassium silicate or bound to the organic matrix.

Figure 4.6 shows that HCl emissions are insignificant at low ER values since most chlorine remains in the ashes. Initially chlorine is mainly retained as solid KCl during gasification, as shown in figure 4.9. This agrees with Kuramochi et al.'s [161] work that showed that five of the six biomasses studied could retain chlorine as solid KCl at low temperatures up to 823–873 K. Solid KCl was not produced in any temperature range only for sewage sludge. They suggested that key elements for the formation of solid KCl are aluminum and silicon, which were employed in a phase

diagram composed of the Al–Si–K–O–Cl system at a fixed concentration of oxygen and chlorine using FactSage software. They found that if the potassium content was lower than the content of either Al or Si in the feedstock, such as in sewage sludge, the HCl emissions were relatively higher in all temperature ranges due to the lack of solid KCl formation. Although KCl easily forms during gasification in the presence of potassium, they identified that there was a specific composition of key elements that made the formation of KCl thermodynamically unstable.

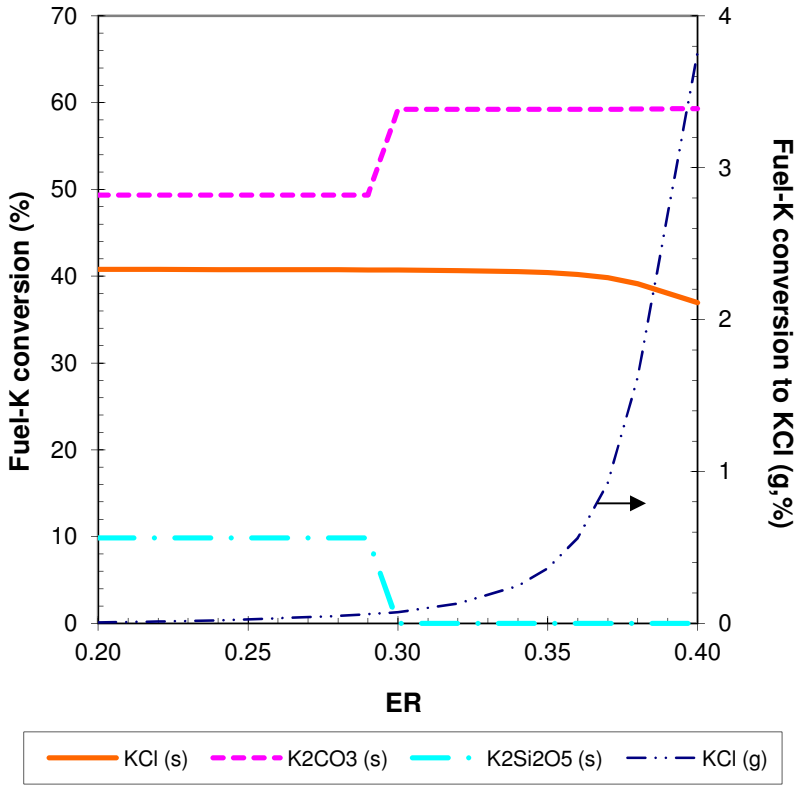

Figure 4.9 Fuel-potassium conversion inside gasifier versus ER

At ER values greater than 0.29, gasification temperatures are higher than 947 K and the chlorine present in ash starts to vaporise as KCl, NaCl and HCl, as shown in figure 4.10a. Fuel-chlorine is converted up to 9.2% to KCl gas and less than 0.6% to NaCl and HCl gases. Figure 4.10b shows that HCl is the main gas generated in the GT combustion chamber. Therefore, low production of chlorine-containing gases during gasification requires the selection of an ER that does not exceeds an ER value of 0.36, which ensures an HCl emission below the WID limit of 10 mg/m^3 (shown in figure 4.6).

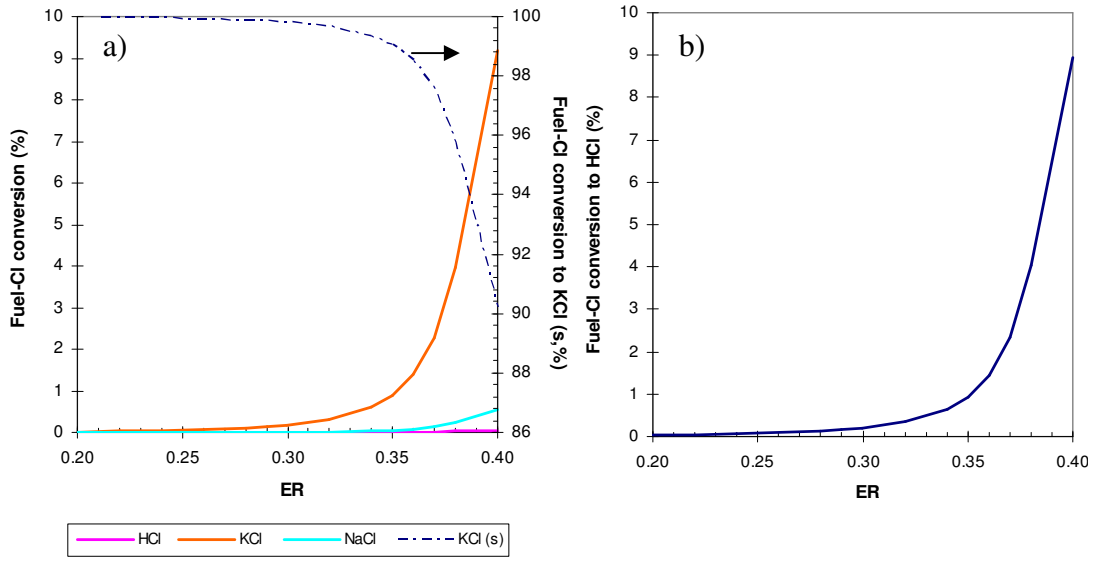

Figure 4.10 Fuel-chlorine conversion versus ER inside: a) gasifier and b) GT combustion chamber

In conclusion, the selection of the proper ER to minimise the emission of pollutants, will be a compromise. Low ER values have the benefit of generating low HCl emissions but with the disadvantage of releasing very high SO_2 emissions. The preferred ER value of 0.29, which can potentially provide the best process efficiency of 33% with a gasification temperature of 940 K, will conveniently emit less than 1 mg/m^3 of HCl, however, the emission of SO_2 will be as high as 368 mg/m^3. Even the selection of a higher ER value, e.g. an ER of 0.36, will emit less than 10 mg/m^3 of HCl but still 172 mg/m^3 of SO_2 at a gasification temperature of 1020 K.

H_2S removal processes include solid sorption and adsorption. Solid sorption is suitable for low H_2S concentrations. Common adsorbents employed are the oxide of Fe, Mn, Zn, Cu and Ca. One example is char-supported Fe–Mo sorbents which showed to be effective reducing sulphur containing impurities from coal gases at temperatures below 773 K. The activated char contributed to the high reactivity of the sorbents due to the active pore structure and uniform dispersion of the metal oxides. Sulphur uptake by the sorbents showed to increase by increasing the iron loading level of the char. The addition of Mo into the char-supported Fe sorbents significantly increased the desulfurization efficiency [50]. However, most sorbents cannot be regenerated and must be disposed after being used. Solid sorption processes that use sorbents such as zinc-titanate and zinc ferrite which can be

regenerated are still under development [163]. Adsorption with molecular sieves is a feasible option when the gas contains heavier S compounds (such as mercaptane and COS) that must also be removed. Also water and CO_2 are removed in large quantity.

4.2 Calorific value of poultry litter

The influence of fuel composition on the LHV of product gases and on process efficiency was examined by varying the LHV of poultry litter. Since the LHV of biomass depends on its elemental composition, mainly the composition of carbon, hydrogen, and oxygen was varied. This variation was carried out over a range of fuel compositions: C/O ratio of 0.8 to 1.4 wt% and C/H ratio from 6 to 15wt%. In order to get comparable results, the ER, moisture content, and ash content were kept constant, as 0.26, 25 wt% and 21.63 wt% (dry), respectively.

Figures 4.11 shows that increasing the LHV of poultry litter increases the LHV of product gases.

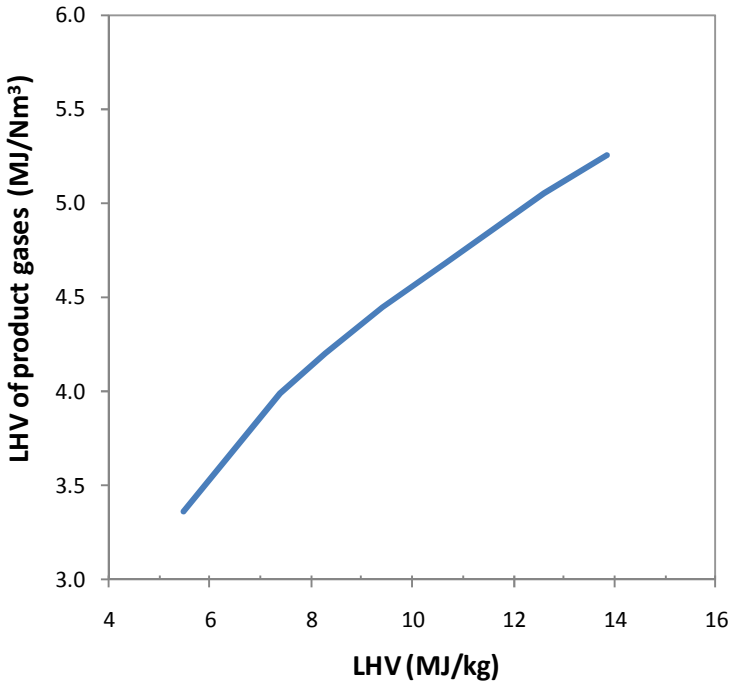

Figure 4.11 LHV of product gases versus LHV of poultry litter with an ER of 0.26 and moisture content of 25%

Figure 4.12 shows a linear relationship between the LHV of poultry litter and the process efficiency, in the range of LHV analysed. The LHV of poultry litter that

has been used in this work is of 11.4 MJ/kg, which delivers a LHV of product gases of 4.8 MJ/Nm^3 and process efficiency of 32% using an ER value of 0.26.

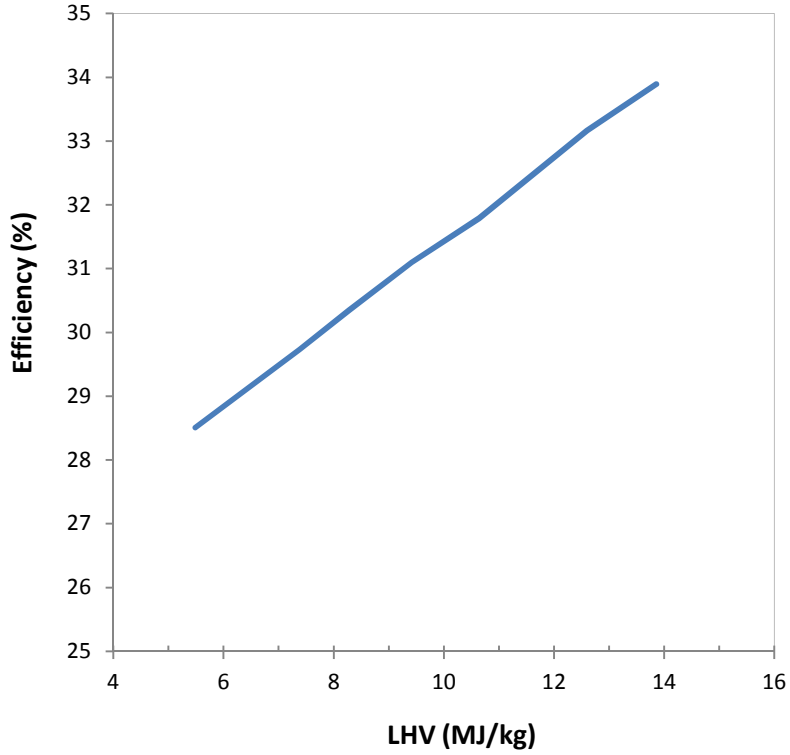

Figure 4.12 Process efficiency versus LHV of poultry litter with an ER of 0.26 and moisture content of 25%

4.2.1 Moisture content

The selection of the operating conditions greatly depends on the quality of the feedstock used. The moisture content in poultry litter can vary depending on the season and the storage practices followed within the farms. The effects of moisture content together with ER changes were evaluated. Figure 4.13 shows a graph of cold gasification efficiency versus a range of moisture content values, each curve represents a different ER value employed for gasification.

Figure 4.13 and 4.14 show that the cold gasification efficiency and process efficiency decrease with increases in moisture content. For ER values greater than 0.30, the efficiencies decrease steadily with increasing moisture content. For lower ERs, the decrease in efficiency is more gradual; for an ER value of 0.20, there is a range of moisture content, 30–40%, where the efficiency remains almost constant.

This range of moisture content corresponds to gasification temperatures lower than 850 K, which allows the reheating of product gases with the hot GT exhaust gases. For this reason, it is seen that at high moisture contents, the efficiencies are higher for lower ER values.

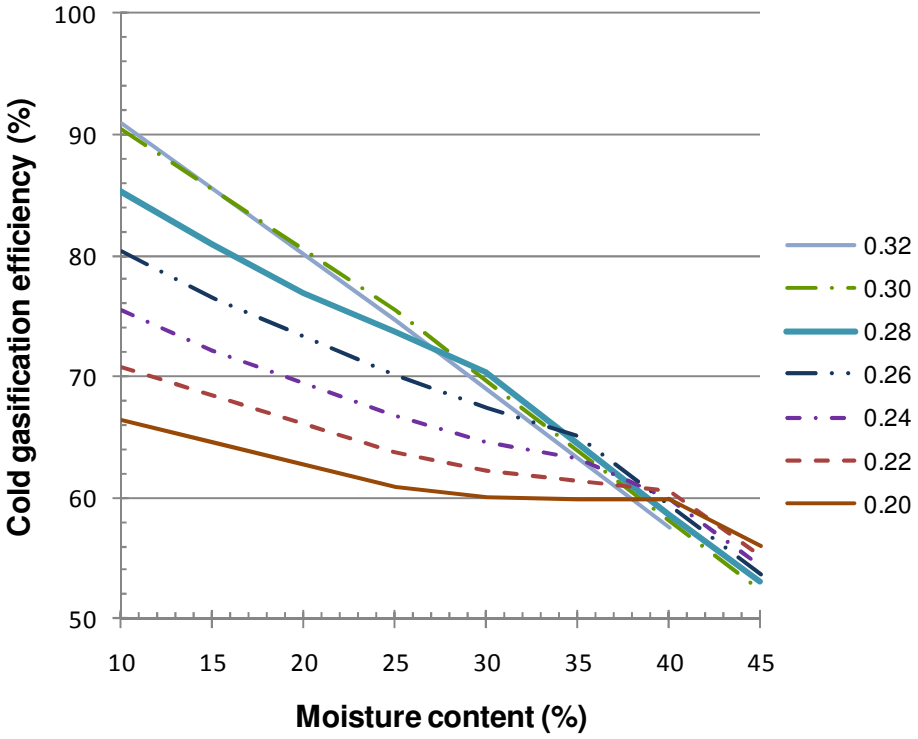

Figure 4.13 Cold gasification efficiency versus moisture content at various ER values

Figure 4.15 shows in bars the composition of inorganics in the gas phase using different values of moisture content of poultry litter, and the line represents the gasification temperature. With increases of moisture content HCl, KCl, NaCl and KOH were minimised in the gas phase because the gasification temperature is reduced with higher moisture content.

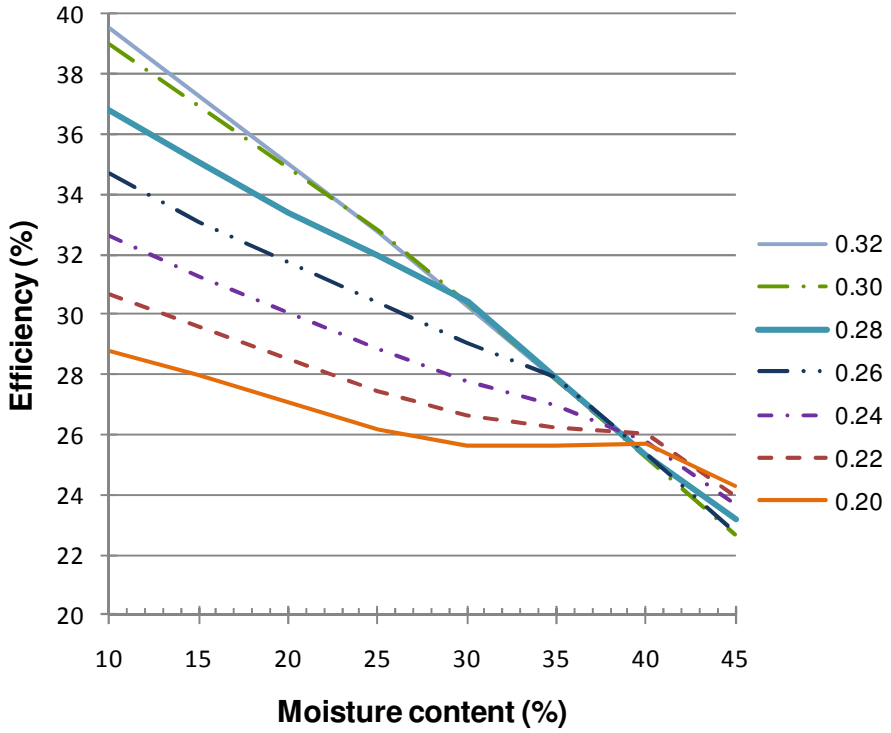

Figure 4.14 Process efficiency versus moisture content at various ERs

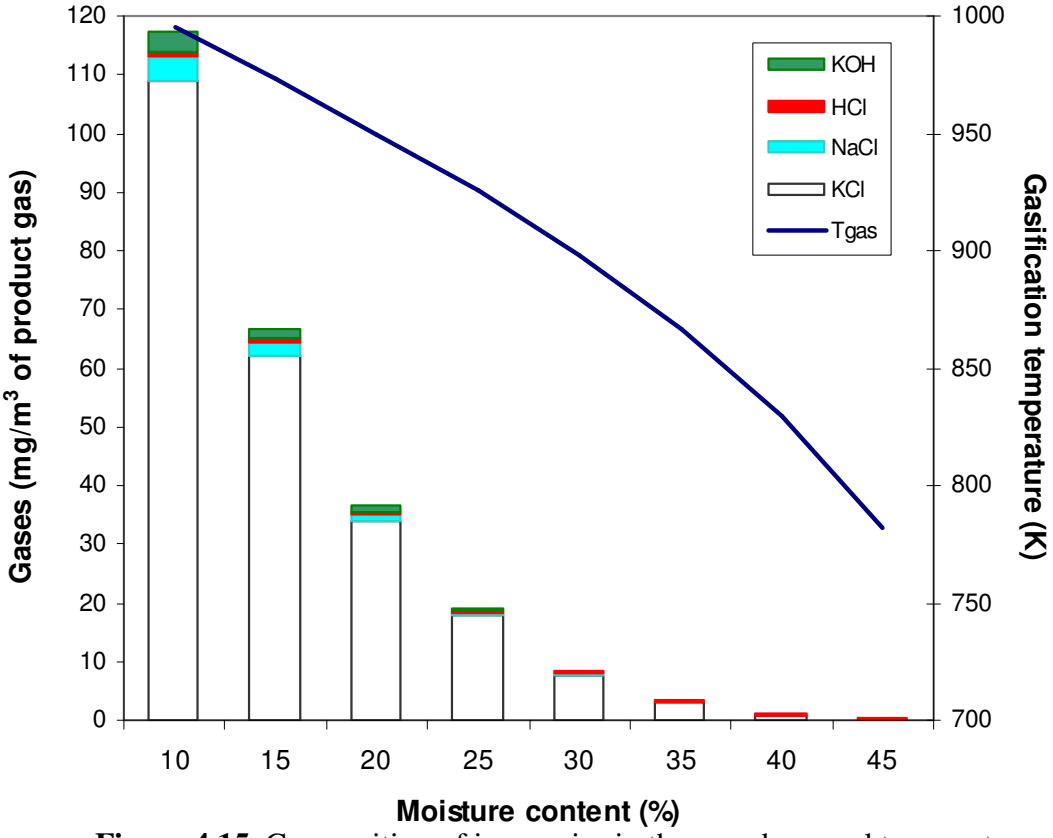

Figure 4.15 Composition of inorganics in the gas phase and temperature of gases varying moisture content with ER of 0.28

Figure 4.16 shows the composition of inorganics leaving the gasifier along with the gas stream as dust. At high temperatures (> 950 K), sulphur was captured in the solid phase as CaS which reduced the amount of H_2S in the gas phase from 3.0 to 0.8 g/m^3 of product gas. At temperatures higher than 950 K, Ca_3SiO_5 also appeared in the solid phase and more potassium was captured as $K_2Si_2O_5$. The concentrations shown in figure 4.16 represent 1% of the solids constituents of the ashes.

The inclusion of ash constituents in the simulation showed that a wetter fuel helps to maintain the vaporisation of chlorine and sodium to lower levels. The total amount of solids was kept fairly constant despite char being completely gasified at moisture contents greater than 25%.

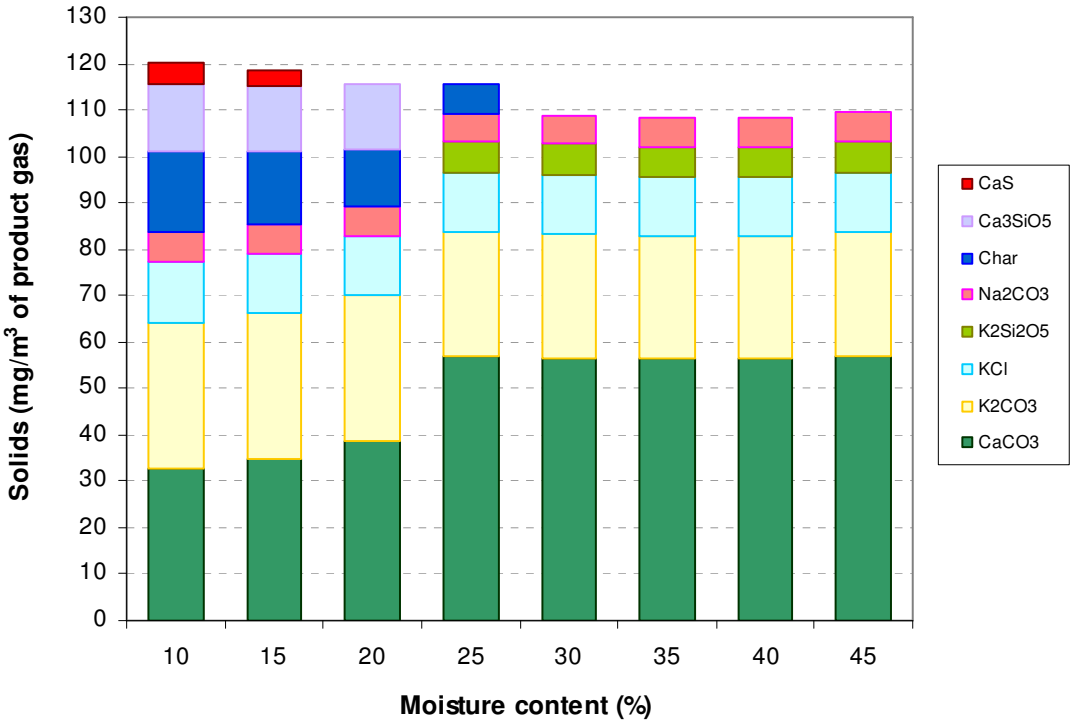

Figure 4.16 Composition of inorganics in gas stream varying moisture content with an ER of 0.28

Table 4.2 shows the inorganic concentrations in the product gases after gasification. The first two columns show the inorganics and their maximum allowable concentration according to the GT fuel requirements as established in [52]. The third column indicates the ER values that satisfy the limits when moisture content of poultry litter is of 25%. The fourth column shows what inorganics are below the limit values at various moisture contents when the ER is of 0.28. The table

shows that Na is under tolerable values at the ER and MC values analysed. For K and HCl, maximum ER and/or MC values should not be exceeded to maintain inorganic gases below fuel requirements. Sulphur exceeds limits at all ranges, only SO_2 is found at insignificant amounts, whilst COS and H_2S exceed limits and are oxidised in the GT combustor.

Although equilibrium calculations provide a good evaluation of the tendencies due to the variation of ER and moisture content, these calculations have been previously proved to predict higher potassium, sodium and chlorine concentrations than the experimental concentration results [164].

Table 4.2 Comparison of fuel requirements for gas turbines and inorganic concentrations after gasification

Component	Allowable concentration [52]	Concentrations and parameters to maintain specifications after gasification (this work)	
		Moisture content : 25%	ER = 0.28
HCl	< 0.5 ppm	< 0.5 ppm (at ER $\leq$ 0.35)	< 0.5 ppm (with any moisture content)
Na	< 1-2 ppm	< 1.5 ppm (at ER $\leq$ 0.36)	< 1.2 ppm (with any moisture content)
K	< 1-2 ppm	< 1.5 ppm (at ER $\leq$ 0.22)	< 2.5 ppm (with MC > 30%)
S (SO_2 + H_2S + etc)	1 ppm	SO_2 << 0.01 ppm COS > 17 ppm H_2S > 320 ppm	SO_2 << 0.01 ppm COS > 17 ppm H_2S > 320 ppm
Other metals	< 1-2 ppm	-	-

4.3 Pressure ratio of gas turbine

The effects of pressure on gas yields [147] and gasifier temperature, lower heating value (LHV) of gas, and exergy efficiency [165] were previously studied for

biomass gasification. In addition, an optimum pressure of approximately 13 bar was found based simply on the maximum cold gasification efficiency achievable; it was assumed that 25% of the amount of air for stoichiometric combustion was employed and air inlet was at ambient temperature during the simulation of wood gasification [140]. However, these studies were only concerned with gasification and did not take into account the effects of pressure when a turbine engine is integrated into the gasification process. Therefore, the effects of varying the pressure ratio of the gas turbine on carbon conversion, product gas temperature, product gas composition, higher heating value of gases and process efficiency were evaluated.

Two conditions were assumed in the energy integration system (EIS), as proposed in [166] for case D. The first one that the temperature of air was constrained to 724 K in order to evaluate the effects of pressure at the same temperature, and the second one that the temperature approach of the EIS was 20 K, for all the pressure ratios evaluated. The latter case represents the use of 'Stage 4' as the EIS.

Figure 4.17 shows the gasification temperature versus pressure when air was preheated to 724 K. It is seen that the temperature increases as expected with increasing pressure. This agrees with the trend previously shown using gasifier pressures of 10-20 bar for manure gasification [165]. The temperature at 10 bar in this work is 952 K and in the Srinivas et al.' work of 1140 K; however, the conditions used were different. In this work an ER value of 0.29 and moisture content of 25% are employed, whilst the other work used an ER of 0.1, steam fuel ratio (SFR) of 1 (steam and air injected at the same temperature and pressure) and the moisture content of manure was neglected. The difference in temperatures is due to the assumption in the present work that energy from the gasification reactions is used to drive the flash pyrolysis. If it were assumed an ER of 0.1, SFR of 1, temperature of air and steam of 614 K and dry litter, the gasification temperature would be 1076 K at 10 bar when eliminating the heat stream Q-DECOMP of figure 3.1.

In the energy integration system when the temperature approach is set as 20 K, the gasification temperature also increases with pressure, especially at lower pressure ratios as shown in figure 4.17. Gasification temperatures with temperature approach of 20 K are higher than in the constrained case at low pressure ratios due to the higher temperatures of preheated air (as illustrated in figure 4.18).

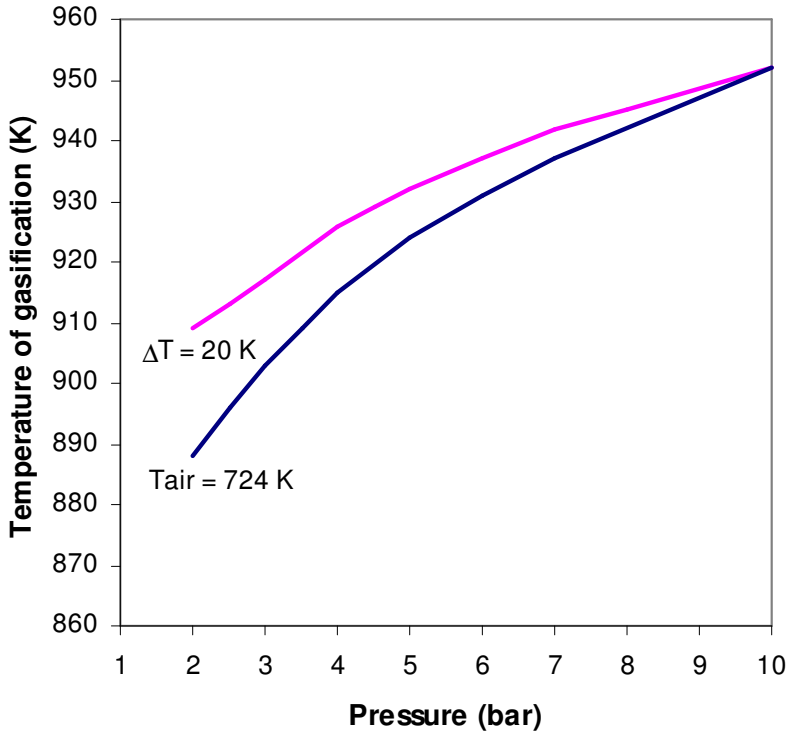

Figure 4.17 Gasification temperature versus pressure when temperature of air is at 724 K, and when temperature approach of energy integration system is 20 K

Figure 4.18 depicts the exhaust temperatures of the turbine and compressor versus pressure ratio. It can be seen that the turbine exhaust temperature decreases with pressure ratio whilst the compressor exhaust temperature increases as expected. More energy is available for integration at lower pressure ratios due to higher turbine exhaust temperatures which can preheat the cooler compressed air.

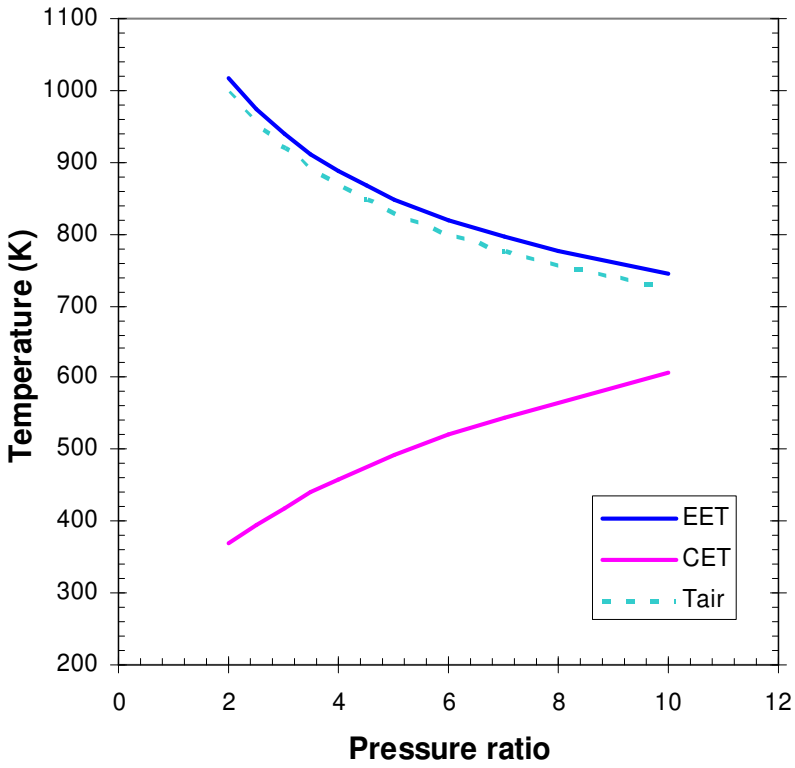

Figure 4.18 Expander exhaust temperature (EET), compressor exhaust temperature (CET) and temperature of preheated air (Tair) vs. pressure ratio with a temperature approach of 20 K in the EIS

Figure 4.19 shows the product gas composition versus gasifier pressure when the temperature of air is at 724 K. This figure shows that methane and water vapour increase with higher pressure, whilst hydrogen decreases. No significant difference is observed for CO and CO_2 concentration with changes in pressure.

For wood gasification, it was earlier found from simulation work that pressure increases favoured CH_4 formation and simultaneously reduced CO and H_2 formation up to a pressure of 12-13 bar [140]. In contrast, other work reported that no significant influence of pressure was revealed on gas composition during the gasification of four types of biomasses [165]. However, in Srinivas et al. [165] work, the temperature of air was not kept constant with pressure changes since the increase in pressure ratio increases the compressed air temperature, which could have neutralised the effects of pressure.

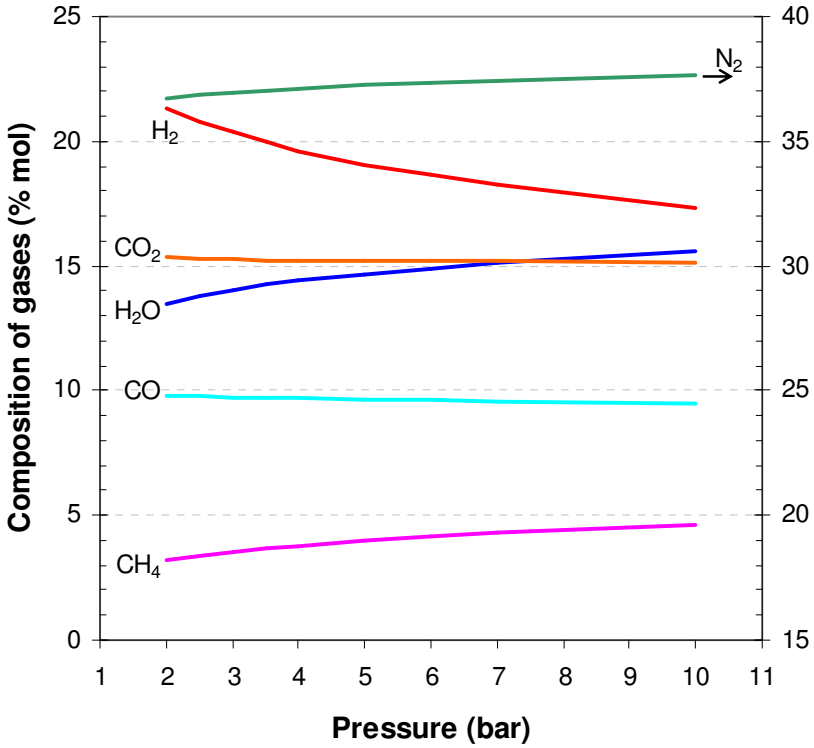

Figure 4.19 Composition of gases versus pressure when temperature of air is at 724 K

Figure 4.20 shows the effects of gasifier pressure on HHV of gases. Since the content of methane, hydrogen and carbon monoxide impact on the HHV, its value is expected to change with pressure. However, the graph shows only a slight increase in the HHV when preheated air is constrained to 724 K. The increase in methane concentration (figure 4.19) and gasifier temperature (figure 4.17) compensate the decrease in CO and H_2 concentrations. When the temperature approach is fixed as 20 K in the EIS, the HHV slightly increases up to a pressure ratio of around 4.5. Afterwards, the HHV decreases steadily because the decline in CO and H_2 concentrations together with the drop in the temperature of the gasifying air overcome the increase in methane concentration.

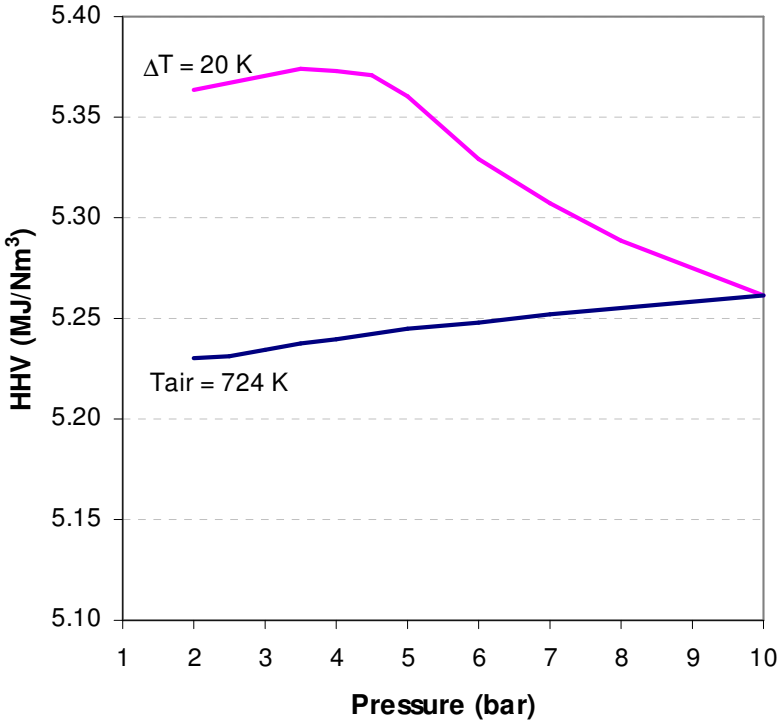

Figure 4.20 HHV of gases versus pressure when temperature of air is at 724 K and with a temperature approach of 20 K

Figure 4.21 illustrates the effects of pressure on carbon conversion. Because the gasifier temperature increases with pressure, carbon conversion slightly improves with increasing pressure when the temperature of preheated gasifying air is kept constant (724 K). When the temperature approach is established as 20 K in the EIS, carbon conversion is complete up to a pressure ratio of 4.17, whilst carbon conversion decreases steadily at higher pressure ratios. This decline in carbon conversion is attributable to the significant reduction of gasifying air temperature, from 998 K at a pressure ratio of 2 to 724 K at pressure ratio of 10, as shown in figure 4.17.

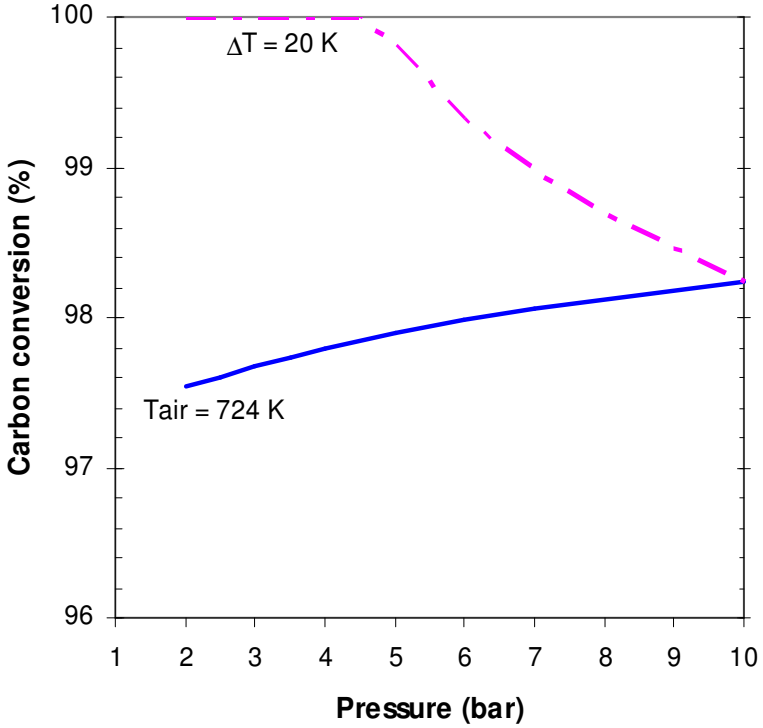

Figure 4.21 Carbon conversion versus pressure when temperature of air is at 724 K and with a temperature approach of 20 K

Figure 4.22 shows that increasing the pressure ratio improved the process efficiency up to a maximum, at a pressure ratio of 7, when the preheated air temperature is constrained to 724 K. At low pressure ratios not all the energy from the GT exhaust gases is recuperated. However, when the heat integration was improved using a temperature approach of 20 K in the energy integration system, lower pressure ratios provided higher efficiencies because for this case all the heat from the GT exhaust gases is integrated into the gasification and GT combustion processes.

These results confirm that higher pressure ratios are recommended for the simple Brayton cycle, but for the Brayton cycle with heat-exchange, lower pressure ratios achieve higher efficiencies.

Nonetheless, at pressure ratios lower than 3.5, the heat exchanger becomes the critical element because it would require the use of high temperature heat exchangers, which are considered when operating at temperatures above 923 K [167]. As a result, intermediate pressure ratios (4–6) seem more convenient because they do not require expensive heat exchangers that have to stand high temperatures and provide low temperature approaches.

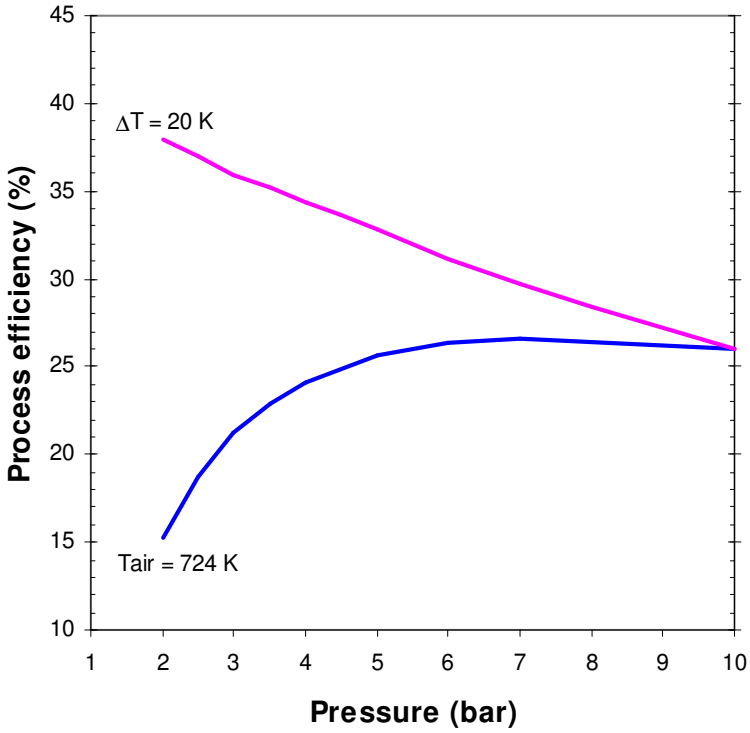

Figure 4.22 Process efficiency versus pressure ratio when temperature of air is at 724 K, and when temperature approach of EIS is 20 K with EIT of 1173 K

4.4 Turbine inlet temperature

In previous sections, the expander inlet temperature was constrained to 1173 K. This section, however, evaluates the effects of increasing the maximum expander inlet temperature (EIT), with the objective of improving the process efficiency. Figure 4.23 illustrates the process efficiency when the EIT was raised to two additional temperatures, 1273 K and 1373 K, at various pressure ratios in the GT.

The two conditions assumed in section 4.3 were used for the energy integration system (EIS) for all the pressure ratios evaluated. The first condition was that the temperature of air was constrained with the purpose of evaluating the effects of pressure when the temperature of air is the same in all the cases. The second condition consisted of using the same temperature approach of 20 K in the EIS. The temperature of air, for the case of the constrained temperature, was selected according to the expander exhaust temperature at a pressure ratio of 10 on account of being the lowest exhaust temperature, as illustrated in figure 4.24.

Figure 4.23 shows that process efficiency was improved by increasing the expander inlet temperature, as a result of the rise in the expander exhaust temperature

(shown in figure 4.24). The higher expander exhaust temperatures allow preheating air and product gases to reach higher temperatures and more energy can be integrated into the system. Therefore, at lower pressure ratios more energy is recuperated by preheating the product gases and air before entering the GT combustion chamber when the temperature approach in the EIS was of 20 K. The increment in efficiency was more pronounced at higher pressure ratios, especially when the temperature of air was constrained. The parameters constrained, such as expander inlet temperature, might entirely depend on the operating specifications of commercial gas turbines.

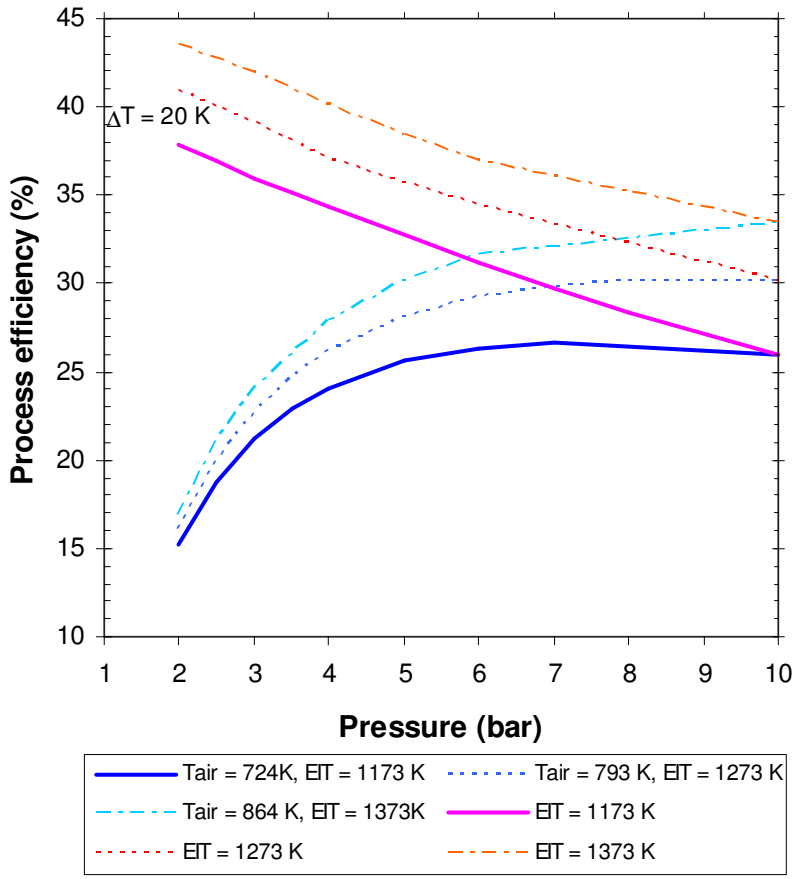

Figure 4.23 Process efficiency versus pressure ratio when temperature of air is constraint and when temperature approach of EIS is 20 K at various expander inlet temperatures (EIT)

One commercially available gas turbine is the Turbec T100 model which is a microturbine with combined heat and power unit [168]. The microturbine is designed to be fuelled with natural gas and can deliver 105 kW of net power output. The Turbec T100 operates with a pressure ratio of 4.5 in the GT compression and

expansion sections. The maximum expander inlet temperature is of 1223 K and the temperature of the exhaust gases is approximately 923 K; therefore, these parameters imply an isentropic efficiency of 80%.

The 501-KB5 gas turbine from Rolls-Royce was designed to deliver 3,938 kW of net power output. This machine utilizes a pressure ratio of 9.4 for the compressor and expander. The maximum allowable operating expander inlet temperature is of 1,308 K and the temperature of the exhaust gases is approximately 833 K, which implies a required isentropic efficiency of 87%.

As a result, the isentropic efficiency assumed in this work of 85% is between the Turbec T100 of lower power capacity and the Rolls-Royce 501-KB5 of much higher power output.

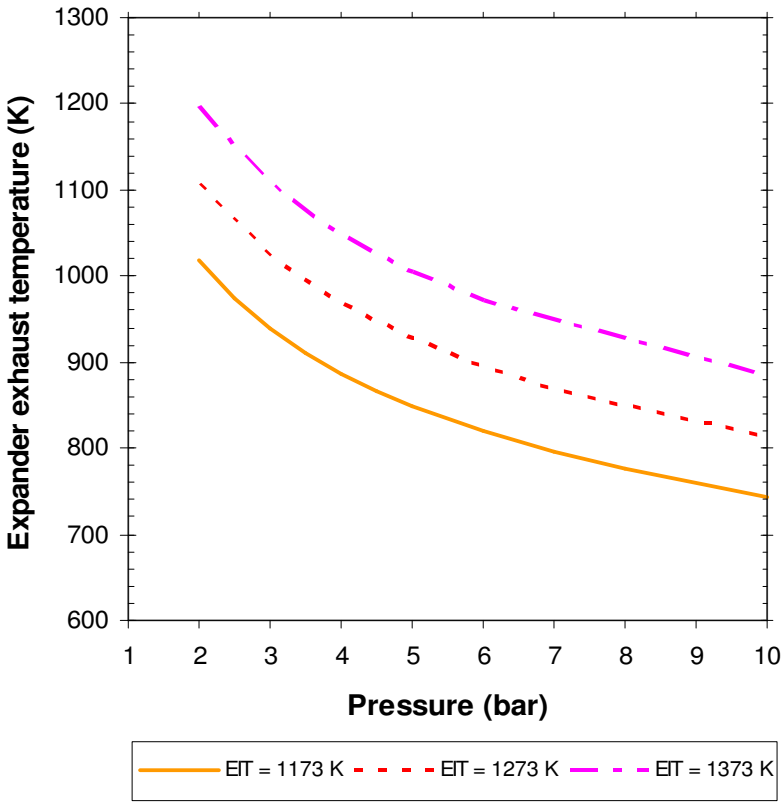

Figure 4.24 Expander exhaust temperature versus pressure for various expander inlet temperatures (EIT)

4.5 Temperature approach of heat exchangers

The temperature approach for the three heat exchangers of the 'Stage 4' network was varied to evaluate possible improvements in the process efficiency. The

efficiency improved linearly from 30% to 34% when changing the temperature approach from 50 K to 5 K, respectively, using an ER value of 0.29, as shown in figure 4.25.

In previous sections, a temperature approach of 20 K was employed. The use of a lower temperature approach, such as 5 K, provides a process efficiency increment of 1.5% points; however, the selection of this value will depend on current commercial equipments and also might require a greater surface area.

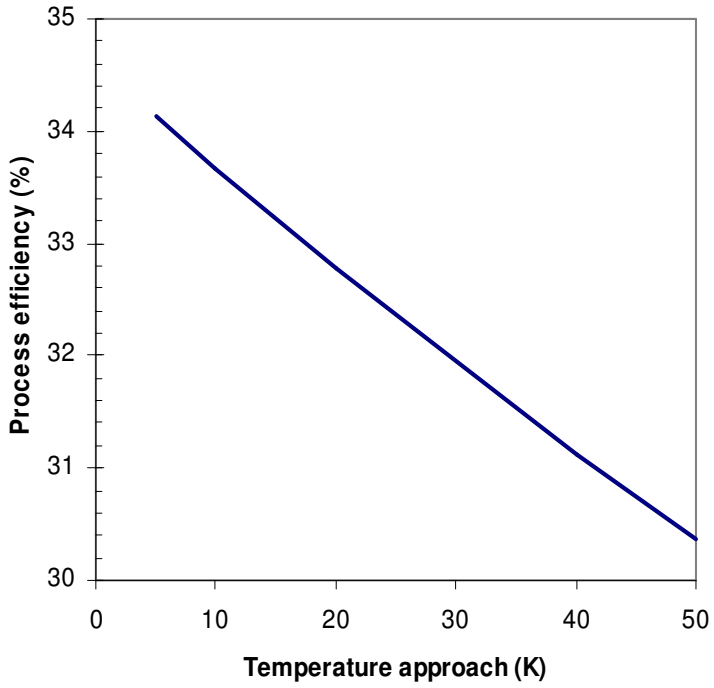

Figure 4.25 Process efficiency versus temperature approach

Meggitt (UK) Limited trading as Heatric produces plate type exchangers PCHE, which are stacked and diffusion-bonded together to form strong, compact, all-metal heat exchange cores. These heat exchangers can stand high temperatures of up to 900°C, incorporate more than two process streams into a single unit, and be up to 85% smaller and lighter than the equivalent shell and tube exchanger. The counter current design enables temperature approaches of 3-5°C [169]. Bronswerk heat transfer BV (The Netherlands) designs and manufactures shell and tube heat exchangers in all kinds of special materials according to international standards. The company claims that these heat exchangers can stand high pressure, corrosive environment and temperatures up to 800°C with temperature approaches of up to

10°C [5]. These two examples of commercial exchangers show the possibility to operate with very small temperature approaches in high temperature heat exchangers.

4.6 Pressure drops in system

In order to analyse the effects of pressure drops, pressure drops were assumed in the gasifier. Figure 4.26 shows that process efficiency decreases linearly with increases in pressure drop. The gasifier pressure was maintained as 5 bar and the compression ratio was increased depending on the pressure drop assumed; therefore, the higher compression ratio requires more power to drive the gas turbine compressor, which ultimately reduces the overall process efficiency. With a pressure drop of 0.3 bar, the process efficiency decreases by only 1.5% points.

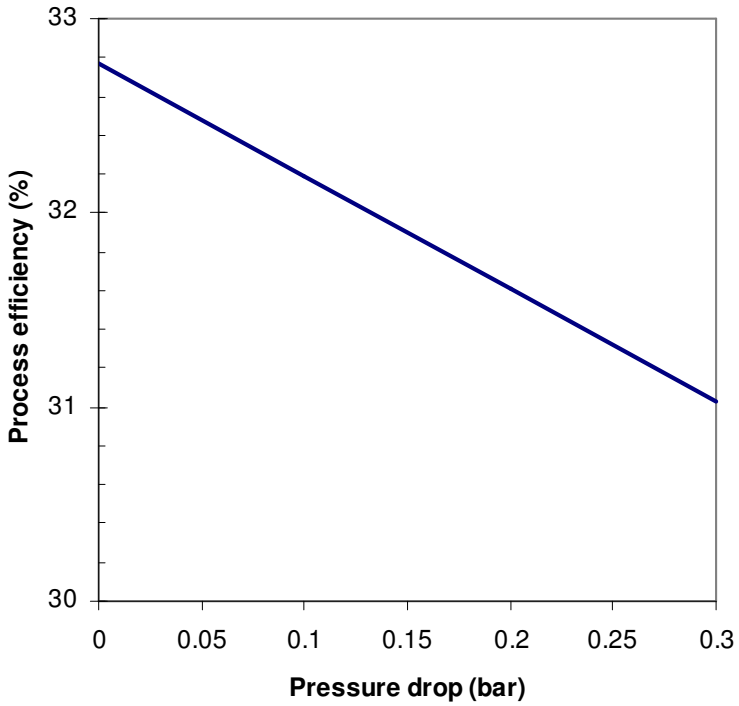

Figure 4.26 Process efficiency versus pressure drop in gasifier

It has been reported that a maximum process efficiency of 33% can be delivered at an ER value of 0.29. However, this value could decrease if the temperature approach of heat exchangers is lower than 20K or if pressure drop is experienced during gasification.

4.7 Summary of findings

This work shows a solution for a small scale process that operates with a comparable efficiency to large scale options. This is due to the effective energy recuperation into the gasification process and gasifying air. The addition of the energy integration system is shown to be much more significant than the effect of pressure.

Four case studies were evaluated, 'atmospheric' versus 'pressurised' layouts with the addition of energy recuperation as chosen in chapter 3. This chapter shows that efficiencies of up to 24% and 33% are achievable with the, 'atmospheric layout' (base case) and 'pressurised layout' (case D), respectively, where 200 kW of net power are generated.

When only cold gasification efficiency was analysed, no significant difference among the two case studies was observed. Therefore, this parameter can mislead the comparison because it only provides the best ER for each layout without a considerable difference in the CGE. Nevertheless, CGE together with LHV and carbon conversion allow identification of the optimum ER for each case. Process efficiency analyses highlighted the best layout to achieve maximum integration.

Two cases in the energy integration system were evaluated to analyse the effects of pressure ratio on the gasifier and gas turbine performances, as well as on the overall process efficiency. Process efficiency analyses showed the best pressure ratio to achieve maximum integration. Pressure ratios from 4 to 6 were recommended as they delivered process efficiencies of 34.4–31%, respectively. Additionally, increasing the turbine inlet temperature improved the process efficiency.

On the other hand, the selection of the proper ER will be a compromise to achieve minimum emission of pollutants. Low ER values have the benefit of generating low HCl emissions and good process efficiency but with the disadvantage of releasing very high SO_2 emissions. High ER values did not show to reduce the SO_2 emissions enough to comply with the guidelines. Therefore, H_2S removal seems to be necessary for the reduction of SO_2 emissions.

Inorganic studies showed that calcium and silicon were found in the solid phase. Chlorine was retained in the solids as KCl. However, at high temperatures (with high ERs or low MCs) NaCl, KCl, HCl and KOH are found in the gas phase. These gases are of great concern in gas turbines because they can increase rates of

hot corrosion on turbine surfaces. At high temperatures (> 950K), H_2S concentration is lower since sulphur remains in the solid phase as CaS. These studies suggest operating at low temperature, selecting low ER values and wet fuels. To minimise the vaporisation of inorganic species, and in particular of potassium, an ER of 0.26 or lower or for greater ERs increasing moisture content is more convenient. For K and HCl, maximum ER and/or MC values should not be exceeded to maintain inorganic gases below fuel requirements. However, H_2S and COS exceed the limits, only SO_2 was found at insignificant amounts.

Chapter 5

Modelling of fluidised bed gasification: kinetic model

The success of biomass gasification requires a reliable system that delivers a quality product. Therefore, tar elimination from the product gas is the ultimate goal to make gasification an attractive option. The presence of tar can cause operational problems because of the possible formation of aerosols, soot formation due to repolymerization, and interaction of tar with other contaminants on fine particles. In addition, heavy tars may condense on cooler surfaces downstream which can lead to blockage of particle filters and of fuel lines. This chapter describes the fundamentals of the proposed mechanism for tar formation and evolution, as well as of the model for the simulation of a fluidised bed gasifier.

5.1 Background on tar formation and evolution

During thermal conversion processes, one by-product formed is tar. The initial pyrolysis tars are often called primary tars, which are further transformed into secondary and tertiary tars at higher temperatures. Primary tars have been identified as consisting of mainly oxygenated compounds produced at 400–700°C. Secondary tars are produced at around 700–850°C and comprise of phenolics and olefins; whilst tertiary tars are formed at temperatures around 850–1000°C and consist of complex aromatic compounds [170]. As part of the tertiary tars, aromatics such as polycyclic aromatic hydrocarbons (PAH) are found. These by-products affect the end-use of the gasification product, causing problems such as pipeline plugging and damage to gas engines. Therefore, some mechanisms are proposed in the literature with the aim to understand the generation of PAH leading to soot formation, as described below:

i. Direct combination of aromatic rings, for example the combination of two rings to produce biphenyl.
ii. H_2-abstraction-C_2H_2-addition (HACA) sequence. Aromatic rings grow by H-abstraction forming a radical compound, followed by acetylene addition which propagates molecular growth by cyclisation.
iii. Phenol precursor for PAH formation. Phenol is transformed to cyclopentadiene and CO is abstracted from the phenol [171]. After that, cyclopendienyl radicals combine to form bigger compounds, e.g. aromatic compounds from naphthalene to chrysene [172].

Figure 5.1 shows a mechanism found in the literature for soot formation according to Fitzpatrick et al. [173]. This mechanism was proposed for the co-firing of coal and pine wood based on the species identified from their experimental findings and known mechanisms for PAH growth. The model consisted of three routes for soot formation: i) starting with coal and/or wood pyrolysis and oxidation products, wherein aliphatic species formed acetylene involved in the HACA mechanism to be transformed into PAH species of one to four aromatic rings; ii) through the so-called soot nucleation, in which soot precursors nucleate by association of the four-aromatic ring species and grow, it included the oxidation of soot particles; and iii) reactions of tar species, including side-chain cracking and decomposition and reaction via cyclopendienyl radicals. Since wood has a less aromatic nature than coal, HACA was suggested as having a more important role for biomass soot formation.

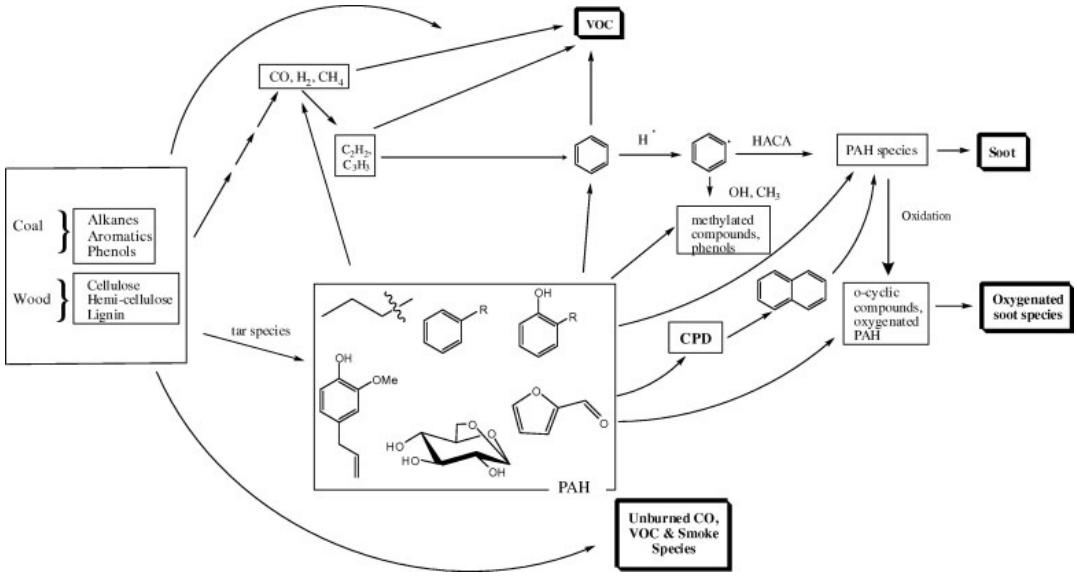

Figure 5.1 Proposed routes for the co-combustion of coal and wood. HACA: H-abstraction-C_2H_2-addition. CFD: cyclopentadiene [173]

5.1.1 Tar precursors

Biomass composition includes lignin, cellulose and hemicellulose. Lignin fraction normally consists of 20–40 wt% dry of biomass. Lignin is a complex racemic polymer and is composed of p-hydroxyphenyl, guaiacyl and syringil units [174]; an example of a typical lignin structure is shown in figure 5.2. Since only the lignin fraction of the biomass is aromatic in nature, lignin represents a potential precursor for PAH formation. In the case of poultry litter, around 6.3% of the total carbon has an aromatic origin [77].

Lignin pyrolysis is known to produce non-condensable gases, char, and condensable tars comprising several low and high molecular weight phenolic compounds, at low to moderate temperatures (<700°C) [174]. Oxygenated compounds are the most dominant products during the pyrolysis of biomass from both cellulose and lignin; mainly guaiacols with some furans and sugar derivatives such as levoglucosan which predominantly arises from cellulose even above 600°C [173].

Experimental studies have shown that cellulose pyrolysis produces levoglucosan as an intermediate product, which then converts to tar compounds [175]. Besides levoglucosan, other primary tar components are produced after

cellulose pyrolysis such as, furfural, glycolaldehyde, hydroxyacetone, formic acid and acetic acid. Increasing yields of CO, CH_4 and H_2 were linked to decreasing yields of levoglucosan, glycolaldehyde, formic acid and furfural [176].

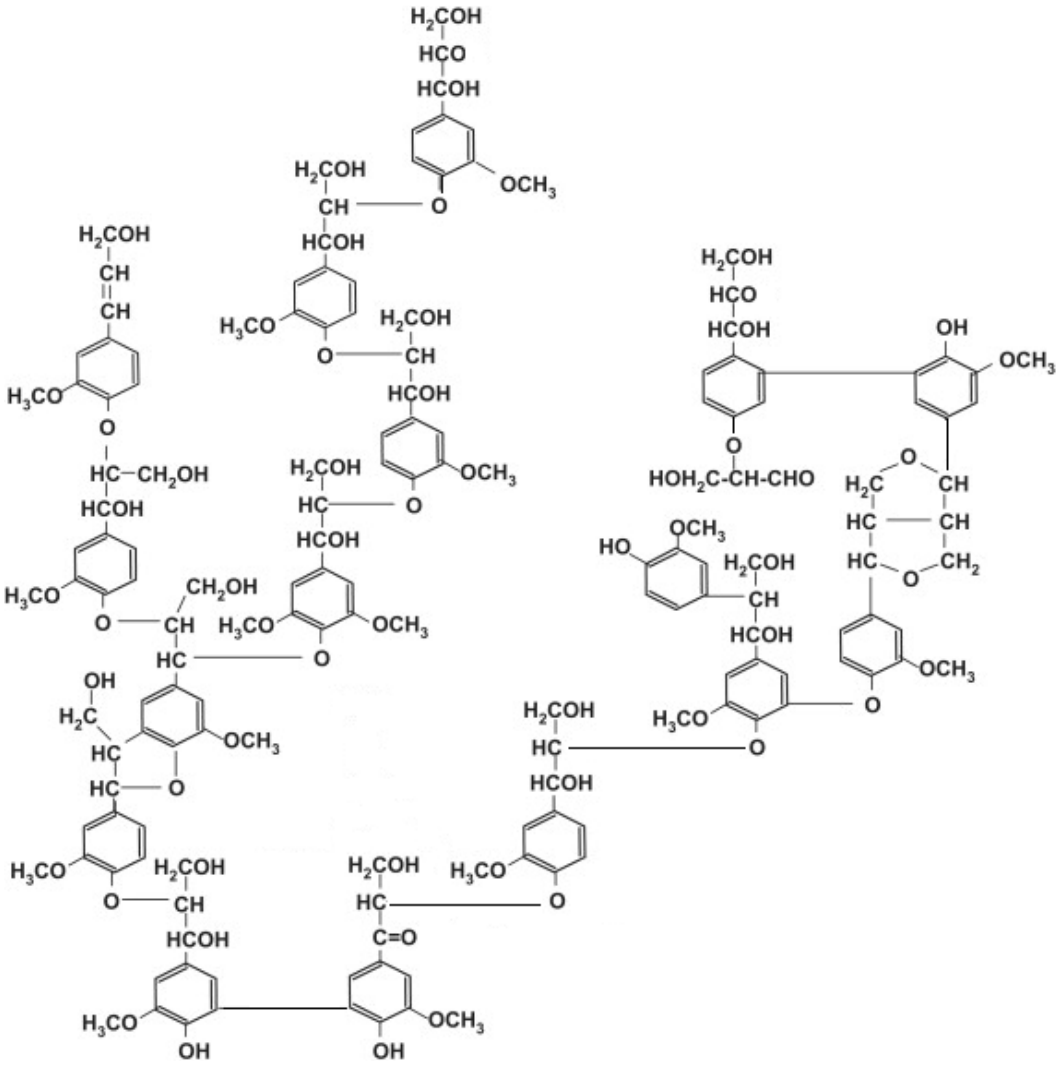

Figure 5.2 Typical structure of a softwood lignin [177]

Figure 5.3 shows three hydroxycinnamyl alcohols considered precursors of lignin, which only differ in their degree of methoxylation. The three species, p-coumaryl alcohol, coniferyl alcohol and sinapyl alcohol, are also called monolignols. These monolignols produce dilignols as the main building blocks of the lignin polymer, p-hydroxyphenyl, guaiacyl, and syringyl phenylpropanoid, respectively [174].

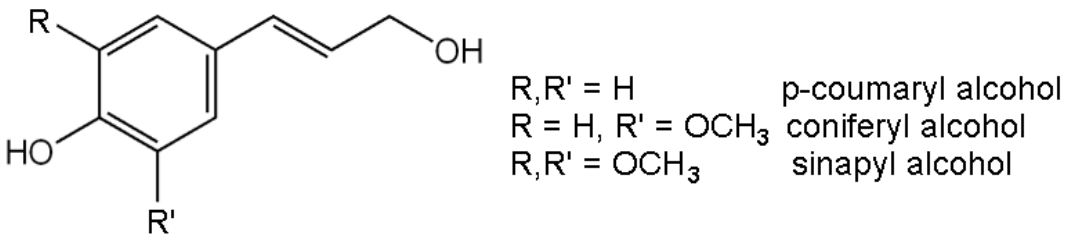

Figure 5.3 Hydroxycinnamyl alcohols precursors of lignin

The lignin monomeric unit is often referred as nine carbon atoms and expressed using a C_9 based formula, e.g. $C_9H_{7.2}O_2(H_2O)_{0.4}(OCH_3)_{0.92}$ for Norway spruce. For spruce lignin a ratio of guaiacyl : p-hydroxyphenyl : syringyl units was estimated as 94:5:1 [177].

Due to the complexity of lignin, model components have been used as reference in experimental works for the characterisation of the different lignin structures and identification of possible devolatilisation reactions. Some examples of model units are shown in figure 5.4. LIG-C represents a softwood lignin without methoxyl groups and with the largest amount of carbon [174]. LIG-O and LIG-H represent structures of hardwood lignin and are richest in O and H, respectively, containing methoxyl groups.

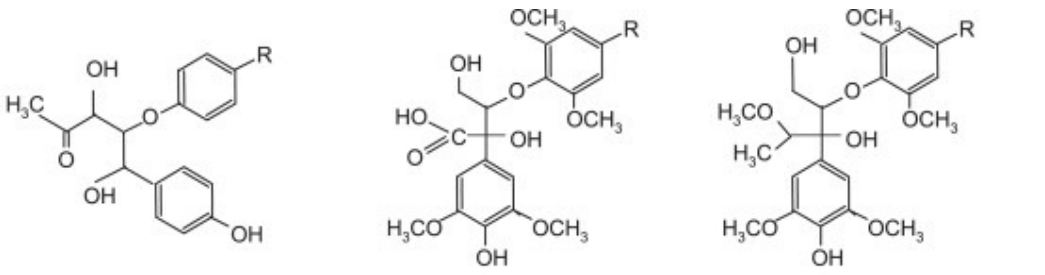

Figure 5.4 Model units in lignin structure [174]

Eugenol (4-Allyl-2-methoxyphenol, $C_{10}H_{12}O_2$) is other model compound that was used in order to represent the structural units of lignin. The major aromatic produced during pyrolysis was naphthalene with methylnaphthalenes and other 2- and 3-ring PAHs [173]; during combustion mainly monoaromatics, such as benzene, toluene and C_2-benzenes, were generated [178].

As another representative of lignin, catechol (o-dihydroxybenzene) has been used because it is a predominant unit in lignin and coal, as well as present in biomass tars [179]. Catechol was pyrolised in the presence of various amounts of oxygen. Two-ring compounds, mainly indene and naphthalene were detected under pyrolysis or oxygen-rich conditions below 800°C; whilst in the absence of oxygen, larger PAHs were produced and decreased with increasing oxygen content above 800°C [178]. Also, experiments using a residence time of 0.4 s in a reactor operated at 500-1000°C showed that benzene was the most abundant aromatic produced during catechol pyrolysis (maximum yield 6.7% w/w at 900°C), followed by naphthalene and indene [179].

Since the lignin fraction in biomass is relatively small, the HACA route to PAH formation was proposed as the more likely mechanism for soot formation [173]. Indeed, acetylene and butadiene were detected in significant concentrations during the combustion of pine wood [178]. The decomposition of methoxyl groups and aliphatic chains are the main sources of light hydrocarbon gases. Acetylene reached a maximum production between 900 and 1000°C and complete destruction at 1200 and 1400°C for gasification and pyrolysis, respectively [180]. It was suggested that acetylene may derive from the decompositions of C_2H_4 and certain aromatic tar components. The yield of non-equilibrium intermediates (e.g. acetylene and ethylene) during pyrolysis was increased by high temperatures and short gas residence times [181].

During experiments using catechol as a model compound of lignin, C_2H_2 was found as an abundant product during pyrolysis and was proposed to add to benzene or phenyl radicals to produce styrene and phenylacetylene, or add to naphthalene, phenanthrene and pyrene to form cyclopenta-fused PAHs [179].

5.1.2 Models of tar destruction

Most reports are mainly concerned with the identification and quantification of PAH from pyrolysis or combustion [170]. In the case of kinetic studies, focus has been given to the determination of either kinetic parameters for the overall weight loss of the fuel or kinetic parameters for the evolution of light gases (such as CO, CH_4 and H_2). As a result, there are still insufficient kinetic data and theoretical

comprehension of the reaction process of gasification. On the other hand, tar is a complex unit with a large number of constituents.

Tar conversion processes have been simulated using numerical methods to understand the cracking of tar as a secondary method inside a second reactor. A kinetic model was used for the thermal degradation of tar in a secondary gasification unit called Turboplasma®, where the plasma gas is air heated to temperatures up to 5000 K close to the torch. Tar was represented by naphthalene and toluene, and a reaction pathway and its associated kinetics were given. This pathway was based on the thermal cracking of tar into soot and hydrogen and on the reforming of naphthalene and toluene into benzene and methane by water [182]. Other model used benzene, phenol, toluene and naphthalene as tar model compounds to simulate the tar destruction under partial oxidation conditions. Hydrocarbons were converted to CO and H_2O by oxidation. Steam reforming reactions were proposed for toluene and phenol. Naphthalene was also formed from phenol pyrolysis and naphthalene reactions produced soot, benzene, CH_4 and H_2 [183].

A detailed kinetic mechanism was developed to predict lignin devolatilisation from TGA pyrolysis experiments. This model used three reference lignin units (shown in figure 5.4) to represent the initial lignin structure, 100 molecular and radical species were involved in the mechanism, and the mass balances included the net rate of formation. Heat and mass transport resistances were ignored. Experimental TGA data from a variety of lignins pyrolysed found in the literature were compared to the model predictions [174]. The model results agreed with the experimental thermal degradation of lignins, only the total mass loss at low pyrolysis temperatures was underestimated at isothermal devolatilisation. However, the supplementary file with the list of species and kinetics shows only half of the species with their reactions and kinetic parameters.

A method to simulate high temperature steam gasification of woody biomass has been reported [184]. The system consisted of an updraft fixed bed gasifier. Heat-up and pyrolysis calculations were based on thermal equilibrium, whilst gas-phase reactions were calculated in a one-dimensional plug flow reactor based on kinetics. The pyrolysis reaction was described as:

$$Biomass \rightarrow a_1 Char + a_2 Tar + a_3 H_2 + a_4 CO + a_5 CO_2 + a_6 CH_4 + a_7 C_2 H_4$$

The pyrolysis product yields were taken from experimental pyrolysis work up to the temperature of 1173 K. The tar composition was calculated as a mixture of acetol, toluene and naphthalene. Eleven reactions that included the evolution of these three compounds were given. They found that tar concentration from steam gasification was higher than from air or oxygen-blown gasification [184, 185]. The numerical analysis over predicted CH_4 and under predicted H_2.

A review of the background on tar evolution, main tar precursors and models that simulate tar formation and evolution was given. A classification of tar compounds based on the evolution of tar as temperature increases divides them into primary, secondary and tertiary tars; a list of typical compounds corresponding to each category can be found in [170]. Due to the identification of tar compounds from experimental work, the most frequent individual tar species studied experimentally and as model tars are acetol, acetic acid and guaiacols (primary tars), phenols, cresols and toluene (secondary tars), and naphthalene (tertiary tar). Tars are normally modelled as a "lump" or using the most stable components such as toluene, benzene and naphthalene; however, these species are known to appear as secondary and/or tertiary tars and the mechanisms and kinetics of their formation are omitted. On the other hand, a detailed kinetic model for lignin devolatilisation that includes as much as 100 species becomes a complex problem when being incorporated to simulate the conversion of biomass inside the gasifier. Among the mechanisms found for the PAH growth, the HACA route seems feasible only at temperatures greater than 900°C wherein acetylene is more abundant. Therefore, a mechanism that could describe the formation of tars while maintaining a minimum number of tar species represents a more practical solution for tar simulation during biomass gasification. This review was taken as the framework to propose a mechanism for tar formation and evolution to be incorporated in a kinetic model of the fluidised bed gasifier.

5.2 Model development

5.2.1 Model assumptions

This section describes the assumptions taken in order to model the fluidised bed gasifier regarding mass and energy balances inside the system. The following

section involves the description of the reaction pathway included in this kinetic model.

The model consists of a bubbling fluidised bed with sand particles and on top a freeboard zone. Air is used as gasifying agent and is previously preheated. A schematic diagram of the fluidised bed is shown in figure 5.5.

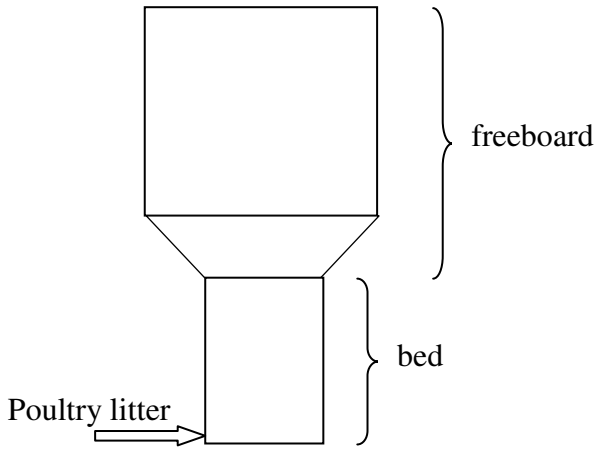

Figure 5.5 Schematic diagram of fluidised bed

The model assumptions are:

- steady-state regime
- one-dimensional fluidised bed, where variations in conditions occur only in the axial z direction
- two-phase model for the hydrodynamic behaviour of the fluidised bed, where the gas flow entering the reactor at u_0 velocity is divided into two phases: the emulsion phase and the bubble phase
- solids in the bed are well-mixed inside the emulsion phase
- the bed consists of sand, ash and carbon
- biomass devolatilisation occurs instantaneously since the mixing of biomass particles proceeds more slowly than pyrolysis [104]; therefore, pyrolysis takes place on entry to the bed
- homogeneous and heterogeneous reactions occur in the emulsion phase, since it contains all the particles and a portion of the gases. The gases are maintained at minimum fluidisation conditions and the excess gas passes through the bed to the bubble phase

- only homogeneous reactions occur in the bubble phase, since it is considered as free of particles
- all gases in both phases are assumed as in plug flow mode
- mass transfer between bubble and emulsion phases occurs through molecular diffusion. Mass transfers in the axial or vertical direction within each phase are considered as negligible compared to transfers in the horizontal direction between phases
- energy balance considers heat of reaction, heat exchange between bubble and emulsion phases, and heat exchange between well mixed particles and gas in the emulsion phase
- the gases that travel to the freeboard zone are assumed in plug flow mode

Differential equations for bubble phase and emulsion phase for each species included in the model were written. The model includes hydrodynamics of the fluidised bed, rate of reactions for homogeneous and heterogeneous reactions, and mass transfer between emulsion and bubble phases. The mass and energy balances of the emulsion phase are:

$$\frac{dC_{e,i}}{dz} = K_{gt,i} \cdot \delta \frac{(C_{b,i} - C_{e,i})}{u_{mf}} + \frac{\sum R_{gge,k}}{u_{mf}} + \frac{\sum R_{gse,k}}{u_{mf}} \quad (5.1)$$

$$\frac{dT_e}{dz} = A_t \left[H_{be} \delta (T_b - T_e) + (1-\delta)\left(1-\varepsilon_{mf}\right) A_p h_p (T_s - T_e) - (1 - \delta)\varepsilon_{mf} \sum_k R_{gge,k} \Delta H_{R,gge,k} - (1-\delta)\left(1-\varepsilon_{mf}\right) \sum_k R_{gse,k} \Delta H_{R,gse,k} \right] / \sum F_{e,i} \cdot C_{pe,i} \quad (5.2)$$

and for the bubble phase:

$$\frac{dC_{b,i}}{dz} = -K_{gt,i} \cdot \delta \frac{(C_{b,i} - C_{e,i})}{u_b} + \frac{\sum R_{ggb,k}}{u_b} \quad (5.3)$$

$$\frac{dT_b}{dz} = A_t \left[-H_{be} \delta (T_b - T_e) - \delta \sum_k R_{ggb,k} \Delta H_{R,ggb,k} \right] / \sum F_{b,i} \cdot C_{pb,i} \quad (5.4)$$

where δ is the bubble diameter; u_{mf} is the minimum fluidisation velocity; u_b is the bubble velocity; $C_{b,i}$ is the concentration in the bubble phase of species *i*; $C_{e,i}$ is the concentration in the emulsion phase of species *i*; K_{gt} is the mass transfer coefficient; R_{gg} is the rate of reaction of gas-gas reactions; R_{gs} is the rate of reaction of gas-solid reactions; ε_{mf} is the bed voidage at minimum fluidisation; T_b temperature of bubble phase; T_e is the temperature of the emulsion phase; T_s is the temperature of

solids; H_{be} is the heat transfer coefficient between emulsion and bubble phases; h_p is the heat transfer coefficient between solids and gas; C_p is the heat capacity, A_t is the cross-surface area of reactor, $\Delta H_{R,gg}$ is the heat of reaction of homogeneous reactions, and $\Delta H_{R,gs}$ is the heat of reaction of heterogeneous reactions.

For the carbonaceous material, a global mass balance is integrated over the gasifier bed zone. The outlet flow is equal to the inlet flow plus the heterogeneous reactions,

$$F_{C,out} = F_{C,in} + \int_{z_0}^{z_{bed}} \sum_i R^i_{gs,C} A_t (1-\delta) dz \quad (5.5)$$

Similarly, a global energy balance,

$$(FH)_{C,out} = (FH)_{C,in} + \int_{z_0}^{z_{bed}} (1-\delta)\left(1-\varepsilon_{mf}\right) A_p h_p (T_s - T_e) dz \quad (5.6)$$

where F_C is the flow rate of carbonaceous material, $H_{C,in}$ is the enthalpy of the carbonaceous material calculated from ultimate analysis, and z_{bed} is the total bed height.

For the freeboard region, it is considered that homogeneous reactions continue as it were a second reactor in series with the fluidised bed. The mass and energy balances in this zone for each species follow the equation:

$$\frac{dC_i}{dz} = \frac{\sum_k R_{gg,k}}{u_f} \quad (5.7)$$

$$\frac{dT_f}{dz} = \frac{A_t \sum_k R_{gg,k} H_{r,k}}{\sum F_{f,i} \cdot C_{pf,i}} \quad (5.8)$$

where u_f is the gas velocity in the freeboard. These parameters were calculated using the following correlations:

a) Hydrodynamics

It was assumed that air is injected from the bottom of the gasifier. Once injected, part of the air will remain in the emulsion phase at minimum fluidisation velocity (u_{mf}) and react with the fuel, and the rest will ascend as bubbles at increasing velocity. Knowledge of the bubble size is important because it affects the bubble rise velocity, the fractions of bubble and emulsion phases, the mixing of solids and the interface mass transfer between bubble and emulsion phases [120]. The growth of bubbles along the bed height is modelled according to the bubble assemblage model for a perforated plate distributor proposed by Mori and Wen [186]. It assumes a perfectly mixed gas entrance region and coalescence of bubbles to calculate the

growth of bubbles (d_b, diameter of bubbles). Table 5.1 also shows the equations to calculate minimum fluidisation velocity (u_{mf}), bubble velocity, bubble diameter, bubble fraction and bed voidage along the bed height.

Table 5.1 Bed hydrodynamics

Parameter	Equation	Reference
Bed voidage at minimum fluidisation	$\varepsilon_{mf} = 0.586\phi_s^{-0.72}\left(\frac{\mu^2}{\rho_f \gamma D_p^3}\right)^{0.029}\left(\frac{\rho_f}{\rho_p}\right)^{0.021}$ $\gamma = g(\rho_p - \rho_f)$, γ : specific weight of particle	[187]
Velocity at minimum fluidisation	$u_{mf} = \frac{\varepsilon_{mf}^3 \phi_S^2 Ar}{150(1-e_{mf})}\left(\frac{\mu}{\rho_g d_p}\right)$ $Ar = \frac{d_p^3 \rho_g (\rho_s - \rho_g) g}{\mu^2}$, Ar: Archimedes number	[32]
Bubble diameter	$d_b = D_{BM} - (D_{BM} - D_{B0})\exp\left(-\frac{0.3z}{D_t}\right)$ $D_{BM} = 0.652\left[A_t(u_0 - u_{mf})\right]^{0.4}$ $D_{B0} = 0.347\left(\frac{A_t(u_0 - u_{mf})}{n_d}\right)^{0.4}$, perforated plate	[186]
Bubble velocity	$u_b = u_0 - u_{mf} + u_{br}$ $u_{br} = 0.711\sqrt{g \cdot d_b}$	[32]
Bubble fraction	$\delta = \frac{u_0 - u_{mf}}{u_b - u_{mf}}$ for fast bubbles, $u_b > \frac{5u_{mf}}{\varepsilon_{mf}}$ For intermediate bubbles or $\frac{u_{mf}}{\varepsilon_{mf}} < u_b < \frac{5u_{mf}}{\varepsilon_{mf}}$ $\delta = \frac{u_0 - u_{mf}}{u_b + u_{mf}}$ when $u_b \cong u_{mf}/\varepsilon_{mf}$ $\delta = \frac{u_0 - u_{mf}}{u_b}$ when $u_b \cong 5u_{mf}/\varepsilon_{mf}$	[32]
Total bed voidage, ε_f	$\varepsilon_f = \varepsilon_{mf}(1-\delta) + \delta$	[32]

b) Mass transfer coefficients

The bubble-emulsion phase mass transfer coefficient was estimated as the sum of convective and diffusive transfer through the bubble surface. The mass transfer coefficients (K_{gt}) were calculated using the work of Sit and Grace [188] on bubble interaction on mass transfer in fluidised beds, and as follows

$$K_{gt} = \frac{u_{mf}}{4d_b} + \left(\frac{4D\varepsilon_{mf} u_b}{\pi \cdot d_b^3} \right)^{1/2} \tag{5.9}$$

where D is the diffusion coefficient. Table 5.2 shows the equations to estimate the mass diffusivity and the mass diffusivity of the mixture.

Table 5.2 Mass transfer parameters [189]

Parameter	Equation
Mass diffusivity	$D_{AB} = \frac{10^{-3} T^{1.75} \left(\frac{1}{M_A} + \frac{1}{M_B} \right)^{1/2}}{P\left(\left(\sum v \right)_A^{1/3} + \left(\sum v \right)_B^{1/3} \right)^2}$
Mass diffusivity of mixture	$D_{1-mix} = \frac{1}{y_2^{'}/D_{1-2} + y_3^{'}/D_{1-3} + \ldots + y_n^{'}/D_{1-n}}$ $y_2^{'} = \frac{y_2}{y_2 + y_3 + \ldots + y_n}$

c) Energy transfer coefficients

The heat transfer coefficient between emulsion and bubble phases (H_{be}) is estimated with the following correlation [32]:

$$H_{be} = 4.5 \left(\frac{u_{mf} \rho_g Cp_g}{d_b} \right) + 5.85 \frac{\left(k_g \rho_g Cp_g \right)^{1/2} g^{1/4}}{d_b^{5/4}} \tag{5.10}$$

For the calculation of the heat transfer coefficient between the solids and the gases (h_p) [32], it was estimated using dimensionless numbers, i.e. Reynolds number (Re), Nusselt number (Nu) and Prandtl number (Pr).

$$Nu = 2 + 0.6 \mathrm{Re}^{1/2} \mathrm{Pr}^{1/3} \tag{5.11}$$

$$\mathrm{Pr} = \frac{Cp \cdot \mu}{k_g} \tag{5.12}$$

$$\mathrm{Re} = \frac{d_p u_0 \rho_g}{\mu} \tag{5.13}$$

$$Nu = \frac{h_p d_p}{k_g} \tag{5.14}$$

d) Thermodynamic and transport properties

Table 5.3 shows how thermodynamic and transport properties were calculated. The heat capacity of the species participating in the reactions was determined as a function of temperature. Thermal conductivity and viscosity of the gas mixtures were both estimated as a function of the temperature and composition of the confined area. Appendix A contains the coefficients to calculate the heat capacity, thermal conductivity, viscosity, Gibbs free energy of formation and enthalpy of formation of each species.

Table 5.3 Thermodynamic and transport properties of species

Property	Equation	Reference
Heat capacity	$C_p = A + BT + CT^2 + DT^3 + ET^4 + GT^5$	[190]
Enthalpy of formation	$H_f = A + BT + CT^2 + DT^3 + ET^4$	[190]
Gibbs free energy	$\Delta G_f = A + BT + CT^2 + DT^3 + ET^4$	[190]
Thermal conductivity	$k_g = A + BT + CT^2 + DT^3$	[191]
Thermal conductivity of mixture	$k_{mix} = \sum_i x_i k_g$	
Viscosity of gas	$\mu = \frac{16.64(M)^{1/2}T}{(\varepsilon/k)^{1/2}\sigma^2}$ in μP $\mu = A + BT + CT^2 + DT^3$	[192]
Viscosity of mixture of gases	$\mu_{mix} = \sum_i x_i \mu_i$	

5.2.2 Proposed mechanism for tar and coke formation

In this work, the proposal of a mechanism that incorporates tar formation is presented and its development consisted of two steps. Firstly, a list of main tar compounds was made based on the tar compounds identified as most abundant from experimental work after biomass pyrolysis. Secondly, possible reaction pathways were evaluated by the selection of the most favourable reactions to occur in the process.

Table 5.4 shows some typical products of lignin pyrolysis identified from experimental work [193]. These pyrolysis products can be mainly grouped in phenolics, such as phenols, guaiacols and catechols, and light gases e.g. carbon oxides. However, this list does not identify if the products are originally generated or evolved after reactions of previous products. To make a distinction, in this work a mechanism is proposed that includes the reaction pathway from lignin precursors to larger PAHs.

Table 5.4 Typical lignin pyrolysis products [193]

Type of product	Group of compound	Examples
Light liquids		H_2O, methanol
Phenolics	Monohydroxyl phenols	Phenol, o-cresol, m-cresol, p-cresol, 2-ethylphenol, 4-propylphenol and xylenols
	Guaiacols	Guaiacol, 4-methylguaiacol, 4-ethylguaiacol, 4-propylguaiacol
	Catechols	Catechol, 4-methylcatechol, 4-ethylcatechol, 3-methoxycatechol
Gases	Hydrocarbons	Methane, ethane, ethylene, propane, propylene, n-butane and isobutene
	Carbon oxides	CO, CO_2
	Sulphur-containing compounds	H_2S, methyl mercaptan

Based on the typical structure of lignin, catechol, guaiacol and vanillin were chosen as primary tar products in the present work. Guaiacol and vanillin were selected because reports have shown that these two guaiacols are dominant products during biomass pyrolysis [170, 173, 194] and lignin is rich in methoxyl groups (OCH_3). Catechol was selected because it is a structure found in lignin and a major component of biomass tars. Other researchers have used catechol and dihydric phenol catechol as model compounds of lignin units [179].

In this work, lignin is represented by seven guaiacol, seven vanillin and two catechol units. The sixteen units are put together and accounted for 70% of the softwood lignin proposed by Adler [177] shown in figure 5.2. The main assumptions were that

- only the lignin fraction is aromatic in nature,
- the main route for soot formation is via tar components reactions, and
- the formation of cyclopentadiene and indene intermediates are responsible for PAH growth.

However, this might underestimate soot formation since biomass has a less aromatic nature than coal and the HACA mechanism in the absence of aromatic precursors was not included, which might have a more important role for biomass soot formation [173], if acetylene is formed which requires temperatures above 900°C and included in the model.

Figure 5.6 shows the proposed mechanism for tar formation assuming lignin units as precursors. The three lignin units, vanillin ($C_8H_8O_3$), guaiacol ($C_7H_8O_2$), and catechol ($C_6H_6O_2$) are pyrolysed and/or react with hydrogen. This figure does not show the release of volatiles, such as CO, H_2 and CO_2, which are also produced. The reaction pathway was chosen according to the reactions that are most thermodynamically favourable.

Table 5.5 shows the reactions identified from the three lignin units to the formation of three-ring compounds. R1 represents the reaction of pyrolysis of vanillin, and R1a is the reaction of vanillin with hydrogen. For example, reaction R3c was not included in the model, this reaction might also occur but it was not considered because it is not thermodynamically favourable.

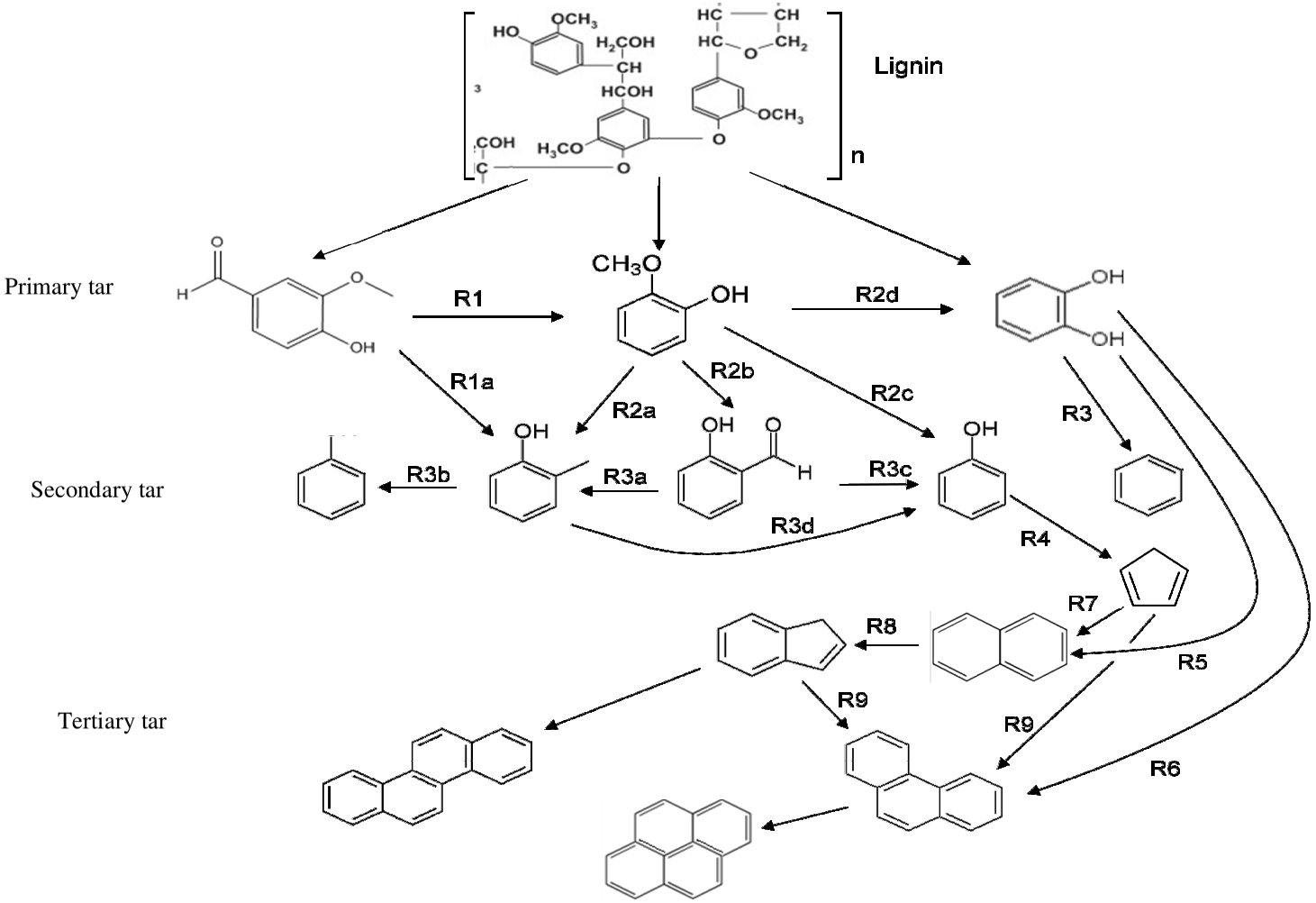

Figure 5.6 Proposed mechanism for primary, secondary and tertiary tar formation

Table 5.5 Reactions of proposed mechanism for tar formation and evolution

		ΔG @ 298K (kJ/mol)	ΔG @ 800K (kJ/mol)
R1	$C_8H_8O_3 \rightarrow C_7H_8O_2 + CO$	-29.2	-91.5
R1a	$C_8H_8O_3 + H_2 \rightarrow C_7H_8O + H_2O + CO$	-153.1	-218.6
R2a	$C_7H_8O_2 + H_2 \rightarrow C_7H_8O + H_2O$	-123.9	-127.1
R2b	$C_7H_8O_2 \rightarrow C_7H_6O_2 + H_2$	-1.7	-69.9
R2c	$C_7H_8O_2 + 2H_2 \rightarrow C_6H_6O + H_2O + CH_4$	-161.3	-223.3
R2d	$C_7H_8O_2 + H_2 \rightarrow C_6H_6O_2 + CH_4$	-94.6	-88.2
R3	$C_6H_6O_2 + 2H_2 \rightarrow C_6H_6 + 2H_2O$	-144.3	-161.6
R3a	$C_7H_6O_2 + 2H_2 \rightarrow C_7H_8O + H_2O$	-122.2	-57.2
R3c	$C_7H_6O_2 \rightarrow C_6H_6O + CO$	57.7	91.7
R3b	$C_7H_8O + H_2 \rightarrow C_7H_8 + H_2O$	-72.0	-81.8
R3d	$C_7H_8O + H_2 \rightarrow C_6H_6O + H_2O$	-48.7	-54.7
R4	$C_6H_6O \rightarrow C_5H_6 + CO$	73.3	-4.7
R5	$2C_6H_6O_2 \rightarrow C_{10}H_8 + 2CO_2 + 2H_2$	-198.5	-379.4
R6	$3C_6H_6O_2 \rightarrow C_{14}H_{10} + 4CO + 2H_2O + 2H_2$	-148.4	-570.1
R7	$2C_5H_6 \rightarrow C_{10}H_8 + 2H_2$	-131.9	-164.1
R8	$C_{10}H_8 + O_2 + H_2 \rightarrow C_9H_8 + CO + H_2O$	-354.8	-378.6
R9	$C_5H_6 + C_9H_8 \rightarrow C_{14}H_{10} + 2H_2$	-104.9	-139.7

i) Reactions

The reactions used for the model included homogeneous and heterogeneous reactions for the emulsion phase and only homogenous reactions for the bubble phase. Biomass pyrolysis was modelled using two reactions: R18 and R21. Reaction R18 represents the flash pyrolysis of biomass that releases volatiles, i.e. non-condensable gases and water, and char. Biomass composition is based on the ultimate analysis minus the lignin ultimate analysis. Char was assumed as only composed of carbon. Reaction R21 corresponds to the formation of primary tars, the three lignin units previously chosen, vanillin, guaiacol and catechol. The evolution of these three tars followed the mechanism shown in figure 5.6, which corresponds to reactions R1 to R9. Reactions R10 to R17, R19, and R20 represent combustion and gasification reactions of carbon and volatiles.

Ash was assumed to contain a fraction of sodium carbonate, the rest was considered as inert. Reaction R22 represents the reaction of Na_2CO_3 with HCl to retain chlorine in the solid phase.

Reaction R23 shows the decomposition of vanillin to non-condensable gases and water. Reaction R24 corresponds to the steam gasification of naphthalene. Finally, reactions R25 and R26 represent the combustion and steam gasification of benzene, respectively. Table 5.6 shows the reactions included in the simulation:

Table 5.6 Homogeneous and heterogeneous reactions

	Reaction	Reference
R1	$C_8H_8O_3 \rightarrow C_7H_8O_2 + CO$	[195]
R2	$0.705C_7H_8O_2 \rightarrow 0.47C_6H_6O_2 + 0.04C_6H_6O + 0.07C_7H_8O + 0.15C_7H_6O_2 + 0.275CH_4 + 0.06CO + 0.01H_2$	[196]
R3	$C_6H_6O_2 + 2H_2 \rightarrow C_6H_6 + 2H_2O$	[179]
R4	$C_6H_6O \rightarrow C_5H_6 + CO$	[172]
R5	$2C_6H_6O_2 \rightarrow C_{10}H_8 + 2CO_2 + 2H_2$	[179]
R6	$3C_6H_6O_2 \rightarrow C_{14}H_{10} + 4CO + 2H_2O + 2H_2$	[179]
R7	$2C_5H_6 \rightarrow C_{10}H_8 + 2H_2$	[197]
R8	$C_{10}H_8 + O_2 \rightarrow C_9H_8 + CO_2$	[197]
R9	$C_9H_8 + C_5H_6 \rightarrow C_{14}H_{10} + 2H_2$	[198]
R10	$C + ½\ O_2 \rightarrow CO$	[199]
R11	$CO + ½\ O_2 \rightarrow CO_2$	[102]
R12	$H_2O_l \rightarrow H_2O_g$	[200]
R13	$CO + H_2O \rightarrow CO_2 + H_2$	[201]
R14	$H_2 + ½\ O_2 \rightarrow H_2O$	[199]
R15	$C + H_2O \rightarrow CO + H_2$	[201]
R16	$C + 2H_2 \rightarrow CH_4$	[201]
R17	$CH_4 + H_2O \rightarrow CO + 3H_2$	[202]
R18	$Biomass \rightarrow a_1CO + a_2CO_2 + a_3H_2O + a_4H_2 + a_5CH_4 + a_6NH_3 + a_7H_2S + a_8HCl + a_9Char$	
R19	$2H_2S + 3O_2 \rightarrow 2SO_2 + 2H_2O$	[203]
R20	$NH_3 + 5⁄4\ O_2 \rightarrow NO + 3⁄2\ H_2O$	[204]
R21	$Lignin = 2C_6H_6O_2 + 7C_7H_8O_2 + 7C_8H_8O_3$	

	Reaction	Reference
R22	$Na_2CO_3 + 2HCl \rightarrow 2NaCl + CO_2 + H_2O$	[205]
R23	$C_8H_8O_3 + 6.68H_2 \rightarrow 2.66CO + 0.085CO_2 + 5.255CH_4 + 0.17H_2O$	[201]
R24	$C_{10}H_8 + 4H_2O \rightarrow C_6H_6 + 4CO + 5H_2$	[206]
R25	$C_6H_6 + 3O_2 \rightarrow 6CO + 3H_2$	[199]
R26	$C_6H_6 + 5H_2O \rightarrow 5CO + 6H_2 + CH_4$	[182]
R27	Ash → Ash	

ii) Rate of reactions

Reactions R18 and R21 represent the primary decomposition of biomass based on a one-component reaction process. This approach is normally adopted for fast heating rates, and the kinetics are derived from yield measurements and weight loss curves of the three product classes (gases, tar and char) formed [87]. The mechanism was chosen as two parallel reactions occurring for the formation of the three product classes. After these three product classes are produced, they are further decomposed and underwent combustion and gasification reactions.

For the rates of reaction of catechol, kinetic parameters and reaction order were taken from work on the pyrolysis of catechol. The kinetics parameters for reactions R3 and R5 were taken from Ledesma et al. [179]. In Ledesma et al. work, experimental product yield/temperature data and observed maximum yields were fitted to obtain the activation energy and pre-exponential factor for each product species when a first order reaction was assumed, at a fixed residence time. Individual kinetics for some benzene and benzenoid PAH, vinyl- and ethyl-substituted aromatics, and cyclopenta-fused PAH compounds were derived.

Phenol is transformed to cyclopentadiene and CO is abstracted from the phenol according to reaction R4 [172]. After that, cyclopendiene combines to form naphthalene in accordance with reaction R7. The reaction rates and kinetic coefficients for all homogeneous and heterogeneous reactions involved in the kinetic model are found in Appendix B.

5.2.3 Numerical method

For the solution of mass equations of individual species (equations 5.1 and 5.3) and energy equations (equations 5.2 and 5.4), the methods available and the one chosen are described in this section. The set of ordinary differential equations (ODE) is solved as an initial value problem, where initial conditions at the bottom of the gasifier were given and concentrations were calculated up the top of the fluidised bed and freeboard zone. Among the solvers commonly employed to solve the differential equations are: the predictor-corrector methods, Richardson extrapolation and the Bulirsch-Stoer method, and the Runge-Kutta methods [207]. The many reactions involved in a gasification process have significantly different reaction rates. Therefore, the wide variation in time scales has severe consequences in the numerical solution of the differential equations that govern the established reaction system. Since stiffness is very likely to occur in this system, methods to solve stiff systems are described:

1) Predictor-corrector methods

These methods first store the solution and then use those results to extrapolate the solution one step advanced, called the predictor step. Then the prediction step value is used to interpolate the derivative, called the corrector step. The difference between the predicted and corrected values gives the local truncation error which is used to control accuracy and adjust the stepsize. These methods are recommended for a high-precision solution of very smooth equations.

2) Generalizations of the Bulirsch-Stoer methods

The Bulirsch-Stoer methods extrapolate a computed result to the value that would have been obtained if the stepsize was zero. The semi-implicit extrapolation method is one of the most important for stiff ODEs. This method is recommended for high-precision applications or when the right-hand sides are expensive. Not recommended for non-smooth functions or with singular points inside the interval of integration.

3) Runge-Kutta methods

The fourth-order Runge-Kutta method evaluates the derivatives four times in each step: once at the initial point, twice at trial midpoints and once at trial endpoint. The final function value is calculated from the four derivatives. When an adaptive stepsize control is included, the method provides the error of the calculation. It uses

the difference between the fifth-order and fourth-order estimates to determine the error and adjust the stepsize with a desired accuracy.

A generalization of the Runge-Kutta method is the Rosenbrock method. This method solves equations and looks for a solution of the form,

$$y(x_0 + h) = y_0 + \sum_{i=1}^{s} b_i \mathbf{k}_i \tag{5.15}$$

where $\mathbf{k}_i$ are the corrections found by solving s linear equations:

$$(1 - \gamma h \mathbf{f}') \cdot \mathbf{k}_i = h\mathbf{f}\left(y_0 + \sum_{j=1}^{i-1} \alpha_{ij} \mathbf{k}_j\right) + h\mathbf{f}' \cdot \sum_{j=1}^{i-1} \gamma_{ij} \mathbf{k}_j, \tag{5.16}$$

where $i = 1,\ldots,s$, $\mathbf{f}'$ is the Jacobian matrix, and γ, c_i, α_{ij}, and γ_{ij} are coefficients fixed as constants independent of the problem.

An automatic stepsize adjustment algorithm is necessary for the success of the stiff integration. Runge-Kutta-Fehlberg method is an automatic stepsize adjustment algorithm that computes two estimates of the form (5.15). One called 'real' for $\boldsymbol{y}$ and a lower-order estimate $\hat{\boldsymbol{y}}$ with different coefficients c_i, $i = 1,\ldots,s$, where $\hat{s} < s$ but with the same $\mathbf{k}_i$. The local truncation error is calculated as the difference between $\boldsymbol{y}$ and $\hat{\boldsymbol{y}}$, and then used for stepsize control. It was shown by Kaps and Rentrop that the smallest value for s is four and for $\hat{s}$ is three which made embedding possible, leading to a fourth-order method. The right-hand side of (5.16) was rewritten to minimise the matrix-multiplications

$$\mathbf{g}_i = \sum_{j=1}^{i-1} \gamma_{ij} \mathbf{k}_j + \gamma \mathbf{k}_i \tag{5.17}$$

The equations become

$$\begin{aligned}
\left(\frac{1}{\gamma h} - \mathbf{f}'\right) \cdot \mathbf{g}_1 &= \mathbf{f}(\boldsymbol{y}_0) \\
\left(\frac{1}{\gamma h} - \mathbf{f}'\right) \cdot \mathbf{g}_2 &= \mathbf{f}(\boldsymbol{y}_0 + a_{21}\mathbf{g}_1) + \frac{c_{21}\mathbf{g}_1}{h} \\
\left(\frac{1}{\gamma h} - \mathbf{f}'\right) \cdot \mathbf{g}_3 &= \mathbf{f}(\boldsymbol{y}_0 + a_{31}\mathbf{g}_1 + a_{32}\mathbf{g}_2) + \frac{c_{31}\mathbf{g}_1 + c_{32}\mathbf{g}_2}{h} \\
\left(\frac{1}{\gamma h} - \mathbf{f}'\right) \cdot \mathbf{g}_4 &= \mathbf{f}(\boldsymbol{y}_0 + a_{41}\mathbf{g}_1 + a_{42}\mathbf{g}_2 + a_{43}\mathbf{g}_3) + \frac{c_{41}\mathbf{g}_1 + c_{42}\mathbf{g}_2 + c_{43}\mathbf{g}_3}{h}
\end{aligned} \tag{5.18}$$

The linear equation (5.18) are then solved by first computing the LU decomposition of the matrix $1/\gamma h - \mathbf{f}'$. Then, the four $\mathbf{g}_i$ are calculated by back-substitution of the four different right-hand sides. The Rosenbrock method was chosen to solve the ODEs because it is a reliable method for moderate accuracies ($\varepsilon < 10^{-4}$–10^{-5}). The subroutines *odeint* and *stiff* from [207] were adapted to perform the calculations.

In section 5.2.2, the reactions included in the system were shown. They consist of 27 reactions involving 27 species. However, these 27 species are not involved in all the reactions and this provokes many zeros within the matrix generated, the so-called sparse matrix. In order to threat sparse matrices properly, a coordinate-storage format was used to store only the non-zero elements of the matrix along with their location by keeping row-index and column-index values.

The system of equations to be solved is of the form

$$\boldsymbol{A}\boldsymbol{x} = b \tag{5.19}$$

where $\boldsymbol{A}$ is the n by n matrix, b the right hand side vector of length n, and $\boldsymbol{x}$ is the solution vector of length n.

The solution of systems of sparse linear equations can be solved by two types of numerical methods: direct and iterative. Iterative methods involves the selection of an initial approximation of the solution vector $\boldsymbol{x}$. The calculation includes an iteration to obtain $\boldsymbol{x}$ until an acceptable approximation is found. Iterative methods require less computer storage, however, they experience some fill-in and generate a filled matrix that has non-zero in locations which are zero in $\boldsymbol{A}$. Direct methods benefit of not having rounding errors and provide a solution after a finite number of arithmetic operations are completed [208]. Therefore, a direct method was chosen as described in the numerical solution scheme.

Reaction R18 (shown in section 5.2.2) represents the flash pyrolysis or devolatilisation of biomass to non-condensable gases, steam and char. The stoichoimetric coefficients of this reaction were calculated based on mole balances between every element (C, H, O, N, S, Cl) present in biomass (ultimate analysis) and tar ($mol_{pyr,i} = mol_{bio,i} - mol_{tar,i}$, where i = C,N,O,H,S,Cl), and the species generated. Nine species were assumed to be generated after the devolatilisation of biomass

according to reaction 18. The reactions used to calculate the stoichiometric coefficients were the following:

$$\sum_i (y_i a_{ik}) = \frac{A_k}{\sum_i n_i} \quad (5.20)$$

$$\sum_i y_i = 1 \quad (5.21)$$

where A_k is the total number of atomic weights of the kth element present in the system as determined by the initial constituents of biomass, n_i is the number of moles of the ith species in the system, y_i is the molar fraction of the species produced, and a_{ik} is the number of atoms of the kth element in each molecule of the chemical species i.

Appendix C contains the details of each of the equations involved and the method used to calculate the number of moles for each species by imposing some constraints to allow all species to be produced.

Numerical solution scheme

The NAGWare f95 Compiler was selected for coding the model, which is a full ISO and ANSI standard implementation of the Fortran 95 language. The Fortran Builder (Professional Edition 5.1) was used for writing the coding; this is an IDE (integrated development environment) for Fortran and comes with numerical and plotting libraries.

The LU decomposition (direct method) was performed using the NAG Fortran Library Routine F01BRF for a real sparse matrix A. F01BRF is used to obtain the LU factorization of a permutation of A,

$$PAQ = LU \quad (5.22)$$

where P and Q are permutation matrices, L is unit lower triangular and U is upper triangular.

A pivotal strategy was used to compromise between maintaining sparsity and controlling loss of accuracy through round-off. The routine first permutes the matrix

into block lower triangular form and then only factorizes the diagonal blocks. This saves considerable storage and execution time.

Then the NAG Fortran Library Routine F04AXF was used to solve the set of *n* linear equations of the form (5.19). This routines requires the right-hand side vector *b* and returns the solution vector $\boldsymbol{x}$.

Figure 5.7 shows a schematic diagram of the simulation program coded in Fortran. Two iteration processes are used; one iteration concerns with the carbon conversion and the other with the temperature of solids. The process starts by giving the input parameters that consist of air flow rate, biomass flowrate, temperature of air, gasifier dimensions, density of solids, particle size, ultimate analysis, lignin content and moisture content. The carbon conversion and temperature of solids are given as an initial guess. The Rosenbrock method is used to solve the ODEs and obtain the temperatures and composition of the different phases. The solid reaction rate is integrated over the bed height using (5.5) and the new carbon conversion is obtained and compared with the initial guess. Once the carbon fraction iteration finishes, the energy equation of the solid is integrated using (5.6) and a new temperature of the solid is obtained and then compared with the initial guess. The tolerance for the convergence of carbon conversion and temperature of solids are established as,

$$\frac{|x_{C,new}-x_{C,old}|}{x_{C,old}} \leq 10^{-4} \tag{5.23}$$

$$\frac{|T_{s,new}-T_{s,old}|}{T_{s,old}} \leq 10^{-3} \tag{5.24}$$

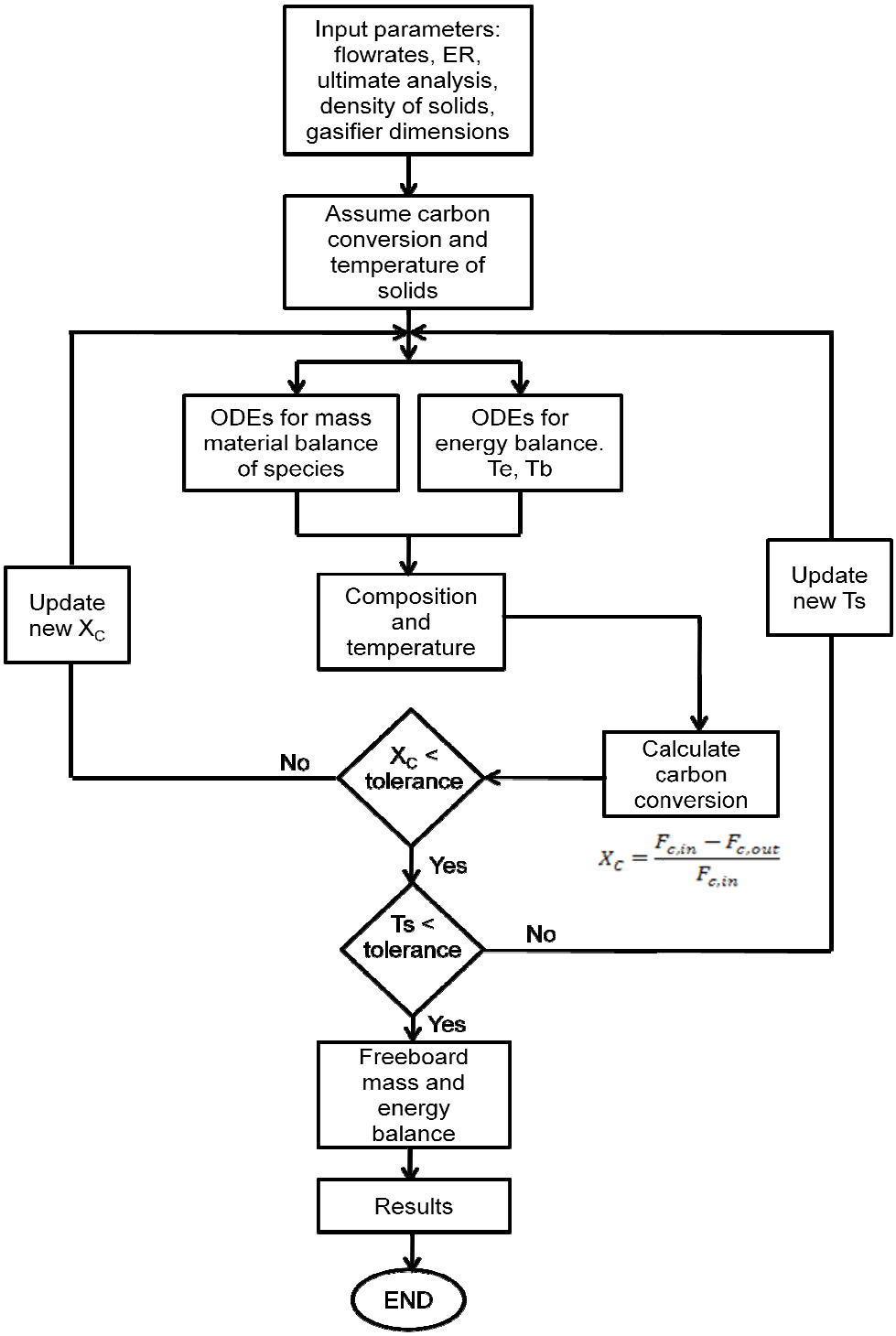

Figure 5.7 Flow diagram of model for the fluidised bed gasifier

5.3 Summary

This section described the development of a method to simulate the fluidised bed gasification of biomass. A two-phase model was used to represent the fluidised

bed. The main contribution of this model is the incorporation of a reaction pathway that includes tar formation and evolution. Lignin was assumed as the precursor of tar compounds due to its aromatic nature. The lignin fraction was described as consisting of guaiacol, vanillin and catechol units which are some of the main species identified in the lignin structure and during lignin pyrolysis. These three compounds were designated as primary tars. Further tar evolution was established based on tar compounds identified from experimental work as most abundant and on most thermodynamic favourable reactions.

The differential equations for bubble phase and emulsion phase for each species were solved using the Rosenbrock method. The model includes hydrodynamics of the fluidised bed, rate of reactions for homogeneous and heterogeneous reactions, and mass and energy transfer between emulsion and bubble phases. In order to verify the proposed model, the following chapter shows the results of the comparison with experimental results previously reported.

Chapter 6

Results and discussion: kinetic model

Since tar elimination from the product gas is necessary to make gasification an attractive option, the presence of tar was included in the kinetic model as described in the previous chapter. Lignin was assumed as the main precursor of tars due to its aromatic nature, therefore, the lignin content of biomass was considered as part of the fuel characterisation. This chapter shows the results from the simulation of the fluidised bed gasifier that incorporates the proposed mechanism for tar formation and evolution into the kinetic model. The model results are validated with experimental data from wood gasification and then compared with the results from the equilibrium model for the gasification of poultry litter.

6.1 Model verification

In order to verify the results generated from the model, experimental data was taken from a previous report since at the present time experimental data from the gasification of poultry litter is not yet available. The inputs used in the model were based on the experimental work conducted in a lab-scale bubbling fluidised bed gasifier of the Energy research Centre of the Netherlands (ECN) [209]. The fuel employed was beech chips and it was used as received. Table 6.1 shows the properties of the beech used during the gasification experiments.

Table 6.1 Properties of fuel [209]

	Beech wood
Ultimate analysis (wt. %, dry)	
Carbon	48.55
Hydrogen	5.97
Nitrogen	0.14
Sulphur	0.017
Oxygen	44.28
Chlorine	0.005
Ash	1.04
Proximate analysis (wt. %, dry)	
Fixed carbon	16.0
Volatile matter	83.0
Moisture	10.2
Lignin	24.0
HHV (kJ/kg)	19071

The gasifier is configured to be heated electrically in order to control the gasifier temperature. The temperatures of bed and freeboard were recorded, and non-condensable gases (CO, CO_2, CH_4, H_2, C_2H_4, and C_2H_6), benzene and toluene were measured on-line by GC-MS and other tars off-line using solid phase absorption (SPA). Table 6.2 shows the gasifier and bed material characteristics.

Table 6.2 Fluidised bed characteristics [209]

Condition	
Bed material	silica sand
Particle diameter	0.27 mm
Bed internal diameter	74 mm
Bed height	500 mm
Freeboard diameter	108 mm
Total length	1100 mm
Gasifying agent	air

Table 6.3 shows a comparison of the results reported from the experimental work, kinetic model and equilibrium model results using the operating conditions indicated in the table, such as fuel feeding rate. The results are shown using two ER values. The table compares experimental and predicted product gas compositions, bed and freeboard operating temperatures, and total tar and tars compositions.

Table 6.3 Comparison between experimental [209] versus kinetic and equilibrium results of beech gasification

	Units	Exp. data	Kinetic Model	Equil. model	Exp. data	Kinetic Model	Equil. model
ER		0.25	0.25	0.25	0.26	0.26	0.26
Biomass feeding rate	kg/h	1	1	1	1	1	1
CO	vol. %	14.09	12.9	16.4	14.20	13.4	17.5
CO_2	vol. %	13.25	13.7	13.6	13.18	13.5	13.02
H_2	vol. %	7.17	9.1	22.7	7.10	8.8	22.6
N_2	vol. %	43.04	57.5	37.2	43.94	58.4	37.5
CH_4	vol. %	4.22	0.54	1.5	4.23	0.37	1.3
H_2O	vol. %	15.6[a]	5.4	8.5	15.5[a]	4.9	7.9
SPA total tar	g/m^3	10.0	21.0		7.6	13.7	
Class 2	mg/m^3	1089	17255		471	10909	
Class 3	mg/m^3	1359	1871		756	1481	
Class 4	mg/m^3	5495	1876		5024	1342	
Phenol	mg/m^3	1015	555		425	339	
Class 5	mg/m^3	311	-		354	-	
Temperature bed	K	1079	969		1103	965	
Temperature freeboard	K	1049	910	910	1073	918	917
Temperature of air	K	298	960	1367	298	967	1367
Carbon conversion	%	97-99	96.7		97-99	97.0	

NA: not available
[a] calculated [209]

The results of tar compounds were reported according to the tar classification system. Class 1 refers to GC-undetectable tars, like heaviest tars that condense at high temperatures even at low concentrations. Class 2 refers to heterocyclic compounds that generally have high water solubility, such as phenol and cresol. Class 3 includes 1-ring aromatic compounds, for example xylene, styrene and toluene. Class 4 refers to 2-3 ring PAH compounds, such as naphthalene, flourene and phenanthrene. Class 5 includes higher PAH compounds, that is, 4-7 ring aromatic compounds from fluoranthene to coronene.

In order to compare the predicted results with the experimental data, the tar concentrations are presented by grouping the simulated tar compounds according to the tar classification system. Vanillin, guaiacol, catechol, phenol, o-cresol and salicylaldehyde were counted as class 2. Cyclopentadiene and benzene were considered class 3. Finally, naphthalene, indene and phenanthrene were added as class 4. Class 5 is not reported since aromatic compounds of four or more rings were not considered in the model.

The results from the kinetic model show that the concentration of class 2 is much higher than expected. This high concentration is mainly due to catechol and salicylaldehyde, where only adding these two compounds gives a concentration of 14.7 g/m^3 and 9.2 g/m^3 with an ER of 0.25 and 0.26, respectively. One of the limitations of the proposed set of reactions is that combustion reactions of catechol and salicylaldehyde, and pyrolysis and gasification of salicylaldehyde were not included due to lack of kinetics. These two compounds are generated from the pyrolysis of guaiacol, which is a primary tar. This reaction causes the decomposition of guaiacol whilst producing primary tar catechol and secondary tar salicylaldehyde among others, according to reaction R2 as shown in chapter 5 (section 5.2.2).

Another difference between the results presented in table 6.3 of the predicted and experimental data is the temperatures of inlet air and gasifier. This difference is due to the fact that the fluidised-bed gasifier from ECN has electrical heaters to control the temperature of the bed and freeboard to particular values. In contrast, the model assumes introducing hot air to achieve high temperatures in both sections. In order to improve the comparison, the model would need to be adjusted to include the option of choosing that the gasifier is externally heated to maintain or achieve certain temperature.

Even though it was observed that the increase of air temperature helped to reduce tar production, the air temperature was established as the one necessary to achieve a carbon conversion of 97%. Allowing the system higher values of conversion made the model unstable.

From the experimental data, it can be inferred that less than 2.6 vol. % and 1.8 vol. % of the total gases correspond to the tar fraction for an ER of 0.25 and 0.26, respectively. The composition of sulphur and chlorine containing gases, ammonia and NO_x was not reported. From the model, 0.9 vol. % and 0.6 vol. % of the gases are tars for an ER of 0.25 and 0.26, respectively. It was previously reported that the total tar yield decreased from 10.15% to 0.26% of the initial biomass feedstock when the ER value was increased from 0 to 0.34; at ER values greater than 0.34, the benefits of adding more oxygen showed to be reduced [183]. The kinetic model also agrees with the experimental data in that the total tar is reduced when the ER value is raised, falling by 24% in the empirical data and 34% in the model, when the ER is increased, from 0.25 to 0.26. Experimental and kinetic model results show that individual tar class concentrations are reduced with the increase of ER and gasification temperature. The experimental data show a greater reduction of classes 2 and 3, and phenol than the kinetic model, whilst the kinetic model decreased greater class 4.

In regard to non-condensable gases, it can be seen that concentrations from experimental data and predicted results by the kinetic model are consistent for some gases, such as CO_2, CO and H_2. The greatest differences are for nitrogen and water. The experimental report presented the concentrations on a dry basis; nitrogen concentration was given as 51% with a note that this value was estimated based on mass balance and for H_2O of 15.6% as calculated, for an ER value of 0.25. Table 6.3 shows that the predicted results present the same trends in the concentration of species for the two compared ER values. The CO_2 composition agrees among the experimental data and both models. The composition of non-condensable gases is lower than the estimated by the equilibrium model, which shows that equilibrium concentrations were not reached. Hydrogen is under predicted and nitrogen is over predicted by the kinetic model with respect to the equilibrium model.

Figure 6.1 shows the composition of tars in the emulsion phase along the gasifier bed and freeboard zone for an ER value of 0.26 using the kinetic model.

Primary tars are shown in dashed lines, vanillin ($C_8H_8O_3$) and guaiacol ($C_7H_8O_2$) in figure 6.1A, and catechol ($C_6H_6O_2$) in figure 6.1B. Vanillin and guaiacol are rapidly produced and then destroyed along the bed. At the top of the bed (0.5 m), guaiacol is completely eliminated and vanillin is significantly reduced.

A very different curve shape can be seen for catechol ($C_6H_6O_2$) in figure 6.1B. This is due to catechol being a primary tar and also produced from guaiacol pyrolysis. Catechol concentration increases progressively with height in the bed zone until it reaches a maximum and then starts decreasing in the freeboard but at a slow rate. Catechol reacts with hydrogen to generate benzene according to reaction R3 and recombines itself to produce naphthalene and phenanthrene in accordance with reactions R5 and R6, respectively. Since the activation energies are relatively high (shown in Appendix B), temperatures greater than 950°C are necessary to decompose catechol into benzene, naphthalene and phenanthrene based on the Arrhenius values determined for the catechol pyrolysis between 500 and 1000°C by Ledesma et al. [179].

Figure 6.2 shows the composition of tars in the bubble phase. The shapes of the curves are very similar to the emulsion phase curves. For vanillin and guaiacol, smaller concentrations are seen as expected, since these two compounds are transferred from the emulsion phase where they are produced.

An abundant secondary tar is phenol (C_6H_6O), which is increasingly produced along the bed, reaching a maximum value of 452 mg/m^3 at the top of the bed. Phenol is considerably reduced in the freeboard zone (above 0.5 m) to a value of 339 mg/m^3.

Another secondary tar is o-cresol (C_7H_8O) shown in figures 6.1B and 6.2B. It can be seen that o-cresol concentration increased with height and remained constant in the freeboard zone. This is another compound that requires the addition of reactions that correspond to the gasification and combustion of o-cresol.

Benzene and indene are considered both secondary and tertiary tars since they often appear in both classes [170]. Figures 6.1A and 6.2A show that benzene and indene are formed in the bed and also continued to be generated in the freeboard zone. Reactions R26 and R27 (shown in chapter 5) correspond to the combustion and steam reforming of benzene, respectively. Even though these two reactions were included in the model, benzene concentration increases which shows that it requires more heat to be destroyed because oxygen is limited in the freeboard.

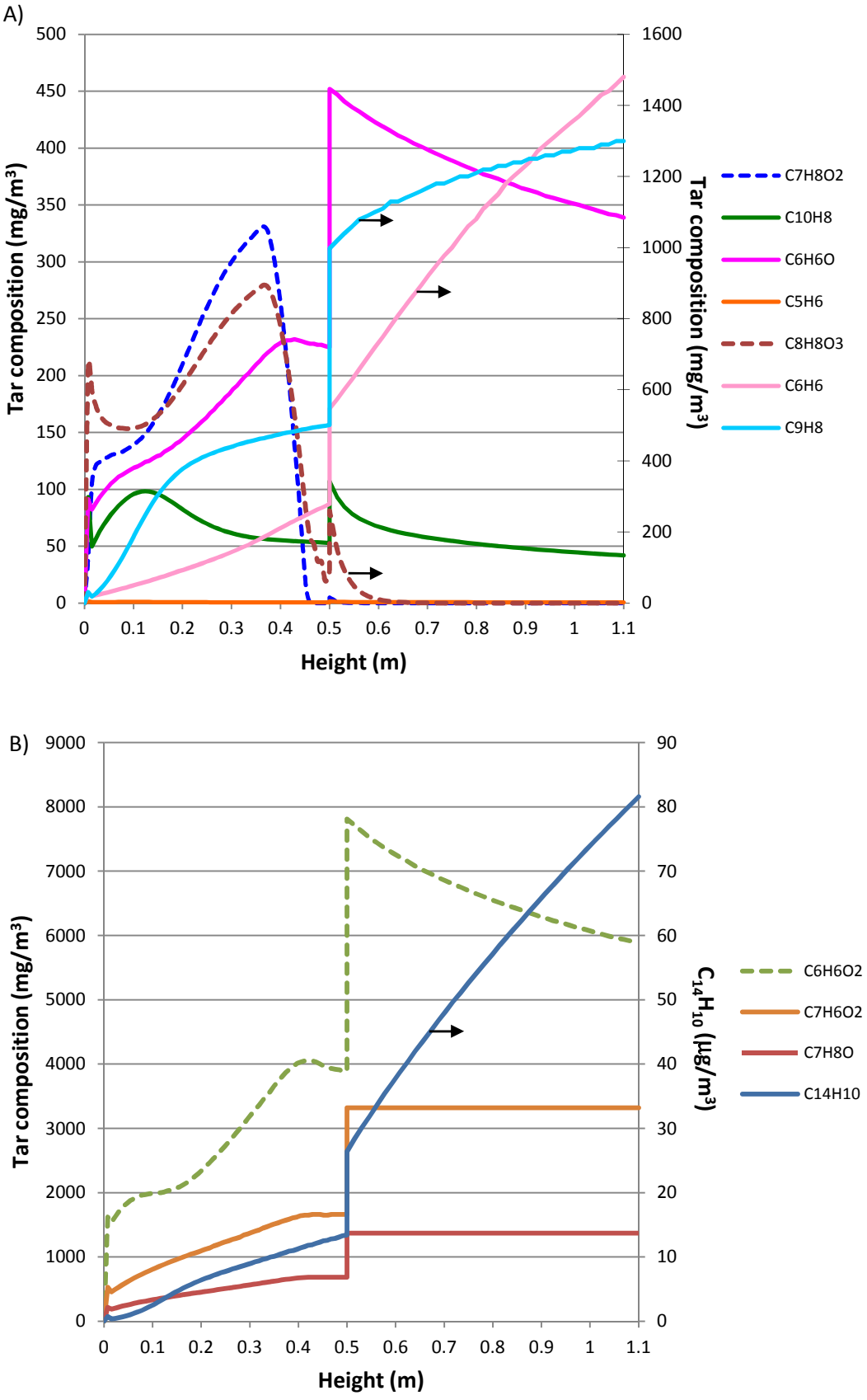

Figure 6.1 A) and B) Tar composition in the emulsion phase from the kinetic model along the gasifier using an ER value of 0.26

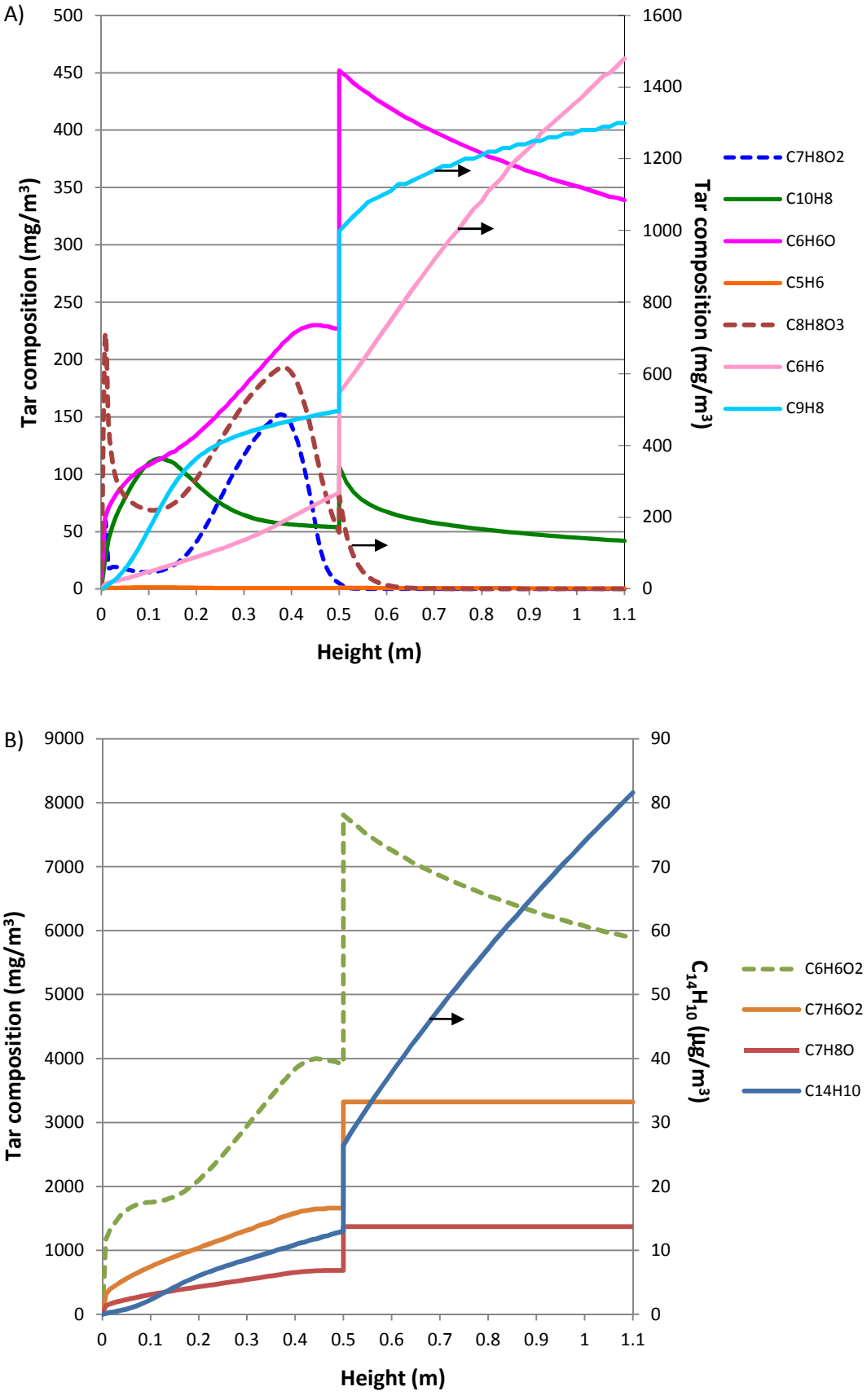

Figure 6.2 A) and B) Tar composition in the bubble phase from the kinetic model along the gasifier using an ER value of 0.26

From experimental work on biomass gasification, it has been reported that benzene and naphthalene are two of the aromatic species present in notable amounts. Whilst most aromatic compounds reached a maximum formation at either 800 or 900°C, followed by a steady destruction with increasing temperature, benzene was one of the most stable one-ring species and was not completely destroyed even at 1200°C [180].

The presence of cyclopentadiene (C_5H_6) is negligible since it is considered an intermediate compound that is produced by reaction R4 where CO is abstracted from phenol [171]. Once cyclopentadiene is generated it immediately reacts to produce naphthalene according to reaction R7 [197].

Very low concentrations are seen for naphthalene ($C_{10}H_8$) and phenanthrene ($C_{14}H_{10}$) as shown in figure 6.2A and 6.2B, respectively. The oxidation of naphthalene according to reaction R8 is more favourable in the bed zone where oxygen is available. In the freeboard, the steam reforming of naphthalene (reaction R24) is more dominant and produces benzene. Phenanthrene is generated mainly in the freeboard at very low concentration (< 135 $\mu g/m^3$). These results agree with work on the characterisation of tars. It was reported that naphthalene is the most quantitatively important tertiary tar analysed and that PAH compounds were present in insignificant amounts up to temperatures of approximately 750-800°C [170].

Figure 6.3 shows the trends of the temperatures of the different phases in the bed zone. In the freeboard zone, the temperature of gases decreased by 32 K from the top of the bed zone. This decrease is consistent with experimental observations. The increase in temperatures of the bubble and emulsion phases in the bed is caused by the combustion reactions occurring closer to the bottom of the bed due to the presence of oxygen. Until the bed height is of 0.4 m or higher, the oxygen content decreases to less than 1% mol and leading to complete absence, respectively, as shown in figure 6.4.

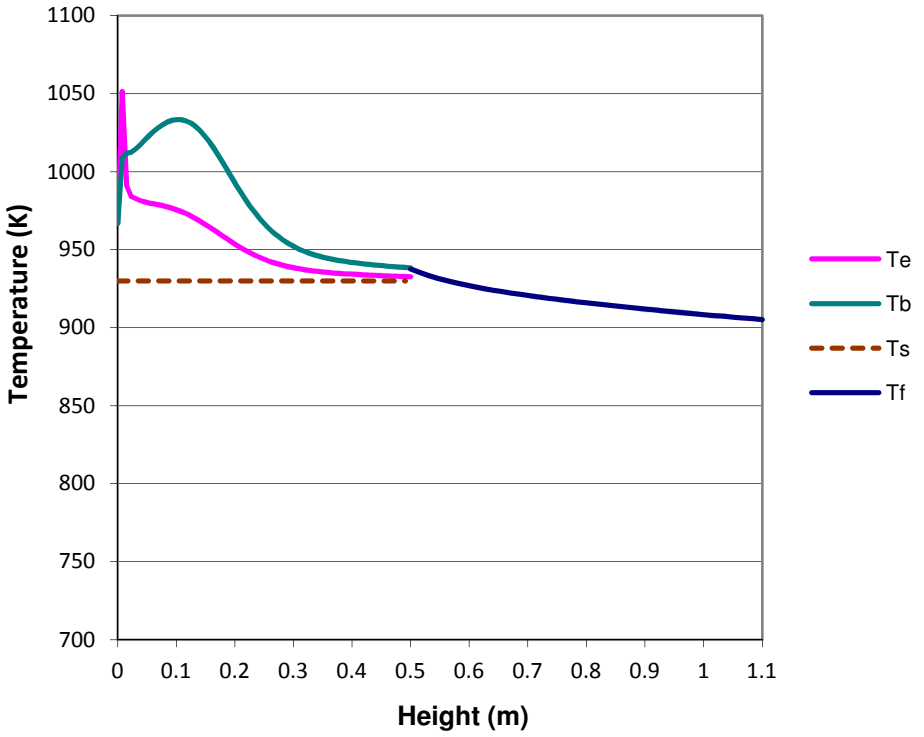

Figure 6.3 Temperatures of gases as a function of gasifier height. Te: temperature of emulsion, Tb: temperature of bubble, Ts: temperature of solids, and Tf: temperature of freeboard zone

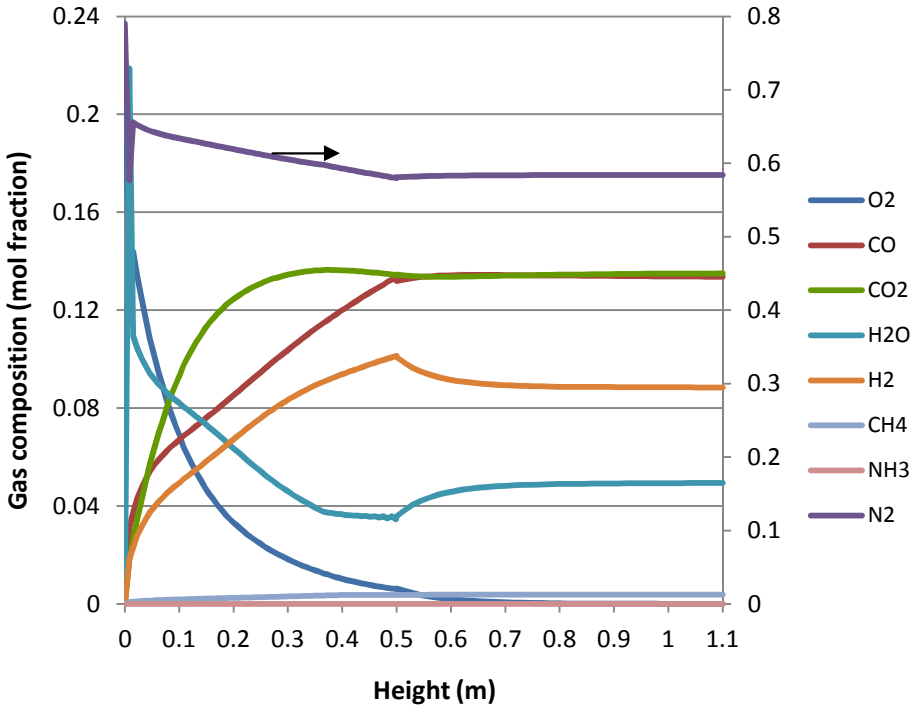

Figure 6.4 Gases composition in the bubble phase from the kinetic model along the gasifier using an ER value of 0.26

This section evaluated the kinetic model using experimental data for wood gasification. The results showed consistency with what is expected during the evolution of primary tars according to experimental work from previous reports. This model requires the knowledge of the lignin content. The measurement of lignin content can be performed by the acid detergent lignin (ADL) method.

6.2 Gasification of poultry litter: Comparison of equilibrium and kinetic models

The results of the kinetic model and equilibrium model are compared in this section. One of the disadvantages of the equilibrium model is that tar components cannot be included because they are not thermodynamically stable; therefore, this model predicts a complete conversion of the tars into non-condensable gas species and water vapour. The kinetic model was compared with the equilibrium model using the input data shown in table 6.4. For both models, flow rates of fuel and gasifying air, temperature of air, and ultimate analysis and moisture content of poultry litter are specified. In addition, lignin content, particle size and density, and gasifier dimensions are required as inputs for the kinetic model.

Table 6.5 shows a comparison of the composition of product gases, temperatures and LHV of gases using the equilibrium and kinetic models. The concentrations of CO, CO_2 and CH_4 are very consistent, whilst the molar composition of H_2 and H_2O are lower for the kinetic model than the equilibrium model. The nitrogen composition is higher for the kinetic model than the equilibrium model. Since the amount of nitrogen is the same for both models, the same ratio of fuel and air was used, non-condensable species that did not reach equilibrium concentration made nitrogen composition higher for the kinetic model.

For the equilibrium model, the achievement of chemical equilibrium is independent of the gasifier height; as a result complete carbon conversion is achieved. In the case of the kinetic model, the bed height was assumed as of 0.4 m. With this bed height, the air temperature was increased in order to raise the temperature of the freeboard to be closer to the equilibrium temperature and achieve high carbon conversions.

Table 6.4 Conditions of kinetic model and equilibrium model

Parameter	Equilibrium model	Kinetic model
Air flow rate	0.0543 kg/s	0.0543 kg/s
ER	0.29	0.29
Temperature of air	830 K	830 K
Poultry litter flow rate	0.0527 kg/s	0.0527 kg/s
Moisture content of poultry litter (wt. %)	25	25
Proximate analysis (wt.%, dry)		
Fixed carbon	24.0	24.0
Volatile matter	54.37	54.37
Ash content	21.63	21.63
Ultimate analysis (wt.%, dry)		
C	37.4	37.4
H	5.11	5.11
O	30.74	30.74
N	3.70	3.70
S	0.45	0.45
Cl	0.97	0.97
Ash content	21.63	21.63
Lignin content (wt %)		25
Particle size		0.35 mm
Particle density		2250 kg/m^3
Reactor diameter		0.6 m
Bed height		0.4 m
Reactor height		1.0 m
Freeboard diameter		1.1 m
Number of holes in distributor		60

Table 6.5 Comparison between equilibrium and kinetic model

	Equilibrium model	Kinetic model
Temperature of solids in bed		880 K
Temperature of emulsion phase		885 K
Temperature of bubble phase		941 K
Temperature of freeboard	940 K	910 K
Carbon conversion	99.9%	96.4%
Gases composition (% mol)		
CO	10.6	9.2
CO_2	15.1	14.5
H_2	19.4	16.0
CH_4	3.8	2.7
H_2O	14.2	12.5
N_2	36.7	43.9
H_2S	0.12	$1.5x10^{-2}$
HCl	$1.7x10^{-5}$	$2.3x10^{-5}$
NH_3	0.025	$4.3x10^{-1}$
SO_2	$6.5x10^{-10}$	$1.0x10^{-2}$
NO	$1.9x10^{-15}$	$6.8x10^{-3}$
Tar		0.74
LHV (MJ/Nm^3, dry, non-condensable gases)	5.58	4.41
LHV (MJ/Nm^3, dry, non-condensable gases including tars)	5.58	4.95

Figure 6.5 shows the composition of main product gases in the emulsion phase of the bed and freeboard zones. Methane shows an increasing concentration with bed height. CO, H_2 H_2O, and CO_2 appear rapidly near the bottom of the bed due to drying and fast devolatilisation of poultry litter. However, their concentrations decrease subsequently with height due to mass transfer to the bubble phase and reactions, such as reaction R11 (oxidation of CO), and reaction R14 (oxidation of hydrogen). H_2O appears near the bottom and is reduced rapidly by heterogeneous

reaction (R15, water gas reaction), and gas-gas reactions such as reaction R13 (steam gasification of CO) and reaction R17 (steam methane reforming).

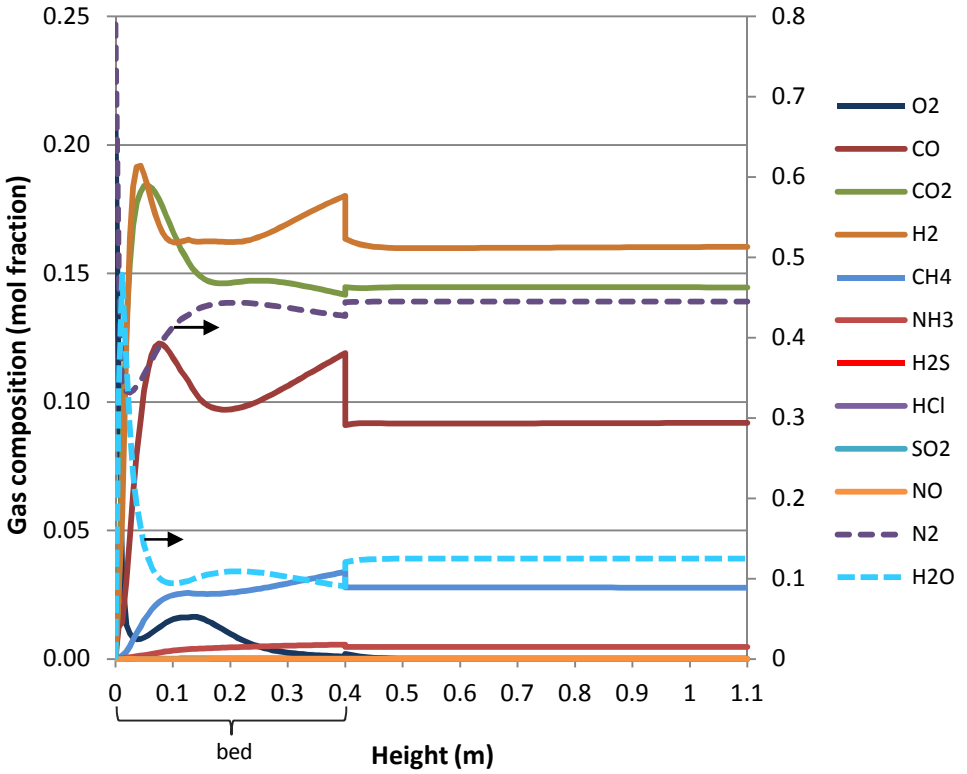

Figure 6.5 Composition of main product gases in the emulsion phase (ER = 0.29)

Figure 6.6 shows the composition of main product gases in the bubble phase of the bed and freeboard zones. Different curve shapes can be seen in figure 6.6 for some of the gases when compared to figure 6.4. Methane, carbon dioxide and ammonia show a monotonic increase in concentration with height. The greatest gases are CO_2, H_2O, and H_2; Nitrogen decreases steadily due to dilution by the generation of fuel gases, and oxygen decreases monotonically due to consumption by combustion reactions. More complex behaviours can be seen for CO, H_2 and H_2O. H_2 reacts to produce more H_2O and CO is also produced by the decomposition of tars (R1, R4, R6, R23, R25 and R26). CO and CH_4 concentrations increase up to a maximum closer to the top of the bed. The concentration of water vapour is quite significant in the bubble phase but when it enters the freeboard it decreases to values lower than 12.5% (mol). This decrease is due to the lower concentrations in the emulsion phase caused mainly by heterogeneous reactions such as water gas reaction, plus homogeneous reactions as steam methane reforming reaction. In

addition, steam gasification of naphthalene according to reaction R25 and of benzene by reaction R27 consume H_2O. The step seen in figures 6.5 and 6.6 is caused by the mixing of gases from the bubble and emulsion phases before entering the freeboard zone.

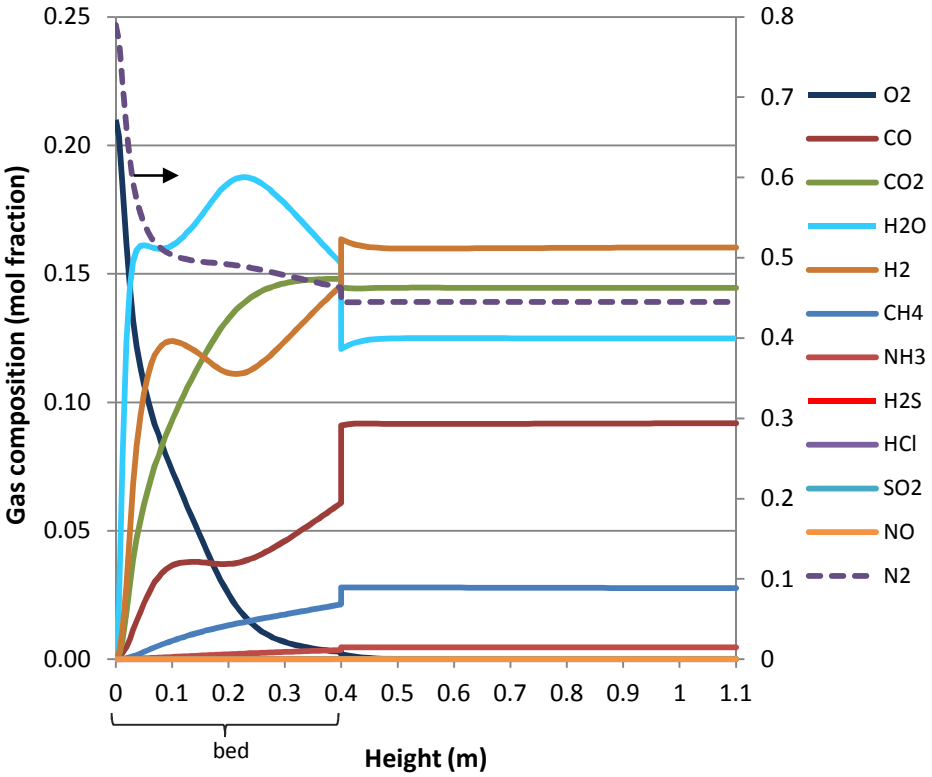

Figure 6.6 Composition of main product gases in the bubble phase (ER = 0.29)

Figure 6.7 shows the tar composition for the emulsion phase in the bed zone plus in the freeboard zone as a function of gasifier height. Benzene and indene concentrations increase in the freeboard while other aromatics decompose, such as guaiacol, vanillin, catechol and phenol. Insignificant concentrations are seen for naphthalene, cyclopentadiene and phenanthrene. These results agree with the findings described for beech gasification in section 6.1.

Figure 6.8 shows the temperatures of gases for the bubble phase, emulsion phase, solids and freeboard zone, as a function of bed height. At the bottom of the bed, the temperature of the emulsion increases abruptly and then remains very similar to the temperature of the solids due to the higher gases-solid energy transfer coefficients. In contrast, the temperature of the bubble phase increases in the middle of the bed due to a decrease in the bubble-emulsion energy transfer coefficients.

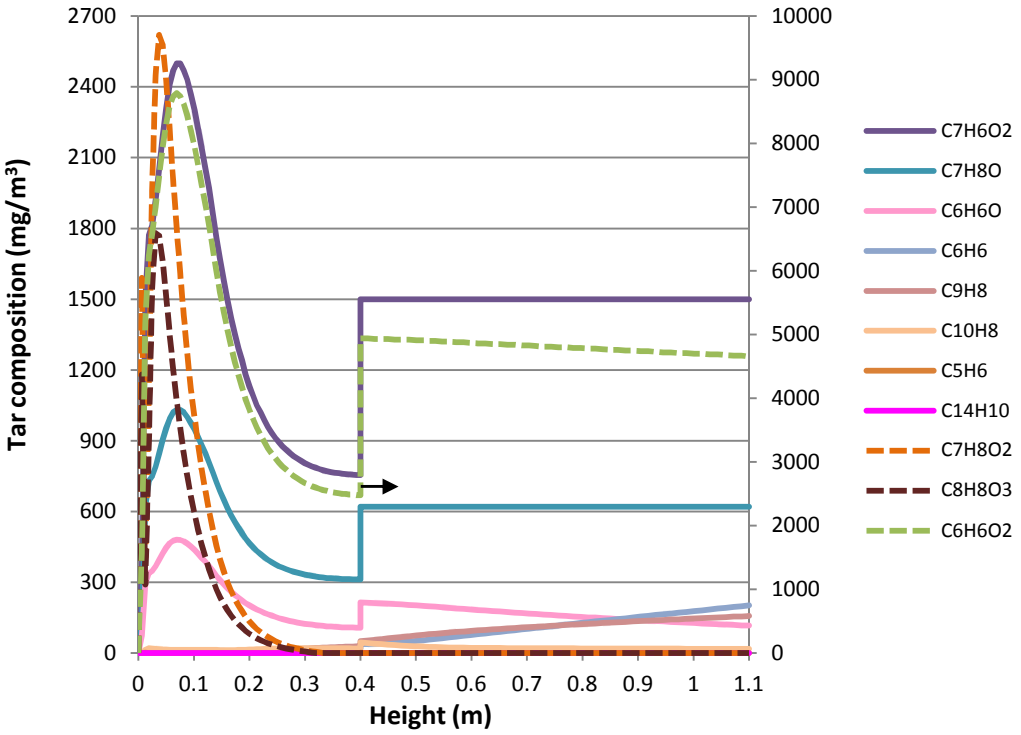

Figure 6.7 Tar composition of emulsion phase in bed zone as a function of gasifier height (ER = 0.29)

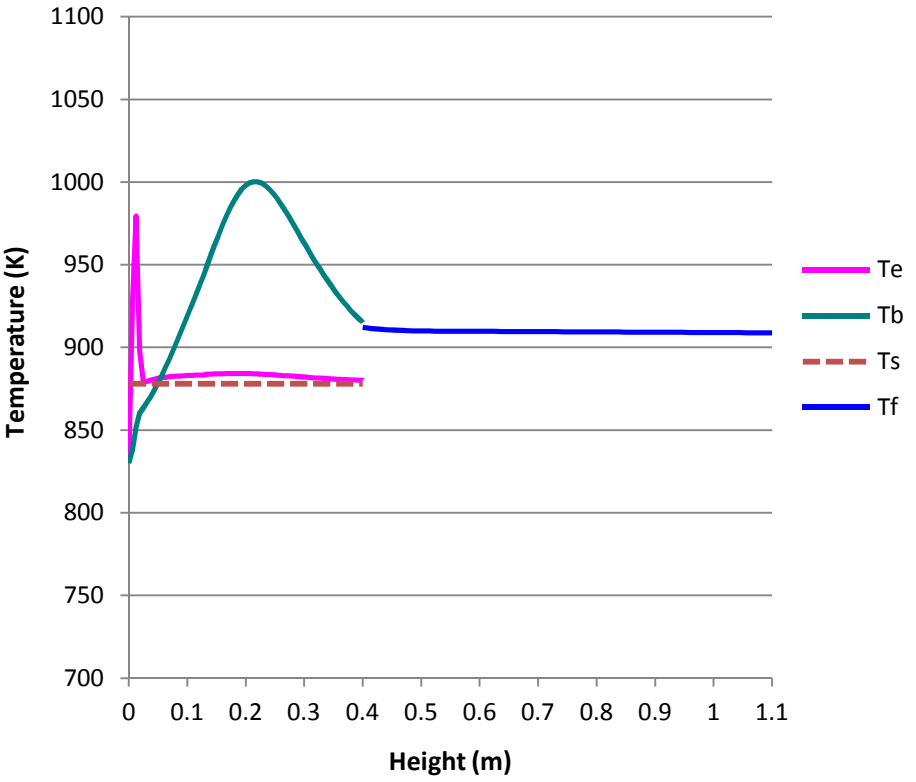

Figure 6.8 Temperatures of gases as a function of bed height. Te: temperature of emulsion, Tb: temperature of bubble, and Ts: temperature of solids

Knowledge of these temperatures is important to identify high temperature regions during the gasifier operation. The temperature of the emulsion shows a hot sport near the distributor which will need to stand this higher temperature. The hot spot in the bubble phase should be considered since it could cause problems to maintain the fluidisation of the bed.

Figure 6.9 shows the composition of product gases when the ER was varied. This figure compares the results between equilibrium model (dashed lines) and kinetic model (solid lines) results using ER values from 0.22 to 0.32. It can be seen that CO, H_2 and CH_4 decreased with increasing ER value, whilst CO_2, H_2O and N_2 increased for both models.

As expected, CO, H_2 and CH_4 decreased while CO_2 increased with increasing ER due to the addition of more air. H_2O increased with greater ER values due to the combustion of hydrogen and methane. Methane decreased due to steam methane reforming reactions. The concentration of methane was higher for the equilibrium model than the kinetic model because methane represents all hydrocarbons in the equilibrium model.

Figure 6.10 shows the tar concentrations of individual tar compounds for various ER values. Catechol and phenol decrease with increasing ER values, whilst benzene and indene increase. Cyclopentadiene and phenanthrene are produced in insignificant amounts (< 35 $\mu g/m^3$). O-cresol and salicylaldehyde concentrations remained quite constant in the range of ER values evaluated. Figure 6.10 agrees with the results of section 6.1. The most abundant tar compounds are catechol, o-cresol and salicylaldehyde, followed by benzene and indene. The total tar concentration decrease with increasing ER value as expected.

This section compared the kinetic model with the equilibrium model. The results showed agreement of the trends of the evolution of main gases when the ER value was varied. The kinetic model provides additional information on the formation of tars and their behaviour when the ER was raised. The increase in ER value has the benefit of reducing the total tar concentration; however, it has the disadvantage of decreasing the LHV of the gases. The model showed that catechol, o-cresol and salicylaldehyde are abundant species for which kinetic parameters for pyrolysis and gasification are not yet available.

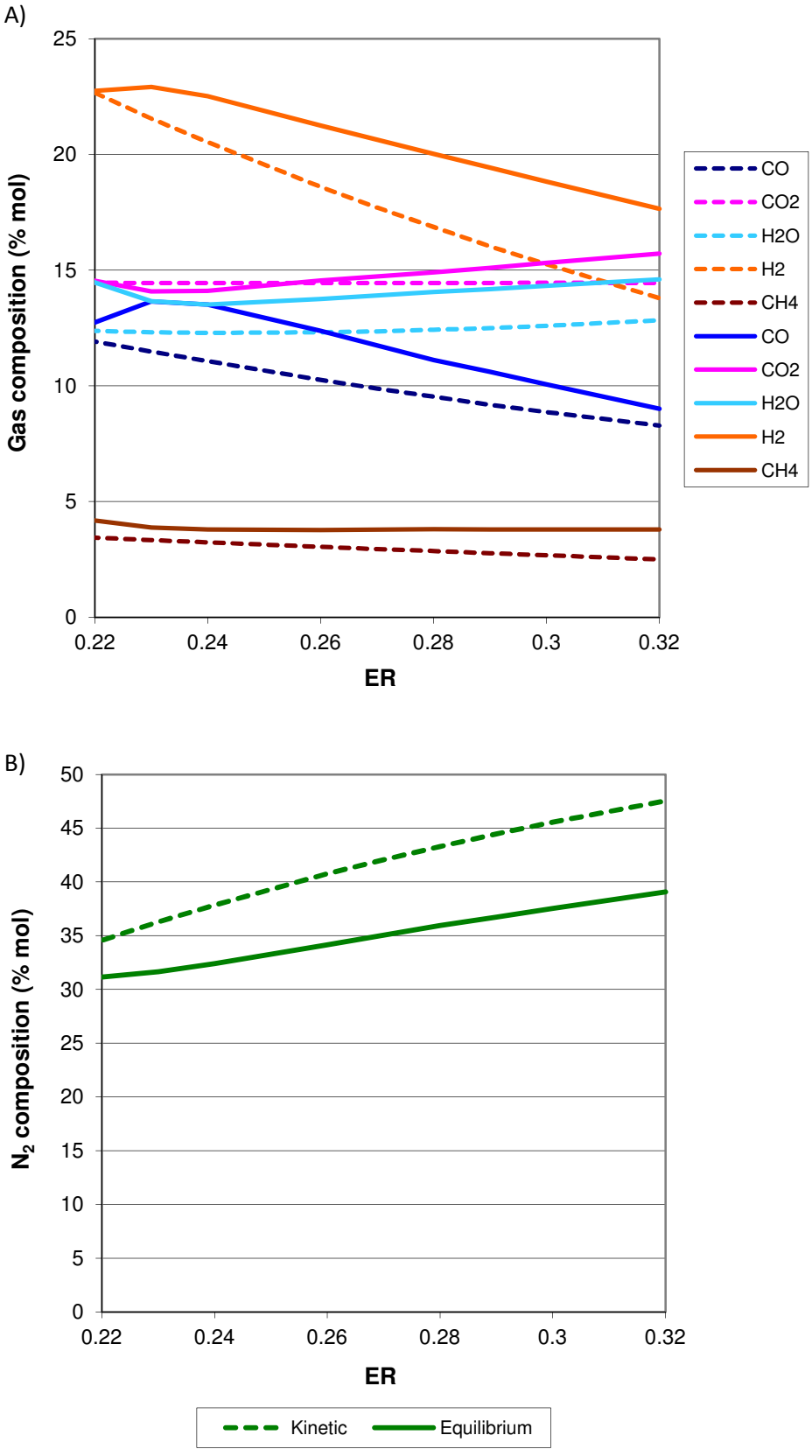

Figure 6.9 A) Gas composition of product gases using various ER values and temperature of air of 830 K, and B) N_2 composition. (solid lines for kinetic model and dashed lines for equilibrium model)

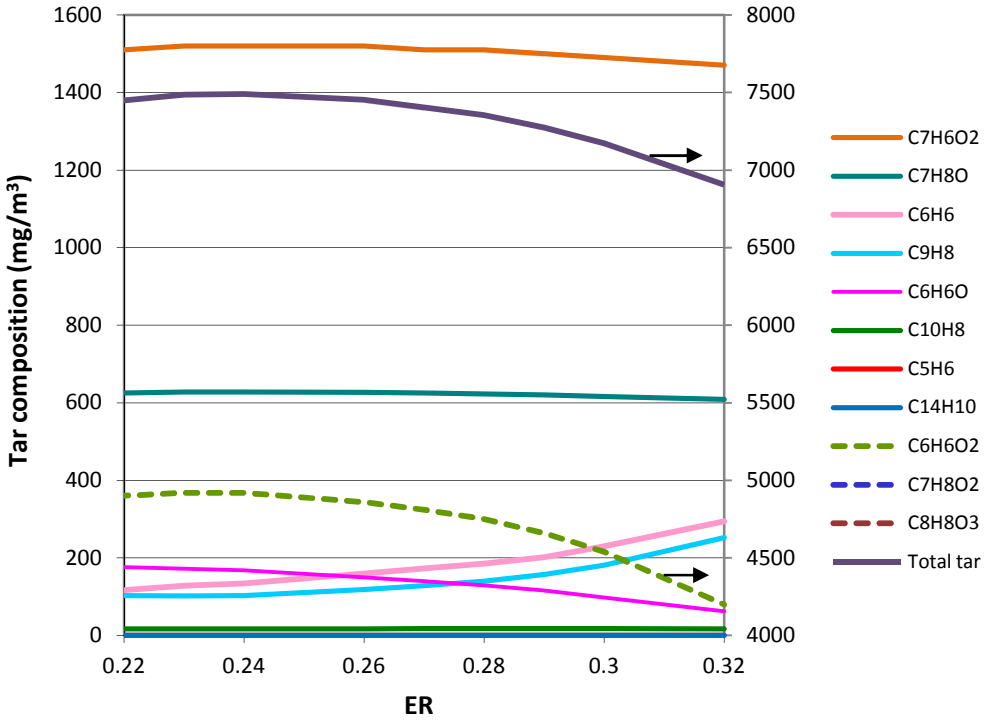

Figure 6.10 Tar composition using various ER values

6.3 Summary

A kinetic model for the gasification of poultry litter that incorporated tar formation and evolution was evaluated in this chapter. Firstly, the model was verified using experimental data from the gasification of beech because at the present time experimental data from the gasification of poultry litter is not yet available. Since lignin was assumed as the main precursor of tars formation, the lignin content of biomass was required as part of the fuel characterisation. The kinetic model results showed consistency with what is expected during the evolution of primary tars according to experimental work from previous reports. However, the model overestimated the total tar concentration and tars of class 2.

Secondly, the kinetic model and equilibrium model were compared for the gasification of poultry litter. The comparison showed agreement between the two models. A sensitivity analysis of the variation of ER values showed similar trends of the evolution of the main gases for both models. In addition, this comparison allowed the validation of assuming that product gases reach equilibrium during gasification in the equilibrium model. Moreover, the kinetic model has the additional benefit of

providing information on the formation of tars and their behaviour when the ER value was raised. The model showed the most abundant tar compounds were catechol, o-cresol and salicylaldehyde, which require further experimental studies to obtain kinetic parameters for their pyrolysis and gasification, since kinetic data for their destruction was not available for inclusion in the model.

Chapter 7

Conclusions

A process for the gasification of poultry litter was examined in this study. This process integrates a fluidised bed gasifier with a gas turbine with the aim of generating combustibles gases for energy production. This process was proposed as a viable solution for a small-scale system to be installed on-site the biomass source. The system allows the treatment of waste with the additional benefit of generation of energy, and is suitable for a poultry farm to avoid the transportation of litter to centralised disposal facilities. A fluidised bed gasifier was chosen because biomass is very rapidly mixed with the bed material, and almost immediately heated up to the bed temperature. During gasification many by-products are generated such as NO_x, SO_2, fly ash and tar. Since tar is a major issue in biomass gasification when implementing this technology, tar formation and evolution was presented as a central part of the evaluation in this work.

After a bibliographic review, the lignin content of biomass was concluded as responsible for tar formation because of its aromatic nature. Therefore, the model requires the knowledge of the biomass lignin content. As lignin components, guaiacol, vanillin and catechol were chosen as tar precursors due to their known presence in the lignin structure. A reaction mechanism and its corresponding kinetics were derived. This mechanism was based on the three-lignin unit decomposition into lighter molecules and greater aromatic rings. Some of the tar products were involved in combustion and/or steam gasification reactions. This model consisted of 27 reactions. The tar reaction mechanism was introduced into the kinetic model for the gasification of poultry litter.

The kinetic model was compared with experimental data from wood gasification for validation purposes. The results showed consistency with experimental work from previous reports for the evolution of primary tars. However, the model overestimated the total tar concentration and tars of class 2.

The kinetic model and equilibrium model were compared changing the ER value. The results showed good agreement on the composition of the main gases when the ER value was varied. The increase in ER value has the benefit of reducing the total tar concentration; however, it has the disadvantage of decreasing the LHV of the gases. The model showed the evolution of tar compounds and which tar species were the most abundant. Three tar species dominated: catechol, o-cresol and salicylaldehyde, with an average composition of 64, 8, and 20 wt. % of the total tars, respectively.

Since there is limited literature on the gasification of poultry litter, the results generated provided a means to evaluate the leading parameters that affect the optimal operation of the gasifier. In addition, tar is a major issue in biomass gasification; therefore, its prediction is relevant for the selection of operating parameters. The kinetic model showed consistent tar predictions as well as a framework to conduct future experimental work.

The full process was evaluated in order to compare layout configurations which included heat recuperation from the GT exhaust gases. On one hand, for the conventional “atmospheric layout”, the fuel gases had to be cooled down before being compressed to the desire pressure; therefore, this caused significant wastage of energy from the hot fuel gases, for the base case 14% of energy was wasted by cooling the fuel gases. On the other hand, the “pressurised layout” benefit was that all process stages could be maintained hot. The maximum efficiency achieved by the conventional “atmospheric layout” was 24%. Process efficiency analyses showed that even when the “atmospheric layout” was set with energy recuperation (28.5%), the “pressurised layout” delivered higher efficiencies with (33%) or without the energy recuperation (31.5%) into the gasifier.

Different energy integration configurations were compared to recuperate energy from the hot exhaust gases from the gas turbine. Pinch analysis was not the most useful tool for the selection of the heat exchanger configurations. The cool streams were air and product fuel gases. However, once the gasifying air was

preheated, the gasification temperature can increase to values higher than the GT exhaust temperature (hot stream), especially at high ER values and low moisture content of poultry litter.

This work reviewed the selection of an optimal ER value. However, it was found that its selection is a compromise between achieving the best process efficiency and the minimum emission of pollutants to comply with environmental standards. Low ER values had the benefit of generating low HCl emissions and good process efficiency but the disadvantage of releasing very high SO_2 emissions. High ER values did not show to reduce the SO_2 emissions enough to comply with the guidelines. Therefore, H_2S removal seems necessary for the reduction of SO_2 emissions.

The incorporation of inorganic constituents of ash in the equilibrium model showed the partition of inorganics in the solid and gas phases. Most of the inorganics remained in the solids. However, at high temperatures (with high ERs or low MCs) chlorine, potassium and sodium can be found in the gas phase. These vapours are of great concern in gas turbines because they can increase rates of hot corrosion on turbine surfaces. At high temperatures (> 950K), H_2S concentration was reduced due to reaction with calcium and sulphur remained in the solid phase as CaS. The studies showed that operating at low temperature, selecting low ER values and/or wet fuels is preferred to minimise the vaporisation of inorganic species and not exceed the fuel requirements for gas turbines.

7.1 Future work

This work has provided an evaluation of the gasification of poultry litter using two models. Since at the present time experimental data from the gasification of poultry litter was not available, future experimental work would not only benefit the design of a commercial facility but also help improving the accuracy of the proposed model.

This work has proposed a tar mechanism and showed how tar evolves during biomass gasification. The evaluation of the simulation results showed that some intermediate reactions require additional kinetic parameters for tar decomposition. It would be beneficial to study individual reactions to gain Arrhenius parameters; in

particular, it is needed to study the reactions of pyrolysis and combustion of o-cresol and salicylaldehyde. The completeness of the kinetics would improve the fidelity of the tar simulation.

For the formation of tar, the main assumption is that tar derives directly from the lignin present in biomass based on its aromatic nature. However, there are experimental studies on cellulose and wood that suggest that acetylene is also responsible for the formation and growth of aromatic rings. During biomass gasification, it would be worth quantifying the generation of acetylene, its implication on benzene formation and PAH compounds growth and its relative importance to lignin aromatics.

In addition, the model could be further improved by making more flexible the design of the gasifier, e.g. allowing the variation of the feeding point of biomass or the use of external heaters to keep certain temperature inside the gasifier. By improving the model to more accurately represent the design and operation of gasifiers, it could provide a better understanding of the reactions occurring during the process and identify optimum conditions to minimise tar production. In order to further validate the model, experiments need to be performed using the operating conditions assumed in the model and required to analyse individual tar compounds and main product gases at various heights of the bed and freeboard zones.

In the kinetic model, a reaction that represents the retention of chlorine (reaction R22) in the ash was included. However, other inorganics, such as sulphur, are also retained in the bed as shown by the equilibrium model. Empirical work on the study of the ash chemistry would benefit the simulation since the incorporation of these reactions would allow the prediction of inorganics partition, ash agglomeration and ash melting, and also benefit the gasifier operation to comply with environmental regulations by predicting the emissions of pollutants, such as SO_x and HCl.

References

[1] Windhorst HW. Bio-energy production - a threat to the global egg industry? World's Poultry Science Journal 2007;63:365-79.

[2] SIAP. Servicio de Información Agroalimentaria y Pesquera. http://wwwsiapsagarpagobmx/.

[3] DEFRA. Department for Environment, Food and Rural Affairs. p. www.defra.gov.uk.

[4] Nicholson FA, Chambers BJ, Dampney PMR. Nitrogen value of poultry litter applications to root crops and following cereal crops. The Journal of Agricultural Science 2003;140:53-64.

[5] Kelleher BP, Leahy JJ, Henihan AM, O'Dwyer TF, Sutton D, Leahy MJ. Advances in poultry litter disposal technology - a review. Bioresource Technology 2002;83:27-36.

[6] Mante OD, Agblevor FA. Influence of pine wood shavings on the pyrolysis of poultry litter. Waste Management 2010;30:2537-47.

[7] Bowen B, Lynch D, Lynch D, Henihan AM, Leahy JJ, McDonnell K. Biosecurity on Poultry Farms from On-Farm Fluidized Bed Combustion and Energy Recovery from Poultry Litter. Sustainability 2010;2:2135-43.

[8] Gerba CP, Smith JE, Jr. Sources of Pathogenic Microorganisms and their Fate during Land Application of Wastes. Journal of Environmental Quality 2005;34:42-48.

[9] Henihan AM, Leahy MJ, Leahy JJ, Cummins E, Kelleher BP. Emissions modeling of fluidised bed co-combustion of poultry litter and peat. Bioresource Technology 2003;87:289-94.

[10] Bitzer CC, Sims JT. Estimating the availability of nitrogen in poultry manure through laboratory and field studies. Journal of environmental quality 1988;17:47-54.

[11] European Commission - Environment. http://ec.europa.eu/environment/water/water-nitrates/index_en.html; 2011.

[12] McKendry P. Energy production from biomass (part 2): conversion technologies. Bioresource Technology 2002;83:47-54.

[13] Leahy MJ, Henihan AM, Kelleher BP, Leahy JJ, O'Connor J. Mitigation of large-scale organic waste damage incorporating a demonstration of a closed loop conversion of poultry waste to energy at the point of source (2000-LS-1-M2). Final Report. Environmental Protection Agency; 2007.

[14] Cantrell K, Ro K, Mahajan D, Anjom M, Hunt PG. Role of Thermochemical Conversion in Livestock Waste-to-Energy Treatments: Obstacles and Opportunities. 2007.

[15] Kirubakaran V, Sivaramakrishnan V, Premalatha M, Subramanian P. Kinetics of Auto-Gasification of Poultry Litter. International Journal of Green Energy 2007;4:519 - 34.

[16] Codling EE, Chaney RL, Sherwell J. Poultry Litter Ash as a Potential Phosphorus Source for Agricultural Crops. J Environ Qual 2002;31:954-61.

[17] Upreti BR, van der Horst D. National renewable energy policy and local opposition in the UK: the failed development of a biomass electricity plant. Biomass and Bioenergy 2004;26:61-69.

[18] Wang L, Weller CL, Jones DD, Hanna MA. Contemporary issues in thermal gasification of biomass and its application to electricity and fuel production. Biomass Bioenergy 2008;32:573-81.
[19] Han J, Kim H. The reduction and control technology of tar during biomass gasification/pyrolysis: An overview. Renewable and Sustainable Energy Reviews 2008;12:397-416.
[20] Liu H, Ni W, Li Z, Ma L. Strategic thinking on IGCC development in China. Energy Policy 2008;36:1-11.
[21] Baratieri M, Baggio P, Bosio B, Grigiante M, Longo GA. The use of biomass syngas in IC engines and CCGT plants: A comparative analysis. Appl Therm Eng 2009;29:3309-18.
[22] Rodrigues M, Walter A, Faaij A. Performance evaluation of atmospheric biomass integrated gasifier combined cycle systems under different strategies for the use of low calorific gases. Energy Conversion and Management 2007;48:1289-301.
[23] Wolf J, Barone F, Yan J. Performance Analysis of Evaporative Biomass Air Turbine Cycle with Gasification for Topping Combustion. J Eng Gas Turbines Power 2002;124:757-61.
[24] Rezaiyan J, Cheremisinoff NP. Gasification technologies. A primer for engineers and scientists: Taylor & Francis Group; 2005.
[25] Goyal HB, Seal D, Saxena RC. Bio-fuels from thermochemical conversion of renewable resources: A review. Renewable and Sustainable Energy Reviews 2008;12:504-17.
[26] Demirbas A. Mechanisms of liquefaction and pyrolysis reactions of biomass. Energy Conversion and Management 2000;41:633-46.
[27] Higman C, van der Burgt M. Gasification: Gulf Professional Publishing; 2003.
[28] Skoulou V, Zabaniotou A, Stavropoulos G, Sakelaropoulos G. Syngas production from olive tree cuttings and olive kernels in a downdraft fixed-bed gasifier. Int J Hydrogen Energy 2008;33:1185-94.
[29] Hamel S, Krumm W. Mathematical modelling and simulation of bubbling fluidised bed gasifiers. Powder Technology 2001;120:105-12.
[30] Demirbas A. Biomass resource facilities and biomass conversion processing for fuels and chemicals. Energy Convers Manage 2001;42:1357-78.
[31] Howard JR. Fluidized bed technology: principles and applications: Bristol : Hilger; 1989.
[32] Kunii D, Levenspiel O. Fluidization engineering. 2nd ed: Butterworth-Heinemann; 1991.
[33] Sharma AK. Equilibrium modeling of global reduction reactions for a downdraft (biomass) gasifier. Energy Conversion and Management 2008;49:832-42.
[34] Warnecke R. Gasification of biomass: comparison of fixed bed and fluidized bed gasifier. Biomass Bioenergy 2000;18:489-97.
[35] Gil J, Corella J, Aznar MP, Caballero MA. Biomass gasification in atmospheric and bubbling fluidized bed: Effect of the type of gasifying agent on the product distribution. Biomass and Bioenergy 1999;17:389-403.
[36] Aznar MP, Caballero MA, Gil J, Martin JA, Corella J. Commercial Steam Reforming Catalysts To Improve Biomass Gasification with Steam-Oxygen Mixtures. 2. Catalytic Tar Removal. Ind Eng Chem Res 1998;37:2668-80.

[37] Gil J, Aznar MP, Caballero MA, Frances E, Corella J. Biomass Gasification in Fluidized Bed at Pilot Scale with Steam-Oxygen Mixtures. Product Distribution for Very Different Operating Conditions. Energy Fuels 1997;11:1109-18.
[38] Whitely N, Ozao R, Artiaga R, Cao Y, Pan WP. Multi-utilization of Chicken Litter as Biomass Source. Part I. Combustion. Energy Fuels 2006;20:2660-65.
[39] Channiwala SA, Parikh PP. A unified correlation for estimating HHV of solid, liquid and gaseous fuels. Fuel 2002;81:1051-63.
[40] Kirubakaran V, Sivaramakrishnan V, Nalini R, Sekar T, Premalatha M, Subramanian P. A review on gasification of biomass. Renewable and Sustainable Energy Reviews 2009;13:179-86.
[41] Turn SQ, Kinoshita CM, Ishimura DM, Zhou J. The fate of inorganic constituents of biomass in fluidized bed gasification. Fuel 1998;77:135-46.
[42] GE. Specification for fuel gases for combustion in heavy-duty gas turbines. General Electric Company; 2002.
[43] Doshi V, Vuthaluru HB, Korbee R, Kiel JHA. Development of a modeling approach to predict ash formation during co-firing of coal and biomass. Fuel Processing Technology 2009;90:1148-56.
[44] Visser HJM, van Lith SC, Kiel JHA. Biomass Ash-Bed Material Interactions Leading to Agglomeration in FBC. Journal of Energy Resources Technology 2008;130:011801.
[45] Werkelin J, Skrifvars B-J, Zevenhoven M, Holmbom B, Hupa M. Chemical forms of ash-forming elements in woody biomass fuels. Fuel 2010;89:481-93.
[46] Arvelakis S, Jensen PA, Dam-Johansen K. Simultaneous Thermal Analysis (STA) on Ash from High-Alkali Biomass. Energy Fuels 2004;18:1066-76.
[47] Tortosa Masiá AA, Buhre BJP, Gupta RP, Wall TF. Characterising ash of biomass and waste. Fuel Processing Technology 2007;88:1071-81.
[48] Devi L, Ptasinski KJ, Janssen FJJG. A review of the primary measures for tar elimination in biomass gasification processes. Biomass and Bioenergy 2003;24:125-40.
[49] Milne TA, Evans RJ, Abatzoglou N. Biomass Gasifier "Tars": Their Nature, Formation, and Conversion.: National Renewable Energy Laboratory; 1998.
[50] Yu J, Yin F, Wang S, Chang L, Gupta S. Sulfur removal property of activated-char-supported Fe-Mo sorbents for integrated cleaning of hot coal gases. Fuel;In Press, Corrected Proof.
[51] Bergman PCA, van Paasen SVB, Boerrigter H. The novel "OLGA" technology for complete tar removal from biomass producer gas. Pyrolysis and Gasification of Biomass and Waste, Expert Meeting. Strasbourg, France; 2002.
[52] Klimantos P, Koukouzas N, Katsiadakis A, Kakaras E. Air-blown biomass gasification combined cycles (BGCC): System analysis and economic assessment. Energy 2009;34:708-14.
[53] Nair SA, Yan K, Pemen AJM, Winands GJJ, van Gompel FM, van Leuken HEM, et al. A high-temperature pulsed corona plasma system for fuel gas cleaning. Journal of Electrostatics 2004;61:117-27.
[54] Abatzoglou N, Barker N, Hasler P, Knoef H. The development of a draft protocol for the sampling and analysis of particulate and organic contaminants in the gas from small biomass gasifiers. Biomass and Bioenergy 2000;18:5-17.
[55] Simell P, Ståhlberg P, Kurkela E, Albrecht J, Deutsch S, Sjöström K. Provisional protocol for the sampling and anlaysis of tar and particulates in the gas

from large-scale biomass gasifiers. Version 1998. Biomass and Bioenergy 2000;18:19-38.
[56] Herguido J, Corella J, Gonzalez-Saiz J. Steam gasification of lignocellulosic residues in a fluidized bed at a small pilot scale. Effect of the type of feedstock. Ind Eng Chem Res 1992;31:1274-82.
[57] Narvaez I, Orio A, Aznar MP, Corella J. Biomass Gasification with Air in an Atmospheric Bubbling Fluidized Bed. Effect of Six Operational Variables on the Quality of the Produced Raw Gas. Ind Eng Chem Res 1996;35:2110-20.
[58] Schuster G, Loffler G, Weigl K, Hofbauer H. Biomass steam gasification - an extensive parametric modeling study. Bioresour Technol 2001;77:71-79.
[59] Zhu X, Venderbosch R. A correlation between stoichiometrical ratio of fuel and its higher heating value. Fuel 2005;84:1007-10.
[60] Narvaez I, Orio A, Aznar MP, Corella J. Biomass Gasification with Air in an Atmospheric Bubbling Fluidized Bed. Effect of Six Operational Variables on the Quality of the Produced Raw Gas. Ind Eng Chem Res 1996;35:2110-20.
[61] Lv PM, Xiong ZH, Chang J, Wu CZ, Chen Y, Zhu JX. An experimental study on biomass air-steam gasification in a fluidized bed. Bioresource Technology 2004;95:95-101.
[62] Kinoshita CM, Wang Y, Zhou J. Tar formation under different biomass gasification conditions. Journal of Analytical and Applied Pyrolysis 1994;29:169-81.
[63] Knight RA. Experience with raw gas analysis from pressurized gasification of biomass. Biomass and Bioenergy 2000;18:67-77.
[64] Devi L, Ptasinski KJ, Janssen FJJG, van Paasen SVB, Bergman PCA, Kiel JHA. Catalytic decomposition of biomass tars: use of dolomite and untreated olivine. Renewable Energy 2005;30:565-87.
[65] Sutton D, Kelleher B, Ross JRH. Review of literature on catalysts for biomass gasification. Fuel Processing Technology 2001;73:155-73.
[66] Gil J, Caballero MA, Martin JA, Aznar MP, Corella J. Biomass Gasification with Air in a Fluidized Bed: Effect of the In-Bed Use of Dolomite under Different Operation Conditions. Ind Eng Chem Res 1999;38:4226-35.
[67] Devi L, Ptasinski KJ, Janssen FJJG. Pretreated olivine as tar removal catalyst for biomass gasifiers: investigation using naphthalene as model biomass tar. Fuel Processing Technology 2005;86:707-30.
[68] Corella J, Toledo JM, Padilla R. Olivine or Dolomite as In-Bed Additive in Biomass Gasification with Air in a Fluidized Bed: Which Is Better? Energy Fuels 2004;18:713-20.
[69] Elliott DC, Baker EG. The effect of catalysis on wood-gasification tar composition. Biomass 1986;9:195-203.
[70] Brown RC, Liu Q, Norton G. Catalytic effects observed during the co-gasification of coal and switchgrass. Biomass and Bioenergy 2000;18:499-506.
[71] Zhang R, Brown RC, Suby A, Cummer K. Catalytic destruction of tar in biomass derived producer gas. Energy Conversion and Management 2004;45:995-1014.
[72] Tomishige K, Asadullah M, Kunimori K. Syngas production by biomass gasification using Rh/CeO2/SiO2 catalysts and fluidized bed reactor. Catalysis Today 2004;89:389-403.
[73] Ketcong A, Vitidsant T, Fujimoto K. The Development of Ni/Dolomite Catalyst in Simultaneous Biomass Gasification and Reforming in Fluidized Bed. American Journal of Environmental Sciences 2009;5:273-77.

[74] Rapagnà S, Jand N, Foscolo PU. Catalytic gasification of biomass to produce hydrogen rich gas. International Journal of Hydrogen Energy 1998;23:551-57.
[75] Swierczynski D, Courson C, Kiennemann A. Study of steam reforming of toluene used as model compound of tar produced by biomass gasification. Chemical Engineering and Processing: Process Intensification 2008;47:508-13.
[76] Davalos JZ, Roux MV, Jimenez P. Evaluation of poultry litter as a feasible fuel. Thermochimica Acta 2002;394:261-66.
[77] Schnitzer MI, Monreal CM, Facey GA, Fransham PB. The conversion of chicken manure to biooil by fast pyrolysis I. Analyses of chicken manure, biooils and char by ^{13}C and ^{1}H NMR and FTIR spectrophotometry. Journal of Environmental Science and Health, Part B: Pesticides, Food Contaminants, and Agricultural Wastes 2007;42:71 - 77.
[78] Abelha P, Gulyurtlu I, Boavida D, Seabra Barros J, Cabrita I, Leahy J, et al. Combustion of poultry litter in a fluidised bed combustor*. Fuel 2003;82:687-92.
[79] YANG Y, IJI PA, CHOCT M. Dietary modulation of gut microflora in broiler chickens: a review of the role of six kinds of alternatives to in-feed antibiotics. World's Poultry Science Journal 2009;65:97-114.
[80] Reardon JP, Lilley A, Browne K, Beard K, Wimberly J, Avens J. Demonstration of a Small Modular Biopower System Using Poultry Litter. DOE SBIR Phase-I Final Report. Community Power Corporation; 2001.
[81] Antares_Group_Incorporated. Economic and technical feasibility of energy production from poultry litter and nutrient filter biomass on the lower Delmarva Peninsula (Technical Report No. 20785) Appendix A.; 1999.
[82] Nicholson FA, Chambers BJ, Williams JR, Unwin RJ. Heavy metal contents of livestock feeds and animal manures in England and Wales. Bioresource Technology 1999;70:23-31.
[83] Proudfoot FG, Jackson ED, Hulan HW, Salisbury CDC. Arsanilic acid as a growth promoter for chicken broilers when administered via either the feed or drinking water. Canadian Journal of Animal Science 1991;71:221-26.
[84] Anderson BK, Chamblee TN. The effect of dietary 3-nitro-4-hydroxyphenylarsonic acid (roxarsone) on the total arsenic level in broiler excreta and broiler litter. Journal of Applied Poultry Research 2001;10:323-28.
[85] Nachman KE, Mihalic JN, Burke TA, Geyh AS. Comparison of arsenic content in pelletized poultry house waste and biosolids fertilizer. Chemosphere 2008;71:500-06.
[86] US Food and Drug Administration (FDA). http://www.fda.gov.
[87] Di Blasi C. Modeling chemical and physical processes of wood and biomass pyrolysis. Progress in Energy and Combustion Science 2008;34:47-90.
[88] Basu P, Kaushal P. Modeling of Pyrolysis and Gasification of Biomass in Fluidized Beds: A Review. Chemical Product and Process Modeling 2009;4:Article 21.
[89] Rapagnà S, Mazziotti di Celso G. Devolatilization of wood particles in a hot fluidized bed: Product yields and conversion rates. Biomass and Bioenergy 2008;32:1123-29.
[90] Thurner F, Mann U. Kinetic investigation of wood pyrolysis. Industrial & Engineering Chemistry Process Design and Development 1981;20:482-88.
[91] Kim S-S, Agblevor FA, Lim J. Fast pyrolysis of chicken litter and turkey litter in a fluidized bed reactor. Journal of Industrial and Engineering Chemistry 2009;15:247-52.

[92] Di Nola G, de Jong W, Spliethoff H. The fate of main gaseous and nitrogen species during fast heating rate devolatilization of coal and secondary fuels using a heated wire mesh reactor. Fuel Process Technol 2009;90:388-95.
[93] de Jong W, Di Nola G, Venneker BCH, Spliethoff H, Wójtowicz MA. TG-FTIR pyrolysis of coal and secondary biomass fuels: Determination of pyrolysis kinetic parameters for main species and NOx precursors. Fuel 2007;86:2367-76.
[94] Agblevor FA, Beis S, Kim SS, Tarrant R, Mante NO. Biocrude oils from the fast pyrolysis of poultry litter and hardwood. Waste Management 2010;30:298-307.
[95] Lima IM, Boateng AA, Klasson KT. Pyrolysis of Broiler Manure: Char and Product Gas Characterization. Industrial & Engineering Chemistry Research 2009;48:1292-97.
[96] Giuntoli J, de Jong W, Arvelakis S, Spliethoff H, Verkooijen AHM. Quantitative and kinetic TG-FTIR study of biomass residue pyrolysis: Dry distiller's grains with solubles (DDGS) and chicken manure. J Anal Appl Pyrolysis 2009;85:301-12.
[97] Rose Energy. http://roseenergy.webbelief.com/.
[98] Zhu S, Lee SW. Co-combustion performance of poultry wastes and natural gas in the advanced Swirling Fluidized Bed Combustor (SFBC). Waste Manage (Oxford) 2005;25:511-18.
[99] EPR. Energy Power Resources Ltd. http://wwweprlcouk/indexhtml.
[100] Fibrowatt_LLC. Power from Poultry Litter™. http://wwwfibrowattusacom/indexcfm.
[101] Priyadarsan S, Annamalai K, Sweeten JM, Mukhtar S, Holtzapple M. Fixed-bed gasification of feedlot manure and poultry litter biomass. Trans ASAE 2004;47:1689-96.
[102] Corella J, Sanz A. Modeling circulating fluidized bed biomass gasifiers. A pseudo-rigorous model for stationary state. Fuel Processing Technology 2005;86:1021-53.
[103] Nemtsov DA, Zabaniotou A. Mathematical modelling and simulation approaches of agricultural residues air gasification in a bubbling fluidized bed reactor. Chemical Engineering Journal 2008;143:10-31.
[104] Radmanesh R, Chaouki J, Guy C. Biomass Gasification in a Bubbling Fluidized Bed Reactor: Experiments and Modeling. American Institute of Chemical Engineers Journal 2006;52:4258-72.
[105] Mansaray KG, Al-Taweel AM, Ghaly AE, Hamdullahpur F, Ugursal VI. Mathematical Modeling of a Fluidized Bed Rice Husk Gasifier: Part I-Model Development. Energy Sources, Part A: Recovery, Utilization, and Environmental Effects 2000;22:83 - 98.
[106] Yuehong Z, Hao W, Zhihong X. Conceptual design and simulation study of a co-gasification technology. Energy Conversion and Management 2006;47:1416-28.
[107] Ruggiero M, Manfrida G. An equilibrium model for biomass gasification processes. Renewable Energy 1999;16:1106-09.
[108] Melgar A, Perez JF, Laget H, Horillo A. Thermochemical equilibrium modelling of a gasifying process. Energy Conversion and Management 2007;48:59-67.
[109] Altafini CR, Wander PR, Barreto RM. Prediction of the working parameters of a wood waste gasifier through an equilibrium model. Energy Convers Manage 2003;44:2763-77.

[110] Smith WR, Missen RW. Chemical reaction equilibrium analysis: theory and algorithms; 1982.
[111] Prins MJ, Ptasinski KJ, Janssen FJJG. From coal to biomass gasification: Comparison of thermodynamic efficiency. Energy 2007;32:1248-59.
[112] Deen NG, Van Sint Annaland M, Van der Hoef MA, Kuipers JAM. Review of discrete particle modeling of fluidized beds. Chem Eng Sci 2007;62:28-44.
[113] Luecke K, Hartge E-U, Werther J. A 3D Model of Combustion in Large-Scale Circulating Fluidized Bed Boilers. International Journal of Chemical Reactor Engineering 2004;2:A11.
[114] Ross DP, Yan H-m, Zhong Z, Zhang D-k. A non-isothermal model of a bubbling fluidised-bed coal gasifier. Fuel 2005;84:1469-81.
[115] de Souza-Santos ML. A new version of CSFB, comprehensive simulator for fluidised bed equipment. Fuel 2007;86:1684-709.
[116] Mostoufi N, Cui H, Chaouki J. A Comparison of Two- and Single-Phase Models for Fluidized-Bed Reactors. Ind Eng Chem Res 2001;40:5526-32.
[117] Fiaschi D, Michelini M. A two-phase one-dimensional biomass gasification kinetics model. Biomass and Bioenergy 2001;21:121-32.
[118] Ji P, Feng W, Chen B. Production of ultrapure hydrogen from biomass gasification with air. Chem Eng Sci 2009;64:582-92.
[119] Chejne F, Hernandez JP. Modelling and simulation of coal gasification process in fluidised bed. Fuel 2002;81:1687-702.
[120] Yan H-m, Heidenreich C, Zhang D-k. Mathematical modelling of a bubbling fluidised-bed coal gasifier and the significance of `net flow'. Fuel 1998;77:1067-79.
[121] Yan HM, Heidenreich C, Zhang DK. Modelling of bubbling fluidised bed coal gasifiers. Fuel 1999;78:1027-47.
[122] Yan H-m, Zhang D-k. Modelling of fluidised-bed coal gasifiers: elimination of the combustion product distribution coefficient by considering homogeneous combustion. Chem Eng Process 2000;39:229-37.
[123] Cui H, Grace JR. Fluidization of biomass particles: A review of experimental multiphase flow aspects. Chemical Engineering Science 2007;62:45-55.
[124] Zabaniotou A, Skoulou V, Koufodimos G, samaras Z. Conceptual design and preliminary hydrodynamic study of an agro biomass bench gasification fluidized bed reactor. International Journal of Chemical Reactor Engineering 2008;6:1-17.
[125] Rao TR, Bheemarasetti JV, Ram. Minimum fluidization velocities of mixtures of biomass and sands. Energy 2001;26:633-44.
[126] Suarez JA, Beaton PA. Physical Properties of Cuban Coffee Husk for Use as an Energy Source. Energy Sources, Part A: Recovery, Utilization, and Environmental Effects 2003;25:953 - 59.
[127] Kim S-S, Agblevor FA. Pyrolysis characteristics and kinetics of chicken litter. Waste Management 2007;27:135-40.
[128] Whitely N, Ozao R, Cao Y, Pan WP. Multi-utilization of Chicken Litter as a Biomass Source. Part II. Pyrolysis. Energy Fuels 2006;20:2666-71.
[129] Di Blasi C, Branca C. Kinetics of Primary Product Formation from Wood Pyrolysis. Industrial & Engineering Chemistry Research 2001;40:5547-56.
[130] Simell PA, Hirvensalo EK, Smolander VT, Krause AOI. Steam Reforming of Gasification Gas Tar over Dolomite with Benzene as a Model Compound. Industrial & Engineering Chemistry Research 1999;38:1250-57.

[131] Lv P, Yuan Z, Ma L, Wu C, Chen Y, Zhu J. Hydrogen-rich gas production from biomass air and oxygen/steam gasification in a downdraft gasifier. Renewable Energy 2007;32:2173-85.
[132] Corella J, Caballero MA, Aznar MP, Brage C. Two Advanced Models for the Kinetics of the Variation of the Tar Composition in Its Catalytic Elimination in Biomass Gasification. Ind Eng Chem Res 2003;42:3001-11.
[133] Kuchonthara P, Tsutsumi A. Energy-recuperative biomass integrated gasification power generation system. Journal of Chemical Engineering of Japan 2003;36:846-51.
[134] Ragland KW, Misra MK, Aerts DJ, Palmer CA. Ash Deposition in a Wood-Fired Gas Turbine. J Eng Gas Turbines Power 1995;117:509-12.
[135] Huang Y, McIlveen-Wright D, Rezvani S, Wang YD, Hewitt N, Williams BC. Biomass co-firing in a pressurized fluidized bed combustion (PFBC) combined cycle power plant: A techno-environmental assessment based on computational simulations. Fuel Process Technol 2006;87:927-34.
[136] Sonobe T, Worasuwannarak N. Kinetic analyses of biomass pyrolysis using the distributed activation energy model. Fuel 2008;87:414-21.
[137] Ferreira SB, Pilidis P. Comparison of externally fired and internal combustion gas turbines using biomass fuel. Journal of Energy Resources Technology 2001;123:291-96.
[138] Stahl K, Neergaard M. IGCC power plant for biomass utilisation, Varnamo, Sweden. Biomass Bioenergy 1998;15:205-11.
[139] Frey HC, Zhu Y. Improved System Integration for Integrated Gasification Combined Cycle (IGCC) Systems. Environ Sci Technol 2006;40:1693-99.
[140] Mathieu P, Dubuisson R. Performance analysis of a biomass gasifier. Energy Conversion and Management 2002;43:1291-99.
[141] Nikoo MB, Mahinpey N. Simulation of biomass gasification in fluidized bed reactor using ASPEN PLUS. Biomass Bioenergy 2008;32:1245-54.
[142] Sotudeh-Gharebaagh R, Legros R, Chaouki J, Paris J. Simulation of circulating fluidized bed reactors using ASPEN PLUS. Fuel 1998;77:327-37.
[143] Doherty W, Reynolds A, Kennedy D. The effect of air preheating in a biomass CFB gasifier using ASPEN Plus simulation. Biomass Bioenergy 2009;33:1158-67.
[144] Hannula I, Kurkela E. A semi-empirical model for pressurised air-blown fluidised-bed gasification of biomass. Bioresour Technol;In Press, Corrected Proof.
[145] van den Enden PJ, Lora ES. Design approach for a biomass fed fluidized bed gasifier using the simulation software CSFB. Biomass Bioenergy 2004;26:281-87.
[146] Shi SP, Zitney SE, Shahnam M, Syamlal M, Rogers WA. Modelling coal gasification with CFD and discrete phase method. Journal of the Energy Institute 2006;79:217-21.
[147] Haryanto A, Fernando SD, Pordesimo LO, Adhikari S. Upgrading of syngas derived from biomass gasification: A thermodynamic analysis. Biomass and Bioenergy 2009;33:882-89.
[148] Puig-Arnavat M, Bruno JC, Coronas A. Review and analysis of biomass gasification models. Renewable and Sustainable Energy Reviews 2010;14:2841-51.
[149] Van Ness HC, Abbott MM. Thermodynamics. In: Perry RH, Green DW, Maloney JO, editors. Perry's Chemical Engineeers' handbook. Seventh ed: McGraw-Hill Co., Inc.; 1997.
[150] Aspen Technology I. Aspen Plus 11.1 user guide. Cambridge, MA.; 2001.

[151] Cohen H, Saravanamuttoo HIH, Rogers GFC. Gas turbine theory. 4th ed: Harlow : Longman 1996.
[152] Li XT, Grace JR, Lim CJ, Watkinson AP, Chen HP, Kim JR. Biomass gasification in a circulating fluidized bed. Biomass and Bioenergy 2004;26:171-93.
[153] Smith R. Chemical process design: McGraw-Hill 1995.
[154] McKendry P. Energy production from biomass (part 1): overview of biomass. Bioresource Technology 2002;83:37-46.
[155] Mevissen N, Schulzke T, Unger CA, an Bhaird SM. Thermodynamics of autothermal wood gasification. Environmental Progress & Sustainable Energy 2009;28:347-54.
[156] Sugiyama S, Suzuki N, Kato Y, Yoshikawa K, Omino A, Ishii T, et al. Gasification performance of coals using high temperature air. Energy 2005;30:399-413.
[157] Brooks FJ. GE Gas Turbine Performance Characteristics, GER-3567 H. GE Power Systems.
[158] Li S, Wu A, Deng S, Pan W-p. Effect of co-combustion of chicken litter and coal on emissions in a laboratory-scale fluidized bed combustor. Fuel Processing Technology 2008;89:7-12.
[159] Nikulshina V, Gebald C, Steinfeld A. CO2 capture from atmospheric air via consecutive CaO-carbonation and CaCO3-calcination cycles in a fluidized-bed solar reactor. Chemical Engineering Journal 2009;146:244-48.
[160] Adanez J, Gayán P, Grasa G, de Diego LF, Armesto L, Cabanillas A. Circulating fluidized bed combustion in the turbulent regime: modelling of carbon combustion efficiency and sulphur retention. Fuel 2001;80:1405-14.
[161] Kuramochi H, Wu W, Kawamoto K. Prediction of the behaviors of H2S and HCl during gasification of selected residual biomass fuels by equilibrium calculation. Fuel 2005;84:377-87.
[162] Smula-Ostaszewska J, Peters B. Evaluation of potassium chloride emissions applying the Discrete Particle Method (DPM). Computers & Chemical Engineering 2011;35:606-14.
[163] van Paasen SVB, Cieplik MK, Phokawa tP. Gasification of Non-woody Biomass Economic and Technical Perspectives of Chlorine and Sulphur Removal from Product Gas. Energy research Centre of the Netherlands (ECN); 2006.
[164] Turn SQ. Chemical Equilibrium Prediction of Potassium, Sodium, and Chlorine Concentrations in the Product Gas from Biomass Gasification. Industrial & Engineering Chemistry Research 2007;46:8928-37.
[165] Srinivas T, Gupta AVSSKS, Reddy BV. Thermodynamic Equilibrium Model and Exergy Analysis of a Biomass Gasifier. Journal of Energy Resources Technology 2009;131:031801.
[166] Font-Palma C, Martin A. Effects of Pressure on the Gasification of Poultry Litter. 18th European Biomass Conference and Exhibition – From Research to Industry and Markets. Lyon, France, 3-7 May 2010; 2010, p. 743-47.
[167] Aquaro D, Pieve M. High temperature heat exchangers for power plants: Performance of advanced metallic recuperators. Appl Therm Eng 2007;27:389-400.
[168] Turbec. http://www.turbec.com/; 2011
[169] Heatric. http://www.heatric.com/.
[170] Morf P, Hasler P, Nussbaumer T. Mechanisms and kinetics of homogeneous secondary reactions of tar from continuous pyrolysis of wood chips. Fuel 2002;81:843-53.

[171] Cypres R, Bettens B. Mecanismes de fragmentation pyrolytique du phenol et des cresols. Tetrahedron 1974;30:1253-60.
[172] Sharma RK, Hajaligol MR. Effect of pyrolysis conditions on the formation of polycyclic aromatic hydrocarbons (PAHs) from polyphenolic compounds. Journal of Analytical and Applied Pyrolysis 2003;66:123-44.
[173] Fitzpatrick EM, Bartle KD, Kubacki ML, Jones JM, Pourkashanian M, Ross AB, et al. The mechanism of the formation of soot and other pollutants during the co-firing of coal and pine wood in a fixed bed combustor. Fuel 2009;88:2409-17.
[174] Faravelli T, Frassoldati A, Migliavacca G, Ranzi E. Detailed kinetic modeling of the thermal degradation of lignins. Biomass and Bioenergy 2010;34:290-301.
[175] Nishimura M, Iwasaki S, Horio M. The role of potassium carbonate on cellulose pyrolysis. Journal of the Taiwan Institute of Chemical Engineers 2009;40:630-37.
[176] Hosoya T, Kawamoto H, Saka S. Pyrolysis gasification reactivities of primary tar and char fractions from cellulose and lignin as studied with a closed ampoule reactor. Journal of Analytical and Applied Pyrolysis 2008;83:71-77.
[177] Adler E. Lignin chemistry—past, present and future. Wood Science and Technology 1977;11:169-218.
[178] Fitzpatrick EM, Jones JM, Pourkashanian M, Ross AB, Williams A, Bartle KD. Mechanistic Aspects of Soot Formation from the Combustion of Pine Wood. Energy & Fuels 2008;22:3771-78.
[179] Ledesma EB, Marsh ND, Sandrowitz AK, Wornat MJ. Global Kinetic Rate Parameters for the Formation of Polycyclic Aromatic Hydrocarbons from the Pyrolyis of Catechol, A Model Compound Representative of Solid Fuel Moieties. Energy & Fuels 2002;16:1331-36.
[180] Zhang Y, Kajitani S, Ashizawa M, Oki Y. Tar destruction and coke formation during rapid pyrolysis and gasification of biomass in a drop-tube furnace. Fuel 2010;89:302-09.
[181] Caubet S, Corte P, Fahim C, Traverse JP. Thermochemical conversion of biomass: Gasification by flash pyrolysis study. Solar Energy 1982;29:565-72.
[182] Fourcault A, Marias F, Michon U. Modelling of thermal removal of tars in a high temperature stage fed by a plasma torch. Biomass and Bioenergy 2010;34:1363-74.
[183] Su Y, Luo Y, Chen Y, Wu W, Zhang Y. Experimental and numerical investigation of tar destruction under partial oxidation environment. Fuel Processing Technology 2011;92:1513-24.
[184] Umeki K, Yamamoto K, Namioka T, Yoshikawa K. High temperature steam-only gasification of woody biomass. Applied Energy 2010;87:791-98.
[185] Umeki K, Namioka T, Yoshikawa K. Analysis of an updraft biomass gasifier with high temperature steam using a numerical model. Applied Energy;In Press, Corrected Proof.
[186] Mori S, Wen CY. Estimation of bubble diameter in gaseous fluidized beds. AIChE Journal 1975;21:109-15.
[187] T. E. Broadhurst HAB. Onset of fluidization and slugging in beds of uniform particles. AIChE Journal 1975;21:238-47.
[188] Sit SP, Grace JR. Effect of bubble interaction on interphase mass transfer in gas fluidized beds. Chemical Engineering Science 1981;36:327-35.
[189] Welty JR. Fundamentals of momentum, heat, and mass transfer. 4th ed: Wiley; 2001.

[190] Yaws CL. Yaws' Handbook of Thermodynamic Properties for Hydrocarbons and Chemicals. Knovel; 2009.
[191] Yaws CL. Yaws' Transport Properties of Chemicals and Hydrocarbons Knovel 2010.
[192] Poling BE, Prausnitz JM, O'Connell JP. The Properties of Gases and Liquids. Fifth ed: McGraw-Hill; 2001.
[193] Jegers HE, Klein MT. Primary and secondary lignin pyrolysis reaction pathways. Industrial & Engineering Chemistry Process Design and Development 1985;24:173-83.
[194] Hosoya T, Kawamoto H, Saka S. Secondary reactions of lignin-derived primary tar components. Journal of Analytical and Applied Pyrolysis 2008;83:78-87.
[195] Shin E-J, Nimlos MR, Evans RJ. A study of the mechanisms of vanillin pyrolysis by mass spectrometry and multivariate analysis. Fuel 2001;80:1689-96.
[196] Wahyudiono, Kanetake T, Sasaki M, Goto M. Decomposition of a Lignin Model Compound under Hydrothermal Conditions. Chemical Engineering & Technology 2007;30:1113-22.
[197] Marinov NM, Pitz WJ, Westbrook CK, Castaldi MJ, Senkan SM. Modeling of Aromatic and Polycyclic Aromatic Hydrocarbon Formation in Premixed Methane and Ethane Flames. Combustion Science and Technology 1996;116:211 - 87.
[198] Norinaga K, Deutschmann O, Saegusa N, Hayashi J-i. Analysis of pyrolysis products from light hydrocarbons and kinetic modeling for growth of polycyclic aromatic hydrocarbons with detailed chemistry. Journal of Analytical and Applied Pyrolysis 2009;86:148-60.
[199] Petersen I, Werther J. Experimental investigation and modeling of gasification of sewage sludge in the circulating fluidized bed. Chemical Engineering and Processing 2005;44:717-36.
[200] Chan W-CR, Kelbon M, Krieger BB. Modelling and experimental verification of physical and chemical processes during pyrolysis of a large biomass particle. Fuel 1985;64:1505-13.
[201] Gerber S, Behrendt F, Oevermann M. An Eulerian modeling approach of wood gasification in a bubbling fluidized bed reactor using char as bed material. Fuel 2010;89:2903-17.
[202] Tinaut FV, Melgar As, PÃ©rez JF, Horrillo A. Effect of biomass particle size and air superficial velocity on the gasification process in a downdraft fixed bed gasifier. An experimental and modelling study. Fuel Processing Technology 2008;89:1076-89.
[203] Chejne F, Lopera E, Londoño CA. Modelling and simulation of a coal gasification process in pressurized fluidized bed. Fuel 2011;90:399-411.
[204] Andersen J, Jensen PA, Hvid SrL, Glarborg P. Experimental and Numerical Investigation of Gas-Phase Freeboard Combustion. Part 2: Fuel NO Formation. Energy & Fuels 2009;23:5783-91.
[205] Verdone N, De Filippis P. Reaction kinetics of hydrogen chloride with sodium carbonate. Chemical Engineering Science 2006;61:7487-96.
[206] Jess A. Mechanisms and kinetics of thermal reactions of aromatic hydrocarbons from pyrolysis of solid fuels. Fuel 1996;75:1441-48.
[207] Press WH. Numerical recipes in FORTRAN 77: the art of scientific computing. 2nd ed: Cambridge University Press 1992.
[208] George A, Liu JW. Computer solution of large sparse positive definite systems: Prentice-Hall; 1981.

[209] Kiel JHA, van Paasen SVB, Neeft JPA, Devi L, Ptasinski KJ, Janssen FJJG, et al. Primary measure to reduce tar formation in fluidised-bed biomass gasifiers. Final Report SDE project P1999-012. Agency for Research in Sustainable Energy; 2004.
[210] Dorrestijn E, Mulder P. The radical-induced decomposition of 2-methoxyphenol. Journal of the Chemical Society, Perkin Transactions 2 1999:777-80.

APPENDIX A. THERMODYNAMIC AND TRANSPORT PROPERTIES OF GASES

Table I. Enthalpies of formation, heat capacities and Gibbs free energy of formation of gases at standard conditions [190]

name	formula	ΔH_f (kJ/mol) @ 298 K	Cp (J/(mol K)) @ 298 K	ΔG_f (kJ/mol) @ 298 K
hydrogen chloride	HCl	-92.312	29.136	-104.41
hydrogen	H_2	0	28.77142	0
water	H_2O	-241.826	33.59	-164.92
hydrogen sulfide	H_2S	-20.502	34.192	-36.212
ammonia	NH_3	-45.898	35.652	-235.836
nitric oxide	NO	90.291	29.845	122.0638
nitrogen dioxide	NO_2	33.095		71.43442
nitrogen	N_2	0	36.974	0
oxygen	O_2	0		0
sulfur dioxide	SO_2	-296.842	29.1134	
methane	CH_4	-74.5	35.69	-50.5
carbon monoxide	CO	-110.5	29.14	-137.2
carbon dioxide	CO_2	-393.5	37.13	-394.4
cyclopentadiene	C_5H_6	134.3	75.4	178
benzene	C_6H_6	82.9	82.43	129.8
phenol	C_6H_6O	-96.4	103.22	-32.5
pyrocatechol	$C_6H_6O_2$	-272	120.09	-183.1
salicylaldehyde	$C_7H_6O_2$	-214.95	132.4771	-140.73
o-cresol	C_7H_8O	-128.6	127.3	-34.3
guaiacol	$C_7H_8O_2$	-249	131.4548	-139
vanillin	$C_8H_8O_3$	-369	163.4713	-247
indene	C_9H_8	163.4	124.31	235.1
naphthalene	$C_{10}H_8$	150.6	131.92	224.1
phenanthrene	$C_{14}H_{10}$	207.5	185.7	308.2

Table II. Enthalpies of formation of gases (kJ/mol) [190]

name	formula	A	B	C	D	E	T_{min} (K)	T_{max} (K)
hydrogen chloride	HCl	-91.55941	-0.00226	-1.3E-06	1.56E-09	-4.1E-13	298.15	1500
hydrogen	H_2	0	0	0	0	0	298.15	1500
water	H_2O	-238.5296	-0.01202	3.32E-06	-3.43E-10	7.24E-14	298.15	1500
hydrogen sulfide	H_2S	-17.82052	0.007989	-9.6E-05	1.66E-07	-1.1E-10	298.15	368.3
ammonia	NH_3	-37.85469	-0.03163	1.68E-05	-4.28E-09	8.74E-13	298.15	1500
nitric oxide	NO	90.117767	0.000881	-1.3E-06	9.77E-10	-2.7E-13	298.15	1500
nitrogen dioxide	NO_2	36.761872	-0.01865	2.54E-05	-1.48E-08	3.26E-12	298.15	1500
nitrogen	N_2	0	0	0	0	0	298.15	1500
oxygen	O_2	0	0	0	0	0	298.15	1500
sulfur dioxide	SO_2	-294.0432	-1.7E-06	-6.3E-05	1.37E-07	-1.1E-10	298.15	368.3
methane	CH_4	-66.63984	-0.02229	-2.2E-05	2.98E-08	-8.4E-12	150	1500
carbon monoxide	CO	-114.1326	0.019801	-3E-05	1.49E-08	-2.8E-12	150	1500
carbon dioxide	CO_2	-393.0721	-0.00185	2.08E-06	-2.62E-09	8.57E-13	150	1500
cyclopentadiene	C_5H_6	153.0614	-0.07584	4.46E-05	-3.62E-09	-2.3E-12	150	1500
benzene	C_6H_6	102.13093	-0.07759	4.55E-05	-4.77E-09	-1.9E-12	150	1500
phenol	C_6H_6O	-77.44987	-0.08099	6.41E-05	-1.94E-08	1.69E-12	150	1500
pyrocatechol	$C_6H_6O_2$	-251.3707	-0.09645	0.000105	-4.86E-08	8.96E-12	150	1500
salicylaldehyde	$C_7H_6O_2$	-198.1099	-0.07486	6.44E-05	-8.47E-09	-2.4E-12	150	1500
o-cresol	C_7H_8O	-106.2013	-0.09164	5.77E-05	-6.96E-09	-2.1E-12	150	1500
guaiacol	$C_7H_8O_2$	-223.0745	-0.10734	7.14E-05	-9.22E-09	-2.8E-12	150	1500
vanillin	$C_8H_8O_3$	-344.3725	-0.10741	8.66E-05	-1.03E-08	-3.9E-12	150	1500
indene	C_9H_8	185.85532	-0.08973	4.91E-05	-1.85E-09	-1.9E-12	150	1500
naphthalene	$C_{10}H_8$	175.29383	-0.10103	6.37E-05	-8.15E-09	-2.2E-12	150	1500
phenanthrene	$C_{14}H_{10}$	236.39397	-0.12049	8.38E-05	-1.55E-08	-1.2E-12	150	1500

Table III. Heat capacities of gases (J/(mol K), Tmax 1500 K) [190]

name	formula	A	B	C	D	E	F	G
hydrogen chloride	HCl	27.914284	0.004098	0	0	0	0	0
hydrogen	H_2	19.670998	0.069682	-0.0002	2.89E-07	-2.2E-10	8.81E-14	-1.4E-17
water	H_2O	33.174382	-0.00325	1.74E-05	-5.98E-09	0	0	0
hydrogen sulfide	H_2S	29.754047	0.014885	0	0	0	0	0
ammonia	NH_3	27.739667	0.026538	0	0	0	0	0
nitric oxide	NO	35.838886	-0.04612	0.00012	-1.26E-07	6.48E-11	-1.5E-14	8.67E-19
nitrogen	N_2	28.716771	0.007346	-4.5E-05	1.16E-07	-1.2E-10	5.9E-14	-1.1E-17
sulfur dioxide	SO_2	32.853121	-0.01037	0.000209	-4.21E-07	3.86E-10	-1.7E-13	3.05E-17
methane	CH_4	44.356584	-0.14623	0.0006	-8.74E-07	6.78E-10	-2.8E-13	4.58E-17
carbon monoxide	CO	28.504576	0.010202	-6.2E-05	1.61E-07	-1.8E-10	9.02E-14	-1.7E-17
carbon dioxide	CO_2	23.506104	0.038066	7.4E-05	-2.23E-07	2.34E-10	-1.1E-13	2.17E-17
cyclopentadiene	C_5H_6	44.492574	-0.29841	0.002429	-4.8E-06	4.54E-09	-2.1E-12	3.87E-16
benzene	C_6H_6	40.445112	-0.2629	0.002457	-4.9E-06	4.64E-09	-2.2E-12	3.93E-16
phenol	C_6H_6O	26.917301	0.001934	0.001683	-3.74E-06	3.68E-09	-1.7E-12	3.22E-16
pyrocatechol	$C_6H_6O_2$	15.430076	0.202621	0.001111	-2.77E-06	2.77E-09	-1.3E-12	2.41E-16
salicylaldehyde	$C_7H_6O_2$	88.605938	-0.38087	0.003131	-5.98E-06	5.44E-09	-2.4E-12	4.31E-16
o-cresol	C_7H_8O	55.302571	-0.10825	0.00219	-4.53E-06	4.31E-09	-2E-12	3.66E-16
guaiacol	$C_7H_8O_2$	109.49991	-0.66604	0.004404	-8.54E-06	8.07E-09	-3.8E-12	6.94E-16
vanillin	$C_8H_8O_3$	94.397033	-0.26327	0.00288	-5.27E-06	4.48E-09	-1.9E-12	3.08E-16
indene	C_9H_8	106.59516	-0.74895	0.004734	-8.89E-06	8.07E-09	-3.6E-12	6.29E-16
naphthalene	$C_{10}H_8$	36.529108	-0.13512	0.002873	-6.01E-06	5.75E-09	-2.7E-12	4.9E-16
phenanthrene	$C_{14}H_{10}$	32.439474	0.042455	0.003097	-6.78E-06	6.57E-09	-3.1E-12	5.62E-16

Table IV. Gibbs Free Energies of Formation of Gases (kJ/mol) [190]

name	formula	A	B	C	D	E	T_{min} (K)	T_{max} (K)
hydrogen chloride	HCl	-91.9142	-0.01293	6.07E-06	-2.8E-09	5.35E-13	298.15	1500
hydrogen	H_2	0	0	0	0	0	298.15	1500
water	H_2O	-240.617	0.035116	2.02E-05	-9.3E-09	1.78E-12	298.15	1500
hydrogen sulfide	H_2S	-17.158	-0.06856	6.02E-05	-4.7E-08	1.98E-11	298.15	368.3
ammonia	NH_3	-43.3381	0.078873	4.53E-05	-2.3E-08	4.47E-12	298.15	1500
nitric oxide	NO	90.28682	-0.01228	-3.3E-07	1.25E-10	-2.2E-14	298.15	1500
nitrogen	N_2	0	0	0	0	0	298.15	1500
oxygen	O_2	0	0	0	0	0	298.15	1500
methane	CH_4	-68.7718	0.03833	9.22E-05	-5.5E-08	1.24E-11	150	1500
carbon monoxide	CO	-111.997	-0.07848	-2.6E-05	2.25E-08	-6.1E-12	150	1500
carbon dioxide	CO_2	-393.333	-0.00403	1.53E-06	-7.4E-11	-3.9E-14	150	1500
cyclopentadiene	C_5H_6	145.1709	0.066956	0.000178	-1.2E-07	2.92E-11	150	1500
benzene	C_6H_6	94.05034	0.075715	0.000182	-1.2E-07	2.96E-11	150	1500
phenol	C_6H_6O	-86.147	0.13963	0.000167	-1.1E-07	2.84E-11	150	1500
pyrocatechol	$C_6H_6O_2$	-261.766	0.223515	0.000169	-1.2E-07	3.09E-11	150	1500
salicylaldehyde	$C_7H_6O_2$	-205.788	0.180836	0.000158	-1.2E-07	2.98E-11	150	1500
o-cresol	C_7H_8O	-115.841	0.222905	0.000208	-1.4E-07	3.44E-11	150	1500
guaiacol	$C_7H_8O_2$	-234.154	0.259937	0.000245	-1.7E-07	4.17E-11	150	1500
vanillin	$C_8H_8O_3$	-355.423	0.308399	0.000232	-1.7E-07	4.29E-11	150	1500
indene	C_9H_8	176.8424	0.141601	0.000222	-1.5E-07	3.63E-11	150	1500
naphthalene	$C_{10}H_8$	164.6348	0.143908	0.000229	-1.5E-07	3.78E-11	150	1500
phenanthrene	$C_{14}H_{10}$	223.5791	0.22025	0.000262	-1.8E-07	4.4E-11	150	1500

Table V. Gas viscosities (Tmax 1500 K) [191]

name	formula	A	B	C	D	Tmin (K)	Gas viscosity @ T_{min} (µP)	Gas viscosity @ 25°C (µP)
hydrogen chloride	HCl	-16.8499	0.598746	-1.8291E-04	3.83E-08	150	68.976	146.423
hydrogen	H_2	1.76113	0.341655	-1.8368E-04	5.11E-08	15	6.8448	88.6535
water	H_2O	22.8211	0.173868	3.2465E-04	-1.4E-07	150	55.7222	99.72
hydrogen sulfide	H_2S	192.146	-0.39855	9.6506E-04	-2.8E-07	150	153.128	151.641
ammonia	NH_3	-7.68191	0.366991	-4.713E-06	4.8E-10	150	47.2623	101.33
nitric oxide	NO	-0.62427	0.738434	-3.7605E-04	9.27E-08	110	76.1766	188.568
oxygen	O_2	-4.94329	0.806733	-4.0416E-04	1.01E-07	54	37.725	202.336
sulfur dioxide	SO_2	-17.0634	0.538327	-1.7010E-04	3.44E-08	150	59.9744	129.229
methane	CH_4	1.26029	0.438036	-2.43E-04	7.1E-08	91	39.161	112.121
carbon monoxide	CO	18.0493	0.63753	-0.0003575	1.03E-07	68	59.7807	179.078
carbon dioxide	CO_2	11.8109	0.49838	-0.0001085	0	195	104.869	150.757
cyclopentadiene	C_5H_6	-10.2343	0.320276	-7.696E-05	1.04E-08	250	65.1862	78.6887
benzene	C_6H_6	2.65848	0.236657	3.7782E-05	-3.4E-08	287	72.8857	75.6733
phenol	C_6H_6O	-1.82232	0.286449	1.0716E-05	-2E-08	250	70.1494	84.0086
pyrocatechol	$C_6H_6O_2$	1.27034	0.188183	2.6795E-05	-2E-08	250	49.6811	59.2337
salicylaldehyde	$C_7H_6O_2$	-2.06469	0.232196	3.5705E-06	-1.4E-08	250	55.984	67.1029
o-cresol	C_7H_8O	-1.38912	0.240873	1.0236E-05	-1.7E-08	250	59.2013	70.8831
guaiacol	$C_7H_8O_2$	-1.30473	0.22241	9.2631E-06	-1.6E-08	250	54.6305	65.4126
vanillin	$C_8H_8O_3$	1.79341	0.193126	3.1116E-05	-2.2E-08	250	51.6829	61.5688
indene	C_9H_8	-1.63087	0.212991	5.5831E-06	-1.4E-08	250	51.7481	61.9994
naphthalene	$C_{10}H_8$	-16.6111	0.252958	-3.356E-05	-1E-09	275	50.3935	55.7984
phenanthrene	$C_{14}H_{10}$	4.12734	0.150174	4.2369E-05	-2.2E-08	250	43.9675	52.072

Table VI. Thermal conductivity of gases, k_g (W/(m K)) [191]

name	formula	A	B	C	D	T_{min} (K)	T_{max} (K)	k_g @ 25°C (W/(m K))
hydrogen chloride	HCl	-2.7488E-03	6.1287E-05	-7.9739E-09	1.2821E-12	159	1500	0.014849
hydrogen	H_2	1.0979E-02	6.6411E-04	-3.4379E-07	9.7283E-11	14	1500	0.181
water	H_2O	5.6199E-03	1.5699E-05	1.0106E-07	-2.4282E-11	150	1500	0.018641
hydrogen sulfide	H_2S	3.1184E-03	3.5162E-05	4.4168E-08	-1.4769E-11	213	1500	0.017137
ammonia	NH_3	9.1414E-03	-7.2945E-06	2.1666E-07	-6.4465E-11	240	1500	0.024517
nitric oxide	NO	2.9995E-03	8.3047E-05	-1.5185E-08	1.8810E-12	121	1500	0.02646
nitrogen	N_2	-2.2678E-04	1.0275E-04	-6.0151E-08	2.2332E-11	63	1500	0.025652
oxygen	O_2	1.5475E-04	9.4153E-05	-2.7529E-08	5.2069E-12	80	2000	0.025917
sulfur dioxide	SO_2	8.5308E-04	8.6212E-06	8.3662E-08	-5.0333E-11	250	900	0.009526
methane	CH_4	5.3767E-03	5.1555E-05	1.6655E-07	-5.7168E-11	97	1500	0.034038
carbon monoxide	CO	9.9186E-04	9.4020E-05	-4.0761E-08	1.3751E-11	70	1500	0.025765
carbon dioxide	CO_2	-1.2000E-02	1.0208E-04	-2.2403E-08	0.0000E+00	195	1500	0.016444
cyclopentadiene	C_5H_6	-9.3915E-03	4.4282E-05	1.0131E-07	-3.8169E-11	250	1500	0.011805
benzene	C_6H_6	-9.7669E-03	5.7816E-05	5.8698E-08	-2.2768E-11	250	1500	0.012085
phenol	C_6H_6O	-7.1128E-03	3.7284E-05	9.4254E-08	-3.4414E-11	250	1500	0.01147
pyrocatechol	$C_6H_6O_2$	-3.3835E-03	1.9421E-05	5.0244E-08	-1.8548E-11	250	1500	0.006382
salicylaldehyde	$C_7H_6O_2$	-0.0040085	2.3154E-05	6.3861E-08	-2.332E-11	250	1500	0.007954
o-cresol	C_7H_8O	-4.9197E-03	2.7464E-05	9.0857E-08	-3.2759E-11	250	1500	0.010477
guaiacol	$C_7H_8O_2$	-4.0641E-03	2.1655E-05	7.1376E-08	-2.6071E-11	250	1500	0.008046
vanillin	$C_8H_8O_3$	-2.2169E-03	1.3456E-05	5.6222E-08	-2.0048E-11	250	1500	0.006262
indene	C_9H_8	-5.9734E-03	2.8944E-05	7.7894E-08	-2.6277E-11	250	1500	0.008884
naphthalene	$C_{10}H_8$	-6.4056E-03	2.0372E-05	8.1863E-08	-2.9543E-11	250	1500	0.006162
phenanthrene	$C_{14}H_{10}$	-3.3919E-03	1.6148E-05	6.6858E-08	-2.3716E-11	250	1500	0.006737

APPENDIX B. KINETIC PARAMETERS OF REACTIONS INVOLVED IN THE KINETIC MODEL

Reaction rate (mol/m^{3}s)	Kinetic coefficient (concentration in mol/m^3)	Reference
$r_1 = k_1 C_{C_8H_8O_3}$	$k_1 = 1.3x10^{11}\, exp\left(-\frac{175309}{RT}\right)$	[195]
$r_2 = k_2 C_{C_7H_8O_2}$	$k_2 = 1.58x10^{12}\, exp\left(-\frac{191000}{RT}\right)$	[210]
$r_3 = k_3 C_{C_6H_6O_2}$	$k_3 = 7.94x10^{10}\, exp\left(-\frac{226354}{RT}\right)$	[179]
$r_4 = k_4 C_{C_6H_6O}$	$k_4 = 1x10^{11}\, exp\left(-\frac{209000}{RT_p}\right)$	[174]
$r_5 = k_5 C_{C_6H_6O_2}$	$k_5 = 5.01x10^{14}\, exp\left(-\frac{310871}{RT}\right)$	[179]
$r_6 = k_6 C_{C_6H_6O_2}$	$k_6 = 2.51x10^{12}\, exp\left(-\frac{352711}{RT}\right)$	[179]
$r_7 = k_7 C_{C_5H_6}^2$	$k_7 = 2x10^{7}\, exp\left(-\frac{2013}{T}\right)$	[197]
$r_8 = k_8 C_{C_{10}H_8}^2$	$k_8 = 4.55x10^{-4}\, T^{3.3} exp\left(-\frac{5690}{T}\right)$	[197]
$r_9 = k_9 C_{C_9H_8} C_{C_5H_6}$	$k_9 = 1x10^{2}\, exp\left(-\frac{33500}{RT}\right)$	[198]
$r_{10} = k_{10} C_{O_2}$	$k_{10} = 0.05 * 5.95x10^{2}\, \mathrm{T_p}\left(\frac{6}{\mathrm{D_p}}\right) \exp\left(-\frac{149440}{T_p R}\right)$	[199]
$r_{11} = k_{11} C_{O_2} C_{CO}$	$k_{11} = 8.83x10^{5}\, exp\left(-\frac{99800}{RT}\right)$	[102]
$r_{12} = k_{12} C_{H_2O,l}$	$k_{12} = 5.13x10^{6}\, exp\left(-\frac{87900}{RT}\right)$	[200]
$r_{13} = k_{13} C_{CO} C_{H_2O} - k_{13'} C_{CO_2} C_{H_2}$	$k_{13} = 2.78\, exp\left(-\frac{12560}{RT}\right)$ $K_w = 0.0265 exp\left(\frac{3966}{T_p}\right)$ $k_{13'} = \frac{k_{13}}{K_w}$	[201]
$r_{14} = k_{14} C_{O_2} C_{H_2}$	$k_{14} = 0.001 * 1.08x10^{10}\, exp\left(-\frac{125525}{RT}\right)$	[199]
$r_{15} = k_{15} C_{H_2O}$	$k_{15} = 3.42 S T_p\, exp\left(-\frac{15600}{T_p}\right)$	[201]
$r_{16} = k_{16} C_{H_2}$	$k_{16} = 3.42x10^{-2} S T_p exp\left(-\frac{15600}{T_p}\right)$	[201]
$r_{17} = k_{17} C_{CH_4} C_{H_2O}$	$k_{17} = 3015\, exp\left(-\frac{125520}{RT}\right)$	[202]

Reaction rate (mol/m^{3}s)	Kinetic coefficient (concentration in mol/m^3)	Reference
$r_{18} = k_{18} C_{Biomass}$	$k_{18} = 1.43x10^4 \, exp\left(-\frac{88600}{RT_p}\right)$	[201]
$r_{19} = k_{19} C_{H_2S}^{1.074} C_{O_2}^{1.084}$	$k_{19} = 2.93x10^9 \, exp\left(-\frac{18956}{T}\right)$	[203]
$r_{20} = k_{20} C_{O_2} C_{NH_3}$	$k_{20} = 5.1x10^{14} \, exp\left(-\frac{35230}{T}\right)$	[204]
$r_{21} = k_{21} C_{Lignin}$	$k_{21} = 4.13x10^6 \, exp\left(-\frac{112700}{RT_p}\right)$	[201]
$r_{22} = k_{22} C_{HCl}$	$k_{22} = 169.9 \, exp\left(-\frac{62281}{RT_p}\right)$	[205]
$r_{23} = k_{23} C_{C_8H_8O_3}$	$k_{23} = 1.13x10^6 \, exp\left(-\frac{109000}{RT}\right)$	[201]
$r_{24} = k_{24} C_{C_{10}H_8}$	$k_{24} = C_{H_2}^{0.4} 1x10^{11} exp\left(-\frac{324000}{RT}\right)$	[206]
$r_{25} = k_{25} C_{C_6H_6} C_{O_2}$	$k_{25} = 1.58x10^{12} \, exp\left(-\frac{202641}{RT}\right)$	[199]
$r_{26} = k_{26} C_{C_6H_6}$	$k_{26} = 4.4x10^5 \, exp\left(-\frac{220000}{RT}\right)$	[182]

APPENDIX C. CALCULATION OF COEFFICIENTS OF VOLATILES PRODUCED FROM DEVOLATILISATION OF BIOMASS (R18)

$$y_{CO} + 2y_{CO_2} + y_{H_2O} = k_O$$

$$y_{\mathrm{CO}} + y_{\mathrm{CO_2}} + y_{\mathrm{CH_4}} + y_{\mathrm{Char}} = k_C$$

$$2y_{\mathrm{H_2O}} + 2y_{\mathrm{H_2}} + 4y_{\mathrm{CH_4}} + 3y_{\mathrm{NH_3}} + 2a_{\mathrm{H_2S}} + a_{\mathrm{HCl}} = k_H$$

$$y_{\mathrm{NH_3}} = k_N$$

$$y_{\mathrm{H_2S}} = k_S$$

$$y_{\mathrm{HCl}} = k_{Cl}$$

The right-side of the equations was calculated as a sum of the initial element composition and the elemental composition that converts to non-condensable gases and water, and tar.

$k_{\mathrm{pyr,i}} = k_{\mathrm{PL,i}} - k_{\mathrm{tar,i}}$

where i = O, C, H, N, S, Cl

To deal with the set of equations, some constraints were imposed to allow the devolatilisation of CO and CH_4. Char is composed of pure carbon and is fixed according to the fixed carbon content based on the proximate analysis of biomass.

$$y_{CO_2} = k_C - y_{Char} - \frac{k_O}{2}$$

$$y_{CH_4} = \left(k_H - 3y_{NH_3} - 2y_{H_2S} - y_{HCl}\right)/4 - y_{Char}$$

$$y_{CO} = k_C - y_{Char} - y_{CO_2} - y_{CH_4}$$

$$y_{H_2O} = k_O - y_{CO} - \frac{y_{CO_2}}{2}$$

$$y_{H_2} = 2k_H - y_{H_2O} - \frac{y_{CH_4}}{2} - \frac{2NH_3}{3} - y_{H_2S} - 2y_{HCl}$$

PUBLICATIONS

C. Font-Palma and A. Martin. Performance of a small-scale gasification process for energy generation. *Biomass and Bioenergy* (submitted)

C. Font-Palma. Characterisation, kinetics and modelling of gasification of poultry manure and litter: An overview. *Energy Conversion and Management*. 2012, 53(1): 92-98

C. Font-Palma and A. Martin. Effects of pressure on the gasification of poultry litter. 18th European Biomass Conference and Exhibition – From Research to Industry and Markets. *Proceedings of the International Conference held in Lyon, France*, 3–7 May 2010, p 743–747, DOI: 10.5071/18thEUBCE2010-VP2.1.39

Performance of a small-scale gasification process for energy generation

Carolina Font-Palma and Alastair D. Martin*

School of Chemical Engineering and Analytical Science
The Mill, University of Manchester
Oxford Road
Manchester, UK, M13 9PL

*Author to whom correspondence should be addressed
E-mail: alastair.martin@manchester.ac.uk
Tel: +44(0) 161 306 4395
Fax: +44(0) 161 306 9321

Abstract

This work reports the integration of a small scale gasification unit with a gas turbine for on-site power generation. This eliminates the need for the transportation of biomass to centralised plants. The poultry industry in Europe is vast and proper waste management is required in order to comply with environmental regulations. Therefore, poultry litter represents a potential fuel candidate since it is an available source. A process simulation was developed for six levels of integration. The model was applied to evaluate integration schemes involving atmospheric gasification, pressurised gasification and recuperation of energy from the gas turbine exhaust gases. The recuperation of residual heat to preheat air and produced gases was performed with the aim of achieving the highest electrical efficiency. The energy integration system showed more significant effects on process efficiency, cold gasification efficiency, carbon conversion and LHV than the gasifier operating pressure. The proposed solution of the small scale process delivered an electrical efficiency comparable to large scale options.

Keywords: Integrated Gasification; Biomass; Gas turbine; Energy Recuperation; Poultry litter; Aspen Plus

1. Introduction

Biomass and agricultural waste used in energy conversion processes has gained attention as a promising alternative to reduce greenhouse gas emissions. Thermochemical processes are preferred since they offer the following advantages: i) the process can be designed to suit on-site application allowing a more compact system, ii) conversion takes shorter times (a matter of minutes) compared to the long periods required in anaerobic digestion, iii) destruction of pathogens due to high process temperatures; the option of employing seasonal residues from farms, and iv) more efficient recovery of nutrients [1]. One thermochemical process is gasification, which converts biomass into a combustible gas mixture by partial oxidation. Gasification is chosen because it solves the problem of waste disposal and represents a viable solution for the on-site generation of energy.

Since the main product of biomass gasification is a valuable mixture of combustible gases, gasification is frequently coupled to power generation systems. Integrated

gasification combined cycle (IGCC) puts together a gasification unit and a combined cycle power system. The combined cycle system combines one or several gas turbines (GT) and/or one or several steam turbines which can include a heat recovery steam generator (HRSG). There are currently 18 installed coal-fired plants of large size (200 – 300 MW) worldwide, mainly located in Japan, the USA, Germany and Holland, which have reached the demonstration stage of commercial-scale IGCC plants [2]. Thus, the IGCC technology focuses on high efficiency and large capacity.

For biomass gasification plants, literature is mostly dedicated to simulation studies. Baratieri et al. [3] compared two plant layouts: a circulating fluidised bed gasifier where one layout was integrated with a gas engine, and the other with a combined cycle gas turbine (CCGT) and a HRSG. The first layout was recommended for 100 – 1000 kW_{el} plants because steam could be produced without the need of an expensive district heating network, and the second layout for medium size plants (10-20 MW_{el}) due to the higher electrical efficiency. In traditional IGCC systems, gasification is performed at atmospheric pressure and the produced gases need to be cooled before being compressed to the required pressure for the GT [3-5]. In addition, systems employing a pressurised gasifier are usually of medium to large scale. At Värnamo, Sweden, a 6 MW BIGCC (Biomass integrated gasification combined cycle) system was installed and consists of a circulating fluidised bed gasifier that operates at 20 bar and 950 – 1000°C [6]. The hot gas is cooled to a temperature of 350–400°C before entering a ceramic filter for particle removal. GT exhaust gases are used in a HRSG to generate steam and then injected into a steam turbine. An IGCC system using air-blown pressurised biomass gasification was suggested within the power range of 10–40 MW_e capable of achieving up to 40% of net efficiency [7]. Indeed, more complex systems are found in the literature, such a modified IGCC system that used a HRSG to generate steam. Air for combustion and fuel gases were preheated before entering the GT burner. However, the fuel gas was previously cooled down to 673 K for hot gas clean-up; after being preheated in the HRSG, the fuel temperature was 50 K lower than after steam gasification. The GT exhaust gases were employed to externally heat the gasifier and the remaining heat used in the HRSG [8]. In addition to a HRSG for generating high and low pressure steam, an air separation unit (ASU) was included for oxygen-blown gasification. The nitrogen generated from the ASU was used to dilute and cool syngas before combustion. The gasifier was modelled at high pressure and temperature, 25 bar and 1600°C, respectively. Co-gasification of coal, petcoke and olive pomace delivered an overall plant efficiency of 35% [9].

The understanding of the gasification process allows the operation and optimisation of the system. A useful tool to explore its complexity is the mathematical simulation of the gasification process. Significant work has focused on biomass gasification using chemical equilibrium models [10-14]. The equilibrium calculation provides the final composition and temperature of the product gases considered. Furthermore, equilibrium models are helpful due to the prediction of the thermodynamic limits of the gasification reaction.

Most biomass gasification work has concentrated on wood utilisation. However, the United Kingdom and in general the European Union have large poultry industries that produce 820 and 5,500 million birds per year, respectively [15]. From poultry operations, litter is generated as a waste consisting of manure, waste bedding and feathers. In the EU, the litter is removed with every new flock and substituted with fresh bedding material; therefore, an estimated production of 1.4 million tons of poultry litter results from broiler operations [16]. Disposal of poultry litter traditionally includes application to land as fertiliser, but the improper application and overuse of poultry litter represent a potential problem due to: spread of pathogens [17]; emission of ammonia, greenhouse gases and

odorous compounds; and ground water pollution through infiltration of nutrients leading to eutrophication [18]. With this growing concern and new regulatory constraints, land spreading is becoming a less acceptable option. Furthermore, poultry litter represents an available source for energy conversion.

Most systems use the hot gas turbine exhaust gases essentially to generate steam. In this work, electricity production is maximised by avoiding the generation of steam and the cost of a HRSG unit. The hot gases from the GT can be used as a heat source for the biomass gasification process as it is proposed in this work. Therefore, the main objectives of this work are the integration of the gasification of poultry litter with a gas turbine using a small-scale and on-site system, and the recuperation of residual heat to preheat air and product gases in order to achieve the highest electrical efficiency.

2. Method

2.1 Process configurations

In order to compare the performance of the proposed pressurised system, it was compared to a conventional arrangement using an atmospheric gasifier. In addition, two more arrangements that include heat recovery were analyzed. Therefore, six case studies were evaluated as explained below.

Base case. This base case does not include any energy integration. This case consists of a gasifier operating at atmospheric pressure where air is used as the gasifying agent as illustrated in figure 1a. Since the product gases carry particles, a filter is used to remove dust from the gas stream. The clean gases are cooled down to 40°C to condense water vapour and lower the work of the syngas compression to reach the required operating pressure. Then the product gases are injected into the combustion chamber of the GT and burnt with the previously compressed air. After combustion, the gases enter the expander and then the De-NO_x unit for NO_x elimination. This arrangement is representative of what has become relatively common practice in the biomass to energy industry in the UK. However, in most installations the combination of syngas compressor and GT is replaced by a converted IC piston engine.

Case 2. This arrangement contains the same process units as the base case, but the hot product gases are used to reheat itself after compression. In this case, the clean gases are cooled down first to 400°C and then further to 40°C. After compression, the cool gases are used to lower the temperature of fuel after gasification to 400°C. Then the reheated gases are injected into the combustion chamber of the GT and burnt with the previously compressed air, as shown in figure 1b.

Case 3. This arrangement contains the same process units as the base case, but in this case, the gasifier is pressurised. A second compressor is used to pressurise the gasifying air as shown in figure 1c. Since the product gases are already at the required pressure, they are not cooled before combustion in the GT.

Case 4. This arrangement includes the same process units as the base case, but in this configuration an energy integration system (EIS) is added as shown in figure 1d. In the EIS, the hot GT exhaust gases are used to preheat air for gasification and air after compression.

Case 5. This arrangement includes the same process units as case 2, but in this configuration an energy integration system (EIS) is added as shown in figure 1e. In the EIS, the hot GT exhaust gases are used to preheat further the product gases after compression, air for gasification and air after compression.

Case 6. This arrangement contains the same process units as case 3, but in this case an EIS is included as shown in figure 1f. In the EIS, the hot GT exhaust gases are used to

preheat air and the gases produced after gasification. Only one compressor is used for air compression; then air is preheated in the EIS. Following pre-heating, the air is divided into two parts. The first part is directed to the gasifier whilst the second part is passed to the burner of the GT as combustion air.

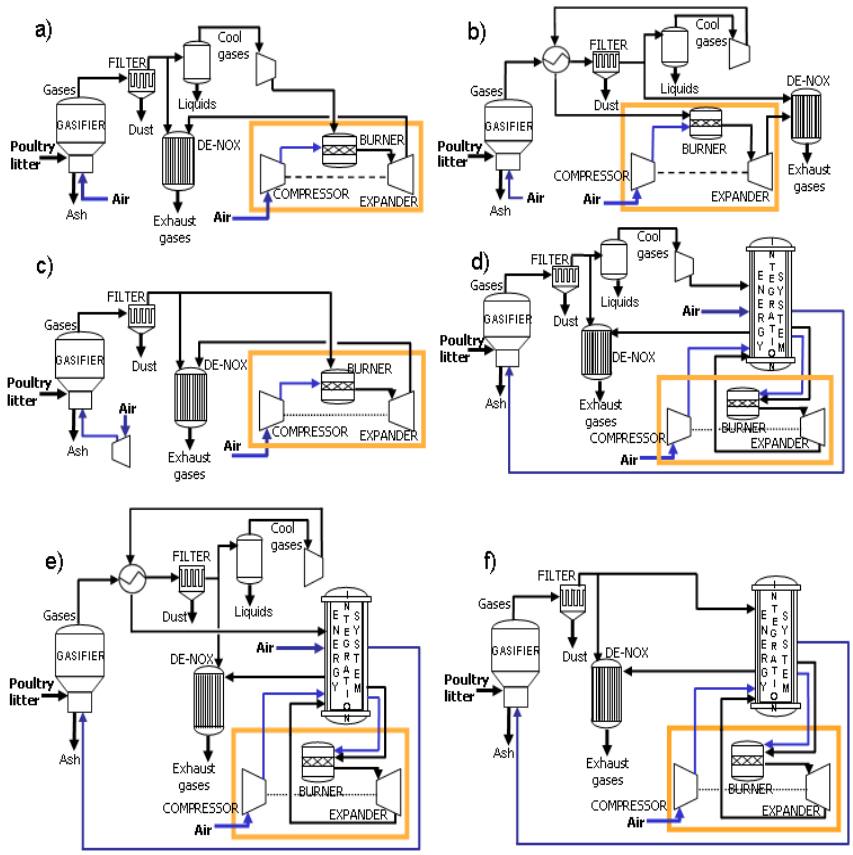

Figure 1 Process configurations: a) Base case, b) Case 2, c) Case 3, d) Case 4, e) Case 5, and f) Case 6

2.2 Model description

A model based on chemical equilibrium was developed to analyse the four layouts. The equilibrium calculation provides the final composition and temperature of the product gases considered. This equilibrium model assumes that the gasifier operates under perfect mixing conditions and uniform temperature, fast reaction rates and sufficiently long residence time to reach equilibrium. Heat losses are ignored since the gasifier is considered to be ideally insulated.

The simultaneous solution of mass and energy balances was performed by modelling in ASPEN Plus [19] software. ASPEN Plus allows the use of processes involving solids and is equipped with physical, chemical and thermodynamic databases. As input data to run the simulations, the ultimate (elemental) analysis, proximate analysis, moisture content, mass flow and HHV of the poultry litter were specified. The ultimate and proximate compositions employed are given in table 1. The HHV for poultry litter was estimated, by ASPEN Plus using the IGT correlation, to be 13.23 MJ/kg (dry basis).

To model the gasification process, the process was split into three component sub-processes, as shown in figure 2, corresponding to: a) the flash pyrolysis of poultry litter was modelled by breaking it into its constituent elements, ash and energy according to its

ultimate analysis. This step used a reactor modelled by a RYIELD block; b) the gasification reactions were simulated based on the chemical equilibrium. The composition of the produced gas was estimated through the minimisation of the Gibbs free energy using a RGIBBS block. The specified products were CO, CO_2, H_2O, H_2, O_2, N_2, C, CH_4, NH_3, H_2S, COS, HCl and HCN. Longer chain hydrocarbons and aromatics were not included as they are thermodynamically unstable under the gasification conditions [12]; and c) Ash separation was simulated by a SSPLIP block using a fractional carryover of the solid components (ash and carbon).

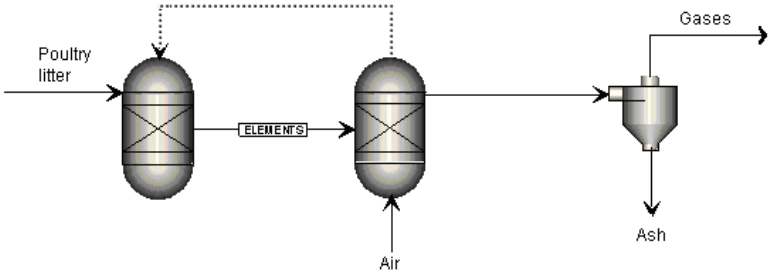

Figure 2 Diagram of the fluidised bed gasification model

In order to model the gas turbine unit, the GT was split into three component sub-processes as shown in figure 1: i) compression of air was modelled using a COMPR block. The isentropic efficiency and the desired pressure ratio were specified; ii) combustion was simulated using an adiabatic stoichiometric reactor with a RSTOIC block. The combustion reactions were specified and established as progressing to completion; and iii) the expansion section simulated the expansion of hot gases to convert their sensible heat into rotational energy. The power generated was used for driving the compressor and the excess work for energy production. The isentropic efficiency and the desired pressure ratio were specified. The expander was modelled using a COMPR block. Table 2 shows further model assumptions.

With the aim of obtaining the best achievable efficiency, the exhaust gases from the GT were used to preheat the air for gasification and the air for combustion in the GT section. In addition, when the outlet product gas temperature was lower than the GT exhaust temperature, product gases were preheated before entering the combustor. The heat exchangers were modelled as counter current using a HEATX block.

3. Results and discussion

The six proposed process layouts were compared by varying the equivalence ratio (ER) and observing its effects on cold gasification efficiency, carbon conversion, lower heating value and process efficiency. ER refers to the ratio of the amount of air supplied and the required air for stoichiometric oxidation.

3.1 Cold gasification efficiency

Cold gasification efficiency is commonly used as a parameter for evaluating the gasification process. The cold gasification efficiency (CGE) was calculated at standard conditions using the following equation:

$$\eta_{CG} = \frac{Q_{gas} LHV_{gas}}{m_{bio} LHV_{bio}} \quad (1)$$

where Q_{gas} refers to the volumetric flow rate of produced gases in m^3/s, LHV_{gas} is the lower heating value of the produced gases in MJ/Nm^3, m_{bio} is the mass flow rate of biomass in kg/s, and LHV_{bio} is the lower heating value of biomass in MJ/kg.

Figure 3 shows the cold gasification efficiency for the six process layouts based on the LHV versus ER. For the six cases, maximum CGEs were obtained. For the base case and case 2, the CGE were identical because the gasifier operating conditions were the same; a similar result was observed for cases 4 and 5. For the base case and case 3, the maximum CGEs were achieved at an ER of 0.33 and 0.32, respectively; whereas for the two energy recuperative layouts, the cases 4, 5 and 6, the maximum CGEs were achieved at a lower ER of 0.29.

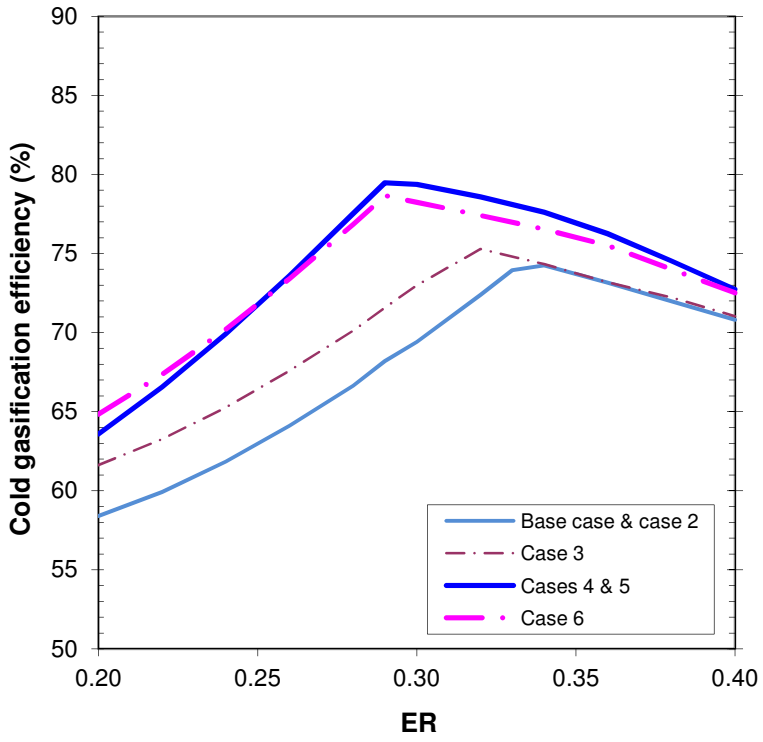

Figure 3 Cold gasification efficiency versus ER for the six cases

The maximum cold gasification efficiency of the base case (74%) was increased by 5% points when the energy recuperative system (cases 4 and 5) was included. These results agree with the trends previously showed for wood gasification with 20% and 40% of wood moisture content [20]; when the air inlet temperature was increased from 298 K to 873 K, the maximum cold gas efficiency showed an increase by nearly 6%. In the present work, the air inlet temperature was 293 K for the base case and case 2, 492 K for case 3, and 830 K for the energy recuperative systems (cases 4, 5 and 6). At an ER of 0.29, the CGE increase of case 5 was up to 11% points higher than the base, which it is the ER where the maximum CGE for case 5 was obtained. As a result, figure 3 confirms that preheating air improves the cold gasification efficiency. Even more advantageous is the fact that air was preheated by recovering heat from the gas turbine exhaust gases.

Figure 3 shows the effect of raising the pressure of gasification from atmospheric (base and case 2) to 5bara (case 3). It can be seen that the cold gasification efficiency of the base case is improved by 3.5% points at the same ER when the pressurised gasifier was

included. However, the maximum CGE was increased by only 1% point but appeared at a lower ER. Previous work investigating the effect of pressure on wood gasification without air preheating found that the CGE increased by approximately 1% between atmospheric and a maximum pressure of approximately 13 bar [21]. For the energy recuperative, atmospheric and 5bara pressurised systems, cases 5 and 6, respectively, the CGEs varied by less than 1%. When pressure was increased, H_2 and CO concentrations decreased; however, CH_4 composition increased. The combined effects of these changes resulted in only small variations in the LHV and gasification efficiency.

Even though the cold gasification efficiency did not drastically improve with every layout modification, each modification from the base case resulted in an optimum ER of lower value. This fact provides some benefits since lower ER under similar air preheat conditions represents operating the gasifier at lower temperatures and obtaining gases with higher LHV. This result is consistent with a previous thermodynamic study of wood gasification, where preheated air reduced the optimum ER for achieving the maximum CGE from 0.29 to 0.25 [20]. However, in that work only the gasification process was evaluated.

3.2 Carbon conversion

Figure 4 shows the carbon conversion as a function of ER for the six cases. Each case shows an increasing conversion up to the maximum 100% and the expected plateau for all higher values of ER. The cases 3, 4, 5 and 6 show complete carbon conversion being achieved at lower ER values than for the base case and case 2. This can be explained by the energy provided by the hotter air which promotes the carbon conversion by endothermic reactions, such as the water-gas reaction ($C + H_2O \rightarrow CO + H_2$) and Boudouard reaction ($C + CO_2 \rightarrow 2CO$).

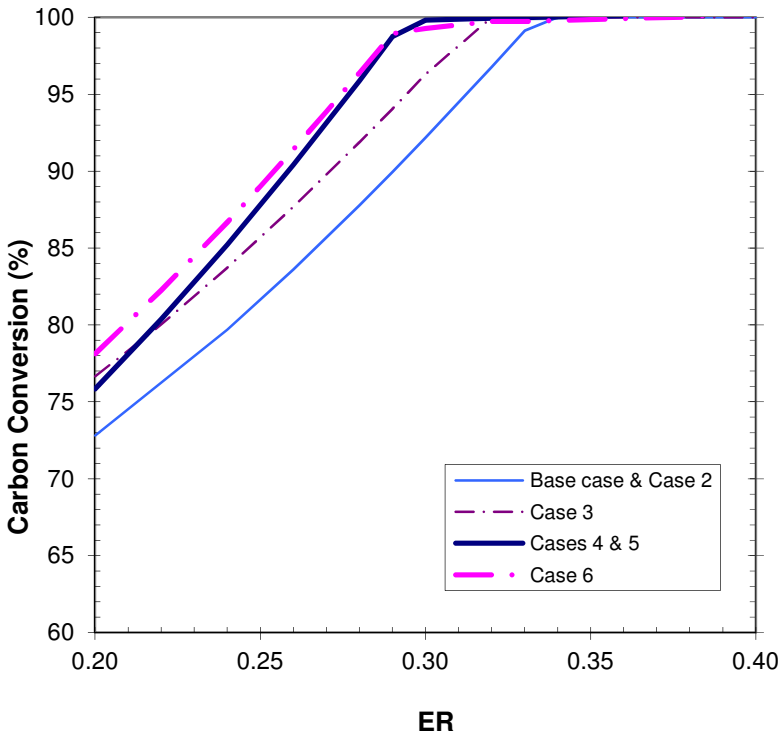

Figure 4 Carbon conversions versus ER for the six cases

When Figure 4 is read in conjunction with figure 3, it can be seen that the maximum CGE coincides with the minimum ER required for complete conversion of the carbon, also referred to as carbon burn-out.

3.3 Lower heating value (LHV)

Figure 5 shows the LHV versus ER for all the layouts. It is observed that the LHV decreases as expected with increasing ER. However, the LHV at low ERs only decreased slightly or remained almost constant for cases 4 and 5 up to the ER where the maximum cold gasification efficiency (figure 3) and complete carbon conversion (figure 4) were achieved.

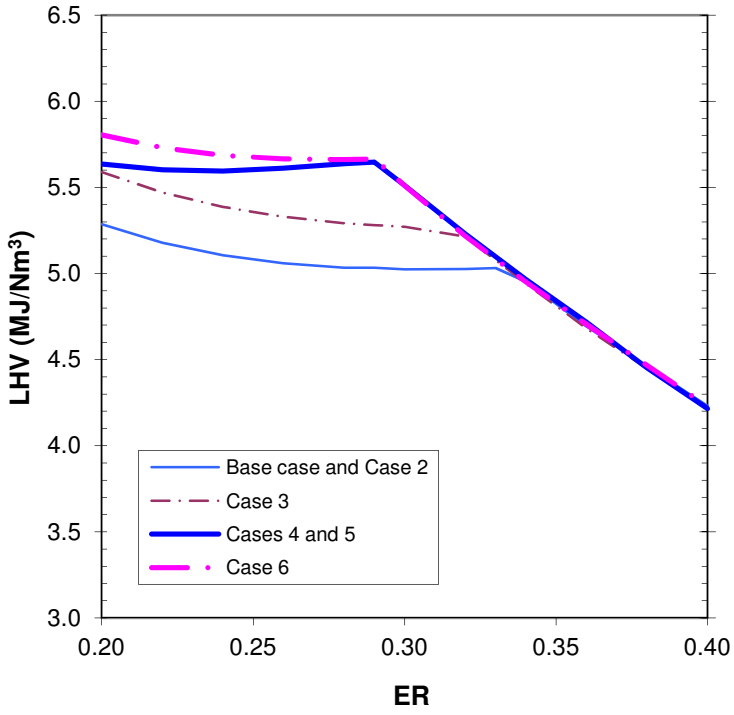

Figure 5 Lower heating value (LHV) versus ER for the six cases

A previous study [22] examining the effect of ER on the gasification of olive kernel found that below a critical value the LHV changes only slightly with ER whilst above the critical value the LHV decreases steadily with increasing ER. Their result supports the trends shown in figure 5; however, they did not associate the critical value of ER with complete conversion of the carbon or the maximum CGE. Furthermore, above the respective critical ER values, the LHV of the gas decreases along a common trend for all six cases. This trend represents the progressive oxidation of the fuel components of the gas.

Higher LHVs were observed for the pressurised cases at low ERs, as already noted; the CH_4 composition increased, while H_2 and CO formation decreased at higher pressure, and CH_4 has greater positive influence on the LHV.

Sugiyama et al. [23] used a pebble bed slagging-gasifier with a high temperature air generator in order to obtain a syngas with higher calorific value. They analysed the effect of increasing the ER when air was preheated to 1000°C. They found that by increasing the ER the carbon conversion efficiency and the cold gas efficiency were improved whilst the HHV of the product gases decreased which is in agreement with our results.

3.4 Process efficiency

Figure 6 shows the process efficiency for the six layouts versus ER. In all cases, the efficiency improved with increasing ER reaching maximum values at the points of carbon burnout and peak CGE. In the base case the maximum efficiency (13%) was achieved at an ER of 0.33. This compares with 19% for the equivalent configuration containing an IC engine with a typical compression ratio of 10:1. For cases 2 and 3, the maximum efficiencies of (14% and 21%) were achieved at ERs of 0.33 and 0.32, respectively. Maximum efficiency in these cases is maintained for all greater ER values studied. For the energy recuperative systems (cases 4, 5 and 6), the maximum efficiencies (25%, 27% and 33.5%, respectively) were achieved at a lower ER of 0.29. However, only case 6 maintained its high efficiency for greater ER values.

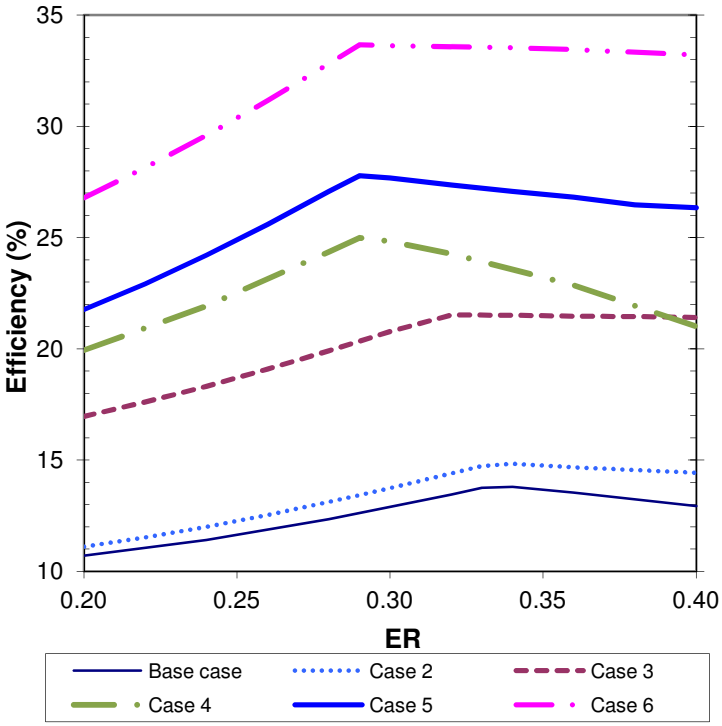

Figure 6 Process efficiency versus ER for the six cases

For the base case and cases 4 and 5, the process efficiency falls for ER values greater than those required for carbon burnout illustrating that it is undesirable to provide gasification air in excess of that required to just achieve burnout. However, for the cases 2, 3 and 6, after the maximum process efficiencies were reached, the efficiencies remained almost constant when ER was increased. Whilst this shows that adding more air does not benefit the efficiency once complete carbon conversion is achieved it indicates that process operation in this region can lead to high efficiency being achieved over range of ER values making process operation and control easier.

For the base case, cases 4 and 5, the reason that the efficiency decreased after reaching their maximum value can be explained with figure 7 which shows the temperature of product gases after gasification (Tgas) and at the entrance to the GT combustor (Tcomb). For all three cases Tgas increases with increasing ER. Tcomb presents a more complex picture as it represents the temperature of the fuel gas after being cooled, compressed and reheated. For all three cases the temperature of fuel gases after cooling and compression was 500 K. For the base case the fuel was fed to the GT combustor at this

temperature, whereas for case 4, the compressed fuel gases stream was reheated to approximately 800K in the heat integration system by interchange with the GT exhaust, and for case 5, the compressed fuel gas was initially reheated by interchange with the hot gasifier product gases before receiving additional reheating from the GT exhaust in the same manner as case 4. In the range of ER between 0.24 and 0.35 the fuel gas in case 5 receives additional heat from the GT exhaust raising its temperature by approximately 30K above that of case 4. However at ERs greater than 0.35 the gasifier product gas is sufficiently hot to reheat the fuel gas following compression to temperatures in excess of the GT exhaust producing the upward "tick" shape of the case 5 Tcomb curve. The loss of process efficiency for ER values greater than 0.29 can be attributed to the additional waste of heat energy arising from the cooling of hotter gasifier product gases in conjunction with the additional mechanical energy required to compress the higher mass flow of gas. Case 5 shows that a proportion of the wasted heat can be recovered through interchange between the gasifier product gases and the compressed gases thus mitigating some of the efficiency losses. At ERs higher than 0.35, the additional heat recovered into the compressed fuel gas results in a slight flattening of the efficiency curve.

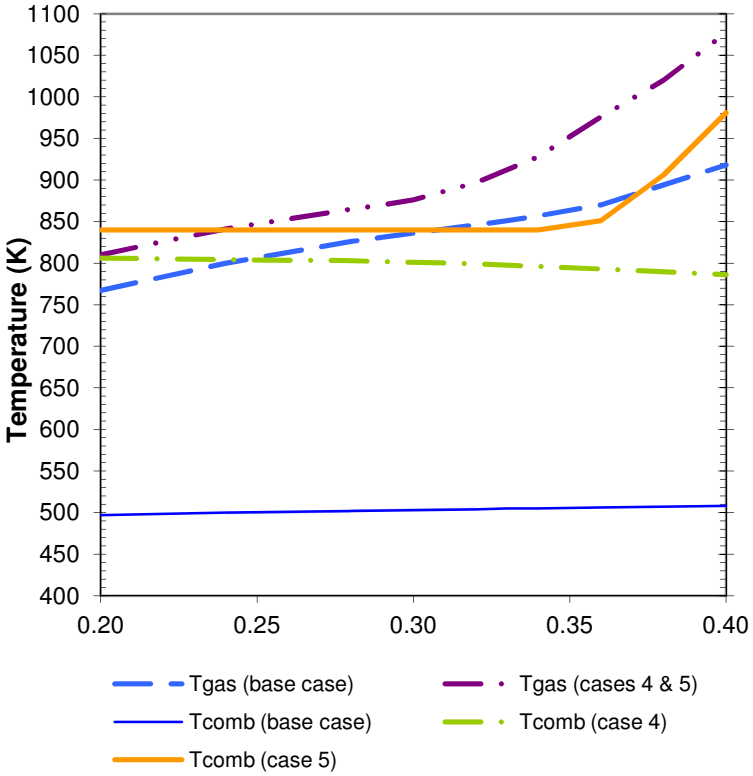

Figure 7 Fuel gases temperature after gasification (Tgas) and fuel gases temperature before entering GT combustor (Tcomb) versus ER for base case, case 4, and case 5

Process efficiency analyses resulted in an alternative approach to evaluate the process configurations that complement cold gasification efficiency, carbon conversion and LHV analyses. Important variations in efficiency were observed as shown in figure 6. The maximum efficiency for the base case was improved by 6% points when a pressurised gasification unit was employed (case 3). However, a bigger improvement was achieved when the energy recuperation system was added to the base case, which increased the efficiency by 11% points (case 4). The addition of a heat exchanger to recover energy from

the hot product gases to reheat itself after compression improved the efficiency by additional 3% points (case 5), that is, 14% points higher than the base case. Figure 6 illustrates that the process efficiencies between cases 5 and 6 differ by 5.5% points which demonstrate an unambiguous difference not observed when only cold gasification efficiency was analysed.

Full integration of the gasifier and GT was achieved by recuperating energy from the GT exhaust gases to preheat air for gasification and combustion, as well as by air extraction from the compressor discharge to avoid the use of a separate air compressor for gasifying air. According to a manufacturer, up to 5% of airflow can be extracted from the compressor discharge without the need of modifications, and air extraction between 6% and 20% may be possible but requires some modifications to the casings, piping and controls [24]. For case 3, an air extraction of 8.6–13% was required for the range of ER evaluated (0.2–0.4). In contrast, for case 6 less than 5% of air extraction was required using an ER of up to 0.3, and at ERs higher than 0.3 approximately 6.7% of air extraction was employed. Since the preferred ER was 0.29 for case 6, the extracted air mass flow was 4.7% of the compressor airflow, which value is within the constraints of the gas turbines as recommended by manufacturers.

The process efficiencies obtained for case 6 in the range of ERs evaluated were between 26% and 33.5%. These results are surprisingly within the efficiencies reported for larger and more complex systems [7, 8, 25]. A conventional IGCC system, with a gasification temperature of 873 K, turbine inlet temperature of 1547 K, turbine pressure ratio of 15 and GT power output of 15.25 MW, gave a net efficiency of 32.6%, and with modification of 33.9%, for coconut husk with moisture content of 50% [8]. Higher net efficiencies have also been reported. One system included an ASU, gas turbine, HRSG, and steam turbine [25]. The efficiencies reported when nitrogen was injected to the combustor of the GT were from 38.2 to 40.8% with a net power output of 275–291 MW. The gasification temperature was 1,589 K and the GT used a pressure ratio of 15.5 and expander inlet temperature of 1,561 K. A second system showed an efficiency of 37.9% with a total power output of 17.9 MW [7]. The simulation parameters used were a pressure ratio of 15.5 and an air-blown gasifier operated at around 850°C. In this work, a small scale system was chosen (200 kW of net power output) with a pressure ratio of 5. These process parameters allow the installation of a compact system with the potential of achieving an efficiency of 33.5%.

4. Conclusions

This work shows a solution for a small scale plant that operates with a comparable efficiency to large scale options. This is due to effective energy recuperation to the gasification process and preheated air. The addition of the energy integration system is shown to be much more significant than the effect of pressure.

Six case studies were evaluated to compare atmospheric versus pressurised gasification and the addition of energy recuperation. When only cold gasification efficiency was analysed, no significant difference between three (4, 5 and 6) of the six cases was observed. However, the overall peak process efficiencies differed by 10% points showing that CGE used in isolation can mislead any process configuration comparison. Whilst the analysis of CGE together with LHV and carbon conversion allows the identification of the optimum ER for an individual case it is still unable to reliably differentiate between all the process configurations. Only overall process efficiency analyses are able to highlight the layout required to achieve maximum efficiency.

Acknowledgements

The Authors would like to thank the National Council on Science and Technology (CONACYT) of Mexico and Keld Energy Ltd. for their financial support.

References

[1] Cantrell K, Ro K, Mahajan D, Anjom M, Hunt PG. Role of Thermochemical Conversion in Livestock Waste-to-Energy Treatments: Obstacles and Opportunities. Ind Eng Chem Res 2007;46:8918-27.
[2] Liu H, Ni W, Li Z, Ma L. Strategic thinking on IGCC development in China. Energy Policy 2008;36:1-11.
[3] Baratieri M, Baggio P, Bosio B, Grigiante M, Longo GA. The use of biomass syngas in IC engines and CCGT plants: A comparative analysis. Appl Therm Eng 2009;29:3309-18.
[4] Rodrigues M, Walter A, Faaij A. Performance evaluation of atmospheric biomass integrated gasifier combined cycle systems under different strategies for the use of low calorific gases. Energy Convers Manage 2007;48:1289-301.
[5] Wolf J, Barone F, Yan J. Performance Analysis of Evaporative Biomass Air Turbine Cycle with Gasification for Topping Combustion. J Eng Gas Turbines Power 2002;124:757-61.
[6] Stahl K, Neergaard M. IGCC power plant for biomass utilisation, Varnamo, Sweden. Biomass Bioenergy 1998;15:205-11.
[7] Klimantos P, Koukouzas N, Katsiadakis A, Kakaras E. Air-blown biomass gasification combined cycles (BGCC): System analysis and economic assessment. Energy 2009;34:708-14.
[8] Kuchonthara P, Tsutsumi A. Energy-recuperative biomass integrated gasification power generation system. J Chem Eng Japan 2003;36:846-51.
[9] Pérez-Fortes M, Bojarski AD, Velo E, Nougués JM, Puigjaner L. Conceptual model and evaluation of generated power and emissions in an IGCC plant. Energy 2009;34:1721-32.
[10] Ruggiero M, Manfrida G. An equilibrium model for biomass gasification processes. Renewable Energy 1999;16:1106-09.
[11] Melgar A, Perez JF, Laget H, Horillo A. Thermochemical equilibrium modelling of a gasifying process. Energy Conversion and Management 2007;48:59-67.
[12] Mansaray KG, Al-Taweel AM, Ghaly AE, Hamdullahpur F, Ugursal VI. Mathematical Modeling of a Fluidized Bed Rice Husk Gasifier: Part I-Model Development. Energy Sources, Part A: Recovery, Utilization, and Environmental Effects 2000;22:83 - 98.
[13] Altafini CR, Wander PR, Barreto RM. Prediction of the working parameters of a wood waste gasifier through an equilibrium model. Energy Convers Manage 2003;44:2763-77.
[14] Sharma AK. Equilibrium modeling of global reduction reactions for a downdraft (biomass) gasifier. Energy Conversion and Management 2008;49:832-42.
[15] FAOSTAT. Food and Agriculture Organization of the United Nations. 2008, p. http://faostat.fao.org.
[16] ADAS. Agricultural Development and Advisory Service, A review of current and impending legislation and its implications for the future disposal of poultry manure. Report

No. ETSU E/GS/00124/REP 1. Energy from biomass Straw, poultry litter and energy crops as energy sources. London, UK: Department of Trade and Industry; 1999, p. 94.
[17] Gerba CP, Smith JE, Jr. Sources of Pathogenic Microorganisms and their Fate during Land Application of Wastes. J Environ Qual 2005;34:42-48.
[18] Bitzer CC, Sims JT. Estimating the availability of nitrogen in poultry manure through laboratory and field studies. Journal of environmental quality 1988;17:47-54.
[19] Aspen Technology I. Aspen Plus 11.1 user guide. Cambridge, MA.; 2001.
[20] Mevissen N, Schulzke T, Unger CA, Bhaird SMa. Thermodynamics of autothermal wood gasification. Environ Prog Sustain Energy 2009;28:347-54.
[21] Mathieu P, Dubuisson R. Performance analysis of a biomass gasifier. Energy Convers Manage 2002;43:1291-99.
[22] Skoulou V, Zabaniotou A, Stavropoulos G, Sakelaropoulos G. Syngas production from olive tree cuttings and olive kernels in a downdraft fixed-bed gasifier. Int J Hydrogen Energy 2008;33:1185-94.
[23] Sugiyama S, Suzuki N, Kato Y, Yoshikawa K, Omino A, Ishii T, et al. Gasification performance of coals using high temperature air. Energy 2005;30:399-413.
[24] Brooks FJ. GE Gas Turbine Performance Characteristics, GER-3567 H. GE Power Systems.
[25] Frey HC, Zhu Y. Improved System Integration for Integrated Gasification Combined Cycle (IGCC) Systems. Environ Sci Technol 2006;40:1693-99.

Characterisation, kinetics and modelling of gasification of poultry manure and litter: an overview

Carolina Font-Palma*

School of Chemical Engineering and Analytical Science
The Mill, University of Manchester
Oxford Road
Manchester, UK, M13 9PL

*Author to whom correspondence should be addressed
E-mail: Carolina.FontPalma@postgrad.manchester.ac.uk
Tel: +44(0) 161 306 4345
Fax: +44(0) 161 306 9321

Abstract

Environmental implications of the disposal of waste from the poultry industry have created the need for proper waste management. As a result, poultry litter has been proposed as a potential fuel candidate for thermal conversion technologies since it is an available source. This review discusses the recent advances in the physical and chemical characterisation of poultry litter. The focus of this review is on gasification for energy generation and current commercial combustion facilities. Significant advances have been made in the pyrolysis, gasification and combustion investigations with the aim to determine their kinetics. These results are important for modelling work and critical issues for the simulation of poultry litter gasification are discussed.

Keywords: Poultry litter; Biomass; Gasification; Pyrolysis; Modelling; Kinetics

1. Introduction

The large poultry industry in the United Kingdom and European Union produces 820 and 5,500 million birds per year, respectively [1]. The increasing demand for poultry supply has resulted in the generation of the so-called litter. Poultry litter is the waste that consists of a mixture of manure, waste bedding, waste food and feathers. The term poultry litter covers total manure and litter generated from chicken and turkey broilers, breeder chickens and layer chickens. Broilers are pullets and cockerels that have not yet reached sexual maturity.

Disposal of poultry litter traditionally includes its utilisation as fertiliser, but its improper application and/or overuse represent potential environmental problems, such as spread of pathogens [2] and emission of greenhouse gases and odorous compounds. Nitrogen present in poultry litter can be converted to ammonia and nitrates. Infiltration of water soluble nutrients can cause ground water pollution and favour high levels of nitrate in drinking water. These high levels of NO_3 can cause cancer, respiratory disease in humans, foetal abortion in livestock and methaemoglobinaemia, a blood disorder in infants commonly known as 'blue baby disease' [3]. Heavy rainfall can sweep the poultry litter applied to land into nearby ditches, streams and lakes. Surface water pollution by nutrients

can lead to eutrophication, which is the excessive growth of algae that consumes aquatic nutrients and oxygen, and block sunlight [4].

Thermal conversion of agricultural waste represents a promising alternative to energy generation and reduction of greenhouse gas emissions. Reviews on the main methods for the conversion of biomass to biofuels, e.g. hydrogenation, pyrolysis and gasification, and the type of biofuels produced can be found in reports by Demirbas [5] and Demirbas et al. [6]. Since gasification of poultry litter represents a viable solution for the disposal of litter and generation of energy, experimental work has been conducted to characterise physically and chemically poultry litter. This work reviews the literature available for the kinetics of gasification of poultry manure and litter, and the advances on experimental work and the challenges of the modelling of its gasification.

2. Characteristics of poultry litter

Biomass properties are important in thermal conversion processes, especially the moisture content, calorific value, fractions of fixed carbon and volatiles, and ash content [7]. Biomass is characterised by lower fixed carbon, and higher moisture and volatile matter contents than coal. However, the higher volatile matter content in biomass favours working at lower gasification temperatures. In addition, poultry manure contains mainly organic matter as showed in table 1.

Table 1 Chemical and physicochemical characterisation of poultry manure [8]

	Poultry manure
Organic matter [a]	85.38
pH	8.8
Moisture [b]	48.69
Total nitrogen [a]	3.56
Inorganic nitrogen [a]	1.74
Ammonia nitrogen [a]	1.76
OCC/nitrogen ratio	10.89
TCC/nitrogen ratio	12.24
P_2O_5 (wt %)	0.71
K_2O_5 [a]	3.79
Paraffinic C [c]	12.4
C in OCH_3, sterols and amino acids [c]	6.7
C in carbohydrates and aliphatics with OH groups [c]	68.1
Aromatic and N-heterocyclic C [c]	3.2
Phenolic C [c]	3.1
C in CO_2H [c]	6.5
Total aliphatic C [c]	87.2
Total aromatic C [c]	6.3
Aromaticity [c]	6.7

[a] in wt % dry basis
[b] in wt % wet basis
[c] distribution of C as % of total C from [9]
OCC: oxidizable carbon content, OCC = (TOMC – 15.356)/1.805
TCC : total carbon content, TCC = (TOMC – 9.33)/1.745
TOMC: total organic matter content, weight loss on ignition at 540°C for 16 h

Nitrogen is present in several forms and is continuously converted by microbial activity and changes in temperature, pH, moisture, and oxygen concentration. Poultry litter contains typically 60–80% of nitrogen in organic form from urea, protein and amino acids present. A large percentage of this organic nitrogen (40–90%) can be transformed to ammonia gas or ionised (NH_4^+) depending on environmental conditions. NH_4 can then be converted to nitrate by microorganisms [10].

Typical composition of poultry litter is shown in table 2; it includes proximate and ultimate analyses, ash fusion and ash analysis, as earlier reported in some publications.

Table 2 Composition of poultry litter

Components	Kirubakaran et al. 2007 [11]	Reardon et al. 2001 [12]	Antares Group Incorporated (1999) [13]	Whitely et al. 2006 [14]
HHV (MJ/kg)	9.56		10.73	12.0
		13.99 (dry)	14.79 (dry)	
		Proximate analysis (wt %)		
Fixed carbon	10.2	14.0	9.8	8.11
Volatile matter	50.3	62.2	47.3	54.72
Moisture	8.2	25.5	27.4	10.59
Ash	28.8	23.9	15.7	26.58
		Ultimate Analysis (wt %)		
C	24.84	35.6	27.22	29.09
H	1.9	4.6	3.72	5.11
O	33.76	29.8	23.10	
N	2.5	5.3	2.69	3.44
S	2.5	0.9	0.33	0.8
Cl	2.5	-	0.71	
Ash	28.8	23.9	15.7	26.58
Moisture	8.2	-	27.4	10.59
		Ash Composition (wt %)		
SiO_2	18.5	22.2	8.1	9.83
Al_2O_3	3.1	2.9	1.9	1.36
TiO_2	-	0.2	0.2	0.06
Fe_2O_3	2.1	1.7	1.16	0.58
CaO	18.5	21.3	17.3	3.72
MgO	4.2	5.0	5.0	1.26
Na_2O	3.6	3.9	9.2	1.61
K_2O	-	-	16.3	3.34
P_2O_5	25.7	20.2	24.4	4.23
SO_3	5.2	7.0	6.7	1.91
BaO	-	-	-	-
SrO	-	-	-	-
CO_2/other	-	0.3	9.4	-
		Ash fusion (°C)		
Initial deformation temperature	1139	-	-	-
Softening temperature	1149	-	-	-
Hemispherical temperature	1161	-	-	-
Fusion temperature	1163	-	-	-

Table 2 illustrates that the composition of poultry litter can vary significantly depending on the litter origin and management practices of the farm. It shows that poultry litter ashes contain high concentrations of potassium (K), calcium (Ca) and phosphorous (P). The presence of K in ashes is known to be dependent on the type of bedding material used. For example, potassium content is very high, around 4–6%, when straw is employed; in contrast, wood shavings reduce the level of K to around 1.5% [15].

A by-product from thermochemical processes, such as combustion and gasification, is ash. The resulting ash contains high phosphorus and potassium concentration that makes it a feasible fertiliser for agricultural crops. Poultry litter ash was evaluated as a potential phosphorus source for wheat and other crops, and showed similar effectiveness as potassium phosphate when the soils were limed [16]. This ash could be potentially sold at a price comparable to fertilisers with phosphorus and potassium of different ratios such as 0:7:30 and 0:10:20, at €11.45 per 50 kg bag. However, the ash might require formulation and granulation which might incur in additional costs. But at least the ash could be used in its original state and save the farmer the expenditure on agricultural fertiliser**.**

Biomass has been pointed out as a source of inexpensive gasification catalyst. Alkali metal salts contained in biomass ash, especially those containing potassium, have been found good promoters of gasification reactions; an almost eight-fold increase in co-gasification rate at 895°C was seen in a 10:90 mixture of coal char and switchgrass ash [17]. Reactivity experiments showed that 20%wt wood ash increased the reactivity of wood by a factor of 32 relative to uncatalysed experiments [18].

Poultry diet contains a range of trace elements, some of which are essential for healthy growth and development, such as zinc, copper, chromium, nickel and manganese, and others which have no known biological functions such as arsenic, cadmium and lead. The addition of Cr, Ni, Cd, Pb and As to animal feedstuffs is not permitted under UK nor European Union regulations. These trace elements should not be added to compound feeds or blended with other feeding stuffs; therefore, levels in diets are those naturally present in the feeds. Arsenic, Cd and Pb are considered to be undesirable substances in livestock feeds.

The presence of arsenic in poultry litter is of great concern; however, arsenic is essential in the poultry diet which benefits arise from pharmacological effects on the gut microflora. The importance of the gut microflora relates to its effects on host nutrition, health and growth performance by interacting with nutrient utilisation [19].

Arsenic was added to poultry diets in the past as a growth stimulant at rates of around 90 mg As/kg DM [20]. Since the benefits were questionable, arsenic is no longer used as a growth promoter in the UK. However, the USA has continued the use of arsenic as Roxarsone (3-nitro-4-hydroxyphenylarsonic acid) because it has shown to increase growth and feed utilisation [21]. This addition causes the presence of 150 mg of As per 4.9 kg of poultry litter generated by a single broiler in a 48-day lifetime in the USA [22]. Recently, the US Food and Drug Administration (FDA) conducted studies of As levels in the liver of chickens; as a result, Alpharma, a subsidiary of Pfizer, Inc., is suspending the sales of Roxarsone by July 2011 [23]. A different situation is found in the UK, arsenic is not included in the poultry diet; therefore, As might be present in an insignificant amount in poultry litter.

The maximum permitted levels of heavy metals in poultry feeds are regulated according to the European Parliament and Council Directive 2002/32/EC and the amended 2003/100/EC, as indicated in table 3. The data reported by Nicholson et al. [24] confirmed that none of the samples of compound or home-mix poultry feeds analysed exceeded the limit. This led to an arsenic content in manure of <0.1–41.1 mg/kg DM with a mean of

9.01 mg/kg DM, as shown in table 3. According to these low values of heavy metals found in poultry litter, the emission of heavy metals are expected to be below the limits established in table 3, which allows emissions of less than 0.5 mg/m^3.

Table 3 Maximum content of heavy metals in poultry feed and their presence in manure

Heavy metal	Maximum content in poultry feed (mg/kg DM) [25]	Content in commercial poultry feed (mg/kg DM) [24]	Content in poultry manure (mg/kg DM) [24]	Estimated content in poultry litter (mg/m^3) [24]
Zinc	284	106 –169	208 – 473	130
Copper	40	24.8 – 52.4	45.7 – 173	19
Nickel	Not stated. Poultry tolerance: 400 mg Ni/kg DM in sulphate or acetate form	1.1 – 3.9	2.2 – 12.3	2.4
Lead	5.6	<1 – 2.4	<1 – 9.28	2.0
Cadmium	0.56	<0.1 – 0.33	0.2 – 1.16	0.33
Arsenic	2.24	0.14 – 0.31	<0.1 – 41.1	0.3
Chromium	Not stated	<0.2 – 3.44	3.57 – 79.8	1.2
Manganese	284			
Fluorine	284			
Mercury	0.11			

3. Experimental work on gasification of poultry litter

Gasification comprises sequential steps: pre-heating and drying, pyrolysis, and char gasification and oxidation. The pyrolysis step normally takes place at 200–500°C, where the fuel decomposes into three often lumped products: char, volatiles (condensable hydrocarbon or tar) and gases (non-condensable) [26, 27]. Since pyrolysis is the first stage of thermal degradation, the mechanisms of biomass pyrolysis have been studied to determine the pyrolysis rate and the amount, properties and composition of the resulting product [26, 28].

There is a vast literature on wood pyrolysis, both experimental and modelling, for various types of wood, such as oak, hardwood, sweet gum, fir wood, pine and beech [27]. However, work on the pyrolysis of poultry litter has shown that the pyrolysis characteristics are very different from wood and other types of biomass [29]. As a result, experimental work on the pyrolysis of poultry litter has started. It has been reported that weight is significantly lost during fast devolatilisation of poultry litter to around 40% of weight loss at 500°C, and to about 94% at 1300°C [30]. Table 4 shows the product yields after the pyrolysis of poultry litter from the yet limited work found in the literature. The yields of products and pyrolysis rates are known to be affected by the heating rate, temperature and pressure, as well as by biomass characteristics, such as chemical composition, ash content, particle size and shape, density, and moisture content [26]. Accordingly, the product yields reported vary greatly because of the quite different

experimental conditions in each work, the type of pyrolyser used, and the differences in the poultry litter composition. The results from Lima et al. [31] were the most different. In Lima et al.'s work, char and non-condensable gases were directly quantified; whereas the condensable gases (tar) might have been overestimated since they included non-condensable gases not calibrated, water vapour and pyrolytic oil vapours, that is, tar and hydrocarbon gases greater than C_4H_{10} which were not measured.

Table 4 Product yields from pyrolysis of poultry litter

Pyrolysis conditions	Reactor	Sample description	Yields (% wt)		
			Gas	Tar	Char
Fast pyrolysis at 550°C, sample feed rate 200 g/h (gas yield calculated by difference) [29]	Fluidised bed reactor of 5.08 cm pipe, 50.80 cm high and 13.97 cm preheater zone	Chicken litter with hardwood shavings	33.04	26.98	39.98
		Chicken litter with softwood shavings	42.28	20.66	37.14
		Wood chip	17.1	34.62	39.28
Heating rate: 100 K/min, sample of 21-37 mg, He flow rate of 400 ml/min [32]	TGA coupled with FTIR (tar calculated by difference)	Chicken litter with straw as bedding	49.75	23.37	26.88
Fast pyrolysis at 500°C, sample feed rate 200 g/h using N_2 flow rate of 18 L/min [33]	Bubbling fluidised bed reactor (50 mm pipe, 500 mm high and 140 mm preheater zone)	Chicken litter after one flock was raised, with hardwood shavings as bedding	13.6±5.7	45.7±2.9	40.6±6.2
		Chicken litter after two flocks were raised, hardwood shavings	22.3±2.5	36.8±1.2	40.8±1.9
		Turkey litter, pine wood	21.7±1.9	50.2±1.6	27.6±1.7
		Hardwood bedding	24	63.3±11.3	12.7±2
Fast pyrolysis 20°C/ms at 700°C, 1 mg sample [31]	CDS analytical pyroprobe, 1-cm quartz tube	Broiler litter, with softwood such as pine	9	66	25
Pyrolysis at 330°C [9]	Advanced prototype pyrolyser	Chicken manure	23	50	27

3.1 Char and ash production

Experimental work has shown that the char yield is favoured at lower temperatures, and in order to maximise char yields low heating rate and long residence time are necessary, i.e. slow pyrolysis [31]. Table 5 shows the composition of poultry litter char as reported in previous works. It is seen that the carbon content is very high. The ash content in char was between 21.55 and 66.26% [29], that is, higher than in the initial poultry litter. This higher ash content is because almost all the ash that was in the initial poultry litter remains in the char. In contrast, the ash content in char for bedding material was much lower between 1.4 and 27.28% [29, 33].

Table 5 Composition of poultry litter char from fast pyrolysis and ash content (% wt, on moisture- and ash-free basis)

Pyrolysis temperature	330°C	575°C	575°C	575°C
Component	Chicken manure[1]	Poultry litter[2]	Poultry litter[3]	Hardwood bedding [33]
Carbon	82.7	41.63	74.20	61.33
Nitrogen	7.0	3.08	5.23	1.62
Oxygen	6.4	48.67	5.89	32.33
Hydrogen	3.3	2.42	3.74	2.70
Sulphur	0.6	1.48	3.56	0.39
Chlorine	-	2.72	7.37	1.22
Ash	48.6	43.79	54.53	27.28

[1] Chicken manure [9]

[2] Poultry litter after one flock was raised, hardwood shavings used as bedding material [33]

[3] Poultry litter after two flocks were raised, hardwood shavings used as bedding material [33]

Char is composed of several inorganics such as, potassium, phosphorous, silicon, calcium and trace elements, for instance cadmium, copper and zinc. Table 6 shows the inorganic speciation of char. The concentration of inorganics such as calcium, potassium and phosphorous were increased 2.8–7 times compared to the original samples [29]. The presence of these inorganic elements is what makes poultry litter char a potential soil conditioner or fertiliser.

Chars from poultry litter contain between 1.68% wt [33] and 3.7% wt of phosphorus; in contrast, chars from coal, coconut shell and wood have less than 0.2% wt [31]. Inorganic species, such as potassium, are known to favour char formation [29].

Table 6 Inorganic components of char from poultry litter pyrolysis

	Chicken litter		Hardwood bedding
Element	% wt [33] [2]	mg/g char [31]	% wt [33]
P	1.68	36.8 ± 2.7	0.09
K	5.65	42.0 ± 5.3	1.06
Ca	6.55	53.0 ± 4.0	1.56
Mg	1.16	14.2 ± 1.2	0.17
Na	1.48	NA	0.17
Al	0.54	NA	0.03
Fe	0.62	NA	0.12
Mn	0.08	NA	0.02
Cu[1]	0.08	NA	0.01
Zn[1]	0.08	NA	0.01
Cd[1]	4.0	NA	1.0
Ni[1]	45	NA	26
Se[1]	1.2	NA	0.2
Mo[1]	11	NA	NA
S	NA	17.3 ± 2.3	NA

[1] ppm

[2] Poultry litter after one flock was raised, hardwood shavings used as bedding material

NA – not available

3.2 Condensable gases production

Table 7 shows the elemental analysis of condensable gases after pyrolysis of poultry litter. The carbon and nitrogen content are higher for poultry litter than for bedding material. The higher nitrogen content was attributed to the presence of manure in the litter. Due to the higher content of carbon, the higher heating value (HHV) of condensable gases for poultry litter is higher than for bedding material. It was attributed that this greater HHV was caused by the higher protein content or lipids content, where decarboxylation and nitrogen lost from proteins cause higher hydrocarbon content [33].

Table 7 Composition of condensable gases from fast pyrolysis of poultry litter at 500°C

Component	Content in % wt				
	Chicken litter	Turkey litter	Wood chip	Chicken litter	Hardwood bedding
	[29]			[33]	
Carbon	58.07	60.62	45.22	63.24	55.25
Nitrogen	8.30	4.21	<0.5	5.05	<0.5
Oxygen	22.77	28.68	48.73	23.89	37.58
Hydrogen	7.22	7.16	7.7	7.22	6.54
Sulphur	-	-	-	0.46	<0.05
Ash	1.37	0.71	0.1	<0.09	<0.08
Moisture	-	-	-	4.6	5.3
HHV (MJ/kg)	27.49	26.24	18.11	28.25	22.64

3.2 Gases production

The composition of the gases released after pyrolysis depend on the characteristics of the feedstock. Attempts to understand the fast devolatilisation of poultry litter have also included characterisation of volatiles. The main released non-condensable gases are carbon dioxide, carbon monoxide and hydrogen and small amount of low molecular weight hydrocarbons such as CH_4, C_2H_6, and C_3H_8 [31]. The yield of gases increased with increasing pyrolysis temperature. Methane yields were found as three to eight times lower than CO and CO_2 yields. CO_2 yields were the highest over the temperature range (400–1300°C) measured and reached an asymptotic value at around 1000°C [30]. At temperatures greater than 700°C, CO_2 increases are considered to be caused by decarboxylation of mineral-matter (such as $CaCO_3$); this mineral-matter in poultry litter might be the reason for lower tar yields than from other fuels and the cause for tar destruction at an early stage [32].

The thermal conversion behaviour of poultry litter has also been analysed using thermogravimetric analysis (TGA). The release of nitrogen species has been studied in detail in order to identify NO_x precursors [30, 32]. Experiments on the pyrolysis of poultry litter used TGA and Fourier Transform Infrared (FTIR) spectrometry to quantify evolved gases, mainly N-gases. A high percentage of chicken litter bound nitrogen converted to NH_3, HCN and HNCO, where NH_3 was the main gas released of the three. These nitrogen species are of interest because they are considered NO_x precursors. However, no correlation was found between the amount of nitrogen species released and the nitrogen content in the litter. The gaseous nitrogen species yields were found to decrease with increasing heating rates. In addition, acetic acid (1.3–3.1 % wt daf) and methane (1.2–3.4% wt daf) were released from poultry litter pyrolysis [32].

Other work employed a heated wire mesh to study fast pyrolysis and it was coupled with a FTIR spectrophotometer for the simultaneous analysis of gas species. It was found that CO_2 was predominant at low temperatures (< 800°C) and CO increased at high temperatures, which was attributed to tar decomposition. At low temperature (< 600°C), nitrogen was mainly retained in the char, and ammonia was the main N-gas product. At high temperatures, more nitrogen was released, high yields of N-tar were produced and HCN was the main N-gas formed [30].

Coupling a Fourier transform infrared spectrometer (FTIR) to a TGA was recommended for slow pyrolysis applications, like carbonization and biochar production, but also for modelling purposes using tools such as FG-Biomass [34]. Giuntoli et al. [34]

showed a differential thermogravimetric (DTG) curve with the compounds analysed by FTIR from chicken manure using a heating rate of 10°C/min. It is seen the drying step at 105°C, where moisture is evolved and the water released subsequently was pyrolytic water. Some ammonia was released already during the drying step and it was assumed as physically absorbed NH_3 contained in the manure. CH_4 was released at around 530°C, probably due to the release of methoxyl groups mainly from lignin decomposition. In chicken manure protein-nitrogen is present mainly due to undigested food, and it was considered responsible for the continuous release of NH_3 at lower temperatures. Since manure has also a high concentration of nitrogen in the form of urea, this component was assumed responsible for the high amount of HNCO released at around 430°C, in correspondence with the release of NH_3 and HCN. HNCO possibly decomposes into NH_3 and CO_2 due to the appearance of their respective peaks. A limitation of these works is that FTIR cannot detect H_2, since FTIR cannot measure diatomic molecules of the same element.

4. Combustion facilities for the disposal of poultry litter

Since the application of poultry litter into land is restricted by the European Union, treatment of this waste has gained attention. One example is the work carried out at the Department of INETI in Portugal contracted by the University of Limerick from Ireland using a small-scale fluidised bed combustor [15]. The combustor is square (30 cm x 30 cm) and height of 500 cm. Due to the fluidising velocity employed (0.4–0.5 m/s) a large amount of the ashes was elutriated out of the combustor and then collected in two cyclones. The measurement of the ashes showed that most remained in the bed (only 10–12%) and the ashes collected in the cyclones allowed to trace the partition of potassium, chlorine and heavy metals. Major problems arose from the feeding of poultry litter into the combustor since its moisture as received was 43% which led to unstable combustion. This high moisture content also affected the ignition temperature, which was found to be over 620°C at a moisture content of 20%. To help the combustion of chicken litter, a mixture with peat has been also studied. The combustion efficiency was improved by introducing part of the air as secondary to the freeboard with some turbulence. This reduced the CO formed, and NO_x and N_2O levels were lower than the permitted emission values. It was reported that the ash fusion was determined as 931.9 K; however, a tendency for ash agglomeration above 1073 K was mentioned, but that in general no agglomeration tendency was observed because the bed was reported as shallow and well fluidised. In September 2010, it was announced the approval of Rose Energy Limited, a consortium of three agri-food companies in Glenavy, Ireland, for converting poultry litter into electricity using a fluidised bed combustion and steam turbine. The combustor will be fed with poultry litter and meat and bone meal (approximately 250,000 tonnes per annum), and power about 25,000 homes [35].

Another example of a small size waste disposal system for the farm industry is the co-combustion of poultry litter with natural gas in a swirling fluidised bed combustor (SFBC), where secondary air was injected in a tangential direction. The resulting hot gas was passed through heat exchangers, one after the combustor and the second after the cyclone; the heat recovery efficiencies were 50 and 20%, respectively, which gave a total heat recovery efficiency of around 75% [36].

Examples of commercial facilities for the conversion of poultry litter to energy were reviewed in [10]. Fibropower opened as a poultry-litter-fired power plant at Eye in Suffolk, UK in November 1993. The plant generates a net output of 12.7 MW to supply a 33 kV power line for distribution of local electricity networks. Fibrowatt constructed two

plants; one is a 38.5 MW plant in Thetford, England. The plant consists of a conventional moving grate boiler and steam cycle that employs 420,000 tonnes/yr of poultry litter [37]. The litter is combusted at more than 850°C with a residence time of 2 s. Based on the experience of the management team that built the world's first three poultry litter-fuelled power plants in the United Kingdom in the 1990s, Fibrowatt LLC was founded in 2000 [38]. In mid 2007, the first poultry litter-fuelled power plant (Fibrominn) in the USA began operation in Benson, Minnesota. The 55-MW power plant uses more than 500,000 tonnes of poultry litter annually mainly supplied by Minnesota turkey growers and produces enough electricity for approximately 40,000 homes. This solution uses the heat from a furnace to produce high pressure and temperature steam in a boiler which is then used in steam turbines to generate electricity. However, this project requires that poultry litter be transported in trucks to the plant storage facility plus truck routing to minimise traffic impact on local communities.

In contrast to combustion applications of small and medium scale, little open literature exits for the gasification of poultry litter. A small scale study was performed at Texas A&M University in a updraft fixed-bed gasifier with a 10 kW capacity [39]. The gasifier worked at atmospheric pressure using air as gasifying agent. The apparatus had an internal diameter of 0.15 m and total height of 0.75 m, with a thick two-stage insulation of castable alumina refractory and insulating blankets. The product gas composition mainly consisted of CO (28%), CO_2 (3.7–11%), H_2 (6.1–7.3%) and CH_4 (0.9–1.4%) with a HHV of 4.28–4.64 MJ/m^3 (dry basis). However, the experiments were performed under a batch-mode operation (approximately for 1 hr) since steady-state was not achieved due to ash accumulation in the bed; tar measurements were not presented. This limited literature supports the need for studies on poultry litter gasification.

5. Modelling of gasification of poultry litter

5.1 Kinetics of thermal conversion of poultry litter

The investigation of the thermal conversion behaviour of biomass includes the study of the mechanism and kinetics by which biomass decomposes. The kinetics parameters are normally determined by the curves obtained from experiments using thermogravimetric analysis (TGA). The weight loss at different temperatures from TGA studies is used to determine the characteristics of devolatilisation and further conversion of biomass, and afterwards to elucidate the kinetics of reaction.

TGA results of wood chips and chicken litter (broiler and flock) were compared since chicken litter can contain wood chips as bedding material. Wood chips showed two weight loss regimes, the first one attributed to the decomposition of cellulose, hemicellulose and lignin and the last one to further devolatilisation of residual charcoal. Whereas chicken litter presented three different weight loss regimes, the second loss regime was attributed to manure and lignin and the third one to further charcoal devolatilisation [40].

The kinetics parameters of pyrolysis of chicken litter has been determined using the differential method from data obtained using DTG. The rate of reaction (-r) was expressed as:

$$-r = \frac{dX}{dt} = k \cdot f(X) \tag{1}$$

The reaction rate constant, k, follows the Arrhenius equation:

$$k = A \exp\left(-\frac{E}{RT}\right) \tag{2}$$

The combination of the equations 1 and 2, and taking the natural logarithm yields the following equation:

$$\ln\left(\frac{dX}{dt}\right) = \ln A + n\ln(1-X) - \frac{E}{RT} \quad (3)$$

where E is the apparent energy of activation, A is the pre-exponential factor, T is the pyrolysis temperature, X is the conversion of sample, t is the pyrolysis time, R is the gas constant and n is the reaction order. E and A were determined by linear regression from the lineal relationship between ln(dX/dt) and 1/T with slope –E/R, since TGA was run at different heating rates [40-42].

Another approach to elucidate the gasification kinetics of poultry litter employed static air and static nitrogen separately at a heating rate of 5°C/min [11]. From the TGA data, the rate of reaction was determined as the average of weight loss (dX/dt) between (t – 1) and (t), and (t) and (t + 1). Assuming a first order reaction, $f(X)$ was defined as the weight of biomass yet to be degraded (w) and calculated for each temperature. Using equation 1, k was calculated for each temperature. With the natural logarithm of equation 2, a plot for ln$k$ versus 1/T showed different zones of conversion; E and A were determined for each zone.

Table 8 summarises the results of kinetics parameters for poultry litter when a first order reaction was assumed. The activation energies shown vary significantly as a result of different heating conditions, experimental devices such as classical thermogravimetry, sample characteristics, and mathematical treatment of the data [43]. These variations make difficult to identify proper kinetics of the primary degradation through fast pyrolysis for the simulation of the gasification of poultry litter.

Table 8 Kinetic parameters for chicken litter considering a first order reaction

TGA	Stages of conversion	E (kJ/mol)	A (s^{-1})	Reference
Pyrolysis carrier gas: N_2 at 20 ml/min Heating rates: 5, 10 and 20°C/min	60% conversion 80% conversion	99 464	$7.66x10^3$ $1.01x10^5$	[40]
Static N_2 Heating rate: 5°C/min	moisture removal: 30-120°C zone I: 200-310°C zone II: 310-440°C zone III: 440-600°C	36.54 87.19 52.46 58.76	1740 $9.82x10^5$ 20.22 29.35	[11]
Static air Heating rate: 5°C/min	moisture removal: 30-120°C zone I: 200-310°C zone II: 310-440°C zone III: 440-600°C	32 88.62 63.8 62.12	245.32 $1.34x10^6$ 193.67 55.09	[11]
Pyrolysis N_2 at 50 ml/min Heating rate: 20°C/min	moisture removal: 20-160°C zone II. 160-290°C zone III. 290-390°C zone IV. 390-500°C	100.6 52.11 193.9 242.3	$2.77x10^{13}$ 808.81 $4.18x10^{15}$ $4.81x10^{17}$	[41]
Combustion Air at 50 ml/min Heating rate: 20°C/min	I. moisture removal: 20-150°C II. Devolatilisation (150-350°C) III. Char precombustion (350-500°C) IV. Char combustion (500-650°C)	61.72 71.43 148.5 157.6	$4.41x10^6$ $2.64x10^4$ $4.49x10^8$ $1.69x10^9$	[14]

A kinetic model based on parallel first-order reactions with a Gaussian distribution of activation energies was proposed for the devolatilisation of poultry litter [32]. In order to fit the experimental data, the pre-exponential factor was fixed to $2.2x10^{13}s^{-1}$. Since each volatile species evolved as one or more peaks, single or multiple precursors were assumed, respectively. Kinetic parameters were given for CO, CO_2, H_2O, CH_4, C_2H_4, CH_3COCH_3, CH_3OH, HCN, NH_3, CH_2O, HCOOH, CH_3COOH, C_2H_4O, HNCO and tar, with activation energies ranging from 124.7 to 323.3 kJ/mol.

5.2 Challenges for the modelling of gasification of poultry litter

For wood pyrolysis, two types of models have been proposed for representing fast heating rates, the one-component mechanism and the multi-component reaction mechanism [26]. In the former mechanism, three parallel reactions produce char, tars and gas. Whilst in the latter mechanism, intermediates are produced, an example is a three-step mechanism suggested for wood pyrolysis, which included secondary reactions for tar decomposition into gas and char [44].

The understanding of the initial devolatilisation is necessary for the modelling of biomass thermal conversion processes. From TGA experiments, it is known that wood chips showed two weight loss regimes, whilst chicken litter showed three different weight loss regimes [40].

Kinetics parameters are normally calculated to slow heating rates as shown in table 8. Therefore, there is a need for kinetic parameters for faster heating rates since devolatilisation occurs nearly instantaneously.

Among the greatest challenges of the gasification technology is the elimination of tars. Tar is a complex mixture of condensable hydrocarbons comprising single ring to 5-ring aromatic compounds plus other oxygen-containing hydrocarbons and complex polycyclic aromatic hydrocarbons (PAH) [45]. Tar is undesirable because of its propensity to condensate at temperatures lower than its dew point which causes blockage and fouling of lines, filters and gas turbines. Furthermore, sampling and measuring tars are difficult tasks that affect the accurate modelling of tars. Tars are produced in series of reactions highly dependent on the operating conditions. For simplification, tar model compounds have been studied to understand tar cracking mechanisms [46]. Another approach is the consideration of all tar compounds as a single lump to obtain apparent kinetic parameters [47].

The presence of ash in fluidised bed gasifiers represents a potential risk since bed agglomerates can lead to loss of fluidisation (defluidisation) and alkali vapours in the product gases can increase rates of hot corrosion on turbine surfaces in integrated systems [48]. Gas-phase concentration of alkali constitutes and low melting temperature of alkali ash components can cause ash deposit formation. TGA/DSC tests combined with the Ash fusion test (AFT) and Thermo-mechanical analysis (TMA) were used to characterise the fusion behaviour of poultry residues [49]. In the TMA, the change of height of a load of ash was measured to evaluate the sintering temperature while heating at a constant rate. The ashes were leached with water and ammonium acetate. For the chicken litter sample, a mass loss at 600-800°C was attributed to the decomposition of calcium carbonate and no clear melting point was observed. In contrast, for the leached chicken litter ashes, two endothermic peaks were noticed, one at 728°C (evaporation peak) with a mass loss of 30% and the other at 958°C (melting point). The difference between the two samples was that the leached ashes were enriched with reactive inorganic and high melting point species. As a final point, ash agglomeration, inorganics partition, and ash melting studies have shown

that ash chemistry should be included in both experimental and modelling work. However, ash constituents are often considered as inert in gasification models.

6. Conclusions

To avoid the direct disposal of poultry litter into land, it can be employed as a fuel source for thermal conversion processes. As a result, commercial combustion facilities already exist that convert this waste into energy. However, gasification of poultry litter offers an alternative option for the disposal of litter which benefits from producing combustible mixture of gases to be used in power engines. On the other hand, more research is needed to understand the gasification process. One of the areas that require further work is the generation of more experimental data that could be then fed into modelling work.

Among the challenges that need to be addressed is the understanding of tar formation and evolution. The presence of tar can cause operational problems; in particular heavy tars may condense on cooler surfaces downstream which can lead to blockage of particulate filters and of fuel lines. Another issue is the influence of the ash chemistry since poultry litter contains approximately 20%wt of ash content and high amounts of potassium. Despite the problems caused by the presence of ash, the resulting ash offers the advantage of being suitable for usage as fertiliser.

References

[1] FAOSTAT. Food and Agriculture Organization of the United Nations. 2008, p. http://faostat.fao.org.

[2] Gerba CP, Smith JE, Jr. Sources of Pathogenic Microorganisms and their Fate during Land Application of Wastes. Journal of Environmental Quality 2005;34:42-48.

[3] Henihan AM, Leahy MJ, Leahy JJ, Cummins E, Kelleher BP. Emissions modeling of fluidised bed co-combustion of poultry litter and peat. Bioresource Technology 2003;87:289-94.

[4] Bitzer CC, Sims JT. Estimating the availability of nitrogen in poultry manure through laboratory and field studies. Journal of environmental quality 1988;17:47-54.

[5] Demirbas A. Biomass resource facilities and biomass conversion processing for fuels and chemicals. Energy Conversion and Management 2001;42:1357-78.

[6] Demirbas MF, Balat M, Balat H. Biowastes-to-biofuels. Energy Conversion and Management 2011;52:1815-28.

[7] McKendry P. Energy production from biomass (part 1): overview of biomass. Bioresource Technology 2002;83:37-46.

[8] Guerra-Rodríguez E, Diaz-Raviña M, Vázquez M. Co-composting of chestnut burr and leaf litter with solid poultry manure. Bioresource Technology 2001;78:107-09.

[9] Schnitzer MI, Monreal CM, Facey GA, Fransham PB. The conversion of chicken manure to biooil by fast pyrolysis I. Analyses of chicken manure, biooils and char by ^{13}C and ^{1}H NMR and FTIR spectrophotometry. Journal of Environmental Science and Health, Part B: Pesticides, Food Contaminants, and Agricultural Wastes 2007;42:71 - 77.

[10] Kelleher BP, Leahy JJ, Henihan AM, O'Dwyer TF, Sutton D, Leahy MJ. Advances in poultry litter disposal technology - a review. Bioresource Technology 2002;83:27-36.

[11] Kirubakaran V, Sivaramakrishnan V, Premalatha M, Subramanian P. Kinetics of Auto-Gasification of Poultry Litter. International Journal of Green Energy 2007;4:519 - 34.

[12] Reardon JP, Lilley A, Browne K, Beard K, Wimberly J, Avens J. Demonstration of a Small Modular Biopower System Using Poultry Litter. DOE SBIR Phase-I Final Report. Community Power Corporation; 2001.
[13] Antares_Group_Incorporated. Economic and technical feasibility of energy production from poultry litter and nutrient filter biomass on the lower Delmarva Peninsula (Technical Report No. 20785) Appendix A.; 1999.
[14] Whitely N, Ozao R, Artiaga R, Cao Y, Pan WP. Multi-utilization of Chicken Litter as Biomass Source. Part I. Combustion. Energy Fuels 2006;20:2660-65.
[15] Abelha P, Gulyurtlu I, Boavida D, Seabra Barros J, Cabrita I, Leahy J, et al. Combustion of poultry litter in a fluidised bed combustor*. Fuel 2003;82:687-92.
[16] Codling EE, Chaney RL, Sherwell J. Poultry Litter Ash as a Potential Phosphorus Source for Agricultural Crops. J Environ Qual 2002;31:954-61.
[17] Brown RC, Liu Q, Norton G. Catalytic effects observed during the co-gasification of coal and switchgrass. Biomass and Bioenergy 2000;18:499-506.
[18] Sutton D, Kelleher B, Ross JRH. Review of literature on catalysts for biomass gasification. Fuel Processing Technology 2001;73:155-73.
[19] Yang Y, Iji PA, Choct M. Dietary modulation of gut microflora in broiler chickens: a review of the role of six kinds of alternatives to in-feed antibiotics. World's Poultry Science Journal 2009;65:97-114.
[20] Proudfoot FG, Jackson ED, Hulan HW, Salisbury CDC. Arsanilic acid as a growth promoter for chicken broilers when administered via either the feed or drinking water. Canadian Journal of Animal Science 1991;71:221-26.
[21] Anderson BK, Chamblee TN. The effect of dietary 3-nitro-4-hydroxyphenylarsonic acid (roxarsone) on the total arsenic level in broiler excreta and broiler litter. Journal of Applied Poultry Research 2001;10:323-28.
[22] Nachman KE, Mihalic JN, Burke TA, Geyh AS. Comparison of arsenic content in pelletized poultry house waste and biosolids fertilizer. Chemosphere 2008;71:500-06.
[23] US Food and Drug Administration (FDA). http://www.fda.gov.
[24] Nicholson FA, Chambers BJ, Williams JR, Unwin RJ. Heavy metal contents of livestock feeds and animal manures in England and Wales. Bioresource Technology 1999;70:23-31.
[25] Foundation PP. Open Congress for the 112th United States Congress. http://www.opencongress.org/.
[26] Di Blasi C. Modeling chemical and physical processes of wood and biomass pyrolysis. Progress in Energy and Combustion Science 2008;34:47-90.
[27] Basu P, Kaushal P. Modeling of Pyrolysis and Gasification of Biomass in Fluidized Beds: A Review. Chemical Product and Process Modeling 2009;4:Article 21.
[28] Rapagnà S, Mazziotti di Celso G. Devolatilization of wood particles in a hot fluidized bed: Product yields and conversion rates. Biomass and Bioenergy 2008;32:1123-29.
[29] Kim S-S, Agblevor FA, Lim J. Fast pyrolysis of chicken litter and turkey litter in a fluidized bed reactor. Journal of Industrial and Engineering Chemistry 2009;15:247-52.
[30] Di Nola G, de Jong W, Spliethoff H. The fate of main gaseous and nitrogen species during fast heating rate devolatilization of coal and secondary fuels using a heated wire mesh reactor. Fuel Process Technol 2009;90:388-95.
[31] Lima IM, Boateng AA, Klasson KT. Pyrolysis of Broiler Manure: Char and Product Gas Characterization. Industrial & Engineering Chemistry Research 2009;48:1292-97.

[32] de Jong W, Di Nola G, Venneker BCH, Spliethoff H, Wójtowicz MA. TG-FTIR pyrolysis of coal and secondary biomass fuels: Determination of pyrolysis kinetic parameters for main species and NOx precursors. Fuel 2007;86:2367-76.
[33] Agblevor FA, Beis S, Kim SS, Tarrant R, Mante NO. Biocrude oils from the fast pyrolysis of poultry litter and hardwood. Waste Management 2010;30:298-307.
[34] Giuntoli J, de Jong W, Arvelakis S, Spliethoff H, Verkooijen AHM. Quantitative and kinetic TG-FTIR study of biomass residue pyrolysis: Dry distiller's grains with solubles (DDGS) and chicken manure. Journal of Analytical and Applied Pyrolysis 2009;85:301-12.
[35] Rose Energy. http://roseenergy.webbelief.com/.
[36] Zhu S, Lee S. Co-combustion performance of poultry wastes and natural gas in the advanced Swirling Fluidized Bed Combustor (SFBC). Waste management 2005;25:511-18.
[37] EPR. Energy Power Resources Ltd.
[38] Fibrowatt_LLC. Power from Poultry Litter™.
[39] Priyadarsan S, Annamalai K, Sweeten JM, Mukhtar S, Holtzapple M. Fixed-bed gasification of feedlot manure and poultry litter biomass. Trans ASAE 2004;47:1689-96.
[40] Kim S-S, Agblevor FA. Pyrolysis characteristics and kinetics of chicken litter. Waste Management 2007;27:135-40.
[41] Whitely N, Ozao R, Cao Y, Pan WP. Multi-utilization of Chicken Litter as a Biomass Source. Part II. Pyrolysis. Energy Fuels 2006;20:2666-71.
[42] Nemtsov DA, Zabaniotou A. Mathematical modelling and simulation approaches of agricultural residues air gasification in a bubbling fluidized bed reactor. Chemical Engineering Journal 2008;143:10-31.
[43] Di Blasi C, Branca C. Kinetics of Primary Product Formation from Wood Pyrolysis. Industrial & Engineering Chemistry Research 2001;40:5547-56.
[44] Thurner F, Mann U. Kinetic investigation of wood pyrolysis. Industrial & Engineering Chemistry Process Design and Development 1981;20:482-88.
[45] Devi L, Ptasinski KJ, Janssen FJJG. A review of the primary measures for tar elimination in biomass gasification processes. Biomass and Bioenergy 2003;24:125-40.
[46] Simell PA, Hirvensalo EK, Smolander VT, Krause AOI. Steam Reforming of Gasification Gas Tar over Dolomite with Benzene as a Model Compound. Industrial & Engineering Chemistry Research 1999;38:1250-57.
[47] Corella J, Caballero MA, Aznar MP, Brage C. Two Advanced Models for the Kinetics of the Variation of the Tar Composition in Its Catalytic Elimination in Biomass Gasification. Ind Eng Chem Res 2003;42:3001-11.
[48] Turn SQ, Kinoshita CM, Ishimura DM, Zhou J. The fate of inorganic constituents of biomass in fluidized bed gasification. Fuel 1998;77:135-46.
[49] Tortosa Masiá AA, Buhre BJP, Gupta RP, Wall TF. Characterising ash of biomass and waste. Fuel Processing Technology 2007;88:1071-81.

EFFECTS OF PRESSURE ON THE GASIFICATION OF POULTRY LITTER

C Font-Palma, A D Martin
University of Manchester
School of Chemical Engineering and Analytical Science
The Mill, Oxford Road
Manchester, UK, M13 9PL

ABSTRACT: The poultry industry is large in the EU which generates litter as waste. Improper application and/or overuse of poultry litter as fertiliser can cause the spread of pathogens and ground water pollution. Therefore, gasification is proposed as a potential solution for disposal and energy generation. Conventional gasification systems are large scale with an atmospheric gasifier that requires cooling of the product gas. This work, however, employs a small on-site pressurised gasifier to maintain all stages hot. A model for the optimisation of air gasification integrated with a gas turbine (GT) engine was developed on ASPEN Plus to achieve 200 kW of net power output. Steady-state and chemical equilibrium were assumed in a Gibbs free energy minimisation gasifier. The effects of varying the pressure ratio and inlet temperature of the GT on carbon conversion, gasification temperature, product gas composition, higher heating value and process efficiency were evaluated. At lower pressure ratios more energy was recuperated by preheating the product gas and air before entering the GT combustion chamber. Increasing the pressure ratio improved the process efficiency up to a maximum with air preheat constrained to 724 K. The increase of the GT inlet temperature also improved the process efficiency.
Keywords: gasification, integration, gas turbine, small scale application, modelling, agricultural residues

1 INTRODUCTION

The European Union has an enormous poultry industry which produces 5,500 million birds every year [1]. Bedding material is spread over the floors within the poultry houses. The purpose of the bedding material is to absorb moisture and promote drying. Litter is removed with every new flock of birds and substituted with fresh bedding material. Thus, poultry litter consists of manure, waste bedding, waste food and feathers. An estimated production of 1.4 million tons of litter results from broiler operations in the United Kingdom [2]. Traditional disposal of poultry litter includes its utilisation as fertiliser but the improper application or overuse represents a potential problem due to: the spread of pathogens [3]; emission of ammonia, greenhouse gases and odorous compounds; and ground water pollution through infiltration of nutrients leading to eutrophication [4]. Due to growing concern and new regulatory constraints, manure disposal on agricultural land is becoming more restricted. Gasification is proposed as an alternative method that solves the problem of waste disposal and represents an environmentally sound option for the on-site energy production.

Conventional integrated gasification combined cycle (IGCC) systems employ gasification at atmospheric pressure, where the produced gases are cooled to facilitate the compression to the required pressure for the gas turbine (GT) engine [5-7]. Pressurised gasification is, therefore, more advantageous to avoid the cooling of gases when compression is required and maintain all process stages hot.

However, systems employing a pressurised gasifier are usually of medium to large scale. At Värnamo, Sweden, a 6 MW BIGCC (Biomass integrated gasification combined cycle) system consists of a circulating fluidised bed gasifier that operates at 20 bar and 950 – 1000°C [8]. The hot gases are cooled to a temperature of 350 – 400°C before entering a ceramic filter for particle removal. GT exhaust gases are used in a heat recovery steam generator (HRSG) to produce steam, which then is introduced into a steam turbine. An IGCC system using air-blown pressurised biomass gasification was suggested within the power range of 10 – 40 MWe capable of achieving up to 40% of net efficiency [9].

Limited work has focused on the effects of pressure and even less in combination with a power generation system. The effects of pressure on gas yields [10] and gasifier temperature, lower heating value (LHV) of gas, and exergy efficiency [11] have been studied for biomass gasification. In addition, an optimum pressure between 12-13 bar was found based simply on the maximum cold gasification efficiency achievable; it was assumed that 25% of the amount of air for stoichiometric combustion was employed and air was at ambient temperature during the simulation of wood gasification [12]. However, these studies were only concerned with gasification and did not take into account the effects of pressure when a turbine engine is integrated into the gasification process. This work considers a small scale on-site pressurised gasification unit to avoid the transportation of litter to centralised plants and maintain all process stages hot. The objective of this work is the assessment of the effects of pressure on the gasifer and gas turbine performance as well as on the overall process efficiency; additionally, the effects of increasing the turbine inlet temperature were evaluated.

2 METHODOLOGY

2.1 Process description

The system consists of a pressurised gasifier where air was used as gasifying agent as illustrated in figure 1. Since the produced gases can carry over particles (ash and unconverted carbon), a filter was included to remove dust from the gas stream. In the energy integration system (EIS), the hot gas turbine exhaust gases were employed to preheat air and the gases produced after gasification. Following pre-heating, air was divided into two parts. The first part was directed to the gasifier as gasifying air, whilst the second part was introduced to the burner of the GT as combustion air. The preheated gases were injected into the GT combustion chamber and burnt with the previously preheated air. After combustion, the gases entered the expander where their sensible heat is

converted to rotational energy and then the De-NO_x unit to destroy NO_x compounds.

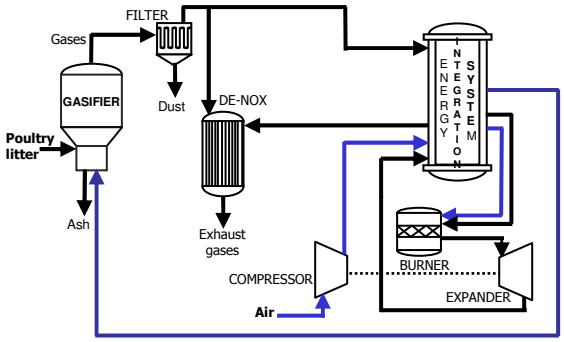

Figure 1: Schematic diagram of pressurised system with energy recuperation

2.2 Process simulation

A model based on chemical equilibrium was developed to analyse the process. The equilibrium calculation offers the temperature and final composition of the product gases considered. This model assumes that the gasifier operates under perfect mixing conditions and uniform temperature, fast reaction rates and sufficiently long residence time to reach equilibrium, and heat losses are ignored since the gasifier is considered as completely insulated.

The software ASPEN Plus was employed for the simultaneous solution of mass and energy balances [13]. ASPEN Plus allows the use of processes involving solids and is equipped with physical, chemical and thermodynamic databases. As input data for the simulations, the ultimate (elemental) analysis, proximate analysis, moisture content, mass flow and higher heating value (HHV) of the poultry litter were specified. The ultimate and proximate compositions employed are given in table I. The HHV for poultry litter was estimated as 13.23 MJ/kg (dry basis) by ASPEN Plus using the IGT correlation.

Table I: Ultimate and proximate analysis of poultry litter

Ultimate analysis	Wt % (dry basis)	Proximate analysis	Wt % (dry basis)
Carbon	37.50	Fixed carbon	24.00
Oxygen	30.62	Volatile matter	54.37
Nitrogen	3.71	Ash	21.63
Hydrogen	5.12	Moisture	25.00
Sulphur	0.45		
Chlorine	0.97		
Ash	21.60		

To model the gasifier, the gasification process was split into three component sub-processes:

- flash pyrolysis consists of the breaking of poultry litter into its constituent elements, ash and energy according to its ultimate and proximate analyses, and is modelled using a RYIELD block,
- gasification is considered as chemical equilibrium and is modelled through the minimisation of the Gibbs free energy using a RGIBBS block. The specified products were CO, CO_2, H_2O, H_2, O_2, N_2, C, NH_3, H_2S, COS, HCl and CH_4,
- ash separation consists of the disengagement of gas from the fluidised bed that allows the separation of ash and unconverted carbon from the fuel gas, and is modelled using a SSPLIP block using a fractional carry over of the solid components (ash and carbon).

In order to model the gas turbine unit, the GT was divided into three component sub-processes:

- compression of air is modelled using a COMPR block,
- combustion is modelled using an adiabatic stoichiometric reactor with a RSTOIC block. The combustion reactions were specified and established as progressing to completion,
- expansion consists of the conversion of the sensible heat of hot gases into rotational energy, and is modelled using a COMPR block. The power generated was used for driving the compressor and the excess work for energy production.

With the aim of obtaining the best achievable efficiency, the exhaust gases from the GT were used to preheat the air for gasification and the air for the GT combustion section. In addition, when the expander exhaust temperature (EET) was higher than the gasifier outlet product temperature, product gases were preheated before entering the combustor. The EIS was modelled as a series of counter current heat exchangers using HEATX blocks. Two conditions were assumed in the EIS, that the temperature of air was constrained to 724 K in order to evaluate the effects of pressure at the same temperature, and that the temperature approach of the EIS was 20 K, for all the pressure ratios evaluated. Table II shows further model assumptions.

Table II: Model input data

Unit	Description	Assumption
Gasifier	Pressure	2-10 bar
	ER	0.29
Gas turbine	Compressor isentropic efficiency	0.85
	Expander isentropic efficiency	0.85
	Expander inlet temperature	1173 K
		1273 K
	Pressure ratio	2-10
	Net power	200 kW
Energy integration system	Temperature of air	724 K
	Temperature approach	20 K

3 RESULTS AND DISCUSSION

The effects of varying the pressure ratio of the gas turbine and the expander inlet temperature (EIT) on carbon conversion, product gas temperature, product gas composition, higher heating value of gas, and process efficiency were evaluated.

3.1 Effects of pressure on gasification

To evaluate the effects of pressure on the gasification of poultry litter, the pressure ratio of the gas turbine was varied, with the two conditions established for the EIS. The effects were studied on temperature of gases, product gas composition, HHV of gases and carbon conversion.

Figure 2 shows the gasification temperature versus pressure when air was preheated to 724 K. It is observed that the temperature increases as expected with increasing pressure. This agrees with the trend previously shown using a gasifier pressure of 10-20 bar for manure gasification [11]. The temperature at 10 bar in this work was 952 K and the previously reported of 1140 K; however, the conditions used in this work were an ER of 0.29 and moisture content of 25%, and in the other work an ER of 0.1, steam fuel ratio of 1 and the moisture content of manure was not mentioned, perhaps it was assumed as dry fuel.

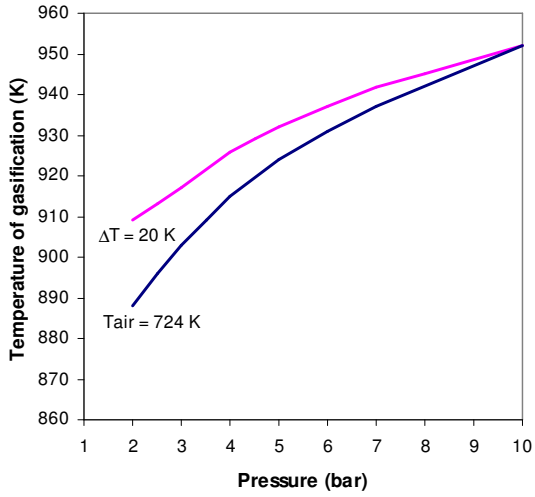

Figure 2: Gasification temperature versus pressure when temperature of air is at 724 K, and when temperature approach of energy integration system is 20 K

Figure 3 depicts the product gas composition versus gasifier pressure. Methane and water vapour increase with higher pressure, whilst hydrogen decreases. No significant difference is observed for CO and CO_2 concentration.

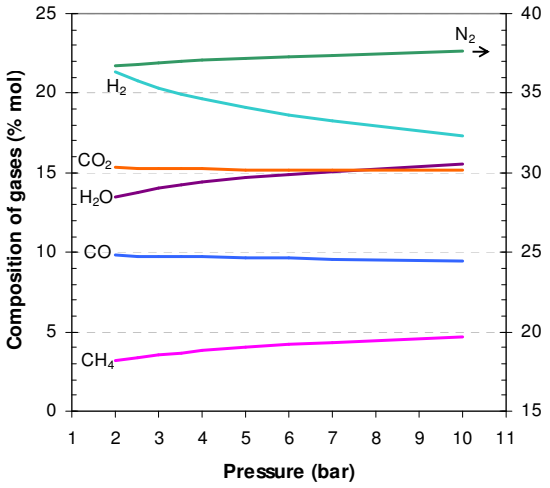

Figure 3: Composition of gases versus pressure when temperature of air is at 724 K

For wood gasification, it was earlier found from simulation work that pressure increases favoured CH_4 formation and simultaneously reduced CO and H_2 formation up to a pressure of 12-13 bar [12]. In contrast, other work reported that no significant influence of pressure was revealed on gas composition during the gasification of four types of biomasses [11]. However, in Srinivas et al. work, the temperature of air was not kept constant with pressure changes since the increase in pressure ratio increases the compressed air temperature, which could have neutralised the effects of pressure.

Figure 4 shows the effects of gasifier pressure on HHV of gas. Since the content of methane, hydrogen and carbon monoxide impact on the HHV, its value is expected to change with pressure. However, the graph shows only a slight increase in the HHV when preheated air is constrained to 724 K. The increase in CH_4 concentration (figure 3) and gasifier temperature (figure 2) compensate the decrease in CO and H_2 concentration.

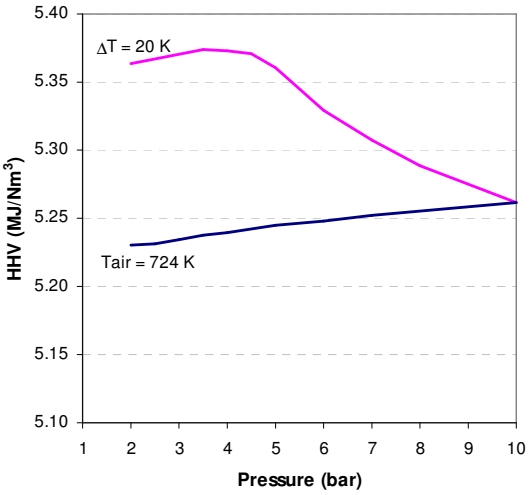

Figure 4: HHV of gases versus pressure when temperature of air is at 724 K and with a temperature approach of 20 K

Figure 5 illustrates the effects of pressure on carbon conversion. Because the gasifier temperature increases with pressure, carbon conversion improves with increasing pressure when the temperature of preheated air is kept constant (724 K).

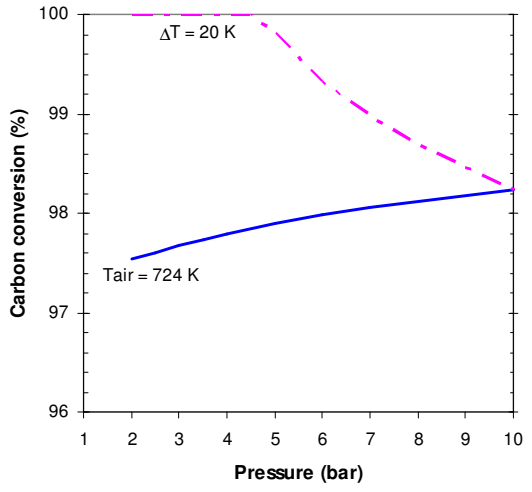

Figure 5: Carbon conversion versus pressure when temperature of air is at 724 K and with a temperature approach of 20 K

3.2 Effects of pressure on gas turbine and energy integration system

Figure 6 depicts the exhaust temperatures of the turbine and compressor versus pressure ratio. It can be seen that the turbine exhaust temperature decreases with pressure ratio while the compressor exhaust temperature increases as expected. More energy is available for integration at lower pressure ratios due to higher turbine exhaust temperatures which can preheat the cooler compressed air.

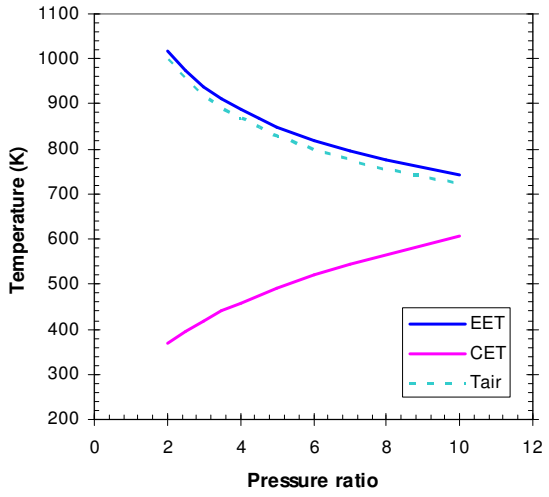

Figure 6: Expander exhaust temperature (EET), compressor exhaust temperature (CET) and temperature of preheated air (Tair) versus pressure ratio with a temperature approach of 20 K in the EIS

In the energy integration system when the temperature approach is set as 20 K, the gasification temperature increases especially at lower pressure ratios as shown in figure 2. Figure 4 illustrates that the HHV increases slightly up to a pressure ratio of around 4.5, afterwards the HHV decreases due to the decrease in the temperature of the gasifying air. Similarly, figure 5 shows that carbon conversion is complete up to a pressure ratio of 4.5, whilst carbon conversion decreases steadily at higher pressure ratios.

3.3 Effects of pressure on overall process efficiency

Figure 7 shows that increasing the pressure ratio improves the process efficiency up to a maximum, at a pressure ratio of 7, with the preheated air temperature constrained to 724 K. However, when the heat integration was improved using a temperature approach of 20 K in the energy integration system, low pressure ratios provided higher efficiencies.

Figure 7 also illustrates the process efficiency when the EIT was raised to 1273 K. The process efficiency was improved by increasing the EIT, since the expander exhaust temperature increased allowing more energy to be integrated into the system. This increment in efficiency was more pronounced at higher pressure ratios especially when the temperature of air was constrained. Therefore, at lower pressure ratios more energy could be recuperated by preheating the produced gases and air before entering the GT combustion chamber when the temperature approach in the EIS was of 20 K.

Nonetheless, at pressure ratios lower than 3.5, the heat exchanger becomes the critical element which would require the use of high temperature heat exchangers, defined as temperatures above 923 K [14]. As a result, intermediate pressure ratios (4 – 6) seem more convenient, because they do not require expensive heat exchangers that could stand high temperatures or provide low temperature approaches.

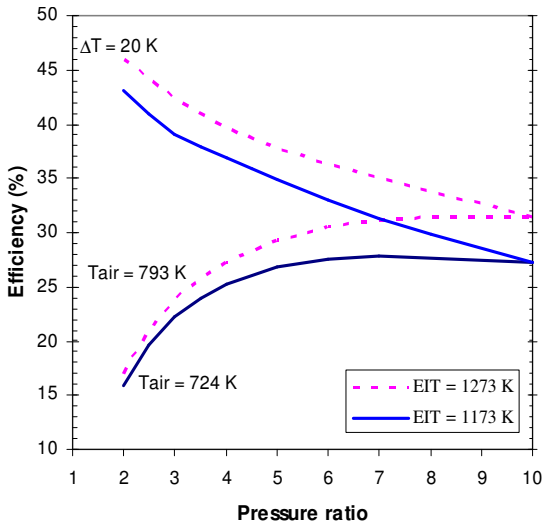

Figure 7: Process efficiency versus pressure ratio when temperature of air is at 724 K, and when temperature approach of EIS is 20 K at EIT of 1173 K, and when temperature of air is at 793 K at EIT of 1273 K

4 CONCLUSIONS

This work shows a solution for a small scale plant that operates with a good efficiency. Two cases in the energy integration system were evaluated to analyse the effects of pressure on the gasifer and gas turbine performances, as well as on the overall process efficiency.

Plant efficiency analyses highlighted the best pressure ratio to achieve maximum integration. Additionally, increasing the turbine inlet temperature improved the process efficiency.

The variation of constraints in the energy integration system showed to be much more significant than the effect of pressure. This is due to the energy recuperation to the gasification process and preheated air.

5 NOMENCLATURE

BIGCC	Biomass integrated gasification combined cycle
CET	Compressor exhaust temperature
EET	Expander exhaust temperature
EIS	Energy integration system
EIT	Expander inlet temperature
ER	Equivalence ratio
GT	Gas turbine
HRST	Heat recovery steam generator
HHV	Higher heating value
IGCC	Integrated gasification combined cycle
LHV	Lower heating value
Tair	Temperature of air

6 REFERENCES

[1] European Union EU. Directorate-General for Agriculture and Rural Development. Agriculture in the European Union - Statistical and economic information 2008.http://ec.europa.eu/agriculture/agrista/index_en.htm

[2] ADAS. Agricultural Development and Advisory Service, A review of current and impending legislation and its implications for the future disposal of poultry manure. Report No. ETSU E/GS/00124/REP 1. Energy from biomass Straw, poultry litter and energy crops as energy sources. London, UK: Department of Trade and Industry; 1999, p. 94.

[3] Gerba CP, Smith JE, Jr. Sources of Pathogenic Microorganisms and their Fate during Land Application of Wastes. J Environ Qual 2005;34:42-48.

[4] Bitzer CC, Sims JT. Estimating the availability of nitrogen in poultry manure through laboratory and field studies. Journal of environmental quality 1988;17:47-54.

[5] Baratieri M, Baggio P, Bosio B, Grigiante M, Longo GA. The use of biomass syngas in IC engines and CCGT plants: A comparative analysis. Applied Thermal Engineering 2009;29:3309-18.

[6] Rodrigues M, Walter A, Faaij A. Performance evaluation of atmospheric biomass integrated gasifier combined cycle systems under different strategies for the use of low calorific gases. Energy Conversion and Management 2007;48:1289-301.

[7] Wolf J, Barone F, Yan J. Performance Analysis of Evaporative Biomass Air Turbine Cycle with Gasification for Topping Combustion. Journal of Engineering for Gas Turbines and Power 2002;124:757-61.

[8] Stahl K, Neergaard M. IGCC power plant for biomass utilisation, Varnamo, Sweden. Biomass and Bioenergy 1998;15:205-11.

[9] Klimantos P, Koukouzas N, Katsiadakis A, Kakaras E. Air-blown biomass gasification combined cycles (BGCC): System analysis and economic assessment. Energy 2009;34:708-14.

[10] Haryanto A, Fernando SD, Pordesimo LO, Adhikari S. Upgrading of syngas derived from biomass gasification: A thermodynamic analysis. Biomass and Bioenergy 2009;33:882-89.

[11] Srinivas T, Gupta AVSSKS, Reddy BV. Thermodynamic Equilibrium Model and Exergy Analysis of a Biomass Gasifier. Journal of Energy Resources Technology 2009;131:031801.

[12] Mathieu P, Dubuisson R. Performance analysis of a biomass gasifier. Energy Conversion and Management 2002;43:1291-99.

[13] Aspen Technology I. Aspen Plus 11.1 user guide. Cambridge, MA.; 2001.

[14] Aquaro D, Pieve M. High temperature heat exchangers for power plants: Performance of advanced metallic recuperators. Applied Thermal Engineering 2007;27:389-400.

7 ACKNOWLEDGEMENTS

The Authors would like to thank the National Council on Science and Technology (CONACYT) of Mexico and Keld Energy Ltd. for their financial support.

Contact: Carolina.FontPalma@postgrad.manchester.ac.uk